Connection Investigations for Cold-Formed Steel Modular Building Structure Systems

by

HANWEN ZHANG

A thesis submitted to the
University of Birmingham
for the degree of
DOCTOR OF PHILOSOPHY

Department of Civil Engineering
School of Engineering
College of Engineering and Physical Sciences
University of Birmingham
October 2017

UNIVERSITYOF
BIRMINGHAM

University of Birmingham Research Archive

e-theses repository

ABSTRACT

Modular construction is a kind of construction that is prefabricated off−site and easily assembled on site. Because of its advantages, such as high efficiency and productivity, modular buildings are widely used for hotel, residential, school and shop buildings. Cold-formed steel (CFS) with its advantages of high strength-to-weight ratio is commonly utilised in the modular constructions. The benefits brought by this kind of structure are prominent and reflected in aspects of technology development, economy and sustainability.

The construction industrialisation promoted construction innovation. The integrated pipeline production process of each module can provide good standardisation and quality control. It lowers down the construction cost and saves building cost due to the economics of scale and the reduced construction timescale. The application of recyclable materials reduces environmental pollution. However, problems of modular construction are also presented. The challenge comes about due to the connections, as generally consume a substantial part of the expenditure. An easy erection and effective connection method could considerably achieve a great cost saving. The investigations for CFS modular structure and connections have been carried out since 1980's. As the types of connections and fasteners between components or units become more complex and diversified nowadays, current codes and standards cannot cover the connection configuration and precision requirements in design.

To investigate and improve the structural behaviours of connections employed in CFS modular building constructions, the unsolved issues in connections of off-site CFS modular building structures were identified in this thesis. The research investigated the connections in the CFS modular panel structure through experimental, analytical and numerical methods including the behaviours of the purlin-to-sheeting, stud-to-track and joist-to-post connections.

In the CFS roof system, purlin sections are often attached to the corrugated steel sheet by self-drilling screws. The magnitude of the rotational stiffness of the purlin-to-sheeting connection

affects the load carrying capacity of the purlin. The current prediction does not provide appreciated accuracy. Off-site CFS modular structures are often organised by thin-walled galvanized stud and track section components. The structural behaviour differences are mainly derived from steel material properties, connections and dimensions of the members. However, due to the limitation of the component dimensions and manufacture tolerance, gaps may exist between the connected sheets. This clearance may lead to warping in the early stages, and may impact the structural behaviour of the connection. The response of the stud-to-track connection is also determined by the connecting method. Progressive collapse of CFS structures has been concerned and specified in the General Service Administration (GSA) guidelines and the Department of Defense (DoD) guidelines. In the structure, the load transfer path can be changed due to the removal of the structural components through potential beam action and catenary action. The alternative loading will be imposed on the connections in a certain range. Considering high strength material (S550) applied in modular structure and complex loading conditions, it is necessary to analyse the entire structural behaviour of the connections, and find out the most efficient and effective connecting method as well as the reasonable fasteners.

A finite element (FE) model was developed which made a good agreement with the numerical results. Based on the numerical studies, a modified calculation method for the rotational stiffness of purlin-to-sheeting connection was proposed in this thesis. This study carried out parametric studies to figure out the influence of the variables on stud-to-track connection performance. A comparison was also conducted between single-bolted connections and double-screwed connections applied in the CFS structure. In order to investigate and improve the performance of the connection between panels under normal and abnormal loading conditions, this research intends to predict the responses of screwed connection with high strength materials under combined loadings. A comparative study of joining solutions was rendered. In this investigation, a series of tests about screw joints under pure and mixed loading scenarios were conducted. The results of a well-established FE model present a great accordance with the test outcomes. The connection configurations applied in CFS panel

system with high strength material were introduced in this research. The screw joint properties were employed in the simulation of the proposed connection configurations. It was proved that the new connecting methods can provide a great improvement to the structural behaviour under either normal or abnormal loading conditions.

ACKNOWLEDGEMENTS

First of all, I would like to express my sincere gratitude to Prof. Charalampos Baniotopoulos for his continues support, encouragement and supervision during my PhD study. He is more than a supervisor. His enthusiasm in life and expertise in the research field have set the great example for me to learn from.

I express my deepest appreciation to Dr. Jian Yang for his supervision throughout my PhD study. He has provided expert guidance and a number of opportunities to improve myself. With his assistance, I have won the Student Development Scholarship during my research period. The thesis would not have been possible to be completed without his valuable suggestions and persistent support.

I am indebted to Dr. Pedro Martinez-Vazquez, Dr. Yingang Du and Dr. Marios Theofanous for their constructive suggestions and advices for the thesis.

I am also grateful to my friends and colleagues for providing help to me in study and life, particularly to Feiliang Wang and Zijun Li who have kindly assisted me completing the experimental work and paperwork issues.

My thanks to the Department of Civil Engineering, School of Engineering, University of Birmingham and School of Naval Architecture, Ocean and Civil Engineering, Shanghai Jiao Tong University, for providing support for assistance, facilities and supports throughout the research.

Finally, I would like to extend my heartfelt thanks to my family. Their love, understanding and caring have always encourage me to continue moving forward.

TABLE OF CONTENTS

LIST OF FIGURES

LIST OF TABLES

LIST OF ABBREVIATIONS

ACI	American Concrete Institute
AEM	Applied Element Method
AISI	American Iron and Steel Institute
AS	Australian Standards
ASCE	American Society of Civil Engineers
BFcsw	Bearing failure in section web around bolt hole
BS	British Standard
BSI	British Standards Institution
CFS	Cold-formed steel
CL	Concentrated load
CPB	Cement particle board
DB	Distortional buckling
DoD	Department of Defence
E	Young's Modulus
EC	Eurocode
FD	Face-down position
FEM	Finite element method
FFcs	Flexural failure of connected cold-formed steel section
FFgp	Flexural failure of gusset plate
FU	Face-up position
GSA	General Services Administration
LB	Local Buckling
LBW	Laser beam welding
LTBgp	Lateral torsional buckling of gusset plate
MBS	Modular building structure
MIG	Metal inert gas

MZ	Modified Z
OSB	Oriented strand board
PCA	Portland Cement Association
SPR	Self-piercing rivet
SHS	Square hollow section
SCI	Steel Construction Institute
UDL	Uniformly distributed load

CHAPTER 1   INTRODUCTION

1.1 Introduction

Innovation in the construction industry has always been slower than in other sectors. In an early UK report by Egan (1998), off-site modular construction was proposed as a modern method for improving aspects of construction performance such as efficiency and quality. An extensive survey by Gibb and Isack (2003) has listed the benefits of modular construction. It concluded that less construction time on site, higher quality and lower costs were considered as the key benefits from the clients' perspective. Additional benefits, such as better health and safety control, less environmental disturbance, and high productivity, were also reported for off-site construction (Hampson and Brandon, 2004).

a) Light steel module with an internal corridor   b) Installation of modules in a social housing project, London

c) Modular student accommodation, Manchester   d) Mixed modules and panels in medium-rise apartments

Figure 1-1 Off-site CFS modular building constructions (SCI., 2006)

Gypsum board
50 mm mineral wool + Z-steel battens
Vapour barrier (PE)
175 mm mineral wool + thermal studs
Gypsum board
80 mm mineral wool
Rendering

1
2
3
4
5
6
7
8
9
10

1. 20 mm surface material
2. 10 mm Sasmox wood-gypsum board
3. 18 mm Sasmox board strips
4. 18 mm Sasmox board
5. 30 mm impact sound insulation
6. 15 mm plywood
7. 300 mm C-profile and 100mm mineral wool
8. 24 mm acoustic profile
9. 13 mm Gypsum board
10. Surface material

a) External wall panel   b) Intermediate floor panel   c) Roof panel

Figure 1-2 Modular panel configurations (From *Rautaruukki Corporation*)

Recently, sustainable construction, the concept of personalisation and an emphasis on customer experience have become the new directions of focus in the construction industry (Zabihi et al., 2013). The pictures in Figure 1-1 illustrate the applications of CFS modular construction.

In practice, off-site cold-formed modular buildings are increasing world-widely because of their numerous advantages, e.g. waste reduction, recyclability, reusability, fast assembling, etc. A great thermal and acoustic insulation performance can be obtained with the in-filled materials (see Figure 1-2).

However, this kind of construction presents both benefits and challenges. Connections between components or units are getting more complex and diversified. But current design guidance cannot cover the state. This research aims to study the connections in off-site CFS modular building structures and provide relevant design guidance. The genetic forms of steel modules are introduced as follows.

Innovation and revolution have always been the driving force behind most industries. In contrast, the automation and productivity of the construction industry are still progressing at a

comparatively slower rate. On the research side, off-site CFS modular building structures are recognised as a future trend in the industrialisation of the construction process.

1.1.1 Containers

Container modular constructions are made of multiple boxes as unit. Boxes can be produced by either used standard containers or open-section steel components. Coupled with mature transportation and handling facilities, this kind of modular construction is recently developing rapidly which is appropriate for temporary registration. Container modular unit realized the maximum proportion of prefabricated structure and notably shorten the on-site construction time. Due to the regular shape of the boxes, container modular construction is widely utilised for hotels, accommodations, offices, canteens as well as garages. In order to obtain larger space, modular units can be designed with partially or fully open sides and placed together. Container buildings represent low-cost, easy build and generally use for low-rise temporary construction.

Besides, sound insulation, air circulation problems and thermal insulation issue are ineluctable to be solved. In order to make freight container be able to satisfy habitation requirements, windows and doors are merged with the steel boxes. The implementation of embedded material in containers leads to good seal and thermal insulation effect. As for the transportation usage, the design of freight container follows general standards. However, the dimensions of containers can be adjusted according to the requirement. The regular dimensions of the boxes are of 6m or 12m in length, 2.5m in height with the width of 2.438m. Although the shape and dimensions of containers are limited, there are many combinations consisting of individual units and sometimes modified boxes.

Containers are mainly used to estabilsh low-rise construction, the corner column and walls carry the vertical loading. Box units can be connected by corner eyes with cleats and bolts. Welding is still the main method to connect components in this system. For some practical requirements, the container can be strengthened by welding a stiffener to either the inside or outside of the walls (see Figure 1-3).

Top end frame
Roof
End wall
Side wall
Corner structures
Top side frame
Corner eyes
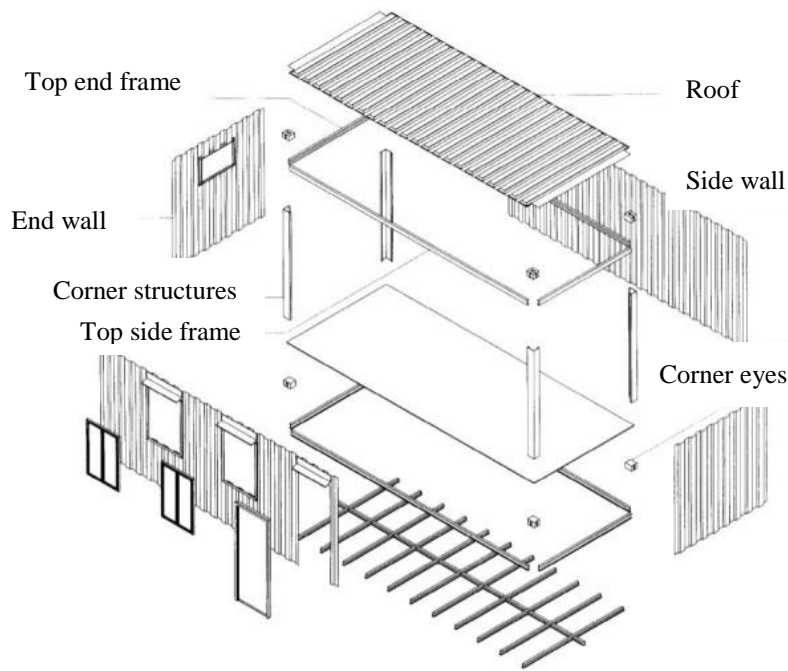
a) Schematic diagram   b) Strengthening in container structure

Figure 1-3 Container structure unit

1.1.2 CFS panel system

Component modular structure is erected by pre-cast 2D wall and floor panels (see Figure 1-4), accompanied by 3D-modules for functional parts, such as kitchens, bathrooms and toilets (Lawson and Ogden, 2008). Despite the lack of relative integrity and easy assemblage, this system is generally applied in low-rise and medium-rise residential sector and more flexible in design. The connection between each panel needs further analysis and innovation, such as connection configuration and the structural behaviours.

For the low-rise buildings with less than 3 floors, it is permitted to place floor panels on walls directly. In terms of medium-rise construction, it is required to make the load transfer directly through the walls by carrying the floors (Gorgolewski et al., 2001a).

This system is very flexible in use. The thermal and acoustic insulation is implemented by embedded materials. Relative to sheeting diaphragms effect caused by corrugated steel sheet and floor slab, it is believed that these panels provide more effective support to the open

section members, preventing torsion caused by eccentric loading. Global stability and strength of the structure are enhanced by the in-filled materials as well. However, this hypothesis needs to be proved and quantified as well.
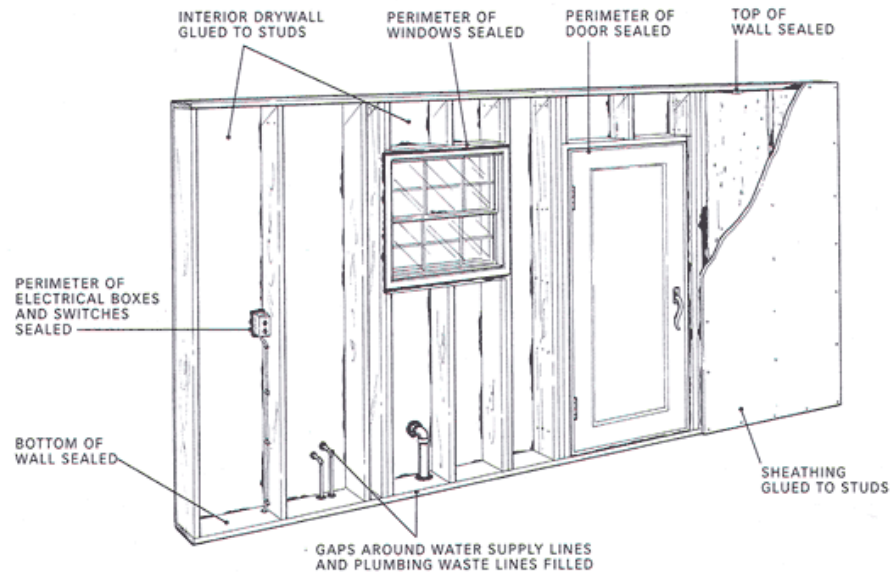
Figure 1-4 Modular wall panel (From *The Modular Home*)

1.1.3 Plate-column system

The steel modular plate-column system consists of truss lattice plates and precast steel columns (see Figure 1-5). Square hollow section (SHS) is usually adopted as columns. At the connection between the floor and the column, the bracings are needed to enhance the strength of the floor and reduce the span of the floor. The imposed loading is carried by the truss floor and transferred to the braced steel column through the connection between the components. Its feature is that there is no beam under the interior floor and the layout is flexible.

This kind of construction is applicable for multi-story buildings, warehouses, public buildings, office buildings and residences. Additional shear walls or other anti-lateral force components, such as diagonal bracing can be added to limit the horizontal displacement of the structure and enhance the ability to resist earthquakes and wind.

Figure 1-5 Interconnection of boxes

1.1.4　Frame structure cassettes

In the frame cassette, corner columns and frames beams are the vertical load carrying members and the diagonal bracing (see Figure 1-6) is used to resist horizontal forces. This system is similar to containers but the shape and dimensions are more flexible in use as compared to container boxes. Unlike traditional light steel constructions, this box is considered as a combination of hot rolled corner column and light steel keel in-filled, of which the corner columns serve as the dominant member resisting vertical loads from upper modules when the boxes are stacked and hoisting the load.
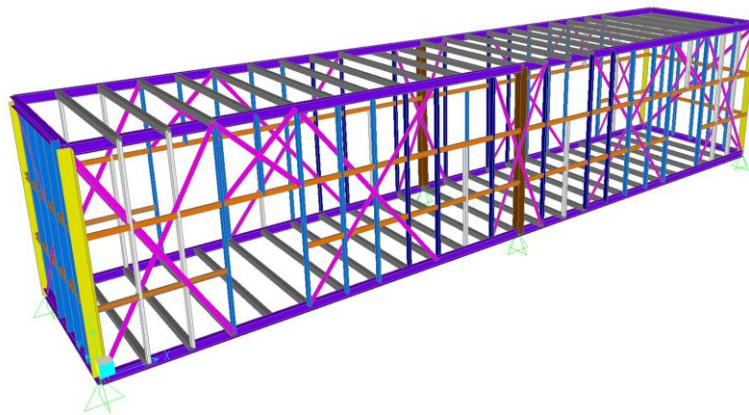
Figure 1-6 Light steel keel structure box sketch

Other components are made of CFS open C or U sections which are supposed to strengthen the steel frame to some extent. Square hollow section (SHS) and angle sections are regularly adopted as corner columns.

In the wall panels, rigid or flexible diagonal bracing is applied to resist horizontal force caused by wind or earthquake. The connections of the modular construction include interconnection between modular cassettes (see Figure 1-7).
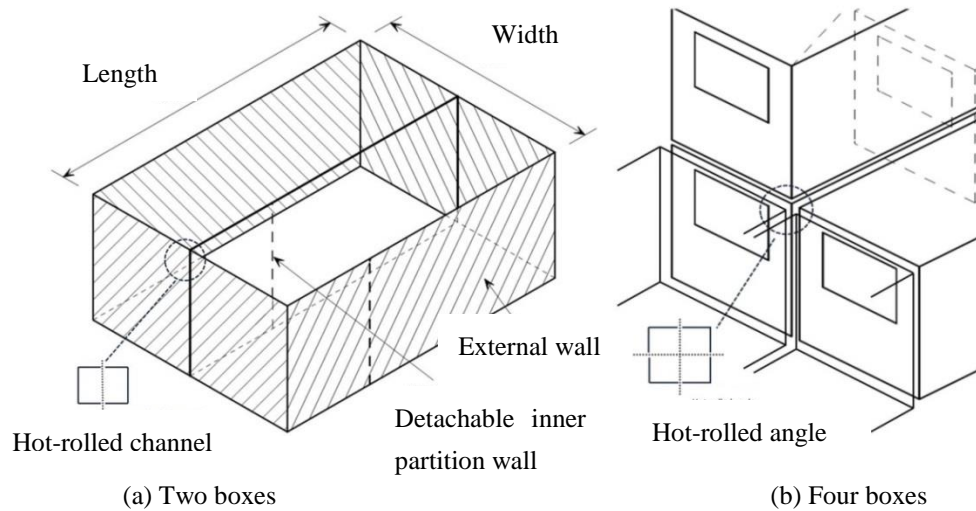
Figure 1-7 Interconnection of boxes

1.1.5 Connections

Table 1-1 shows the connections involved in steel modular building structure systems. Connection behaviour is the key factor to ensure the safety of the structure under loading conditions, including the resistance of each unit and the integrity of the assembled construction. The strength redundancy of each connection determines the structure responses event under abnormal loading conditions, like fire and blast.

According to the scope of application, the connections can be divided into connections linking accessory structures, connections installing units and connections assembling units. The current design method cannot cover the practical situations, and the predictions accuracy need to be further improved. Therefore, this thesis studied the connections applied in CFS modular building structures.

Table 1-1 Connections involved in steel modular systems

Scope of application	Connection position	Annotation
Connections linking accessory structures	1. <u>Purlin-to-sheeting connection</u>	Roof system
	2. Floor-to-frame connection	Concrete slab, composite slabs with corrugated steel sheet
	3. Wall-to-frame connection	Connection between in-filled light steel stud wall and structural frame
	4. Connection to attach finishing materials	Such as plasterboard, sheathing, floor boarding, insulation and decking to light steel structures
Connections installing a unit	1. <u>Stud-to-track connection</u>	In modular panels
	2. Connection between structural sections and bracings	Connections between vertical and horizontal load carrying element
Connections assembling units	1. <u>Joist-to-post connection between floor panel and wall panel</u>	In modular panel system
	2. Connection between column and floor panel	In column-floor panel system
	3. Connection to link adjacent frame cassettes	In frame structure cassette system
	4. Connection to link adjacent containers	In frame container system

The investigation of this thesis involves purlin-to-sheeting connection, stud-to-track connection and joist-to-post connection between wall panel and floor panel. Purlin-to-sheeting connection is used in roof system. The rotational stiffness of the connection significantly affects the system performance. Stud-to-track connections play crucial role to guarantee the resistance of modular panels. These units are assembled by joist-to-post connections. The behaviour of the connections determines the structural integrity and the responses under normal and abnormal loading conditions.

1.2 Novelty

The main novelties that are worth to be investigated in this thesis are listed as follows:

- Analysis of benefits and challenges of off-site CFS modular building construction systems and the supply chain.

- Modified calculation method of rotational stiffness of Σ purlin-corrugated sheet

connections.

- Analysis of bolted and screwed stud-to-track connections with gaps.

- Screw joint tests under pure and mixed loading conditions.

- Simulation method of screw joint connecting high strength steel (S550) sheets subjected to shear, tension and combined shear and tension loading scenarios.

- Analytical method of screw joint subjected to mixed loads.

- A comparative study of proposed connection configurations and the current typical connection.

- Structural behaviour and load resistance mechanism of CFS modular panel structures with different connection configurations under normal and abnormal loading conditions, with regard to geometric shape and nonlinear resistance of the connections as well as the attached materials.

1.3 Aim and objectives

The aim of this research is to investigate and improve the structural behaviours of connections employed in CFS modular building constructions under normal operational or abnormal loading conditions. This is achieved through the following objectives.

- To develop a design method for predicting the rotational stiffness of the screwed purlin-to-sheeting connection.

- To compare joining solutions of the CFS stud-to-track connections.

- To examine the structural properties and develop a resistance prediction method of the screw joint under pure or mixed loading conditions.

- To develop numerical methods to simulate the screw joint applied in the CFS structures.

- To measure the structural properties of different connection configurations of the joist-to-post connection.

- To evaluate influence of the connections on the robustness of the structures.

1.4 Methodology

To achieve the aforementioned aim and objectives and thoroughly understand the structural performance of the connections in CFS modular constructions, an extensive literature review is conducted to understand the state-of-the-art research development in this field and identify the existing knowledge gaps. A series of laboratory tests are carried out to obtain the first hand data of screw and bolt joint behaviour. The existing test outcomes from the previous studies are also used for reference. The test results are used as the basis and validation of numerical simulation. FEM is employed for numerical analysis to extend the range of geometric dimension beyond the tested specimens. For the investigation of structural robustness, 2D and 3D analytical models are adopted. Based on the test and numerical analysis, design recommendations for the connections are developed through the analytical models.

1.5 Outline of thesis

Chapter 1 introduces the background knowledge of the investigation. An extensive literature review is conducted in this field in Chapter 2. Based on the comprehension of development of CFS connections and modular construction systems, knowledge gaps are identified. In consequence, the corresponding problems are addressed by using numerical, experimental and analytical approaches. Finite element methods (FEMs) are developed to predict the structural responses of the joints and connections. In Chapter 3 and Chapter 4, the proposed simulation methods are verified by existing experimental results and specification predictions, and the modified design methods of purlin-to-sheeting connections are achieved through numerical and analytical approaches. As a validation of the numerical studies of screw joints under complicated loading conditions, a series of tests are conducted in Chapter 5. When the screw joints are subjected to mixed loads, the thesis uses the derived equations to predict the ultimate resistance of the joints. For the further investigation of connection configurations, FEM is employed to carry out the analysis of joist-to-post connections under tension, shear

and rotation actions. The connection properties are attached to the 2D and 3D construction simulations by using commercial software package ABAQUSv6.13 and SAP2000v14.1 in Chapter 6. The collapse reaction mechanism of the CFS modular panel constructions is studied through analytical method, and the theory to analyse the load carrying capacity of the structure under abnormal loading conditions is established, which is verified using the numerical results. The thesis studied the structural performance of the connections applied in CFS modular building structures. Chapter 7 provides a summary of the investigations conducted in each chapter and recommendations for the future works.

1.6 Summary

This chapter addressed the background, novelty, the aim and the objectives and methodology of the investigation. The outline of each chapter has been presented in this chapter. The details of the research are presented in the following chapters.

CHAPTER 2   LITERATURE REVIEW

2.1   Introduction

The conventional construction process is usually completed on construction sites. Cast-in-place concrete structure is one of the representatives. The connection featuring high strength and stiffness can achieve a high level of structure continuity. However, the off-site CFS construction consisting of light steel components provides advantages in sustainability, quality control, economic benefit, etc. The connection configurations and joint performance determine the structural behaviour of the structure. To understand the development of the research about CFS connections, literature review was carried out to illustrate research background and mechanism. The researches on the relevant areas were presented as the foundation of the further study. The knowledge gaps of connections and joints in CFS modular constructions were identified based on this following analysis in aspects of modular construction, purlin-sheeting system, connection and joints as well as structural robustness.

2.2   Modular construction

Energy conservation and environmental protection are becoming major concerns in various industrial sectors particularly in the construction industry, which normally accounts for 40% of energy consumption and one third of carbon emissions. In the past two decades, modern construction methods, such as off-site modular construction, have been actively encouraged and pursued by policy makers and industrial leaders in order to tackle these problems throughout the world. Meeting all conventional requirements such as safety, serviceability and durability, off-site modular construction has emerged as a more advantageous construction method featuring material efficiency, high quality, flexible adaptability, reduced waste and lower energy demands. This new construction technology has been adopted worldwide but with variations in the extent and scope of technological progress and engineering applications. Nowadays, modular construction is mainly used for residential projects, schools, hotel

buildings or shops, and the building components or the entire building units are produced at manufacturing sites. One of the most commonly used materials for this type of construction is CFS.

The use of modular buildings has not been without challenges. The high upfront costs, the long lead time, the complex connections and the acceptance level all affect the appeal of building modularisation (Pan et al., 2007). By 2004, the use of off-site construction in the UK was still at a low level (Goodier and Gibb, 2005). With current high demands for housing in the UK (Barker, 2003), it is necessary to promote the development of construction industrialisation. In parallel with this, it is prerequisite to enhance the overall understanding of off-site construction (Pan et al., 2005). This status similarly occurs in other countries. Recent surveys in Sweden (Larsson et al., 2014), Australia (Blismas and Wakefield, 2009) and China (Zhai et al., 2014) reveal that a lack of skills and sufficient knowledge together with conventional social attitudes are the biggest obstacles in implementing off-site construction. With the development of technology and a change in people's perception of construction industrialisation, the number of off-site modular buildings is continuously increasing in Europe, particularly in the UK (SCI., 2007). One of the key materials that facilitate off-site construction is CFS. Its favourable features, such as high strength-to-weight ratio, excellent structural performance, high recyclability, and good compatibility with other fill-in materials help promote its use in modular buildings.

By conducting an extensive survey, this section reports the enabling benefits and challenging obstacles in off-site modular construction with CFS and identifies problems that need to be addressed in the construction process for off-site modular buildings. The state-of-the-art development of off-site modular building construction with CFS is reviewed in terms of the technical progress, economic behaviour, sustainability and social impact, and based on this a market outlook is proposed.

2.2.1 Technology development

2.2.1.1 Technical enablers of modular construction

One of the main merits of modular construction is the construction speed. Based on existing experience, the construction time on-site can be reduced to 20% of that taken under conventional construction methods (Miles and Whitehouse, 2013). In addition to the economic benefits due to saving time, this advantage is also important when modular construction is applied in emergency circumstances, such as post-disaster reconstruction. Moreover, modular construction can also be used together with new building products and technologies to create energy efficient buildings. Many projects completed in the UK have proved successful in this field. For instance, with additional mineral wools placed between the steel frame sections, nearly 90% (Miles and Whitehouse, 2013) of direct heat loss can be prevented, and the U value of wall components can reach $0.25w/m^2 \, ℃$ or below. Excellent acoustic performance can also be achieved by the incorporation of inner gypsum boards attached to the wall panels.

From manual fabrication to automated production, standard modular units have proved popular and necessary due to their flexibility as well as for their better controlled construction quality. In traditional construction, the quality of buildings depends to a large extent on the skills of the construction workers on site. However, this is difficult to quantify or standardise. In contrast, with the development of manufacturing techniques, the components made from CFS can be accurately manufactured off site.

In addition, cold-formed structures are much lighter in weight than other structures such as concrete frame structures, or even timber frame structures. The high strength-to-weight ratio can reduce the foundation loads and allows for a longer span and larger structures, which also significantly improves the flexibility of buildings. As modular cold-formed structures can be easily disassembled and reinstalled, and most steel members can be reused and recycled, this type of building can be moved in part or as a whole.

2.2.1.2 Technical challenges of off-site modular construction

In general, applications have shown that galvanised CFS can meet the structural and functional requirements of the projects (Outinen et al., 2000). However, as a newly emerging construction method, there are many technical challenges that need to be addressed.

Modern method of construction is supposed to achieve benefits with highly automated manufacture and fast construction and is widely used for low and medium rise buildings (Miles and Whitehouse, 2013). The study (Lawson and Ogden, 2008) introduced generic forms of light steel framing and modular constructions by case study. Wind forces on K-braced frame were also evaluated by using FE method. The wall panel shear tests were summarised. The results indicated that the additional elements attached on structure provide considerable structural behaviour reserve in global stability. The 'Hybrid' construction and the corresponding design methods were proposed as the economic form in medium-rise sector.

High-rise modular buildings (12 storeys or more) have more complex and higher requirements for their structural properties, in particular, concerning wind and seismic resistance and stability. The investigation (Lawson and Richards, 2010) reviewed main technologies employed in high-rise residential buildings and some application cases. It was indicated that wind loads, robustness as well as the eccentricities caused by tolerances, leading to the horizontal forces, are important due to the scale and height of the construction. The research (Lawson et al., 2012) presented some typical cases related to the application of modular constructions in multi-story buildings, including high-rise residential buildings up to 25 stories. The essential modular technologies and structural behaviour analysis of high-rise modular construction were also demonstrated. Based on the information and modular building design concept derived from the cases, a summary of sustainability, economic benefits as well as the issues that required attention were presented in this research. In general, clustered modular construction and corridor arrangement of modules are applied as typical layout of modules in high rising modular buildings, see Figure 2-1. For high-rise construction, resistance of horizontal forces caused by wind loads or robustness to accidental actions is one

of the crucial elements in the design process. Given this consideration, concrete or steel core is employed. The corners of modules are tied together to transfer horizontal loads and alternative load paths will occur in the event of accident damage. For taller buildings, technologies of improving stabilities in medium rise building, such as diaphragm action, bracing in lifts and stair area using hot-rolled steel components are not applicable. Nevertheless, compression resistance and overall stability of the light steel sections and connections in load-bearing walls require a deeper understanding. Moreover, robust performance is also very important when accident failure occurs in partial structure.

a) Clustered arrangement of modules   b) Corridor arrangement of modules
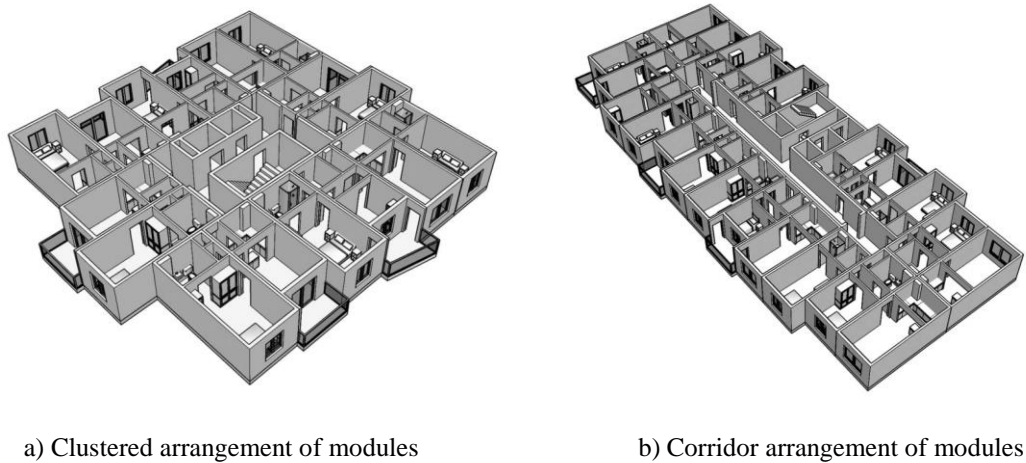
Figure 2-1 Typical arrangements of modules (Lawson et al., 2012)

Shear walls are recognised as one of the key load bearing components of modular buildings. The choice of in-fill materials for the walls, floors and roofs, along with the arrangement of the internal studs and fasteners, significantly determines the strength, stiffness, overall stability, and other structural performance (Landolfo et al., 2010). Compression tests on modular walls were carried out taking into account the effects of attached boards (Lawson and Richards, 2010). It was found that the minor axis buckling can be prevented, event only one side attached board. The carrying capacity of walls increased by 10 to 40 present compared with BS 5950-5 due to the attached boards. The bending stiffness significantly increased up to 62 present resulted from the attachment of OSB and CPB boards on both sides. The effect of eccentricity was also determined in this research. For the highly stacked modules, tolerance due to installation and manufacture was evaluated and considered in the design. The design

method of stability of corner post in modular construction was proposed, involving the shear stiffness of the wall panel and second-order effects. The design of such members is not well covered by codes of practice or other design guides. Hence, research into the design of modular buildings should be carried out in order to standardise the design method.

Connection is one of the key challenges in design. A wide variety of connection types are used for building components or units, but there is a lack of standardisation. Components in modular building structures may be subjected to complicated loadings, such as the combined action of bending, shear and torsion. The connections dominate the performance of a structure and occupy a large proportion of construction cost. Further research is required on the connections and joints within and between the modular units.

As the case stands (Nair, 2004), the components of construction can be suddenly ineffective or compromised due to abnormal loadings, such as fire, blast or impact, which may lead to disproportional or progressive collapse. Existing guidelines DoD and GSA permit the structure to respond nonlinearly once a column was removed in the disproportional or progressive collapse analysis. If the horizontal and vertical tie force is sufficient, the catenary may occurs, leading to the change of the load transfer path. Whereas, the structure may remain elastic in the construction, causing no plastic hinge to dissipate energy through inelastic material deformation (Ruth et al., 2015) which is performed as a beam action. The inherent characteristic of robustness and integrity of CFS modular construction is relevant to construction shapes and connection configurations (Foley et al., 2007). In case of unaccounted scenarios, load resistance mechanism of the initial connections may be changed from pure shear to rotation and tension which puts forward new demands on the connection ductility and bearing capacity. The reduction of structural redundancy increases the economic efficiency but weakens robustness to some extent.

Intermediate plates, end plates, fin plates, and tee or angle cleats are frequently used in structural connections to transfer the forces from one member to another. Plates or cleats are relatively strong and stiff to transfer the forces by in-plane actions. However, they are weak to

transfer the forces in out-of-plane bending (Trahair et al., 2007). For thin-walled steel members, due to the thin thickness and stress concentration around fasteners, local buckling likely occurs in connection zones. Gussets and cleats can directly increase connected thickness, stiffen partial components or redistribute force transfer path to improve structural performance of the original connection. Connections with stiffeners are proposed in this research. In order to find out the most effective and efficient connection configuration and comprehend the connection response in the modular construction, a numerical investigation was carried out involving either normal or abnormal loading conditions.

2.2.2   Economic benefits

The cost of off-site construction can be divided into four main categories: fabrication, transportation, erection and operation costs.

Most components of CFS modular buildings can be produced off-site. They can be transported and assembled on site in the form of panels and prefabricated shapes and hence significant savings can be made to construction time. This method also requires fewer site workers and cranes. Therefore, costs of labour, equipment and on-site overheads can be significantly reduced. For developers, shorter construction duration means a shorter payback period.

In traditional construction, material waste on construction sites accounts for 10% of the construction material, most of which ends up as landfill. Factory manufacture can avoid such wastage and can even optimise the use of raw materials.

Manufacturing units in the factory can also enhance their quality and can reduce the number defects occurring in products and thus also reduce the operational costs for maintenance and repairs (SCI., 2006).

According to a report (SCI., 2007), high volume production can further reduce the cost of manufacturing due to the economies of scale.

2.2.3 Sustainability

2.2.3.1 Environmental sustainability

The steel frames used in modular buildings are galvanised and hence are durable even under hostile environmental conditions. Steel is a highly recyclable material, and no steel frames should end up in landfill. The water used in production is also reused with this pollution-reducing and energy saving construction method (SCI., 2006). Moreover, for CFS structures, CO_2 emissions can be reduced both in construction and during the life-cycle of the buildings (Coimbra and Almeida, 2013).

Since the prefabrication process is carried out in the factory, there is significantly less pollution from noise, dust and waste on site. By using this type of construction, a clean and less environmentally damaging construction site can be created leading to a reduced impact on the environment and improved air quality.

2.2.3.2 Energy consumption

Steel itself is a heat conductive material. However, the air-tightness of steel framed buildings can reduce heat loss due to the leakage of air through the building envelope. This is further improved by added insulation materials such as mineral wool and gypsum. Nowadays, modular units can also incorporate renewable energy systems such as solar panels.

Another important factor is that less transportation is needed for the construction materials for off-site construction, leading to less pollution and lower energy consumption. A report (Miles and Whitehouse, 2013) indicated that on-site energy consumption can be reduced to around 20% of that of traditional construction projects.

2.2.3.3 Reduced waste

In the traditional construction industry, a lot of waste is produced from construction materials, including cutting bricks or boards, packaging, damaged elements, and material wasted on site or in transportation. In Europe, cement and brickwork make up the largest proportion of waste produced, at percentages of 32% and 25%, respectively (SCI., 2006). Unfortunately, the

majority of this waste cannot be reused or recycled and is usually sent to landfill. Consequently, how to reduce the levels of waste is a major challenge for the construction industry. Off-site cold-formed structures can minimise wastage in production to 90% of that in conventional construction (Miles and Whitehouse, 2013), in the following ways. Firstly, the great majority of the materials used in modular building are reusable or recyclable. Most CFS components can be reused or recycled at rates approaching 90%. With good practice, there could be reduced waste both on-site and off-site. Secondly, off-site CFS modular buildings are easily disassembled or extended, which provides flexibility, potentially leading to reduced building demolition waste as well. In addition, considering the current excessive levels of steel production capacity, this type of structure is also efficient in the use of resources.

2.2.4 Society

Compared with traditional construction, the construction duration is notably reduced in modular construction. The off-site construction supply chain is also significantly more integrated and better controlled. At least 60% (Miles and Whitehouse, 2013) of the completed construction product is made off-site, requiring fewer workers on site but creating more manufacturing based jobs. As a result, off-site construction tends to convert jobs for low skilled construction workers into properly trained technicians or engineers.

Because the construction methods and skills are quite different from those of traditional building construction, some new jobs will be created. For example, experienced designers and engineers in this field are needed for the design of modular building structures. Based on the requirements of the construction process, a highly skilled and transferrable workforce (Miles and Whitehouse, 2013) is indispensable for the prefabrication and assembly processes in order to ensure engineering quality and efficiency.

Particularly in developing countries (Zhang et al., 2014), high initial cost, low level supply chain, the lack of a developed legal system and government incentives, poor productivity, low skilled labour and product quality problems emerge as the factors which hinder the progress

of construction industrialisation. In the initial stages of development in construction modularisation, developing countries may invite a number of overseas workers from developed countries, which will generate high costs. It is also necessary to carry out training of the local workforce at an early stage.

In fact, the challenges of modular construction are not only confined to the technical level. The growth of this construction method coincides with a rapidly developing society and the on-going process of integration of suppliers. Therefore, it cannot achieve its full potential benefits without the support of government and optimised supply chains (Doran and Giannakis, 2011).

2.3 Purlin-to-sheeting system

In recent decades, the screw connections of CFS sections have been studied extensively by various researchers through experimental and numerical approaches (Tan, 1996, Mills, 2004, Kwon, 2006, Bambach, 2007, Fiorino et al., 2007, Gutierrez et al., 2011). Special considerations of the connection performance of purlins attached to sheeting have been implemented into design standards such as EC3 (Eurocode, 2006b). In the code, the lateral and rotational restraints provided by the sheeting are considered as lateral and rotational springs respectively, and the spring stiffness is obtained analytically. However, the method in EC3 for modelling rotational stiffness has been criticized over years due to its relatively low accuracy (Vraný, 2002). Hence modifications to the current design standard are required and the topic has drawn increasing interests from researchers. An analytical model was developed in (Vraný, 2006) to determine the effect of external loading on the rotational restraint. It was found that a higher stiffness of the rotational restraint provided by sheeting results in a reduction of stress in the free flange and a reduction of buckling length in hogging moment areas. Mechanics-based expressions were introduced by (Gao and Moen, 2012) for calculating the rotational restraint provided by through-fastened metal panels to Z- and C-section girts or purlins. The equations considered the effect of local panel deformation at a screw, and the girt or purlin flange bending at a through-fastened connection. An analytical formulae was derived

by (Ren et al., 2012) to calculate the bending stress of the partially restrained C-section purlins by using the classic bending theory of thin-walled beams. In order to further consider the interactional effect at screw points and the effect of loading directions, an improved analytical method based on experimental studies was proposed in (Zhao et al., 2014) to predict the rotational stiffness of cold-formed Z and Σ purlin/sheeting systems.

The restraining effect provided by sheeting has an influence on the buckling (see Figure 2-2) resistance capacity of the purlin. For the purlin-sheeting system under uplift loading scenario, it was found that translational spring stiffness can affect the local buckling of purlin while rotational spring stiffness has influence on lateral-torsional buckling, and the rotational spring stiffness has no influence compared to the translational spring stiffness on the maximum tensile and compressive stress (Ye et al., 2004, Ye ZM, 2002). Moreover, the influence of the initial geometric imperfections on the purlin performance was found only in purlins of medium or long length with no or low rotational spring stiffness (Zhu et al., 2013). For the purlin subjected to pure bending, the lateral restraint provided by the sheeting has almost no effect on the lateral-torsional buckling of the member (Li, 2004). The influence of lateral restraint provided by cladding on the lateral-torsional buckling of Z-purlin beams was examined in (Chu et al., 2005) by using the energy method. Moreover, an analytical model that describes the bending and twisting behaviour of partially restrained CFS purlins subjected to uplift loading was further developed by (Li et al., 2012). For a fully restrained thin-walled C- or Z-section beam subjected to uplift loading, it will not buckle in lateral-torsional mode, but may exhibit a web-flange distortional buckling mode (Yuan et al., 2014).

a) Local buckling   b) Distortional buckling   c) Lateral-torsional
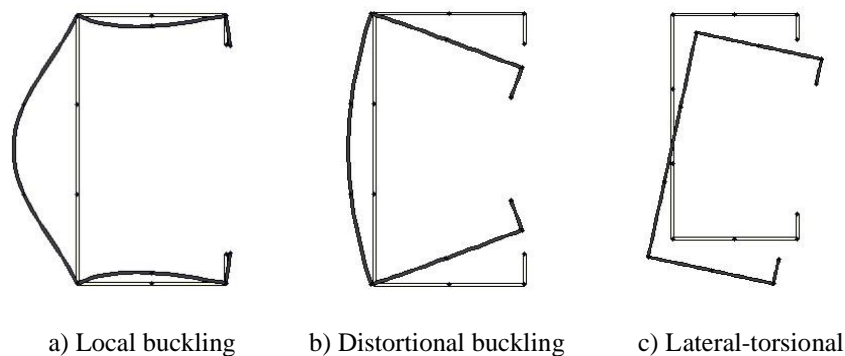
Figure 2-2 Buckling models of CFS section

2.4 Joints and connections

A plethora of research studies have been recently performed on the structural behaviour of steel connections where the failure modes, strength and stiffness of joints and connections have been examined through experimental, numerical and theoretical studies.

2.4.1 Experimental studies

2.4.1.1 Joints

The joint properties normally affect the structural performance of the connection. The bolt joint has been studied. As early as 1986, Kirk (1986) presented a comprehensive review on the research development of cold-formed construction, including stiffness and strength of their joints, design and materials standards, technical developments, etc. A full scale tests of cold-formed section portal frame building system was carried out in this research, which emphasized that cold-formed sections not only can be utilised as secondary structural members but can be qualified for primary framing as well. In the tests, it was found that the stiffness and strength of joints were strong enough, leading to the failure occurred in the members. The study suggested that the eaves and ridge connections with bolt joints can be considered as fully rigid connections but for elastic design. However, because of the small thickness of the member section, bolted connections in cold-formed structure cannot provide a full rigidity in practice. Through analysis and tests, Zadanfarrokh and Bryan (1992) quantified the affecting factors of the strength and rigidity of bolt joints, e.g. the thickness of the section, full shank diameter, threaded portion, etc. They also presented the design expressions for calculating the bearing strength and flexibility of the bolt joints and compared it with those calculated using AISI, EC3 Part 1, BS 5950 Part 5 and BS 5950 Part 1. Based on tensile tests of bolted lap joints and parametric analysis, Bryan (1993) developed the design equation for the joint with compliance of a single lap bolt joint made of Z28 steel with the yield stress of 280MPa and the ultimate bearing strength of 390MPa, and γ_M=1.25 was recommended as safety factor for design. An investigation (He and Wang, 2011) of the whole load-deflection behaviour of bolted thin-walled steel plates in shear was performed using experimental,

numerical and analytical approaches. It was found that the initial stiffness of thin-walled steel connections can be predicted using the equations in Eurocode3 (Eurocode, 2006b). Three pure failure modes (e.g. solely bearing, shear and tearing) and combined failure modes were identified. The bolt-hole elongation determines the resistance of the joint. The elongation is the sum of effects from the deformation of the bolt-hole circumference in tension and the wrinkling in front of the bolt. The methods of calculating the ultimate deformation were proposed and the calculated deformation agreed well with experimental and numerical ones (He and Wang, 2011). In a research (Draganić et al., 2014), bolt joints were studied to ensure bolt-hole elongation that enables a progressive collapse mechanism, focusing on the plastic behaviour of single lap joints. Experimental, numerical and analytical analyses were conducted using bolt-hole centre to plate edge distance as a parameter. S235 steel and M16 of class 5.6 were adopted in the tests. It was found that with the centre to edge distance increasing from 22mm to 40mm, 7.9% higher ultimate load and 20.2% larger plate rotations at ultimate load were achieved. The ARAMIS optical system was employed to record the displacement and deformations of the joints in experimental testing. In contrast with European and American standards, improved prediction equations of ultimate and serviceability loads were proposed.

There are also some other connecting methods which provide both advantages and disadvantages. Based on Eurocode 3, Tomà et al. (1993) performed research on the mechanical properties of joints with fasteners, welding and adhesive bonding in the cold-formed construction. Predreschi et al. (1997) came up with the press-joining, which is a new technique of cold-formed section joints (see Figure 2-3). This joint was demonstrated by small-scale shear, bending tests as well as full-scale tests of trusses. Correspondingly, calculation method of the strength was presented as Eq. 2-1.

$$\text{Peak load} = (5.63 \times 10^{-3} - 2.65 \times 10^{-5} \cdot \alpha) \cdot (\text{UTS}^{0.98} \times \text{t}^{1.45}) \qquad \text{(Eq. 2-1)}$$

where α is the angle of applied shear, t is the thickness of the steel, and UTS stands for the ultimate tensile strength of the steel.

The behaviour of the press-joins of cold-formed components under pure bending moment was also investigated in detail by Davies et al. (1997). It was found that the peak moment is highly positively related to thicknesses of members and the spacing of the joints. It was also influenced by the angle of shear added to an individual joint. From the comparison between calculated and experimental results, the researchers provided a calculation method used to predict the peak load, stiffness, and plastic limit of the joint more accurately.
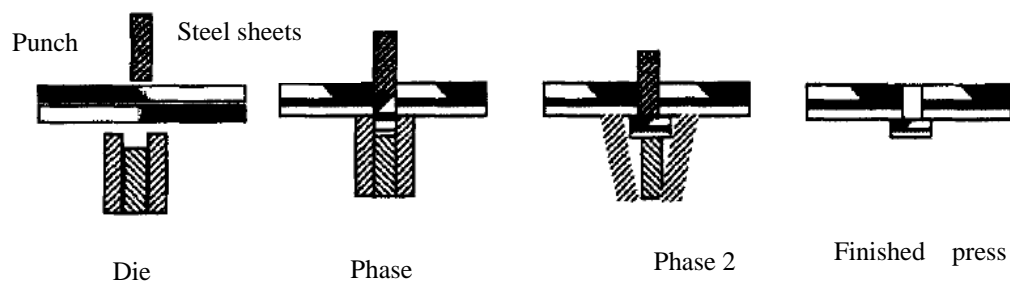
a) Sequence of forming press join
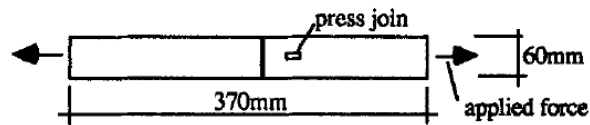
b) Shear test sample of press join

Figure 2-3 Schematic diagram of press join (Pedreschi et al., 1997)

Mäkeläinen and Kesti (1999) studied a new type of joint for thin-walled members, namely Rosette joint (see Figure 2-4), which has several advantages in comparison with traditional joining methods.
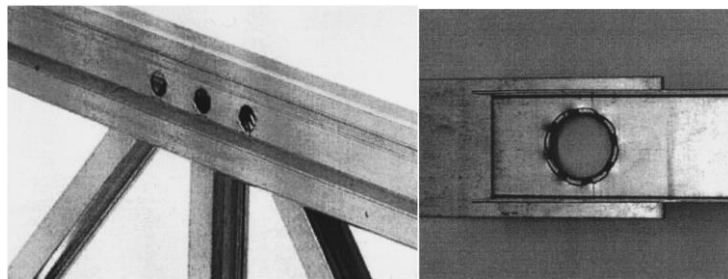
Figure 2-4 Rosette joint (Mäkeläinen and Kesti, 1999)

Rosette joint is made of a part of the components without extra fastenings or heating in the installation process. In the study, the new type of connection was verified by shear, compression and tension tests and was compared with traditional joints. The tests given demonstrated that Rosette-joining has very good capacity of tensile and shearing resistance, which can be applied in roof-truss structure. Laser beam welding (LBW) is widely utilised in auto industry. Landolfo et al. (2009) studied the application of LBW in CFS beam connections. The lap-shear and tension tests were carried out. It was found that the parameters of sheet thickness, gap, loading direction, weld shapes and zinc coating influenced the strength or deformation of the joints in various degrees. Compared with the experiments, for spot welds loaded in shear, the results of Eurocode 3 overvalued the strength of the joint. In contrast, for tensile strength, the code obtained good collaboration with the test results. Mucha and Witkowski (2013) investigated double and single joints in the destruction process by means of uniaxial shearing tests. Fasteners, e.g. clinch rivet, blind rivet, self-piercing rivet (SPR), self-drilling screw, etc., were applied in the tests and diverse actions in failure were detected in details. In the conclusion, clinch rivet joints achieved high efficiency and peak load; for the overlap joints, the alignment order of fasteners is important, but self-drilling screw is less sensitive; the combination of different fasteners leads to considerable change of separation work, particularly for a combination made by blind rivet and self-drilling screw; the SPR joint presented nonlinear characteristic in the test. Researchers (Wahyuni, 2015) also investigated CFS joins with screw, adhesive and combination connection method. The ultimate loads and failure modes were achieved by conducting materials, single lap joint and flexural joint tests. Material properties of epoxy resin and polyester resin were obtained. Screw and combination joints on CFS structures could prevent premature structural collapse and both epoxy resin and polyester resin have good properties to minimize the bearing failure, while increasing structural rigidity of combined connection. However, an anomaly occurred with the screw and a polyester resin adhesive combination joint, since polyester adhesive was not distributed uniformly in the joint area by screw drilling. This caused a dislocation of the adhesive connection, resulting in reduction in the maximum performance of joint strength.

However, the joint may not only be subjected to pure shear or tension, but also to a combination of them, which makes the prediction of the structural behaviour of a joint more complicated. Sønstabø et al. (Sønstabø et al., 2015) reported an investigation on the force-displacement responses and failure behaviour of the aluminium sheet joints using the flow-drill screws (FDS) under tension, shear and the combined tension and shear loading by the experimental study. The experiments included the single connection tests and the connection component tests. A literature review of the SPR joints subjected to the combined loads with various shear/tension was carried out. It was found that the strength of the joints increased while the ductility decreased with the ratio of shear to tension. Deformations and four failure modes of the screw joints were observed in the component tests, i.e., the screw rotation, the screw pull-over, the screw push-out and the screw fracture, which do not occur in the single lap tests. Based on these comparisons, the differences of the structural behaviour between FDS and SPR can be identified under the shear dominated loading condition. Another research investigated the failure mechanisms of the spot weld joint used in vehicle industry subjected to tensile, shear or their combination (Asme, 2003). The strength, the overall deformation and failure process were identified from the cross tension and the lap-shear sample tests. The model for calculating the failure load of a lap-shear sample was proposed. Based on the classical von Mises and Tresca failure criteria as well as the respective stress distribution, the ultimate load of cross tension tests can be predicted by the developed equations. Moreover, as for the combined normal/shear loading, design equations were also proposed in the chapter to examine their resistance. The theoretical analysis has been validated by previous experimental or numerical results. A special testing rig was designed for the connection specimens under the mixed loading conditions (Barkey and Kang, 2010, Lee et al., 1998, Lin et al., 2002).

2.4.1.2 Connections

Except for the performance of the joint and fastener, the well-designed connection configuration can also significantly improve the structural properties of the connection. Researchers (Chung and Lau, 1999) presented system tests on bolted moment connections of

cold-formed components. It was found that at the structure failure, the moment carried by bolted moment connections with four bolts per member ranged from 42% to 84% of the moment carrying capacity of the connected members, which embodied the efficiency and effectiveness of the bolted moment connections. Subsequently, an experimental study (Chung and Lawson, 2000) about the shear resistance of connection using CFS cleats was presented. Four connection configurations (see Figure 2-5) and three failure modes were identified.
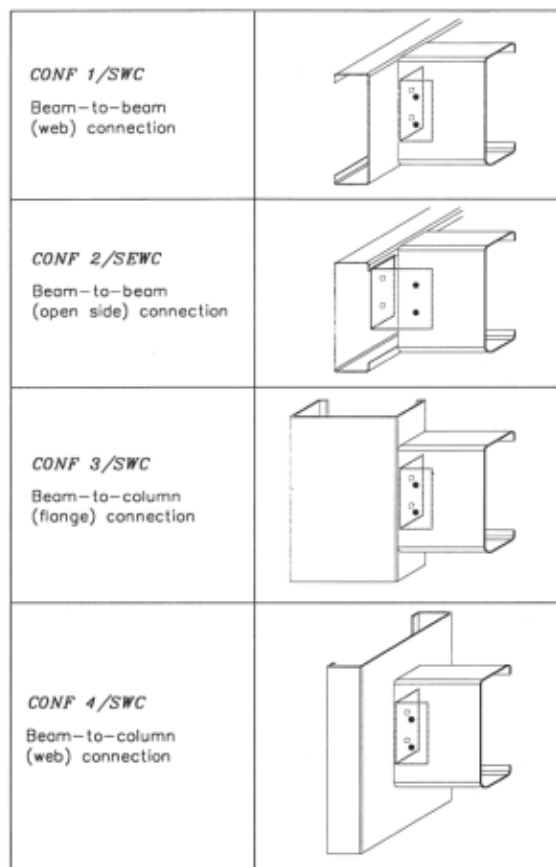
Figure 2-5 Details of connection configurations (Chung and Lawson, 2000)

This joint is made of a part of the components without extra fastenings or heating in the installation process. In their study, the new type of connection was verified by shear, compression and tension tests and was compared with traditional joints. The tests given demonstrated that Rosette-joining has very good capacity of tensile and shearing resistance, which can be applied in roof-truss structure. In a later research (Wong and Chung, 2002), bolted moment connections of CFS structure were studied by means of a series tests of

connections in CFS beam-column and sub-frames. Four typical failure modes were identified namely BFcsw, LTBgp, FFgp and FFcs. In general, the proposed connection configurations could transmit moment effectively. It was demonstrated that, for mode BFcsw, the bearing moment of the connections were below 50% of the moment capacity. For mode LTBgp and FFgp, the proportions were raised up to 60% and 75% respectively. However, for mode FFcs, the connections have the best transmission efficiency with the figure of over 85%. Dundu and Kemp (2006) performed experimental investigation about portal frames comprising cold-formed channels connected back to back at the eaves and apex. The study involved semi-rigid and inelastic joints and the lateral-torsional buckling of the eaves region. It was shown that the back to back bolted connections provided considerable ductility. Further ductility was achieved in mild steel channels than that of high-strength channels. In the comparison of the purlin-rafter connections with two vertical (marked 1-1 in Figure 2-6), two diagonal (marked 1-2 in Figure 2-6), and four bolted (see Figure 2-6) systems under critical elastic lateral buckling load, the two vertical and two diagonal bolts did not reduce the effectiveness of the connection.
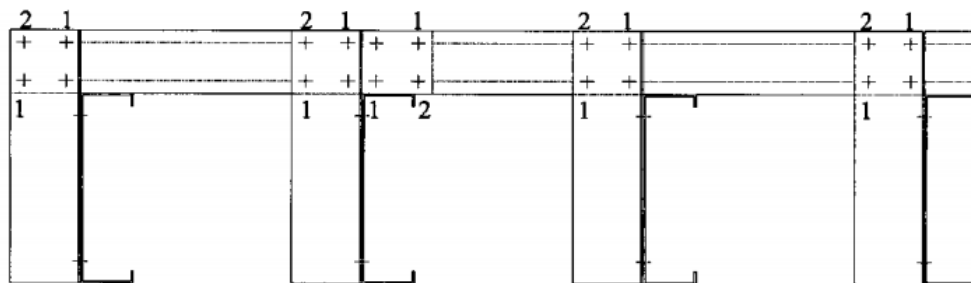
Figure 2-6 Purlin-rafter connections with four bolts (Dundu and Kemp, 2006)

Ho and Chung (2006) presented experimental and theoretical investigation on the CFS Z sections with lapped connections. Comparisons were carried out between connections with different lap lengths and different numbers of bolts configured on the webs and flanges. It was found that the performance of connections with *Config. W2F2* and *W4F2* were close to those with *Config. W4* and *W6* (see Figure 2-7). Furthermore, rational design rules for overlapped multi-span purlin systems were proposed.
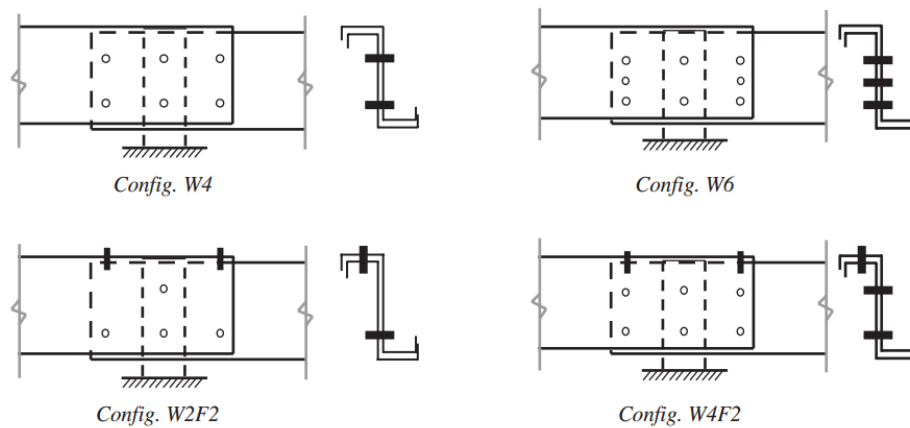
Figure 2-7 Configurations of lapped Z section connection (Ho and Chung, 2006)

Yang and Liu (2012) studied sleeve connections of CFS Σ purlins. In their investigation, response of the sleeve connections was divided into three stages, the friction at the contact interfaces, slips of bolt and the interaction among purlin, sleeve and the bolts. It was also found that, with low level of loading, the slippages of bolts significantly impacted the response of rotation. In contrast, the bearing forces between bolts and the components in sleeve connection presented a limited adverse effect on the moment resistance.

Tensile membrane action tests (TMA) and bending-prying action tests (BPA) were carried out by Bewick et al. (2013). It showed that current codes use large safety factors to design stud-to-track connection and therefore are not economical. Through laboratory experiments considering large deformations and inelastic material response, the results showed that the overall stiffness and strength of steel stud walls can be significantly greater than those calculated using the standards. According to the tests, using single screw connection is insufficient to reach tensile membrane behaviour of the stud wall system. Additional screws enhance the ductility and strength of the connection which help to achieve tensile membrane response. In the load tree tests (LTT), three studs were placed with space 406mm on the centre. The variables of the analysis included the screw size, the stud and track geometry and the type of sheathing. It was found that sheathing effectively resist rotation caused by the eccentricity to the shear centre of the applied load. In terms of the unsheathed load tree specimens, the magnitude of the strength increase was less than that of the TMA series. It was

because that a pure tension load acted on the connection in the TMA series, whereas the screws in unsheathed load tree specimens were subjected to bending and prying, torque and tension loads.

2.4.2   Numerical studies

The accuracy of finite element software and computer computing power are greatly improved in the past decades. Based on the technology development, numerical method has become a powerful tool for studying complex subjects and being a supplement to the limited experimental data. Bursi and Jaspart (1997) used three-dimensional FEM to study tee stub bolted steel connections by means of LAGAMINE program. This model simulated the large deformation and the natural strain-true stress curves and reproduced the property of displacement field. The comparison between numerical and test results verified the effectiveness and the accuracy of the suggested model. The LAGAMINE finite element program was also used to study lap screw joints to predict the ultimate resistance, the deformation, screw rotation behaviour and the stress distribution of the joints between thin steel sheets and the results corresponded well to the test results. The precise finite element model presented provided a good demonstration for the further research (Fan et al., 1997a, Fan et al., 1997b). For CFS strips with high strength but low ductility, current expressions may not be applicable. Chung and Ip (2000) established a three dimensional solid nonlinear finite element modelling to study the performance of the bolt joints between high strength CFS strips and hot rolled steel plates under the action of shear force. In order to accurately predict the load-extension curves and the bearing resistance of the strips, a stress-strain curve was suggested and also validated by experimental results. It should be noticed that around 20% of the load bearing capacity of the bolted connection is contributed by frictional resistance between element interfaces. Ju et al. (2004) simulated the crack behaviour of the steel bolt joints under shear loads by using three-dimensional plastoelastic FEM. In the modelling, bolt clearance, bolt head, washer, deformable bolt, friction, plate distortion and bolt bending were included which made the simulation closer to the actual and obtained good agreement with the AISC specification. It was suggested that the linear elastic fracture mechanics is

applicable in most cases. At nonlinear stage, the bolt nominal capacities are nearly linearly proportional to the number of the bolts. Kim et al. (2007) introduced four FE solid bolt models, coupled bolt model, spider bolt model and no-bolt model and compared the FEM results with the tests. It was found that the solid bolt model predicted the physical characteristics of the structure most accurately. Gutierrez et al. (2011) investigated slotted Z profile sleeve connections on the performances of strength and rotational stiffness by means of experimental and numerical methods. An adequately accurate FEM model with semi-rigid connection in multi-span model was proposed. Researchers (Bewick and Williamson, 2014) developed a model to predict the ultimate load and deformation of steel stud wall systems. In details, the screws were simulated using nonlinear discrete beam element and a piecewise linear plasticity constitutive relationship for the CFS according to LS-DYNA, which were capable of capturing the essential failure modes (local buckling and lateral-torsional response), peak strength and peak displacement. It was suggested that additional screws in stud-to-track connections can improve the carry capacity; a 76.2mm track is recommended to allow for extra screws and satisfying the specification of AISI (2007) and a fixed-track wall presents better structural behaviour than the slip track wall. Screwed joint featuring with easy installation and the economic efficiency is extensively employed in thin-walled steel constructions nowadays. Bondok et al. (2015) studied the effects of utility holes and sheathing in stud-to-track wall systems with screw joint was conducted. In the study, full-scaled tests and modified finite element model acted quasi-static loading were conducted. Three phases were presented in the resistance-to-deflection curve, elastic flexure range, yielded beam with plastic hinge and softening and plastic tension range. In general, the stud was conservatively supposed to fail when more than 8% of the stud length deforms plastically, which may lead to a local buckling or a lateral torsional buckling. It was also noted that failure of the track-to-floor connection commonly started with the middle bolt pulled over. In contrast, a stud-to-track connection failed where screw tilting and bearing failure mixed. In general, oriented strand board (OSB) sheathing made positive contribution to the stud behaviour in either the softening zone or the ultimate load, however, for the specimens with utility holes, the effects

turned to be negative. In the numerical modelling, the screws joining the stud and the lateral wood bracing were simulated by Multi-Point Constraint (MPC) connectors as a rigid connection. Since the bolted floor-to-track connection was not the research objectives, it was simplified as pinned joint. In the stud-to-track connection, beam connector elements were employed to model the screw behaviour. To simulate screw tilting and bearing capacity, an additional defined spring element with linear stiffness k were adopted. The numerical modelling presented good agreement with test results.

2.4.3   Theoretical studies

In the global analysis of a structure, the connections can be assumed not to transmit bending moments and hence are simple connections. If a connection is strong enough and does not influence the force transmission of the model, it is considered as continuous connection. Otherwise, the behaviour of the semi-continuous connection should be considered in the analysis model. The characteristics of connection affect the load distribution and the structural behaviour. The classification system is generally based on the stiffness or strength of the connection. In EC3 (Eurocode, 2005), if the connections are classified by stiffness, connection categories include nominally pinned connections, rigid connections and semi-rigid connections (see Figure 2-8).
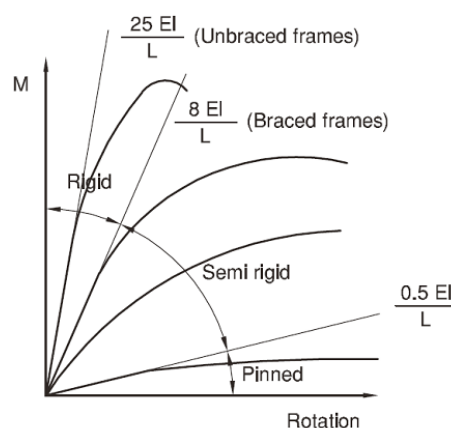
Figure 2-8 Connection classification (From *SteelConstruction.info*[1])

---

[1] http://www.steelconstruction.info/Modelling_and_analysis

Pinned connections are capable of transmitting the internal forces and the allowable rotations but developing insignificant moments in the structure. Rigid connections are supposed to have amply rotational stiffness to obtain full continuity of connected components. The stiffness of semi-rigid connections is between pinned and rigid connections. The classification boundaries are shown in Figure 2-8. This classification is commonly used in elastic analysis.

In terms of strength classification criterion, connections can be divided into nominally pinned connections, full-strength connections and partial-strength connections which can be applied in plastic analysis. The design resistance of full-strength connections is not less than that of the connected components. The pinned connections can resist the internal forces, but the design ultimate moment needs not be larger than 25% of the requirement for full-strength connections. Connections with structural properties between the upper boundary of nominal pinned connections and lower boundary of full-strength connections are defined as partial-strength connections. Stiffness and strength of the connection changes in the entire process of the connection response and the connection with high moment resistance but low stiffness may be not capable of a full-strength connection. However, the aforementioned classifications concerned stiffness and strength criteria separately. While Nethercot et al. (Nethercot et al., 1998) proposed a classification method in which both of the stiffness and strength were involved simultaneously by the developed expressions and the ultimate limit state and serviceability limit state were taken into account:

$$M_j = \frac{qL^2}{12} \left[\frac{\alpha}{2 + \alpha + 2\alpha \frac{EI}{KL}} \right] \qquad \text{(Eq. 2-2)}$$

$$\alpha = \frac{K_c}{EI/L} \qquad \text{(Eq. 2-3)}$$

where M_j is the connection moment; q is the uniformly distributed load; L is beam span length; EI is beam section rigidity; K is connection stiffness; α is column-to-beam rotational stiffness ratio; K_c is the sum of the rotational stiffness of the connected member except the beam considered. EI_c is column section rigidity; L_c is column height; if the connection moment capacity is over 95% of that of the beam, it can be considered as a fully-connected connection. If the connection moment capacity is smaller than 25% of that of the beam, the connection is

classified to pin-connected connection. The partially-connected connection is between these two categories. If the connection cannot deliver the required rotation capacity, this connection is categorized as non-structural connection.

The design of structure includes deflection and carrying capacity at serviceability and ultimate states. The deflection consists of end slip of connections and beam deflection involving bending and shearing deflection. In the light of the serviceable limitation, the deflection criteria (see Table 2-1) of joists under working condition are proposed below, including static deflection criteria (a and b) and vibration sensitivity criteria (c and d) (Gorgolewski et al., 2001a, Kraus, 1997, Lawson et al., 2008).

Table 2-1 Deflection criteria (Kraus, 1997)

Serial number	Scope of application	Criteria
a	static	The maximum deflection under dead and imposed loads is limited to span/350, or a maximum of 12 mm, including the effect of composite actions – this generally ensures that the minimum natural frequency is satisfied (see criterion c).
b		The maximum deflection under imposed loads is limited to span/450 - this only applies to floor areas under higher imposed loads, such as corridors and public areas, as in general, criterion a) will control.
c	vibration	The natural frequency of lightweight floors should exceed 8 Hz for the loading case of self-weight plus 0.3 kN/m^2, which represents the permanent loading considered in domestic buildings. This criterion is satisfied by limiting the maximum deflection of the floor to 5 mm for this loading condition. The natural frequency limit should be increased to 10 Hz for corridors and public areas, where impulsive actions may increase.
d		The local deflection of the floor, using the relevant value of Neff under a nominal 1kN point load, is limited to a maximum of 1.5 mm or (3/span^2) for spans (in m) exceeding 4m, based on the criteria suggested by Kraus and Murray (Kraus, 1997) This reduction in deflection limit with span reflects the need for higher stiffness to counteract the increase in the possibility of impulsive actions that may occur in longer spans. The structural response is different at the serviceability and ultimate limit states. And the failure modes should be detected.

This reduction in deflection limit with span reflects the need for higher stiffness to counteract the increase in the possibility of impulsive actions that may occur in longer spans. The structural response is different at the serviceability and ultimate limit states and the failure modes can be detected.

The research development of CFS bolt joints and the comparison of current design rules was presented by Chung and Ip (2001). However, these design rules are not competent to CFS

strip with high strength low ductility. Based on parametric study by using FEM model, calibrated semi-empirical design rules were proposed (see Appendix I). It is shown that this calculation method can be utilised to predict bearing resistances of the bolt joints of low or high strength steels with variable ductility.

New CFS connecting systems were developed by Di Lorenzo and Landolfo (2004). Shear experimental investigation was carried out in order to evaluate the shear strength and ductility of them which made contribution to the choice of mechanical fasteners. The comparative study included mono-component blind rivets, bi-component blind rivets, circular press-joints and self-piercing rivets. Based on the results in the tests, the bi-component blind rivets achieved better strength and ductility. In contrast, there was no significant difference in strength and ductility between bi-component blind rivets and mono-component blind rivets. According to test results, ductility is the mostly negative factor for carrying capacity of the joints. Particularly, for mono-component blind rivets, the strength reduced by around 50%. It is also concluded that bi-component blind rivets fully fit for ductility-restoring joints. The circular press-joints can be used for the connection with shear strength no more than 3kN. Furthermore, the shear resistance of the symmetrical joints is underestimated in previous regulation due to the wrong bearing coefficient for circular press-joints, which was revised by the author (see Appendix II).

As the eaves and apex connections are not rigid in practice, Lim and Nethercot (2004) developed a process (see Appendix III) to predict the stiffness of bolted moment connections between CFS components of portal frames using nonlinear spring FEM modelling. Full-scale tests were also carried out, which verified the results of the numerical simulation.

Yu et al. (2005) investigated bolted moment connections of CFS beam-column sub-frames under lateral loads. With larger bolt pitches and thick gusset plates in the connections, flexural failure of the connected sections was always the governing factor. Taking into account the combined action of bending and shear force, design rules for the bearing resistance of the connection were proposed. A nonlinear finite element model of the beam-column sub-frames

was shown and semi-rigid connections were presented in the FEM modelling. The results of the modelling followed closely to the experimental investigation. Based on the test results, a modified semi-empirical formula for calculating the flexibility of the bolted moment connections was proposed (see Appendix IV).

As the AISI CFS Truss Design Standard do not provide predictions for the connection stiffness, Zaharia and Dubina (2006) studied the stiffness of the bolted connections in CFS trusses. Tests were carried out on single lap joints, typical truss connections and a full-scale truss. It was demonstrated that rotational stiffness and axial stiffness of the connections mutual affect the response of the truss structure. It was also found that the initial rotational slippages did not notably influence the initial rotational stiffness of the truss connection. The formulas for predicting the rotational stiffness and axial stiffness of the bolted connection were developed. Moreover, considering the rotational stiffness of the connections, equations for calculating buckling length of truss web members were presented (see Appendix V).

Dubina (2008) investigated the stiffness and strength of the bolted connections in cold-formed truss structure by experimental and numerical methods. Three factors affecting the stiffness of the given connection bolts in shear, bolts in bearing on cold-formed member and bolts in bearing on the bracket were taken into consideration and a set of formulas for connection stiffness and moment resistance were presented (see Appendix VI). Furthermore, it was found that the connection model with combined initial rigid and semi-rigid response was more close to the experimental results.

Kwon et al. (2008) investigated the stiffness and strength of PRY sections applied in CFS portal frames. Tests on the connections were carried out with variation of plate thicknesses and connection types. According to the results of numerical analysis and full scale tests, semi-rigid concept and secant stiffness of the connections are applicable in the portal frames. Moreover, simple expressions for calculating the shear resistances of the screwed connections were proposed (see Appendix VII).

Yu and Panyanouvong (2013) considered the effect of gaps in CFS bolted connections, e.g. connections in truss structure. It was concluded that the current norm (AISI S100 2007) works for the truss connections with thick plates. However, for thin materials, AISI prediction overestimated the test results. Therefore, according to the tests, calibration factors (see Appendix VIII) for design of the truss connection with gaps were proposed.

Ye et al. (2013) presented an investigation of sleeved connection on the load-deflection behaviour. A modified Z purlin section (see Figure 2-9) was presented in the tests. It was found that the interlocking and friction made greater contributions to the rotational stiffness of the connections than the bolts. For the flexural stiffness of the sleeved modified Z connections, the length of sleeve and the bending moment of the connections played critical roles. Furthermore, the expression for predicting the flexural stiffness of the connections was proposed (see Appendix IX).
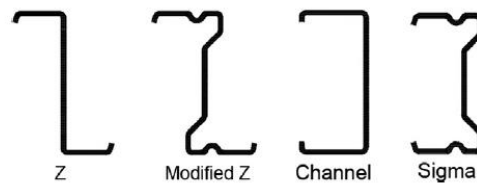
Figure 2-9 Common purlin sections (Ye et al., 2013)

2.5 Construction robustness

2.5.1 Research status

Apart from the traditional design scenario considering the failure of the floors above the removed column with regard to kinetic energy transmission, a progressive collapse assessment of multi-story buildings impacted from above failed floor was investigated. Researchers (Vlassis et al., 2009) have proposed a theoretical method to calculate the energy transfer with regard to the fully plastic and the fully rigid impact scenarios. The crucial parameters, such as energy absorption capacity, strength and ductility of the floor as well as the shear capacity of typical steel bolted connection were taken into account. It was shown that the latter scenario presents greater energy transfer ratio (close to 100%) from the

impacting floor to the impacted floor (around 40%). Numerical study was also carried out using ADAPTIC and shows good agreement with the theoretical method. Gerasimidis and Baniotopoulos (2015) investigated progressive collapse of strengthened moment-resisting steel frames, considering suddenly missing single column in the ground floor. Finite element software ABAQUS was employed to simulate the 2D steel frames selected in the analysis, ranging from 6 floors to 15 floors. Six schemes of strengthening were proposed involving beam and column reinforcement. The results illustrated that the removal of column negatively influences the stability and carrying capacity of the frames. However, the mitigation of the affect due to strengthening varied in different scenarios. There is no general method that is applicable for all collapse mechanisms. A research (Foley et al., 2007) intended to quantify the level of inherent robustness. The 3D numerical analysis of progressive collapse of moment-resisting steel frames from 3 to 20 storeys was conducted. With the successive removal of the structural element, two-way membrane and catenary action likely affect the load transfer mechanisms in the rest system. DoD guidelines (DoD., 2009) provide the requirement of tie force as follows.

If it was an interior tie element, the calculation of the required tie force is

$$F_t = 0.5 \cdot [GRAV] \cdot s_t \cdot L_t \qquad \text{(Eq. 2-4)}$$

If it was an exterior tie element, the calculation of the required tie force is

$$F_t = 0.25 \cdot [GRAV] \cdot s_t \cdot L_t \qquad \text{(Eq. 2-5)}$$

where $GRAV$ (psf) is the gravity loading taken as 1.2D+1.6L; s_t is the spacing between ties; L_t is the beam or girder span. The minimum interior tie force is 16.9 kips, and the minimum exterior tie force is 8.4 kips.

However, based on the inelastic analysis of the 3-storey frame, it was found that the axial force demands in the beam-to-column connections were less than 5% of the carrying capacity.

Based on the design specifications GSA guidelines and DoD guidelines, the possibility of progressive collapse of the CFS frame structure due to the damage of a part of the exterior wall stud column was evaluated by Bae et al. (2008). It was point out that improving the

column compression capacity and the horizontal connection capacity which is directly associated with the removed stud column is the efficient measure to stop the collapse. In 2013, Mohamed et al. (2013) investigated the framing components of CFS stud bearing wall system according to the nonlinear static analysis by Applied Element Method (AEM). It was proved that enhance the lateral bracing and use double studs beside the removed wall panel can improve the system performance of progressive collapse resistance. One element loss in a structure possibly affects not only one adjacent structural element. A research (Gerasimidis et al., 2014) demonstrated the partial damage of structural elements through the alternate load path method. Finite element method was employed in analysis of damaged steel frame. Based on the result of numerical simulation of disproportionate collapse, robustness measures were presented involving single and multiple column damage. A sudden loss of one or more structural members may lead to a catenary action in progressive collapse, which can be assessed by the tensile tie force method. However, in some certain circumstance, TF method seems to be unsafe. Therefore, a study (Tohidi et al., 2014b) has identified the alternative load path in catenary effect (see Figure 2-10) and the corresponding calculation method. Moreover, the 3D nonlinear numerical studies of steel strand and floor-to-floor joint system were carried out by using ABAQUS and verified by full scale tests. The parametric analysis illustrated that the bond behaviour of ties determines the joint reaction in developing the catenary action. In the analytical analysis, the catenary action was taken into account. The connection is assumed to provide ample ductility. The study neglected the local damage in the progressive collapse process. The alternative force transfer path is derived (see Eq. 2-6 to 2-8).
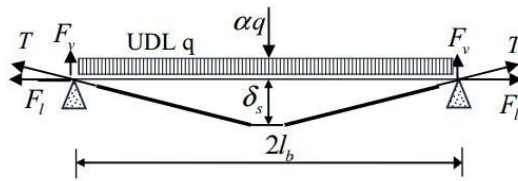
Figure 2-10 Catenary action sketch (Tohidi et al., 2014b)

$$F_l = \frac{(wl_b + \alpha q)b_p l_b}{2\delta_s}$$

(Eq. 2-6)

Let,

$$q = wl_b \tag{Eq. 2-7}$$

$$F_l = (1 + \alpha)\frac{wb_p l_b^2}{2\delta_s} \tag{Eq. 2-8}$$

where w is the uniformly distributed load (including permanent and variable loads); b_p is the spacing of ties; l_b is the floor span length; F_l is the force in the longitudinal tie joining adjacent slabs; δ_s is the vertical displacement at the middle wall support; q is the line load exerted by the upper wall and α is the percentage increase of the line load considering the number of storeys.

In the view of the steel frame with abrupt removal of a column, researchers (Chen et al., 2016) established a simplified beam model and developed the progressive collapse assessment method with regard to structure energy absorption and catenary action at large deflections. This method presents a good agreement with the experimental results.

2.5.2 Load redistribution mechanism

The disabled member caused by abnormal loading actually changes the force transferring path in the structure. In the frame structure, if the internal load carrying column failed, structure general response can be divided into three stages i.e. beam action stage, transition phase stage and catenary action stage. Besides the main frame, accessories, such as slab floor and in-filled walls of the construction, can also influence the structural behaviour due to abnormal loading. Therefore, membrane action needs to be taken account in progressive collapse analysis.

2.5.2.1 Beam action

The connections provide moment resistance to carry the upper loads (see Figure 2-11). The removed column possibly leads to the local damage of the joint. Plastic hinge is firstly formed in the middle connection and then it occurs in the end connections. Thus, the beam action may be transferred to catenary action and the force transfer path will change. Based on analysis of

reinforced concrete frame structure, Yi et al. (Li et al., 2011) suggested the ultimate deformation for beam action as 0.06L.
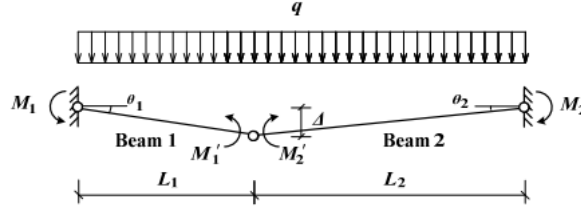
Figure 2-11 Beam action (Li et al., 2011)

$$M_1 + M_1' = \frac{qL_1^2}{2} \qquad \text{(Eq. 2-9)}$$

$$M_2 + M_2' = \frac{qL_2^2}{2} \qquad \text{(Eq. 2-10)}$$

Due to the plastic hinge, the moment resistance of the middle connection is conservatively neglected,

$$M_1 = \frac{qL_1^2}{2} \qquad \text{(Eq. 2-11)}$$

$$M_2 = \frac{qL_2^2}{2} \qquad \text{(Eq. 2-12)}$$

It is similar in the perpendicular direction.

2.5.2.2 Compressive arching action

This action is formed in the transition phase between beam action and catenary action. Cracks occur at top beam end section and bottom middle span section. As a result, the neutral axis of cross section shifts down at the ends and shifts up at the middle span. The force transferring route forms an arc shape.

2.5.2.3 Catenary action

The horizontal forces are needed to be taken into account for the robustness of accident action. The code (BS., 1997) requires the horizontal resistance of each floor should more than 15% of the dead load. If the horizontal restraint of the connections is sufficient, catenary action can occur during column loss and the beams are supposed to be in tension (see Figure 2-12).
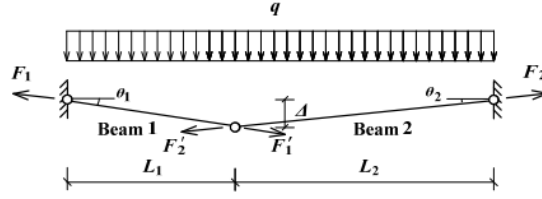
Figure 2-12 Catenary action (Li et al., 2011)

$$\frac{L_1}{\sqrt{L_1^2 + \Delta^2}} \times F_1 = \frac{L_2}{\sqrt{L_2^2 + \Delta^2}} \times F_2 \qquad \text{(Eq. 2-13)}$$

Considering $\Delta = L_1/5$ and $L_1 < L_2$. (Eq. 2-13) can be simplified as

$$F_1 \approx F_2 \qquad \text{(Eq. 2-14)}$$

$$q(L_1 + L_2) = \frac{\Delta}{\sqrt{L_1^2 + \Delta^2}} \times F_1 + \frac{\Delta}{\sqrt{L_2^2 + \Delta^2}} \times F_2 \approx \Delta \times (\frac{1}{L_1} + \frac{1}{L_2}) \times F_1 \quad \text{(Eq. 2-15)}$$

$$F_1 = F_2 = qL_1L_2/\Delta \qquad \text{(Eq. 2-16)}$$

It is similar in the perpendicular direction.

The beams appear like a bridge arch, hanging the upper weight, supported only by the ends. There are two shapes of the arches (Lu et al., 2011). One is the curve (see Figure 2-13), with the axial pull force $T_1 = w_0(L_1 + L_2)^2/8h$.
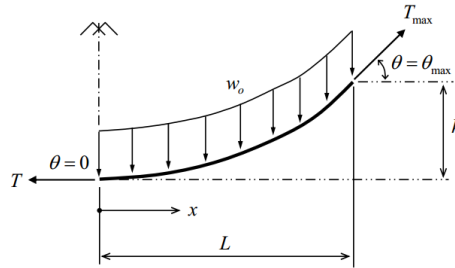
Figure 2-13 Catenary action with curve arch

If it is straight line arch, with reference to Figure 2-12, the axial pull force is $T_2 = L_1 L_2 w_0/h$ (where L_1 and L_2 are the span of each beam. w_0 is the uniformly distributed load (UDL). h is the allowable deflection of the beam). When the span lengths are equal ($L_1 = L_2 = L$), the axial pull force is given by: $T_1 = T_2/2$. The shape of the curve depends on the horizontal restraint which can be assumed as a spring. PCA (1979) performed full scale floor-to-floor tests to

evaluate the longitudinal ties. Based on the results, the catenary action can be achieved in the range of 0.05L to 0.15*L*. For beams with a span-to-depth ratio greater than 5, the maximum deformation due to catenary action is suggested as 0.2L ($\theta = 12°$) in specifications (DoD., 2013).

2.5.2.4 Membrane action

The floor panel in construction is composited with concrete slab floor above the CFS joists. As is shown in Figure 2-14, the joists are forced to deform with slab floor in a compatible fashion of both directions. The interaction between joists and slab can lead to restrain on the deflection caused by the ineffective interior column or panel. In fact, the membrane action also affects the joists under normal working condition.
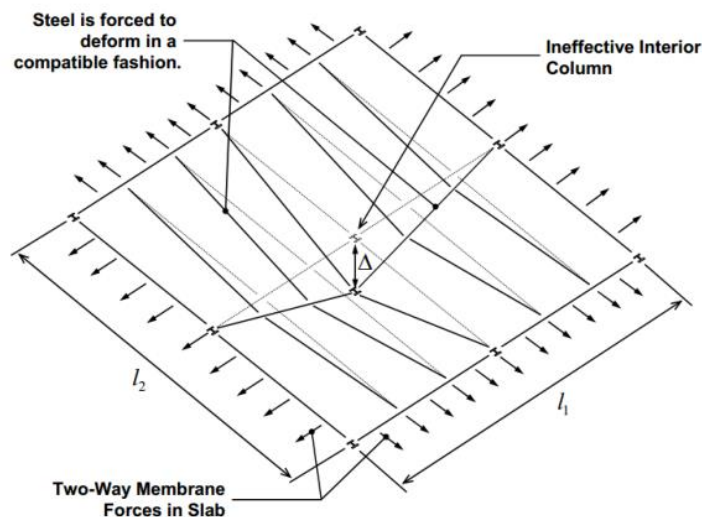
Figure 2-14 Membrane action

Due to the abnormal loads, load path is changed in the connection and structural members. The potential failures of the structure are listed Shear rupture of the screw; Pull-over failure or pull-out failure of screw; bearing tear-out failure in the connected sections; bearing tear-out failure in the cleats; block shear rupture in the connected sections; block shear rupture in the cleats; tension rupture in the cleats; beam failure and column failure.

2.5.2.5 Cantilever action

The removal of the external primary column or wall may result in cantilever action of the adjacent beam or the floor in the structure. The cantilever element is anchored at one end to the support which is forced against by moment, shear or tensile stress.

2.5.3 Design method

2.5.3.1 Tie force (TF) method

The Tie Force (TF) method is an indirect design approach for progressive collapse e.g. ties to columns and walls and vertical ties, in which the horizontal and vertical tie force capacity must be satisfied. In 1968, the British Standards (BS., 1997) firstly started to incorporate provisions to deal with the problem of progressive collapse of concrete structure. The design of internal ties at each floor and roof panel in each direction requires ties to carry tensile force F_l in each direction, which is determined from the greater of

$$\frac{(g_k + q_k)}{7.5}\frac{L}{5}F_t \qquad \text{(Eq. 2-17)}$$

and

$$1.0F_t \qquad \text{(Eq. 2-18)}$$

In the expressions, g_k is the characteristic dead load and q_k is the imposed floor loads (in kN/m^2). L is the length of the floor span. The basic tie strength F_t is obtained from the minor value of $4n_0+20$kN/m, where n_0 is the number of stories and 60kN/m. The former is an empirical formula, which emphasized the floor influence of basic tie strength. The latter is obtained according to Figure 2-15.
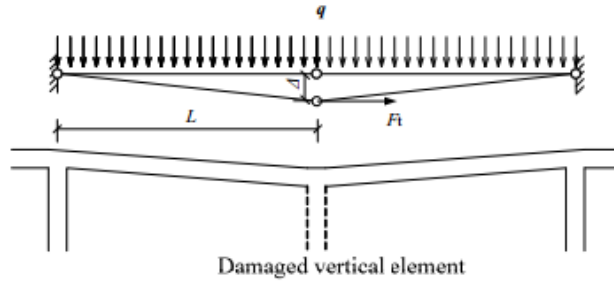
Figure 2-15 Basic tie strength calculation in the British code (BS., 1997)

It is assumed that the horizontal members effectively provide ample tie strength resulting in a catenary behaviour. The tie force $F_l = qL^2/(2\Delta) = 60$kN/m ($\Delta$ is the middle deflection which is adopted as $L/5$. The typical values were supposed in the expression $L=5$m, $q=5$kN/m^2).

The prescriptive tie requirements were adopted in engineering practice and employed in DoD (DoD., 2005). Base on British standard (BS., 1997), researchers (Li et al., 2011, Tohidi et al., 2014a) developed an improved TF method for progressive collapse resistance. Numerical and experimental studies of reinforced concrete (RC) frame structures were also presented by Li et al. (Li et al., 2011) to reveal that the current TF method cannot make assurance to prevent progressive collapse of all the RC structure and may lead to underestimation of the design demand for low-rise frames by using fibre beam element model THUFIBER. The resistance of progressive collapse can be improved in proportion to the number of frame stories. A typical moment-to-curvature relationship of the plastic hinge was found out through the test, presenting the reduction of the connection maximum moment due to the rotation. It was suggested that the tie force F_i and F_j for beams i and j and the beam-end moment capacity M_i in each direction should satisfy the following expressions:

$$F_i = F_j > \beta q L_i L_j / \Delta \qquad \text{(Eq. 2-19)}$$
$$M_i > \beta q L_i{}^2 / 2 \qquad \text{(Eq. 2-20)}$$

where $\beta=0.67$ is the internal force correction factor; q is the imposed loading; L_i, L_j are the span lengths of beams i and j in specific directions respectively; Δ is the allowable limit of the middle joint deflection (1/5 of the shortest span length).

Tohidi (Tohidi et al., 2014a) proposed a calculation of pull-out slip of longitudinal ties in floor-to-floor system (see Figure 2-16) of precast concrete cross wall structures. The equilibrium equation of the catenary system can be derived.

Based on the compatibility condition of deformation,

$$\delta_l = \sqrt{l_b^2 + \delta_s^2} - l_b \qquad \text{(Eq. 2-21)}$$
$$\delta_l = \delta_{ls} + \delta_{lm} \qquad \text{(Eq. 2-22)}$$
$$F_v = \frac{(q \cdot 2l_b + \alpha q)b_p}{2} \qquad \text{(Eq. 2-23)}$$

$$F_l = \frac{(q \cdot 2l_b + \alpha q)b_p l_b}{2\delta_s} \qquad \text{(Eq. 2-24)}$$

$$T = \sqrt{F_v^2 + F_l^2} \qquad \text{(Eq. 2-25)}$$

where δ_l is the increase in the length of each floor slab; δ_{ls} and δ_{lm} represent the extension experienced at the side and middle supports respectively; b_p is the spacing of ties.
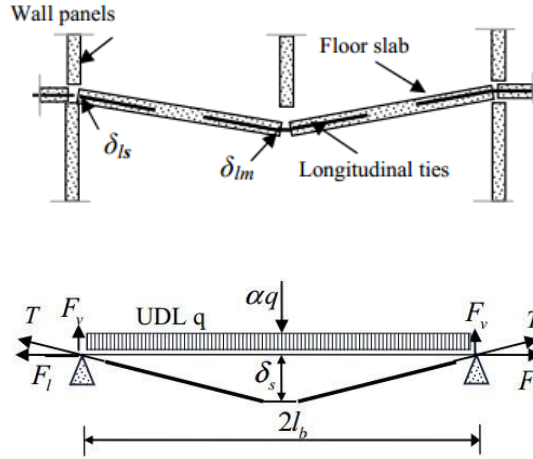
Figure 2-16 Catenary action sketch (Tohidi et al., 2014a)

Nair (2004) conducted a case study based on five current codes and standards, which was considered would not provide assurance against the progressive collapse. The inadequacy of the TF method was also revealed in (Abruzzo et al., 2006). To achieve the efficiency of TF method, DoD (2013) developed an improved TF method in which the required tie strength F_l (lb/ft or kN/m) in the longitudinal or transverse direction is

$$F_l = 3w_F L_1 \qquad \text{(Eq. 2-26)}$$

where floor load w_F=1.2DL+0.5LL (DL=dead load, LL=live load). L_1=either the greater of the distances between the centres of the walls supporting any two adjacent floor spaces in the longitudinal direction or the lesser between $5h_w$ and the building width in the transverse direction (ft or m). h_w = clear story height (ft or m).

2.5.3.2 Alternative path (AP) method

The Alternative Path (AP) method requires the designer to seek an alternate load path for the event of losing a member. The compromised member may be located at internal or peripheral area where the surrounding components may mechanically tie together to provide the

alternative load path, carrying the dead and imposed loads (BS., 1997). According to the position of the ineffectiveness occurred, the alternative load resistance mechanism can be classified into seven types catenary action of beams or floors panels in one or two direction: cantilever action of beam or panels; vertical tie action of wall panels; membrane action of floor panels; partition wall action; vierendeel action; compressive arching action.

The current TF method is a static design method which is an idealized assumption. In order to simulate the dynamic effect acting on the structure because of the sudden compromised column, in accordance with the GSA guidelines (GSA., 2000), an amplified factor 2 for the typical structural configuration or 1.5 for the atypical structural configuration is applied to the evaluation, and the vertical static load is presented.

$$Load=2 \text{ or } 1.5 \ (DL+0.25LL) \tag{Eq. 2-27}$$

For linear and nonlinear static analyses of all construction types, DoD guidelines (DoD., 2005) requires the amplified factored load combination as follow.

$$Load=2[(0.9 \text{ or } 1.2) \ DL+ (0.5LL \text{ or } 0.2SL)] +0.2WL \tag{Eq. 2-28}$$

where SL=snow load, WL=wind load.

It was also specified that the collapse area of the floor directly above the removed element must be less than the smaller of $70m^2$ or 15% of the total area. In addition, for the structures with low level of protection (LLOP), AP method is not mandatory. Base on DoD and GSA guidelines, (Bae et al., 2008) conducted a case study of the CFS framed structures (the army barracks) under abnormal loading conditions using SAP2000. In each scenario, the vulnerable part of the structure was detected. According to 2D and 3D numerical analysis carried out by Ruth et al. (Ruth et al., 2015) the dynamic amplified factor of 2.0 suggested by both GSA guidelines and DoD guidelines for static-nonlinear design is conservative relative to dynamic-nonlinear analysis and the equivalent dynamic factors obtained in 3D models were higher than that of 2D models but slightly lower than 1.50.

2.5.3.3 DoD and GSA guidelines

DoD and GSA guidelines provide the design methods of buildings, involving reinforced concrete, structural steel, masonry, wood and CFS constructions, to resist progressive collapse. The purpose of these guidelines is to reduce the progressive collapse risk in new and renovated buildings when the primary element failed. In the new version (DoD., 2016, GSA., 2016), the incongruities between DoD and GSA guidelines have been reduced in order to bring uniform standard. These guidelines apply to constructions with three or more stories.

The design approaches include direct and indirect design approaches. The former includes Alternate Path (AP) method which requires the structural can bridge over the missing structural element, Enhanced Local Resistance (ELR) method which requires sufficient strength of the building or parts to resist the specific load and Tie Force (TF) method is used to enhance continuity, ductility and structural redundancy to resist abnormal load. The design approach selection depends on the risk category (see Table 2-2) of the structure.

Table 2-2 Risk categories and design requirements

Risk Category	Nature of Occupancy[a]	Design requirement
I	Low occupancy buildings that represent a low hazard to human life in the event of failure	No specific requirements
II	Inhabited buildings with less than 50 personal, primary gathering buildings, billeting, and high occupancy family housing	Option 1: TF for the entire structure and ELR for the corner and penultimate columns or walls at the first story. Option 2: AP for specified column and wall removal locations.
III	Buildings and other structures that represent a substantial hazard to human life in the event of failure, for example, the primary occupancy is public assembly with an occupant load greater than 300.	AP for specified column and wall removal locations and ELR for all perimeter first story columns or walls.
IV	Buildings and other structures designed as essential facilities, for example, fire, rescue, ambulance and police stations and emergency vehicle garages.	TF and AP for specified column and wall removal locations and ELR for all perimeter first story columns or walls.

[a] Section 1604.5.1 Multiple occupancies of the International Building Code (IBC).

The frame columns and load-bearing walls are used to carry the required vertical tie strength. The connections and the structural elements should be capable of carrying the tie forces and meet the continuity requirement (see Figure 2-17).

$$\phi R_n \geq R_u \qquad \text{(Eq. 2-29)}$$

where

ϕR_n = Design strength

ϕ = Strength reduction factor in LRFD approach

R_n = Nominal strength

R_u = Required strength $\sum \gamma_i Q_i$

γ_i = Load factor

Q_i = Load effect
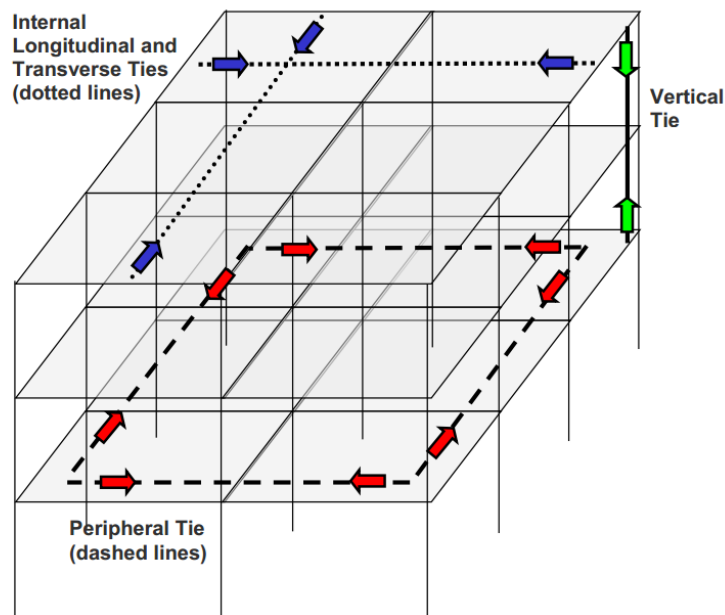
Figure 2-17 Tie forces in the structure

The guidelines suggest the floor load to determine the required tie strengths:

$$W_F = 1.2D + 0.5L \qquad \text{(Eq. 2-30)}$$

where

W_F = Floor Load (lb/ft^2 or kN/m^2)

D = Dead Load (lb/ft^2 or kN/m^2)

L = Live Load (lb/ft^2 or kN/m^2)

The required longitudinal tie force F_i (lb/ft^2 or kN/m^2) is

$$F_i = 3W_F L_1 \qquad \text{(Eq. 2-31)}$$

where

W_F = Floor load (lb/ft^2 or kN/m^2)

L_1 = Greater of the distances between the centres of the columns, frames, or walls supporting any two adjacent floor spaces in the direction under consideration (ft or m)

The required peripheral tie strength in framed and two-way load-bearing wall buildings is

$$F_P = 6W_F L_1 L_P + 3W_C \qquad \text{(Eq. 2-32)}$$

In terms of one-way load-bearing wall buildings,

$$F_P = 6W_F L_1 L_P + 3W_C + 3W_W \qquad \text{(Eq. 2-33)}$$

where

L_P = 3.3 ft or 1.0 m

W_C = 1.2×Dead load of cladding over the length of L_1

W_W = 1.2 ×Dead load of cladding over the length of h_W

h_W = Clear story height (ft or m)

In AP analysis procedure, the structural elements and components resisting collapse due to removal of a vertical load-bearing element are classified as primary components. All other

elements and components are considered as secondary. The secondary beams are assumed to be pinned at both connections without any flexural strength. The analysis includes force- and deformation-controlled actions (see Table 2-3). The continuity of the element directly above the removed component is assumed to be maintained (see Figure 2-18).

Table 2-3 Deformation-Controlled and Force-Controlled Actions

Component	Deformation-Controlled Action	Force-Controlled Action
Moment Frames:		
Beams	Moment (M)	Shear (V)
Columns	M	Axial load (P), V
Joints	--	V[1]
Shear Walls	M, V	P
Braced Frames:		
Braces	P	--
Beams	--	P
Columns	--	P
Shear Link	V	P, M
Connections	P, V, M[2]	P, V, M

[1] Shear may be a deformation-controlled action in steel moment frame construction. [2] Axial, shear, and moment may be deformation-controlled actions for certain steel and wood connections
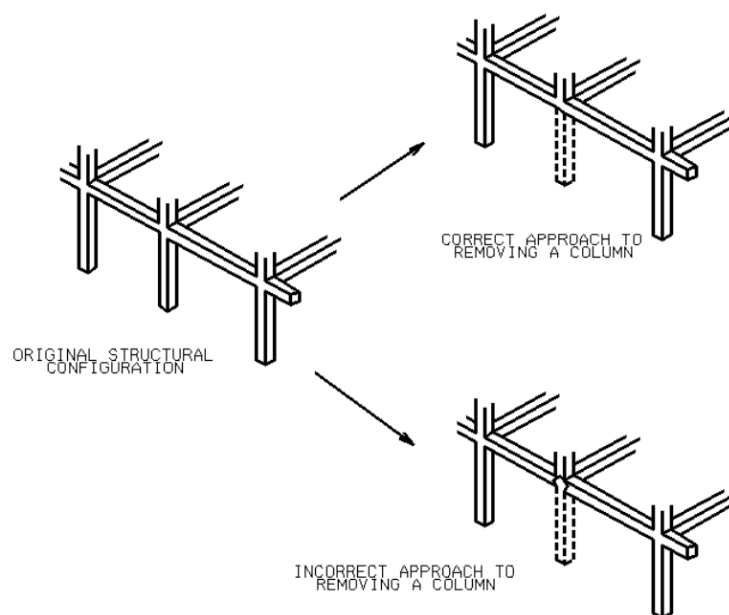
Figure 2-18 Continuity of the structure

The AP method includes three analysis procedures: linear static (LS), nonlinear static (NS) and nonlinear dynamic (ND) procedures. To evaluate a building, a three-dimensional model should be employed rather than two-dimensional models. In the linear static procedure (LSP),

The *DCRs* are introduced for the deformation controlled actions, which can be calculated by the ratio of resulting actions and expected strength of the component or element. The increased gravity loads for floor areas above removed column or wall is applied (see Table 2-4). The *m*-factor is defined in the guidelines for deformation controlled actions.

Table 2-4 Load increase factors for LSP

Material	Structure Type	Deformation-controlled	Force-controlled
Steel	Framed	0.9 m_{LIF} + 1.1	2.0
Reinforced Concrete	Framed	1.2 m_{LIF} + 0.8	2.0
	Load-bearing Wall	2.0 m_{LIF}	2.0
Masonry	Load-bearing Wall	2.0 m_{LIF}	2.0
Wood	Load-bearing Wall	2.0 m_{LIF}	2.0
Cold-formed Steel	Load-bearing Wall	2.0 m_{LIF}	2.0

m_{LIF} is the smallest *m* of any primary beam, girder, spandrel or wall element that is directly connected to the columns or walls directly above the column or wall removal location.

All primary and secondary components shall be checked by:

For deformation-controlled actions,

$$\phi m Q_{CE} \geq Q_{UD} \qquad \text{(Eq. 2-34)}$$

For force-controlled actions,

$$\phi Q_{CL} \geq Q_{UF} \qquad \text{(Eq. 2-35)}$$

where

ϕ = Strength reduction factor from the appropriate material specific code (such as ACI 318, AISC Steel Construction Manual, etc).

m = Component or element demand modifier (m-factor).

Q_{CE} = Expected strength of the component or element for deformation-controlled actions.

Q_{CL} = Lower-bound strength of a component or element for force-controlled actions.

Q_{UF} = Force-controlled action from Linear Static model.

It should be note that overall and local stability must be considered, however, a P-Δ analysis is not required for the LS approach due to the small deformations. In NSP, the dynamic increase factors (DIF) Ω_N are given in Table 2-5 to simulate the dynamic effects. Gravity loads modified by DIF are applied to the entire structure.

Table 2-5 Dynamic increase factors for LS analysis

Material	Structure Type	Ω_N
Steel	Framed	$1.08 + 0.76/(\theta_{pra}/\theta_y + 0.83)$
Reinforced Concrete	Framed	$1.04 + 0.45/(\theta_{pra}/\theta_y + 0.48)$
	Load-bearing Wall	2.0
Masonry	Load-bearing Wall	2.0
Wood	Load-bearing Wall	2.0
Cold-formed Steel	Load-bearing Wall	2.0

θ_{pra} is the plastic rotation angle. θ_y is the yield rotation.

In NDP, the loads starting at zero monotonically and proportionately increase to the entire model until equilibrium is reached. Then, the column or wall section shall be removed instantaneously less than one tenth of the period associated with the structural response mode for the vertical motion of the bays above the removed element. The analysis shall stop when the maximum displacement is reached or one cycle of the vertical motion occurs.

The ELR method requires the column, wall and connections between the structural elements must not fail in shear before the maximum flexural strength reached. All strength reduction factors ϕ (see Eq. 2-29) shall be 1.0. The material strengths for shear, flexure and all other actions shall be the expected material strength (i.e., with the appropriate over-strength factor applied to the lower bound material strength = 0.85 ×expected strength values for CFS structures).

2.6 Knowledge gaps

2.6.1 Purlin-to-sheeting system

Eurocode3 (EC3) provides the calculations for the rotational stiffness of purlin-to-sheeting connection. Based on the test results (Zhao et al., 2014), it was found that the prediction of

EC3 is not accurate due to the neglect or underestimate the effect of parameters, such as purlin thickness, depth and flange width.

2.6.2 Stud-to-track connection

As for stud-to-track connection, the joining methods employed in light steel modular construction has been introduced by researchers (Gorgolewski et al., 2001b, Trahair et al., 2007). Many types of joints can be used in CFS construction industry, including bolts, screws, rivet, etc. (SCI., 2015). Previous studies focusing on the optimization of conventional stud-to-track wall systems have suggested using extra screws as a practical and an efficient solution for the improvement of the resistance of the thin-walled systems. Although bolts with nut and head are expected to be overly strong when applied in thin-walled structures, they might be an alternative for extra screws.

The current norms and specifications have provided the design provision of single lap screw and bolt joints. However, in the CFS component assemblies, there usually are gaps between the connected sheets. The clearance of the joint may reduce the bearing strength of the screwed or bolted connections because of warping or local buckling occurs. It needs to be further investigated.

2.6.3 Screw and bolt joints

Connections with bolt/screw joints have been widely adopted in CFS constructions. Although codified models are available to predict the initial stiffness and resistance of CFS bolt joint (Eurocode, 2005), no method has been yet proposed to evaluate its overall behaviour which significantly impacts the entire structural behaviour in progressive collapse analysis (Stoddart and E., 2012, Stylianidis and Nethercot, 2015, Lim and Krauthammer, 2006, Liu, 2010) and the quasi-plastic analysis (Liu et al., 2011).

Specification AISI-S100 provides a model to predict the resistance of connections subjected to the combined tension and shear, which is only based on one failure mode, i.e. the pull-through. Chinese technical code (GB., 2002) for cold-formed thin-walled steel structures

suggests an interaction model for the combined shear and tension, in which the resistance models for the sole tension or shear and their corresponding failure models are not clearly indicated though.

The structural behaviour of the screw joint has rarely investigated, in particular, when they are subjected to the combined shear and tension. The use of high strength steel also causes new challenges due to its differing material properties. One of the key differences is that the high strength steel has lower ductility compared with the mild steel. The yield stress of high strength steel is closer to its ultimate strength. Therefore, further research is required to illustrate the potential implications on the structural behaviour of the connections made of high strength steel. The design recommendation should be made through examining the resistance, the stiffness and the ductility of the screw connected joints.

2.6.4   Joist-to-post connection

Thin-walled members are often open sections. Transverse loads applied on cold-formed open section joists do not pass through the shear centre of the section, leading to torsion acting on the connection. The torsion may induce twisting and/or warping deformations in the connected zones, which is likely to lead to local failure in the connection. The more effective and efficient connection method needs to be developed to improve the structural performance.

2.6.5   Robustness of CFS modular structure

The design methods described in current guidelines (DoD and GSA) apply to the framed and load-bearing wall buildings do not include modular panel systems. The ineffectiveness of the unit in the modular structure may lead to different load resistance mechanism.

The connections for modular building systems seem to be more complicated than traditional cast-in-place construction. These guidelines could not cover the design requirements for modular construction systems, and the suggestion of connection configurations is not involved in these guidelines.

In fact, the robustness and the load redistribution of the structure due to the removal of the structural element may be determined by the responds of the load carrying members and the connections between primary elements. The mechanical properties, involving stiffness and strength under tension, shear and rotation actions, of the connection are usually nonlinear and vary depending on the type of connection configuration between modules. The entire structural behaviours of different connection configurations under normal and abnormal loading conditions and the influence of that on the robustness of the CFS modular constructions have not been widely studied.

2.7 Summary

An extensive literature was reviewed for understanding the status of relevant research development. Basic concepts of modular constructions were established. A limited knowledge scope of connection technologies was presented, such as screwed connection, bolted connection, press joint, rosette joint, etc. The advantages of this construction such as waste reduction, recyclability, reusability, fast assembling, energy saving, carbon emission reduction, etc. have been realized in construction industry. However, challenges still exist. Connection is known as the pivotal issue in CFS structures as well as modular structures. The various fasteners, high-strength materials, thin-walled sections and various configurations applied have made the connection become one of the key issues in the development of off-site CFS modular structures. In the progressive collapse process, beam action and the catenary action usually lead to mixed loads imposed on the connection. In order to find out the effective and efficient connection method, the entre response of the connection should be estimated with regard to the structural robustness.

CHAPTER 3   PURLIN-TO-SHEETING CONNECTION

3.1 Introduction

In roof systems, CFS purlins attached to corrugated sheeting are widely used due to its shorter construction time. Traditional CFS purlin cross-section types include C-section and Z-section; the former is usually applied on flat roofs and the latter is generally used on the pitch roofs. Σ-section purlin, which evolved from C-section purlin but with two more insets, has been proposed since it has better torsional resistance capacity. These open-section purlins are known to be vulnerable to various buckling modes. The attachment of corrugated sheeting can provide lateral restraints to the purlins and therefore enhance the overall load bearing capacity.

The magnitude of the additional rotational stiffness offered by the sheeting will affect the load bearing capacity of the purlin. A series of laboratory tests of purlin-sheeting system were conducted in the companion study (Zhao et al., 2014). The rotational stiffness of the each purlin specimen was obtained by the vertical load and the corresponding rotation captured. The scenarios of uplift and gravity loads were involved.

Based on the test results, it was found that the current design method in Eurocode3 (EC3) cannot accurately predict the purlin-sheeting rotational stiffness. The effect of wall thickness, flange width and depth of the purlin are neglected in EC3.

In this chapter, an integral model established numerically for predicting the rotational stiffness provided by corrugated sheeting to the Σ purlin is presented. The model is validated against existing experiments. Parametric studies are conducted to reveal the effect of varying the geometric dimensions of the purlin and the interval of the screws on the rotational stiffness. Based on the numerical results, compensation coefficients are proposed to the current EC3 approach to calculating the rotational stiffness of Σ purlin-corrugated sheeting system.

3.2 Experimental and analytical studies

3.2.1 Laboratory tests

Laboratory tests of purlin-sheeting system were conducted and the results were presented in the companion study (Zhao et al., 2014). The experiment was set up according to requirements stated in EC3 (Eurocode, 2006b). During the test, the Σ purlin with a length of 1m was attached to the corrugated sheeting by five self-drilling screws with a diameter of 5.5mm. The screws were located at the centreline of one flange of the purlin connected to the sheeting's trough, as shown in Figure 3-1. The point load was distributed on the free flange by using a steel bracket with 7 bolts.

In the test, the sheeting was fixed on the ground via bottom cleats and M10 bolts. Two scenarios: face-up (gravity/downward loading case) and face-down (uplift loading case), were conducted during the test as shown in Figure 3-1.
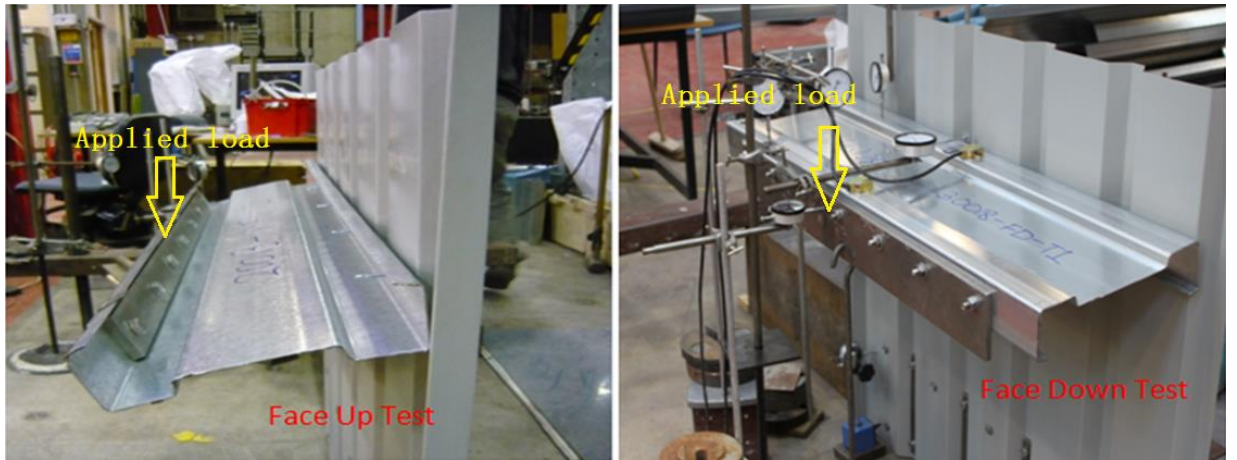
Figure 3-1 Test setup

The configurations of tested purlin sections and corrugated sheeting are shown in Figures 3-2 and 3-3, where W is the total cross-section depth; F is the flange width; t is the thickness; L is the lip length; O is the depth of the top and bottom parts of the web adjacent to the flanges in the Σ-section; I is the middle part of the modified web in the Σ-section; S is the width of the inward bend of the web and r is the corner radius Figure 3-2.

a) Σ-section b) C-section c) Z-section
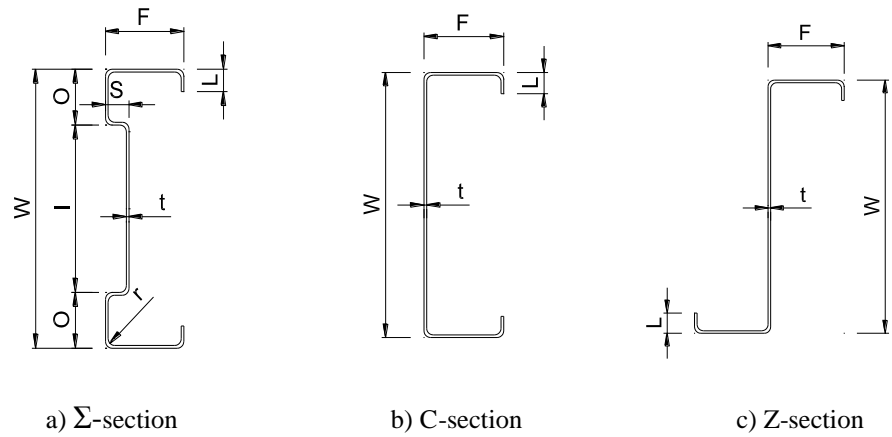
Figure 3-2 Diagram of Σ-, C- and Z- sections
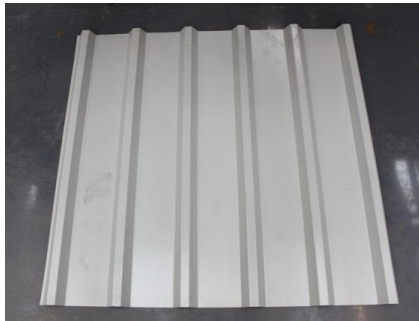
(a) Profile of the sheeting
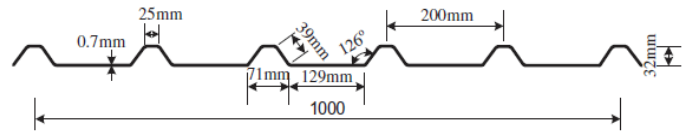
(b) Geometric dimensions of sheeting

Figure 3-3 Configurations of sheeting (Zhao et al., 2014)
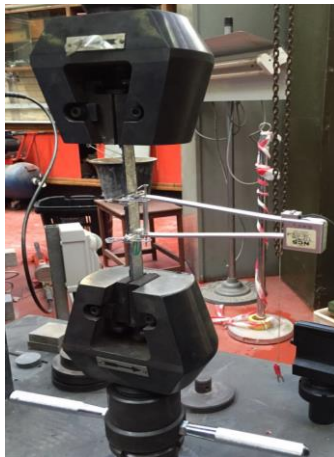
Figure 3-4 Coupon test setup
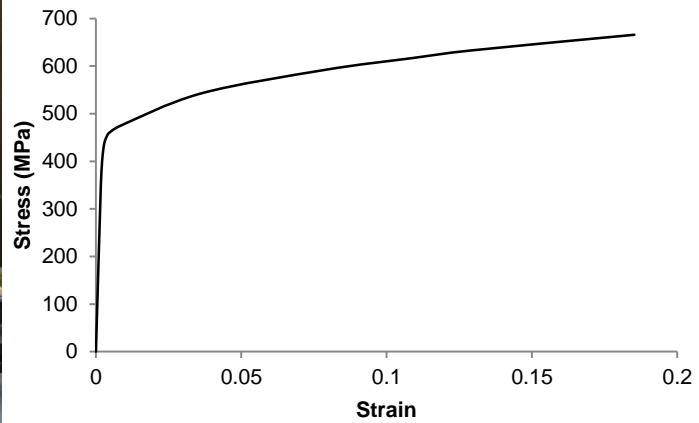
Figure 3-5 Stress-strain curve of the material

The cross-section dimensions of each specimen are provided in Table 3-1 and 3-2. The material properties of the specimen were obtained from tensile coupon tests (BSI., 2009). The coupons were cut from the flat region of CFS Σ-sections and the tests were conducted by

using a SANS 20t displacement controlled test machine (see Figure 3-4). The average stress-strain curve is shown in Figure 3-5.

Table 3-1 Geometric dimensions of Σ- sections

Specimen	W(mm)	F(mm)	L(mm)	O(mm)	S(mm)	t(mm)
Σ20012	200	62.5	20	45	16	1.2
Σ20016	200	62.5	20	45	16	1.6
Σ20025	200	62.5	20	45	16	2.5
Σ24015	240	62.5	20	45	16	1.5
Σ24023	240	62.5	20	45	16	2.3
Σ24030	240	62.5	20	45	16	3.0
Σ30018	300	75	20	60	16	1.8
Σ30025	300	75	20	60	16	2.5
Σ30030	300	75	20	60	16	3.0

Table 3-2 Geometric dimensions of C- and Z- sections

Specimen	W(mm)	F(mm)	L(mm)	t(mm)
C20012	200	62.5	20	1.2
C24023	240	62.5	20	2.3
C30030	300	75	20	3.0
Z14614	145	62.5	20	1.4
Z14618	145	62.5	20	1.8
Z20617	200	65	20	1.7
Z30720	300	75	20	2.0

3.2.2 Analytical design approach in EC3

The analytically derived equation for calculating the total rotational stiffness (C_D) contributed by the sheeting to the purlin is specified in Equation 10.14 of EC3 (Eurocode, 2006b) and given by:

$$C_D = \frac{1}{(1/C_{D,A} + 1/C_{D,C})}$$
(Eq. 3-1)

where $C_{D,A}$ is the rotational stiffness of the connection between the sheeting and the purlin; and $C_{D,C}$ is the rotational stiffness corresponding to the flexural stiffness of the sheeting.

The value of $C_{D,A}$ can be determined by using Eq. 3-2.

$$C_{D,A} = C_{100}.k_{ba}.k_t.k_{bR}.k_A.k_{bT} \qquad \text{(Eq. 3-2)}$$

where

$k_{ba} = \left(\frac{b_a}{100}\right)^2$ if $b_a < 125mm$;

$k_{ba} = 1.25\left(\frac{b_a}{100}\right)$ if $125mm \leq b_a < 200mm$;

$k_t = \left(\frac{t_{nom}}{0.75}\right)^{1.5}$ if $t_{nom} < 0.75mm$;

$k_t = \left(\frac{t_{nom}}{0.75}\right)^{1.5}$ if $t_{nom} \geq 0.75mm$; negative position;

$k_t = \left(\frac{t_{nom}}{0.75}\right)^{1.1}$ if $t_{nom} \geq 0.75mm$; positive position;

$k_{bR} = \frac{185}{b_R}$ if $b_R > 185mm$;

$k_A = 1.0$ when the sheet thickness less than 0.75mm;

$k_{bT} = \sqrt{\frac{b_{T,max}}{b_T}}$ if $b_T > b_{T,max}$ otherwise $k_{bT} = 1$;

b_a is the width of the purlin flange;

t_{nom} is the thickness of the sheeting;

b_R is the corrugation width;

b_T is the width of the sheeting flange through which it is fastened to the purlin;

$b_{T,max}$ is given in Table 10.3 EN 1993-1-3;

C_{100} is a rotation coefficient, representing the value of $C_{D,A}$ if b_a=100mm.

The value of $C_{D,C}$ may be taken as the minimum value calculated based on the models of the type shown in Figure 3-6, taking account of the rotations of the adjacent purlins and the degree of continuity of the sheeting, using:

$$C_{D,C} = m/\theta \qquad \text{(Eq. 3-3)}$$

where m is the applied moment per unit width of sheeting; θ is the resulting rotation.

The conservative value of $C_{D,A}$ may be obtained from:

$$C_{D,C} = \frac{kEI_{eff}}{s} \qquad \text{(Eq. 3-4)}$$

where k is the numerical coefficient with values as shown in Figure 3-6; E is the Young's module of the material; I_{eff} is the effective second moment of area per unit width of the sheeting; s is the spacing of the purlins.
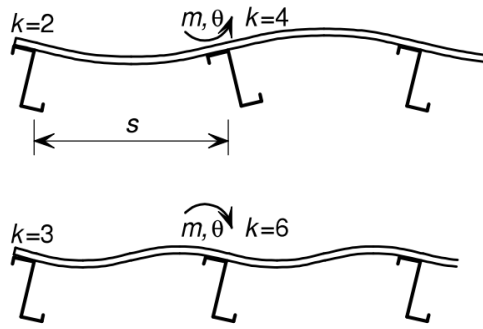
Figure 3-6 Model for calculation $C_{D,C}$

Base on the experimental study, the value of k is 2 as end, upper case of Figure 3-6. The distance between the purlin and the fixed end of the sheeting is 700mm. I_{eff} is determined by the dimension of the corrugated sheeting as shown in Figure 3-3b. The Young's module E is obtained by the result of coupon test (see Figure 3-4 and 3-5). The specimen geometric dimensions of Σ-sections have been introduced in Table 3-1. The analytically rotational stiffness C_D can be calculated involving downward and uplift loading scenarios. The results are shown in Table 3-3.

In the test, the total applied load and the applied moment per unit width of the sheeting M can be obtained. The test electrical inclinometer recorded the rotation angle of the purlin θ_1. The total rotation angle includes the rotation angle of the cantilever sheet θ_S, the rotation angle caused by the localised deformation of the sheet θ_L (see Figure 3-11), the rotation angle

because of the separation between the sheeting and the purlin at the connected point θ_K and the rotation angle due to the bending of purlin flange θ_P (see Figure 3-7).

Table 3-3 Geometric dimensions of Σ- sections

Specimen	k	E(MPa)	I_{eff} (cm^4/m)	s (mm)	$C_{D,C}$ (Nm/m/rad)	$C_{D,A}$ (Nm/m/rad)	C_D(Nm/m/rad)
Σ20012						970 (downward) 470 (uplift)	946 (downward) 464 (uplift)
Σ20016						970 (downward) 470 (uplift)	946 (downward) 464 (uplift)
Σ20025						970 (downward) 470 (uplift)	946 (downward) 464 (uplift)
Σ24015						970 (downward) 470 (uplift)	946 (downward) 464 (uplift)
Σ24023	2	210000	6.21	700	37260	970 (downward) 470 (uplift)	946 (downward) 464 (uplift)
Σ24030						970 (downward) 470 (uplift)	946 (downward) 464 (uplift)
Σ30018						1397 (downward) 677 (uplift)	1347 (downward) 665 (uplift)
Σ30025						1397 (downward) 677 (uplift)	1347 (downward) 665 (uplift)
Σ30030						1397 (downward) 677 (uplift)	1347 (downward) 665 (uplift)
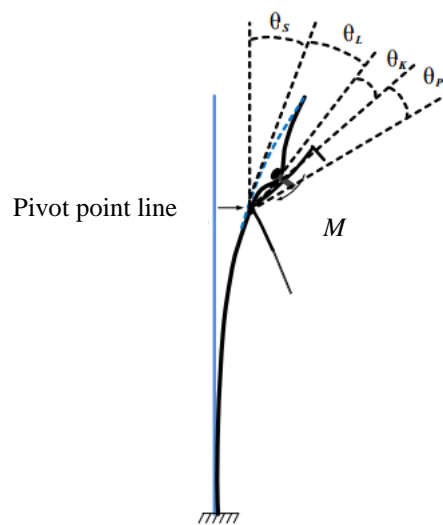
Figure 3-7 Illustration of the rotational deformation (Zhao et al., 2014)

It can be observed that the flexural stiffness of the sheeting not conspicuously influence the total rotational stiffness within the scope of 4%. The flexural stiffness of the sheeting $C_{D,C} = M/\theta_S$ is negligible as the value of which is considered to be much larger than $C_{D,A}$.

During the test process, the purlin profile tends to separate from the corrugated sheeting due to the rotation action under the applied load. However, in the linear stage that the displacement of the loading point no more than 1/10 of the web depth, it has been observed from the test that the total rotation angle caused by this factor is relatively much less than others. Thus, θ_K is neglected in the calculation model.

Therefore, the laboratory results of rotational stiffness $C_{D,A}$ can be calculated by the following equation:

$$C_{D,A} = \frac{M}{\theta_1}$$
(Eq. 3-5)

where M is the applied moment per unit width of the sheeting and θ_1 is the resulting rotation angle of the purlin at the connection point (see Figure 3-1).

According to the assumptions and validations, the further investigation aimed at rotational stiffness $C_{D,A}$ was carried out through numerical and analytical analysis.

3.3 Numerical approach

3.3.1 Modelling process

The comparison between the test and EC3 has between illustrated in Table 3-4, showing a big difference. Numerical method was introduced herein using the commercial FE package ABAQUS (Abaqus-6.13, 2013) to model the laboratory tests. The purlin and sheeting were modelled by 4-node 3D deformable shell elements S4R. The fastener was modelled by 4-node 3D rigid shell elements R3D4. According to the geometries of the purlin and the sheet, different mesh densities were chosen through an extensive trial-and-error process. The most optimal result was obtained when using the discretisation pattern in which the basic mesh size

of 13mm for the member and a refined mesh of 1mm were applied around the bolt hole. An example of the mesh pattern is shown in Figure 3-8.

The interaction between the shell and bolt was "tie" contact and the "hard contact" condition was applied between purlin and the sheeting to remove over-closure between surfaces and the sheeting was simply supported and the purlin was restrained in the longitudinal direction (z axis) to prevent overall movement because of the previous assumptions.

A point load was applied at the mid-span of the purlin by creating a reference point located at the flange-to-web junction line or the flange-to-lip junction line to represent the uplift or downward case (as shown in Figure 3-9). A nonlinear incremental-iterative, Full-Newton solution was adopted in the analysis for solving the nonlinear equilibrium equations. The principal advantage of Newton's method is the high convergence rate. The material property for the purlin element was simulated by a multi-linear stress-strain curve based on the true stress-strain curve from the coupon tests (see Figure 3-5); for the sheeting element, the material property was given by a bilinear stress-strain curve with nominal yield strength of 235MPa.
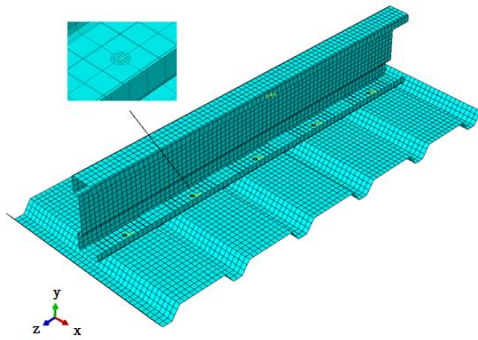
Figure 3-8 Meshed model   Figure 3-9 Boundary conditions
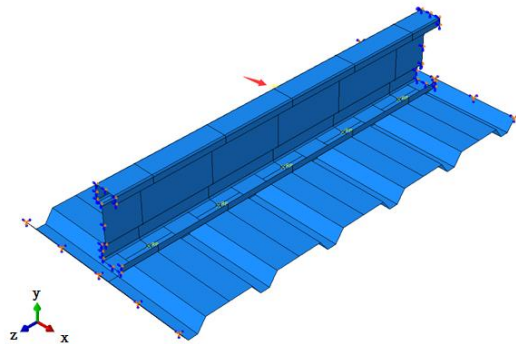
3.3.2 Result discussions

The structural displacement of the purlin and the local deformation of the sheeting in the FE model are shown in Figures 3-10 and 3-11 respectively. The comparison of the moment-rotation curves from experimental and numerical results is shown from Figure 3-12 to 3-20.
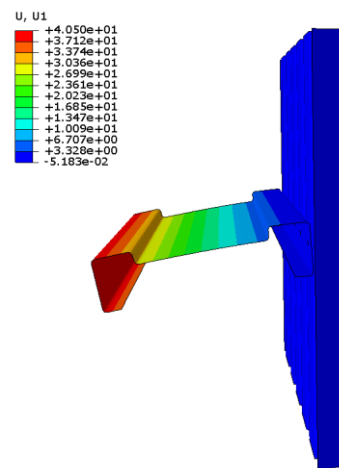
a) Under uplift load
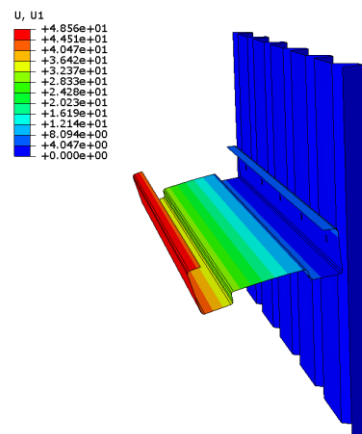
b) Under downward load

Figure 3-10 Structural displacement of the purlin
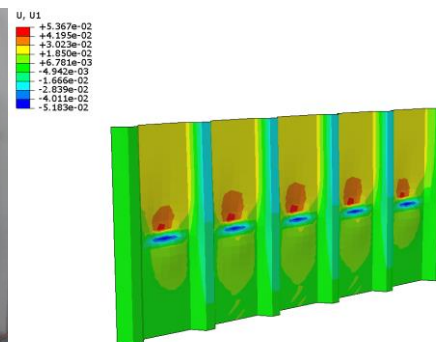
Figure 3-11 Deformation of the sheeting

Rotational stiffness $C_{D,A}$ obtained from the FEM C_{FEM} is compared with the calculated ones using EC3 ($C_{D,A}^A$) and the measured ones from the laboratory test C_{Test}, as listed in Table 3. The $C_{D,A}$ values in FEM are determined when the displacement of free edge of the purlin equal to 1/10 of the web depth (Zhao et al., 2014). It can be observed that some FEM results are above the test ones, but some below the test results. The deviation may be caused by the measurement error in the tests.
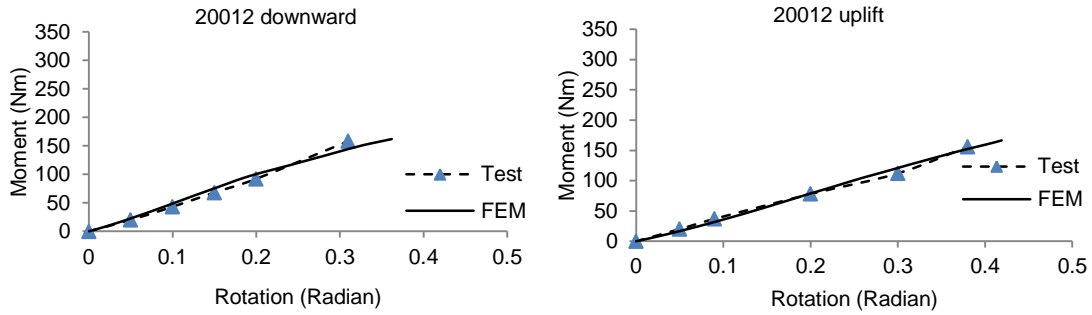
Figure 3-12 Moment to rotation curves (20012)
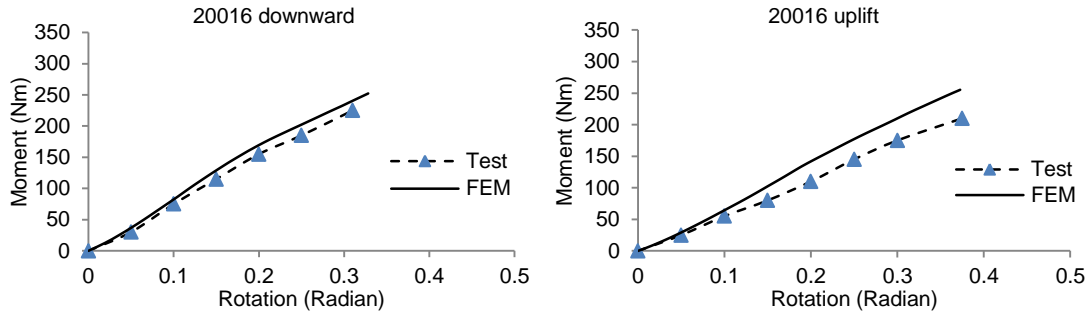
Figure 3-13 Moment to rotation curves (20016)
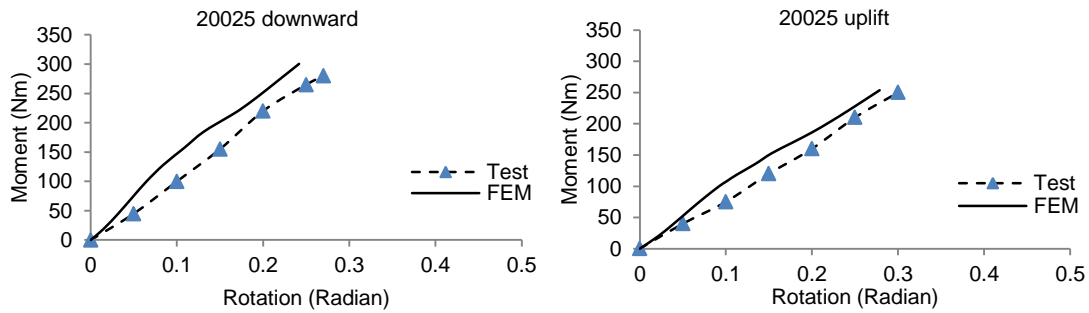
Figure 3-14 Moment to rotation curves (20025)
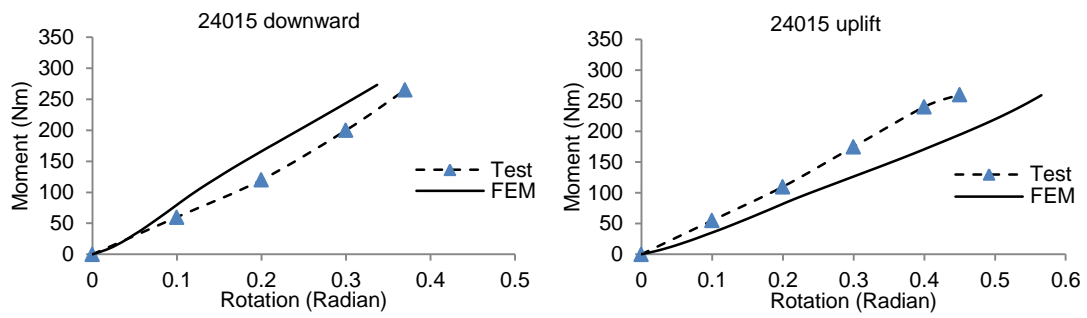
Figure 3-15 Moment to rotation curves (24015)
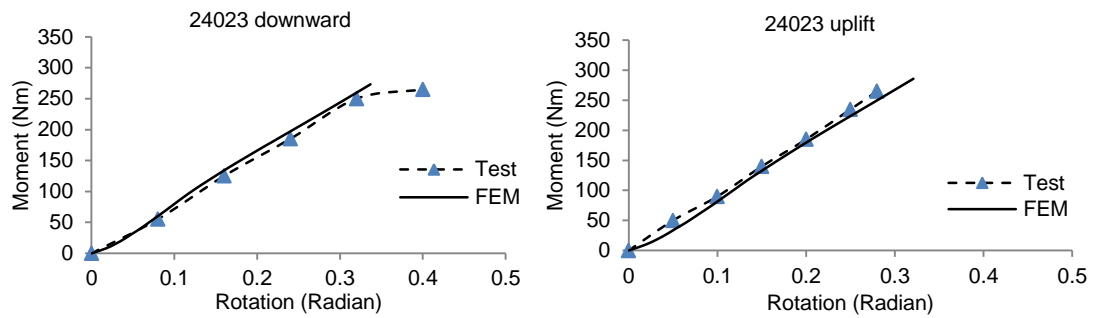
Figure 3-16 Moment to rotation curves (24023)
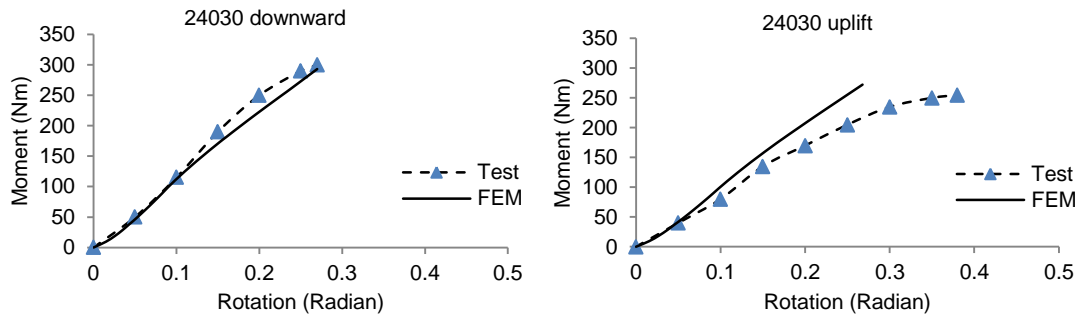
Figure 3-17 Moment to rotation curves (24030)
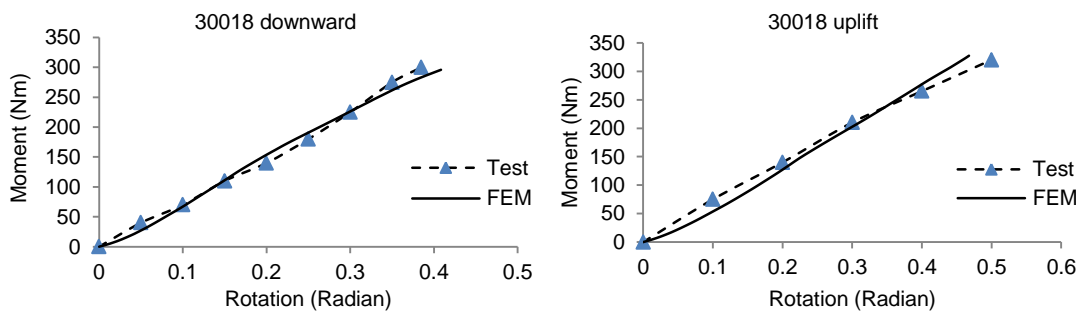
Figure 3-18 Moment to rotation curves (30018)
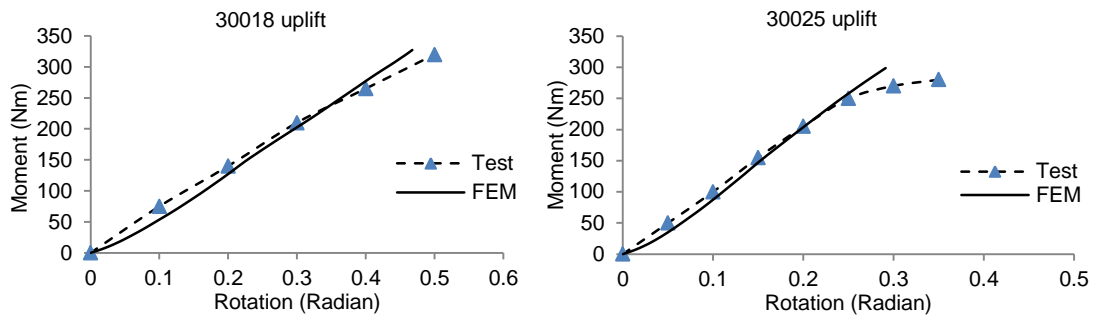
Figure 3-19 Moment to rotation curves (30025)
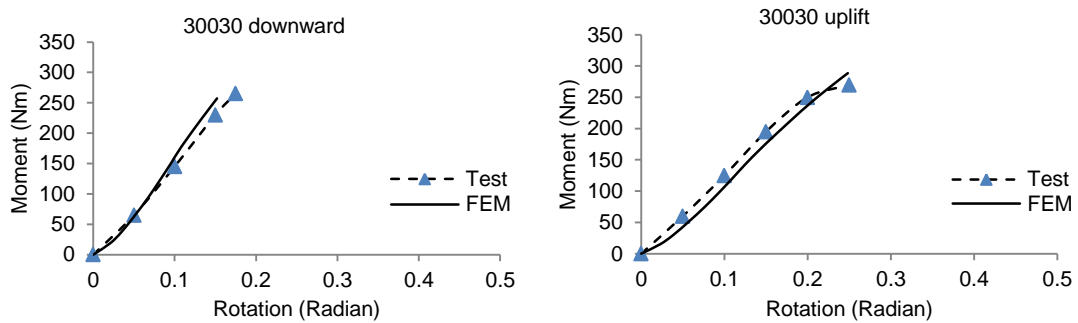
Figure 3-20 Moment to rotation curves (30030)

According to Figure 3-12 to 3-20, a good agreement can be found between the FEM and the test results, implying that the numerical model is valid.

Table 3-4 demonstrates that the average ratio of the predicted rotational stiffness between the numerical model and the test is 1.09, with a standard deviation of 0.07, whereas the average analytical-to-test ratio is 1.03, with a standard deviation of 0.42. The test results indicate that the purlin thickness significantly affect the rotational stiffness. However, this factor is not concerned by EC3, leading to the rotational stiffness for thinner purlins (no less than 1.5mm) overestimated and for thicker purlins (less than 1.5mm) under-estimated by the analytical method in downward load cases. The similar outcomes happen in upward load cases.

It can be concluded that FEM has a better capability in predicting rotational stiffness than the current analytical expressions. One reason for the discrepancy between FEM and test result is the negligence of the washer in the numerical model, which was used in the test to avoid local failure by reducing concentration stress around the bolt hole. In the modelling, the screws

were simulated as rigid element and the mutual movement between the fastener and components was restrained, which leads to an enhancement of the screw joint stiffness in the connection. As a result, the rotational stiffness is overestimated by 9% in FEM.

Table 3-4 Comparison of $C_{D,A}$ results

| Specimen | FEM | | | | Comparison | | |
	Load (N)	θ (rad)	C_{FEM} (Nm/m/rad)	C_{Test} (Nm/m/rad)	C_{FEM}/C_{Test}	$C_{D,A}^A$ (Nm/m/rad)	$C_{D,A}^A/C_{Test}$
$\sum$20012D	150	0.065	573	502	1.14	970	1.93
$\sum$20012U	125	0.073	450	394	1.14	470	1.19
$\sum$20016D	256	0.066	756	691	1.09	970	1.40
$\sum$20016U	238	0.077	638	622	1.03	470	0.76
$\sum$20025D	606	0.079	1049	1024	1.02	970	0.95
$\sum$20025U	606	0.089	943	895	1.05	470	0.53
$\sum$24015D	230	0.060	760	696	1.09	970	1.39
$\sum$24015U	148	0.066	582	593	0.98	470	0.79
$\sum$24023D	484	0.081	980	1009	0.97	970	0.96
$\sum$24023U	438	0.085	876	848	1.03	470	0.55
$\sum$24030D	641	0.091	1156	1047	1.10	970	0.93
$\sum$24030U	641	0.099	1057	909	1.16	470	0.52
$\sum$30018D	202	0.074	943	753	1.25	1397	1.86
$\sum$30018U	150	0.073	785	735	1.07	677	0.92
$\sum$30025D	338	0.080	1181	1078	1.10	1397	1.30
$\sum$30025U	275	0.080	1050	921	1.14	677	0.74
$\sum$30030D	430	0.085	1292	1191	1.08	1397	1.17
$\sum$30030U	353	0.083	1171	977	1.20	677	0.69
Mean					1.09		1.03
S.D.					0.07		0.42

Note: C_{FEM} is the rotational stiffness obtained from FEM; $C_{D,A}^A$ is the analytical rotational stiffness achieved by EC3; C_{Test} is the rotational stiffness obtained from the laboratory tests; D represents the downward load case and U represents the uplift load scenario.

3.3.3 Parametric studies

A series of parametric studies are conducted to investigate the influence of the fastener spacing and sheeting thickness on the rotational stiffness, and only one variable is changed at a time during the analysis.

3.3.3.1 Fastener spacing

In the following figures, the *y*-axis represents the rotational stiffness and the *x*-axis represents the ratio between fastener spacing (*e*) and corrugation width b_R ($b_R = 200$mm according to the test). The fastener used in the models is rigid shell elements with the diameter of 5.5mm. From Figure 3-21 to 3-23, the rotational stiffness decreases with the increase of e/b_R. In general, the results of FEM are in good accordance with the test outcomes. It can be observed that the prediction of EC3 does not change with the increase of the specimen thickness, while the results of FEM and test increase.

The figures show that as the fastener spacing increases, the rotational stiffness decreases as expected. The FEM results show good accordance with the test results. The mean value in FEM drops by 36% and 33% for downward loading case and uplift loading cases, respectively, when increasing fastener spacing from $1.0b_R$ to $2.0b_R$.
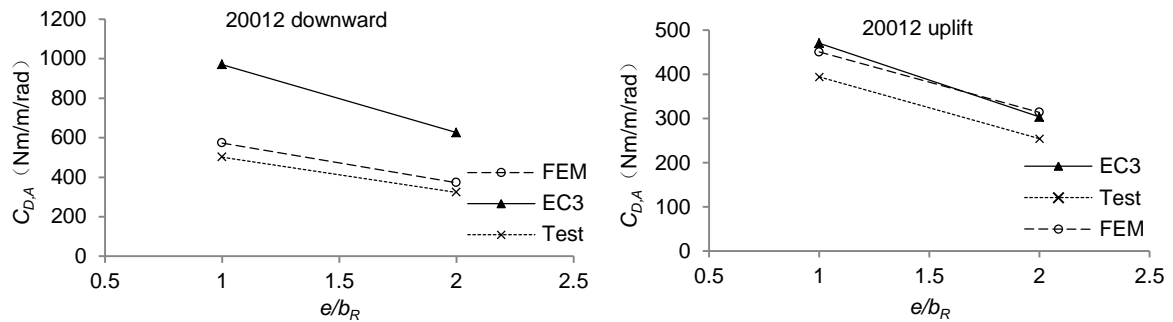
Figure 3-21 The effect of fastener spacing (20012)
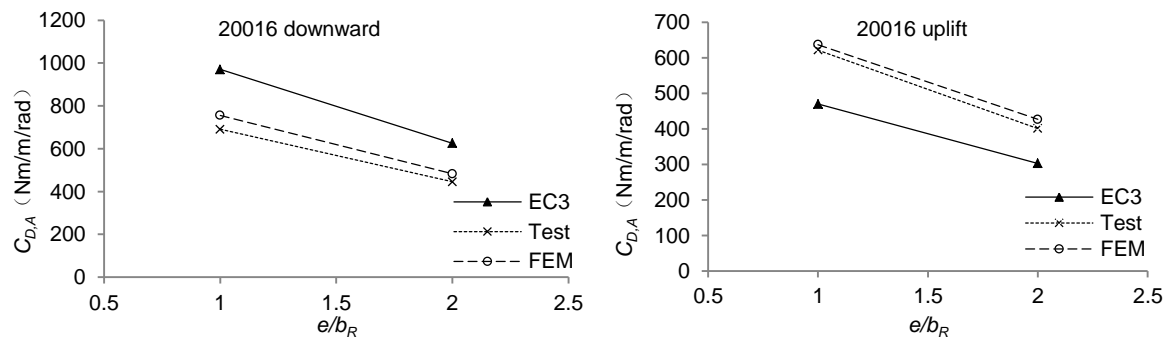
Figure 3-22 The effect of fastener spacing (20012)

72
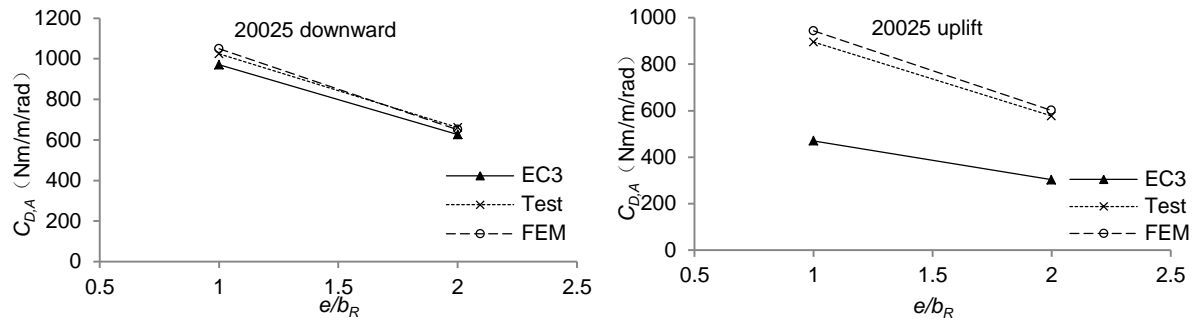
Figure 3-23 The effect of fastener spacing (20025)

3.3.3.2 Sheeting thickness

The corrugated sheeting with three thicknesses (t_s), 0.7mm, 1.0mm and 1.5mm, are analysed herein (see Figure 3-24 to 3-26). With the increase of the shell thickness, the rotational stiffness obtained by FEM presents the same trend with EC3. However, the deviation also can be found. When the purlin thickness changes from 1.2mm to 2.5mm, this deviation grows significantly in the uplift load cases and the ratio between EC3 prediction and FEM result decreases in the downward load cases. It is found that the sheet thickness has a significant effect on the rotation behaviour of the Σ purlin-corrugated sheeting system. Rotational stiffness increases for the 200 series purlin with increasing sheet thickness from 0.7mm to 1.2mm. The EC3 and FEM show an increase of 71% and 87% in the rotational stiffness under downward load when the thickness increases from 0.7mm to 1.0mm, and an increase of 31% and 43% when the thickness increases from 1.0mm to 1.2mm, respectively. A similar trend can be identified for the 200 series purlin under uplift load, with the corresponding values being 71% and 31% for EC3 method, and 75% and 35% for FEM.
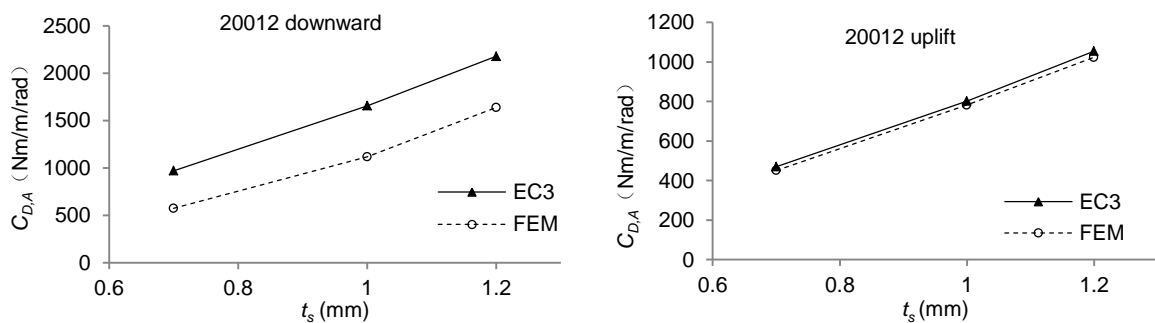
Figure 3-24 The effect of sheeting thickness (20012)

73
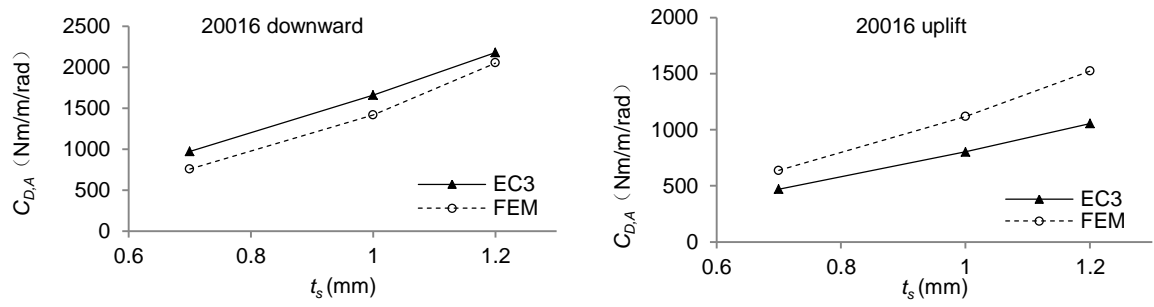
Figure 3-25 The effect of sheeting thickness (20016)
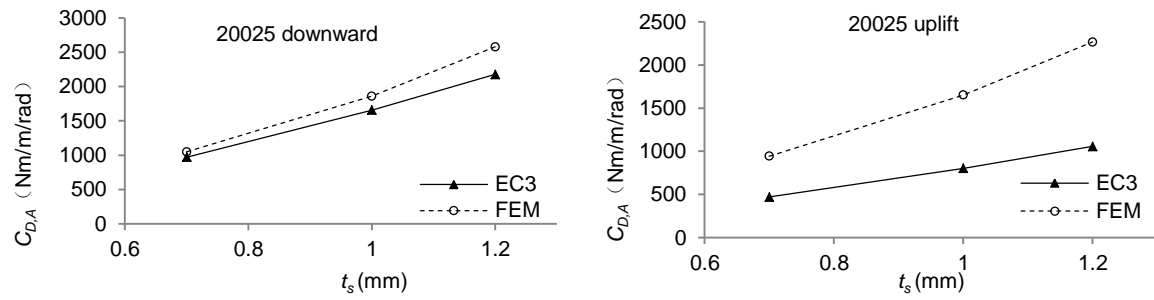
Figure 3-26 The effect of sheeting thickness (20025)

3.3.3.3 Purlin web depth, flange width and shell thickness

The effect of varying web depth (W), shell thickness (t) and flange width (F) on the rotational stiffness of the purlin-sheeting connection is demonstrated in Figure 3-27 to 3-29.
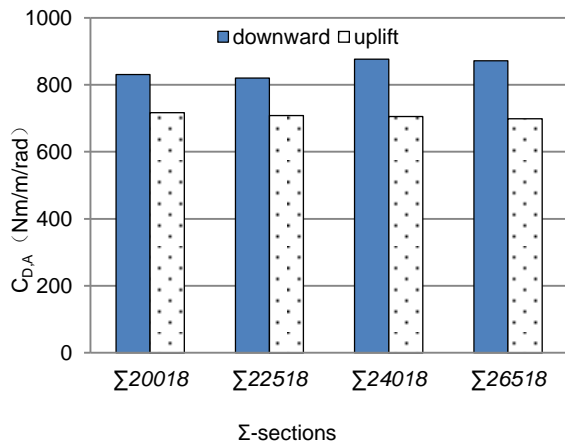
Figure 3-27 $C_{D,A}$ with different web depths
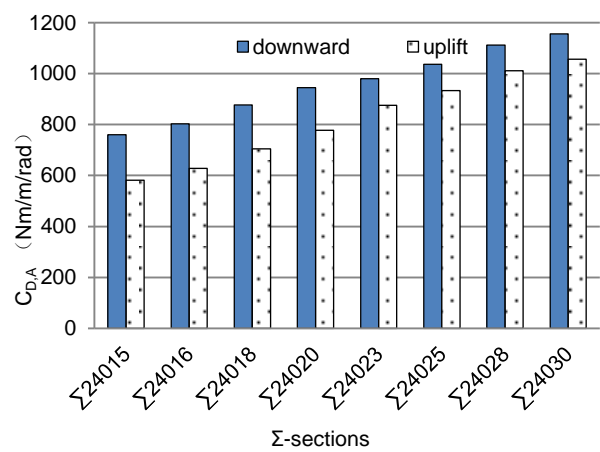
Figure 3-28 $C_{D,A}$ with different shell thickness
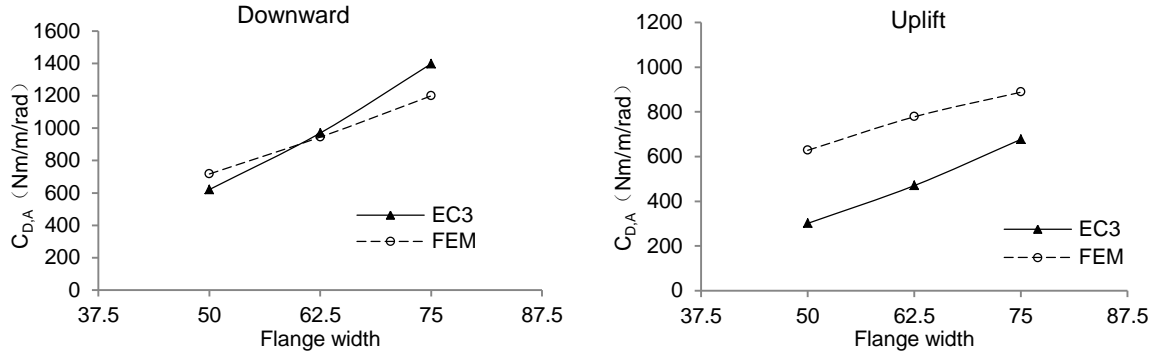
Figure 3-29 $C_{D,A}$ with different flange widths

Comparisons demonstrated in Figure 3-27 indicate that the effect of increasing web depths on the rotational stiffness is not obvious. It shows in the Figure 3-28 that the rotational stiffness increases remarkably with increasing section thickness for both downward and uplift load. Figure 3-29 also demonstrates an increase trend with increasing flange width. Since the analytical method does not consider factors such as the thickness and the overall depth of the purlin, a modification method is hence presented herein to improve the accuracy of the codified method. Since the influence caused by web depth is insignificant on the rotational stiffness, the effect is discarded in the following modification process.

3.4 Modification approach

The experimental and numerical outcomes show that the codified design approach in EC3 is less accurate for predicting the rotational stiffness as it neglects the effect of the purlin thickness and underestimate the effect of flange width. Therefore, a compensation coefficient $\varphi(t, F)$, given by Eq. 3-6, is introduced herein to modify the EC3 approach. The relationship between $C_{D,A}$ obtained by the modified analytical value $C_{D,A}^M$ and the $EC3$ codified value $C_{D,A}^A$ is given by Eq. 3-7.

$$\varphi(t,F) = \beta_t \beta_F \qquad \text{(Eq. 3-6)}$$

$$C_{D,A}^M = \varphi(t,F) C_{D,A}^A \qquad \text{(Eq. 3-7)}$$

where β_t and β_f are the correction coefficients for shell thickness and flange width respectively; $C_{D,A}^M$ is the modified analytical value.

75

The design formula for β_F is derived from the parametric study and the formulae for β_t is obtained based on the regression analysis. In the analysis, the purlin thickness (t) is determined as the main variables affecting stiffness of purlin system. According to the relationship between (t) and dependent variable(y), the nonlinear expectation function is assumed to be parabola (see Figure 3-30 and 3-31):

$$y = a + bt + ct^2$$
(Eq. 3-8)

The expressions (Eqs. 3-10 and 3-11) of β_t for downward and uplift load can be obtained using data analysis software ORIGIN8.0. In order to improve the accuracy of the analysis, the equations (Eqs. 3-9 to 3-11) are employed when determination coefficients are over 0.98 in the regression analysis.

$$\beta_F = \frac{10}{F - 20}$$
(Eq. 3-9)

For downward load,

$$\beta_{t,d} = -0.4t^2 + 3.1t - 0.6$$
(Eq. 3-10)

and for uplift load,

$$\beta_{t,u} = -0.7t^2 + 6.1t - 2.2$$
(Eq. 3-11)

where t is the thickness of section and F is the width of flange.
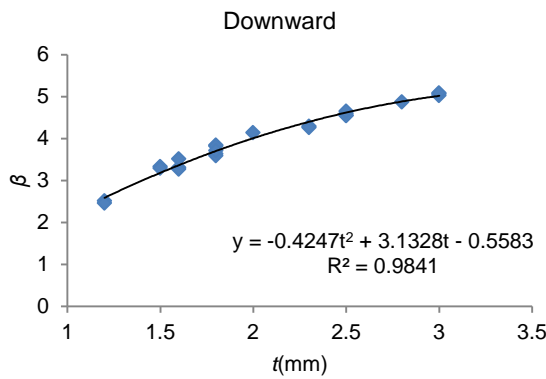
Figure 3-30 β-t relationship under downward load   Figure 3-31 β-t relationship under uplift load
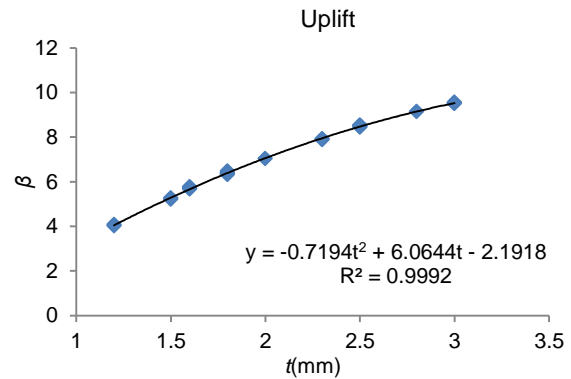
The comparison of rotational stiffness ($C_{D,A}$) between modified analytical method and other approaches is shown in Figure 3-32 and 3-33.

As shown in Figure 3-32, in contrast to test results, predictions obtained by the current specification (EC3) generally overestimate the rotational stiffness of the purlin-to-sheet connection under gravity load. On the contrary, when uplift load is applied on the sheet, conservative results are obtained from the analytical approach (EC3).

Meanwhile, the modified method shows better agreement with the test results, with the average ratio being 1.10 and 1.00, and the standard deviation being 0.07 and 0.08 for the download and uplift scenario, respectively (see Figure 3-33).
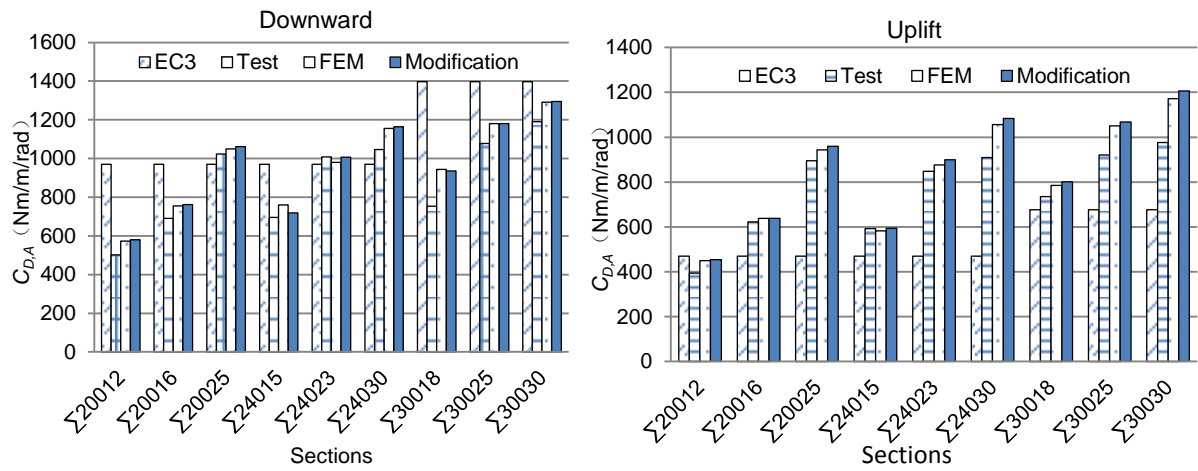
Figure 3-32 Rotational stiffness $C_{D,A}$ with downward & uplift load
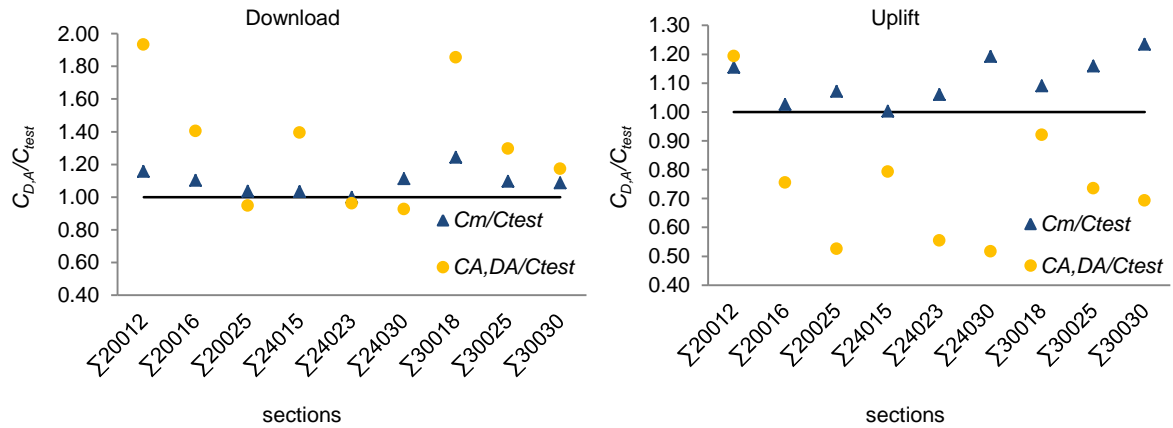
Figure 3-33 Results comparison of $C_{D,A}$

In order to further validate the modified method, more purlin-sheeting models with C- and Z-sections are analysed. The comparison is listed in Table 3-5.

Table 3-5 Comparison of $C_{D,A}$ with C- and Z-section purlins

Specimen	β_t	β_F	C_{Test} (Nm/m/rad)	$C_{D,A}^A$ (Nm/m/rad)	$C_{D,A}^M$ (Nm/m/rad)	$C_{D,A}^A/C_{Test}$	$C_{D,A}^M/C_{Test}$
C20012D	2.54	0.24	579	970	581	1.68	1.00
C20012U	4.12	0.24	455	470	456	1.03	1.00
C24023D	4.41	0.24	986	970	1007	0.98	1.02
C24023U	7.95	0.24	883	470	879	0.53	1.00
C30030D	5.10	0.18	1297	1397	1295	1.08	1.00
C30030U	9.53	0.18	1176	677	1173	0.58	1.00
Z14614D	2.96	0.24	762	970	675	1.27	0.89
Z14614U	4.89	0.24	512	470	541	0.92	1.06
Z14618D	3.68	0.24	820	970	841	1.18	1.03
Z14618U	6.39	0.24	730	470	707	0.64	0.97
Z20617D	3.51	0.22	876	1050	820	1.20	0.94
Z20617U	6.04	0.22	680	508	682	0.75	1.00
Z30720D	4.00	0.18	955	1397	1016	1.46	1.06
Z30720U	7.06	0.18	791	677	869	0.86	1.10
Mean						1.01	1.00
S.D.						0.33	0.05

It is showed that the test results of C- and Z-section purlins are also in good agreement with the modified analytical method. The average value of $C_{D,A}^M/C_{Test}$ shows a very slightly better agreement than $C_{D,A}^A/C_{Test}$ (1.00 to 1.01), and the former also shows more stability than latter, with the standard deviations being 0.05 and 0.33, respectively.

3.5 Summary

In this chapter, the investigation on rotational stiffness in the purlin-sheeting system under both downward and uplift load scenarios has been presented. Based on the comparison between the test results and the analytical values predicted by current design code, it is found that the purlin thickness and flange width have a significant impact on the rotational stiffness in the purlin-sheeting system and therefore modification of the current design method is required. In order to improve the accuracy of codified method, a series of numerical and parametric studies are carried out involving Σ-, C- and Z- sections, and the following conclusions can be drawn based on the studies.

The purlin thickness has a significant effect on the rotation behaviour of the purlin-corrugated sheeting system whereas the effect of increasing web depths is negligible. It shows that the rotational stiffness increases remarkably with increasing section thickness for both downward and uplift load scenarios.

The compensation coefficient that consider the influence of shell thickness (β_t) and flange width (β_F) on the rotational stiffness can lead to a better agreement with the test results for Σ purlins. This approach is also approved to be applicable on Z and C purlins.

CHAPTER 4   STUD-TO-TRACK CONNECTION

4.1   Introduction

A numerical comparison was conducted between a double screw connection and a single bolted connection with similar opening areas. In addition, a parametric study was performed to investigate the influence of factors contributing to optimization of the stud-to-track wall systems, such as width of the stud flange, depth of the stud and the stud thickness. In order to predict the ultimate strength of the stud-to-track connection with a gap, numerical methods were discussed in this chapter. The finite element analysis (FEA) results are in good accordance with those of the existing experimental studies. The parametric findings show that thickness plays a more important role in raising the resistance of the stud-to-track walls compared to effects of other potential parameters. The resistance of samples considerably reduced with the presence of gap between the sheets. In contrast, bolts and self-drilling screws are more suitable for the stud-to-track wall system and mostly applied to link cold-formed components in the modular structures. The stud and track connection as the basic connection employed in modular construction was selected to conduct a comparative study of connection solutions. The predictions of current specification AISI (2007) are presented in this chapter as a comparison. It should be noted that the safety factors are excluded in calculations of AISI. The characteristics of the common connection methods are listed as follows.

4.1.1   Bolted connection

Bolts are a common choice for connecting steel members. The bolted joints (see Figure 4-1) require to be pre-punched in the molding process and are often arranged to be subjected to shear and tension. The washer also affects the structural resistance of the bolted joint. In practice, because of the bolt intensity and rigidity far above thin-walled component, the bearing capacity of the bolted connection is often dominated by the bearing strength of the thinner material. Therefore, this connection method does not fully utilise the resistance of its bolts.

In general, bolts are classified by steel materials as class 4.6, class 8.8, class 10.9, class 12.9 and A-2 stainless bolts[2]. As for class 8.8 bolt, the applied material is quenched and tempered medium carbon steel. It is galvanized at the surface to resist corrosion. In this research, M8 class 8.8 bolt was selected as the study object (see Table 4-1). The material properties are shown in Table 4-2. In order to prevent loose in the connection, bolts are usually tightened properly. The versions of the pre-tightening force are varied. As for M8 bolt, the bolt load of 1640N was applied in the following analysis in accordance with engineering application. However, CFS is covered with galvanizing coat which has a very smooth surface. Hence, the influence of the friction resulted from preload is not significant (Zadanfarrokh and Bryan, 1992, Bryan, 1993).

Results of tests initially conducted by George Winter (Winter, 1956) indicated that there are four basic types of failure usually occur in the CFS bolted connections, i.e., longitudinal shearing failure, ring buckling in front of the bolt, tearing failure in the net cross section and shearing of the bolt. In practice, the minimum distance between centres of bolt holes is suggested to be 3*d*, where *d* is the diameter of the bolt. The distance from the centre of any standard hole to the end or other boundary of the connecting member should not be less than 1.5*d*. The clear distance between edges of two adjacent holes should not be less than 2*d*. The distance between the edge of the hole and the end of the member should not be less than *d* (AISI., 2007).

4.1.2 Screwed connection

Self-drilling and self-tapping screws are widely adopted in light steel structures (see Figure 4-2). The drilling or tapping part of the screw forms a hole in the steel section with a single operation. Without pre-drilled opening, screws are compatible with the installation tolerance. This technique is also used to inter-connect either steel panels or frames on site. It should be note that the protruding head of the screw may interfere with other components. Two or more

---

[2] https://www.boltdepot.com/fastener-information/materials-and-grades/Bolt-Grade-Chart.aspx

screws are suggested to be used for each connection. In addition, self-drilling and self-tapping screws also provide a form of attachment between finishing materials, such as plasterboard, sheathing, floor boarding, insulation and decking and light steel structures.

Screw is made of high quality grade casehardened carbon steel. JT2-NH3 Range self-drilling screw (see Table 4-1) was applied in this research. The material of the screws is based on the reference from E-Z LOK[3,4]. The details of the properties are presented in Table 4-2. Screwed connections can be assembled without pre-openings, which will avoid the effect caused by installation deviations. Screws can carry shear and tension strength in structures. Without nuts, screws may be pulled out or pulled over under tension action, which is determined by the thicknesses of the connection sections. Moreover, the screw joint may fail with bearing failure in the connected sheet, tilting or mix modes. The bearing capacity of the screw joint depends on the minimum value of the tilting resistance and bearing strength of the sheet. Under shear force, the tilting of the fastener is more notable within thin-walled sheets.

In applications, the distance between the centres of fasteners shall not be less than $3d$. The distance from the centre of a fastener to the edge of any part shall not be less $3d$. If the connection is subjected to shear force in one direction only, the minimum edge distance shall be $1.5d$ in the direction perpendicular to the force (AISI., 2007).

4.1.3   Welded connection

The thin-walled sections can be also joined by the continuous metal inert gas (MIG) welded (see Figure 4-3) or spot welded joints (see Figure 4-4). Because of the parent metal is extremely thin, the damage may be occurred during the MIG welding process. After welding, the joint should be protected by zinc rich paint for the durability reason. Spot welding is commonly applied for workshop fabrication as shown in Figure 4-3. The steel elements can be joined through the arc created between the tips of the welding tool on either side, which

---

[3] http://www.ezlok.com/TechnicalInfo/MPCarbonSteel.html

[4] http://www.ejot.co.uk/medias/sys_master/products/8797589045278/JT2_NH3_range.pdf

requires the welding tool can be supported and easily moved into the position to form the joint. A minimum of 3 spot welds should be used for each connection.
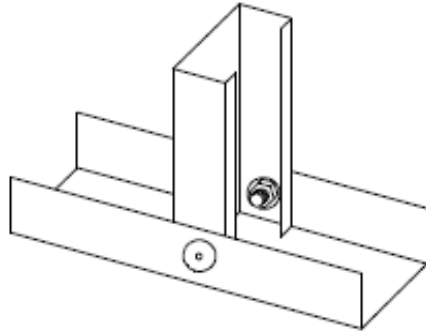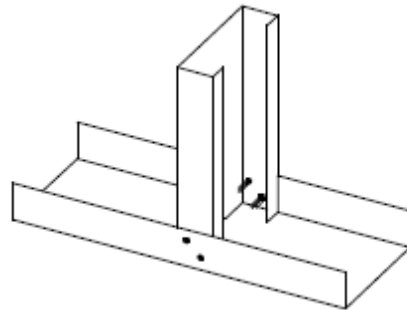
Figure 4-1 Bolt   Figure 4-2 Screw
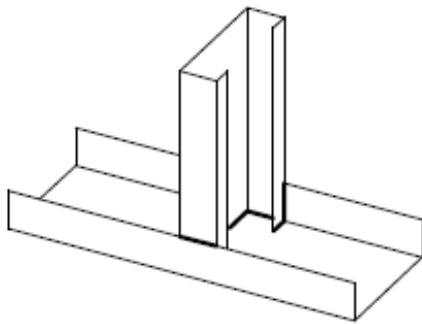
Figure 4-3 MIG welding   Figure 4-4 Spot welding
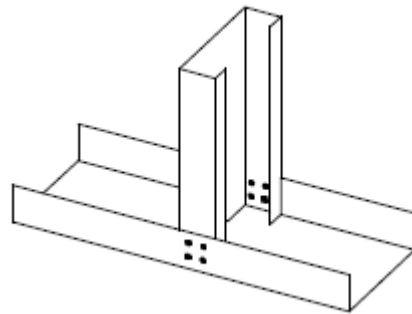
4.1.4 Other connections

Blind rivets are fitted into pre-drilled holes and a mandrel is pulled by a special tool so that the rivet expands into and around the hole. Different from the blind rivet, pre-drilled hole is not required for self-piercing rivet. The rivet can be used both to pierce and to form a permanent fastening within the materials and provide relatively good pull-out resistance between thin-walled attachments. The assembly of rivet joints needs the special tool, which requires sufficient installation space on both sides.

Press joint does not need any additional fastener which is proved to be applicable in light steel connection. A specific tool is required during the installation process. Clinching joint is also a

fastener-less method that can lock two or more layers of thin-walled steel components together. A hydraulically operated punch is needed to drive the layers into a die and make an impression. The cost of making a press joint is high because of the machining required and difficulties in assembly.

Table 4-1 Bolt dimensions and properties of fasteners
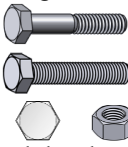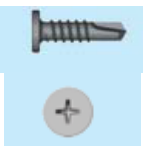
SERIES	FASTENER	APPLICATION	EMBEDMENT	PILOT HOLE DIA	LENGTH/MATERIAL
F1	M8 grade 8.8 Bolt head and nut	With washers on both sides		8.4mm	Carbon Steel quenched and tempered
F2	EJOT JT2-NH3 5.5x19 P2 Drive	Fixing cold rolled section to cold rolled section to a total of 3.0mm in thickness where a flat headed fastener is required.			Organically coated carbon steel.

Table 4-2 Material properties

| Components | Density (g/cm^3) | Elastic | | Plastic | |
		Young's Modulus (GPa)	Poisson's Ratio	Yield Stress/ Ultimate Stress (MPa)	Plastic Strain
S450 Section S450GS+Z	7.85	200	0.3	450 500	0 0.14
Bolts M8 grade 8.8	7.85	200	0.3	580 800	0 0.12
Screw JT2-NH3 5.5×19	7.87	200	0.3	415 540	0 0.1

4.2 Specimens of connection

Specimens selected in the research were selected from Albion Sections products. Twenty seven specimens were modelled in the simulation. They were divided into 2 series and 3 groups. Each of series respects either bolted or screwed T-joint. To be noticed, with the same group, the only differences between series F1 and F2 were the number and the type of fasteners, where F1 means the T-joint with one single bolt (see Figure 4-1); F2 stands for the

T-joint with two screws (see Figure 4-2). The variant in group 1 (G1) was the thickness of the stud section. Group 2 (G2) aims to find out the effect caused by the dimensions of the sections, with the same thickness. The influence of flange width and stud thickness was considered in group 3 (G3). Each group contents three specimens (A, B and C). The sections (see Figure 4-5) are manufactured from S450 steel with Z275 galvanized coating sheets. Dimensions and information of the fasteners are presented in Table 4-3.

Table 4-3 Dimensions and properties of Specimens

Specimen	Sections	WEIGHT Kg/m	DEPTH mm	FLANGE mm	LIPS mm	THICKNESS mm	Area cm^2
G1A	AS1005712	2.15	100	57	12	1.2	2.80
	AT1045013	2.03	104	50	0	1.3	2.62
G1B	AS1005713	2.32	100	57	12	1.3	3.03
	AT1045013	2.03	104	50	0	1.3	2.62
G1C	AS1005715	2.66	100	57	12	1.5	3.48
	AT1045013	2.03	104	50	0	1.3	2.62
G2A	AS2007620	5.75	200	76	15	2.0	7.48
	AT2046320	5.06	204	63	0	2.0	6.52
G2B	AS2257620	6.14	225	76	15	2.0	7.98
	AT2297520	5.82	229	75	0	2.0	7.50
G2C	AS3007620	7.32	300	76	15	2.0	9.48
	AT3067220	6.94	306	72	0	2.0	8.92
G3A	AS1506012	2.74	150	60	15	1.2	3.54
	AT1545820	4.11	154	58	2.0	5.32	190.23
G3B	AS1506320	4.55	150	63	15	2.0	5.96
	AT1545820	4.11	154	58	2.0	5.32	190.23
G3C	AS1506730	6.84	150	67	15	3.0	9.06
	AT1545820	4.11	154	58	2.0	5.32	190.23

a) AS section   b) AT section
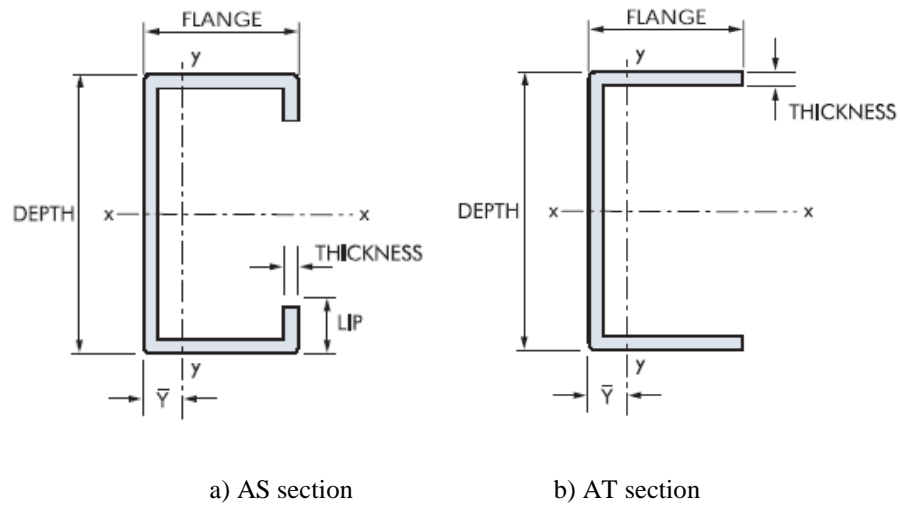
Figure 4-5 Sketch of the sections

4.3 Modelling process

Two FEM models were established in the analysis. The differences between the initial and modified models came to the constraint and interaction properties and the element type and meshing. The modelling process is listed as follows.

4.3.1 Material properties

Material properties of the steel C-sections were modelled by using a double linear stress-strain model (see Figure 4-6) with Von Mises yield criterion and the isotropic hardening rule.
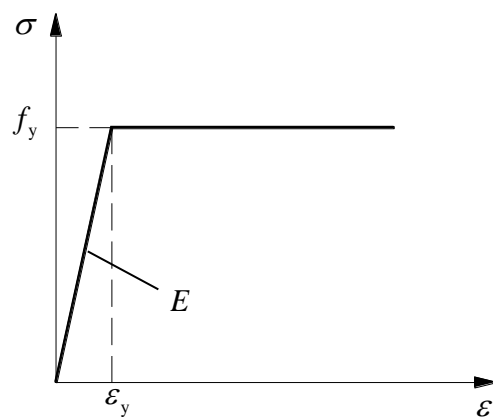
Figure 4-6 Double linear stress-strain curve

4.3.2 Loading and boundary conditions

With regard to the bolt in the simulation, the bolt load of 1640N was applied on each bolt (see Figure 4-7) to simulate pre-tightening force in the installation process. It was added by Apply force method. The Fix at current length method was selected in the following analysis step. In the third step of the T-joint analysis, a displacement load (DL) was directly applied at the top of the cross-section in the analysis step. In order to increase the computing efficiency, only half of the specimen was modelled. Symmetry constraint was applied at the symmetrical sections. The bottom of the T-joint was fixed. The lengths of the stud and track sections were 600mm and 300mm respectively (see Figure 4-8).
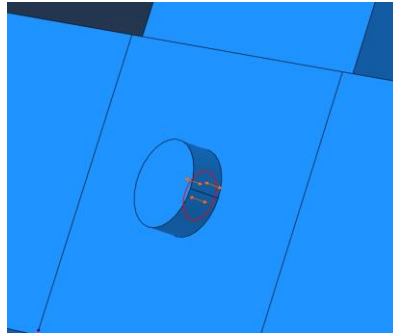
Figure 4-7 Bolt load
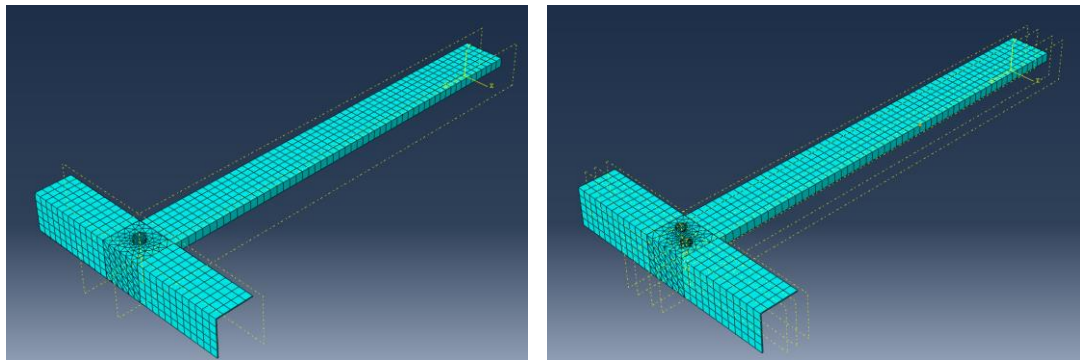
a) Bolted T-joint   b) Screwed T-joint

Figure 4-8 Configurations of T-joint

4.3.3 Constraint and Interaction properties

General contact was employed in the modelling. Friction coefficient 0.3 was considered in all contact surfaces and was isotropic. The modelling applied "Hard" contact relationship to the

minimizes the penetration of the slave surface into the master surface at the constraint locations and does not allow the transfer of tensile stress across the interface. "Tie" constraint was applied on bolts and screws. In details, the inner faces of the nuts and heads were tied on the surface of the contacted components. As a simplification for screw joint, the tie constraint was also applied between screw shank and the edges of the openings with regard to the occlusal force around the holes.

In the contact definition, the surface-to-surface discretization method includes two sliding formulations, being finite sliding and small sliding. The finite-sliding formulation permits any arbitrary motion of the surfaces. The software continually tracks the interactive master surface and the slave nodes, even if the contacting parts are deformable. It is a complex calculation in the software. The small sliding assumes relatively little movement between the surfaces even the two element undergo large motions. The relationship of the slave nodes and the master surface are established at the beginning. Through the analysis, the determined master surface and the interacted slave surface maintain the original relationships. Any rotation and deformation of the master surface and the load path update are only considered in the geometric nonlinear analysis.

In the modification of bolted connection, small-sliding interaction was set between nut and correspondingly contacted surfaces. A quarter of the bolt head interface was tied to the track. Besides, the interaction of the shank surface and the bolted holes was defined by finite-sliding. As for the self-drilling screw, in the contact surfaces between screw and components, finite-sliding was also applied. But tie constraint was used in the second drilled plate. It is assumed that, in the drilling process, the first drilled hole is supposed to be loose. However, the second plate can present better occlusion.

4.3.4 Solution scheme

This research focused on obtaining the full range of load-deflection connection responses in the FE modelling. The pre-load of the bolt was added in the previous analysis steps by using general static method. The geometric nonlinearity and a nonlinear incremental-iterative Full

Newton solution technique were applied in the following analysis step. The linear and nonlinear global buckling analysis of the stud components is not the research emphasis. The installation procedure of the fasteners may cause deficiency around the opening holes. In the experiments, this deficiency is infinitesimally small. Therefore, the imperfection settings were not included in this case.

4.3.5   Element type and meshing

3D solid element was used in the simulation process, which is more capable of analysing connections and fasteners (Kim et al., 2007). The 10-node solid element C3D10 (A 10-node quadratic tetrahedron) was applied around pre-opening area the area. While the 8-node solid element C3D8R (An 8-node linear brick, reduced integration, hourglass control) was used for the rest parts and fasteners (see Figure 4-9). The degrees of freedom of each node include 3 translations for the solid element.

Meshing is closely related to the convergence and precision of FEM modelling. For the fasteners, the approximate global sizing was defined as 1.6mm. In terms of CFS components, the value was 10mm. The area with open hole was separated by using the element shape of Tet (see Figure 4-10). Other parts were meshed by the element shape of Hex-dominated with Sweep technique.

a) Linear element   b) Quadratic element   c) Second-order element

(8-node brick, C3D8)   (20-node brick, C3D20)   (10-node tetrahedron, C3D10)
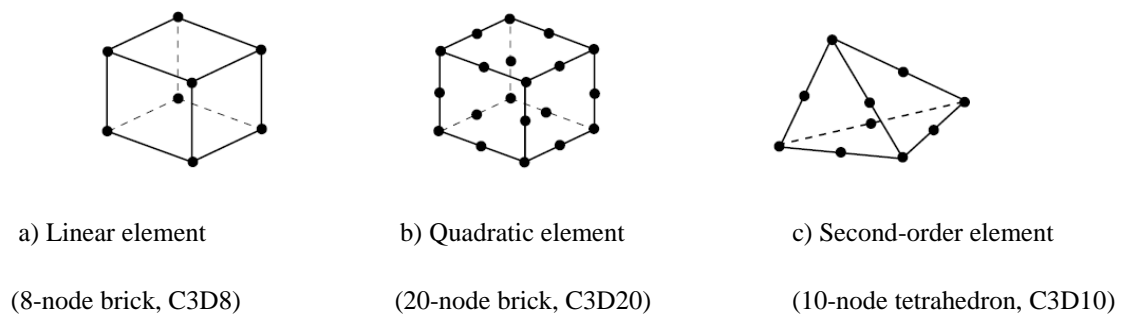
Figure 4-9 Element types of ABAQUS (Abaqus-6.13, 2013)

| a) Meshing near bolt holes | b) Meshing near screw holes |
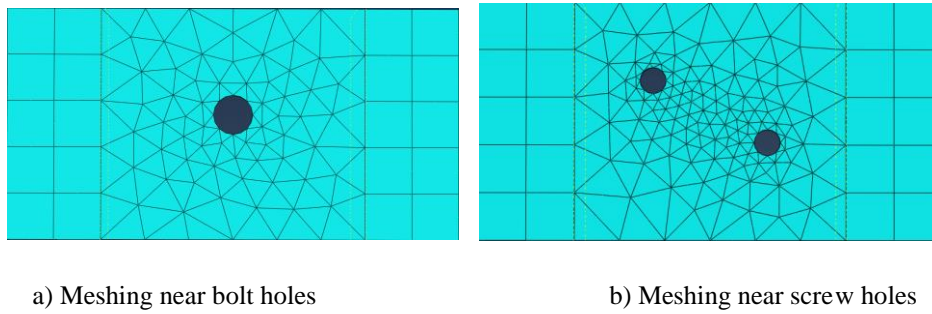
Figure 4-10 Finite element meshing

By experience, Hex or Hex-dominated element shape are more regular, presenting more accurate and better convergence than other element shapes (Shi and Zhou, 2006). Therefore, Tet element shape was replaced by Hex element shape with structured technique in the modified modelling (see Figure 4-12). The element type was C3D20 (20-node quadratic brick). For the the fasteners, the approximate global sizing was defined as 1.6mm. In terms of CFS components, the value was 10mm.

4.4 Sensitivity

Finite element analysis software ABAQUSv6.13 was employed in the numerical study. The sensibility of modelling, as an indication, assists to find out the effective and efficient numerical analysis method. Taken single lapped shear joint as study subject, the dimension of connected plates was: length 100mm; width 50mm; thickness 1mm. The diameter of the screw shank was 5.5mm. The results of FEM simulation are presented in Figure 4-11.

In general, higher density meshes produce more accurate results. On the other hand, more number of elements needs more computing time in the analysis. As a result, the resistances of the models changed with the increasing of the mesh density. However, when number of the element exceeded 2000, the sensibility of the modelling became insignificant (see Figure 4-11). After making balance between the accuracy and time consumption, the appropriate meshing was selected as the sixth modelling and applied in the following simulation.
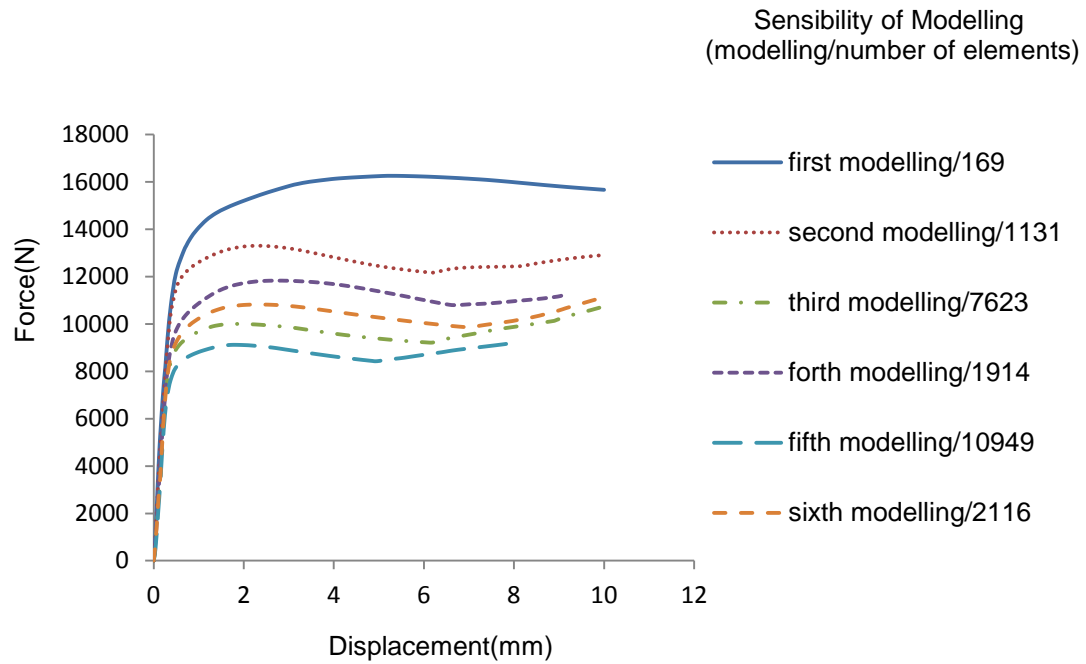
Figure 4-11 Sensibility of modelling

4.5 Results

The stress distribution of specimen F1G1A is demonstrated in Figure 4-12. Figure 4-13 illustrates four steps in the failure process. In the first step, friction between the surfaces of bolt and plates resists the loading. As the force rises, the displacement of the connection increases linearly. After that, the curve reached a flat. The reason is that the diameter of pre-opening hole (8.4mm) is larger than that of the shank (8.0mm). The clearance is supposed to lead to the slipping between the contacted interfaces. In the next step, shearing, slope and tension developed in the bolt. The stiffness of the connection is reduced along this period. With the displacement of the stud increased by the pressure, the bottom surface of stud hit the track, which is the reason that the force-to-displacement curves go up dramatically in the last step.

The gap of 0.7 mm exists in the specimen F1G1A. The gap can be eliminated by slightly adjusting section AS1005712. It can be found that, even the magnitude is very small, the strength and stiffness of the connection are changed considerably (see Figure 4-13). It should

be noticed that, in the third step, the connection without gap reaches the peak load 15.98kN with the displacement of 2.3mm. The corresponding load that with gap is 14.98kN being reduced 6.6%.

The warping and buckling in the stud may influence the resistance of T-joint. Thus, tensile force was applied as comparison. In order to eliminate the redundant support of the track, the web of the track was removed in the modelling. In that case, the descent stage of the load-displacement curve was obtained. It can be found that the bolted connection subjected to tensile force have better structural performance in the post-failure stage (see Figure 4-14).

Figure 4-15 demonstrates the meshing and stress distribution of the screwed connection in specimen F2G1A, with the gap of 0.7mm between stud and track. With the displacement of 0.75mm, the peak load is achieved as 11.48kN, which is much lower than the predictions of AISI (2007) and Kwon et al. (2008) (see Table 4-4).

a)   b)

c)   d)
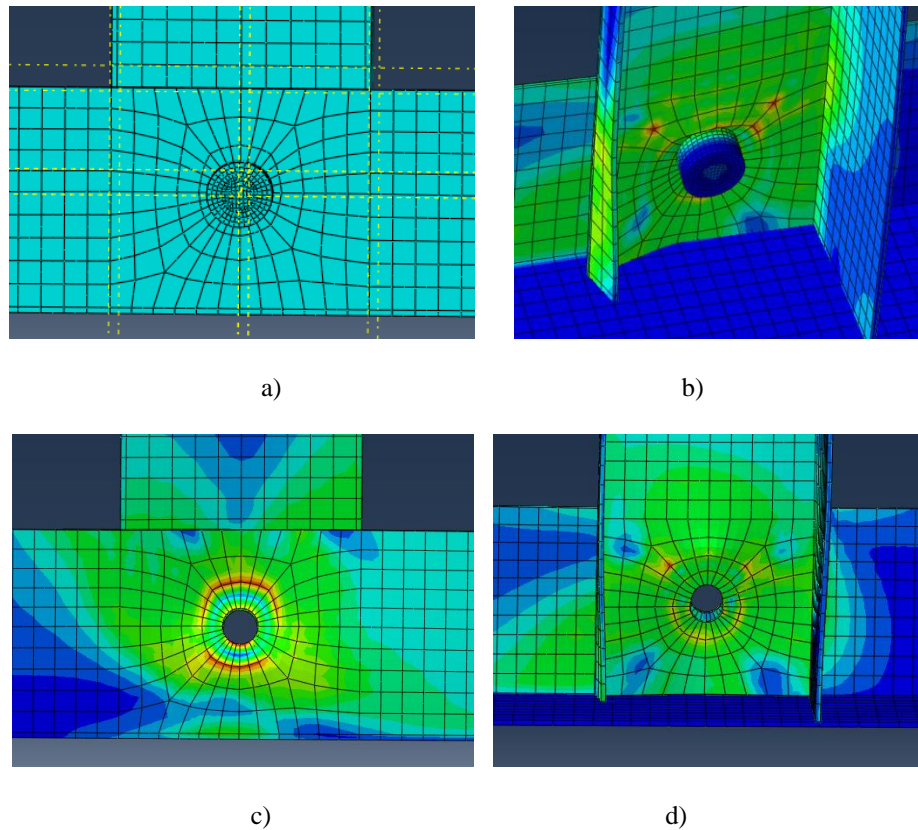
Figure 4-12 Meshed by Hex element shape (F1G1A)
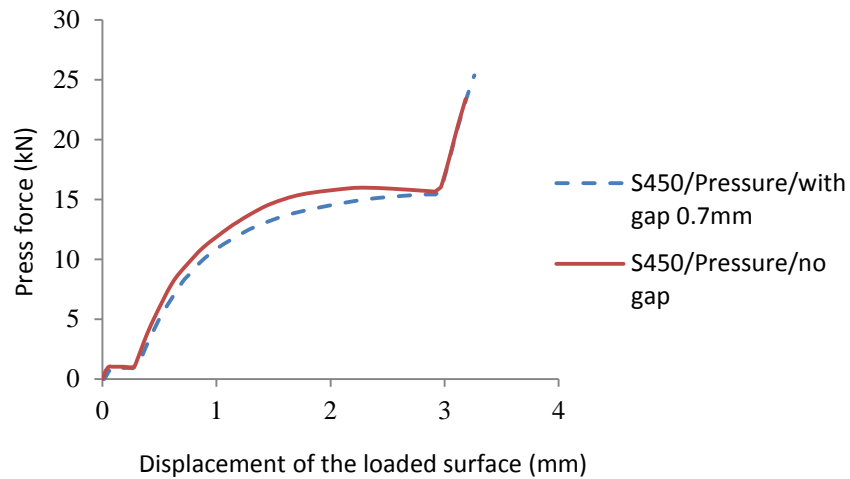
Figure 4-13 The effect of gap in bolted connection
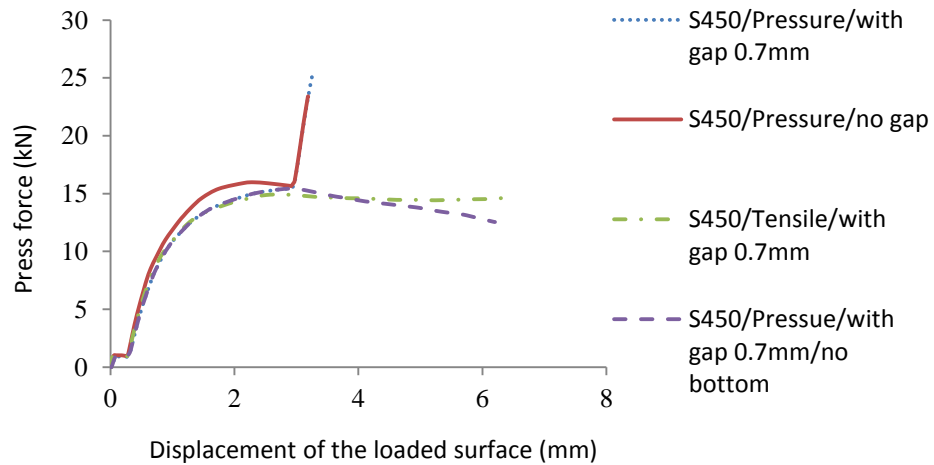
Figure 4-14 Comparison of bolted connection

As shown in Table 4-4, there is notable difference between the resistance predictions of the initial and modified modelling. The peak load of specimen F1G1A dropped from 47.03kN to 14.98kN. The initial modelling provides stronger constraints, leading to the ultimate load of the bolted connection apparently higher than the modified modelling. The result of the modified modelling is in good accordance with the bearing strength predicted by the semi-empirical formula (Yu and Panyanouvong, 2013). Whereas, the bearing strength obtain by the modified modelling is supposed to undervalue the resistance of the screwed connection, indicating that the constraints between the fastener and connected components were insufficient.

a)   b)

c)   d)
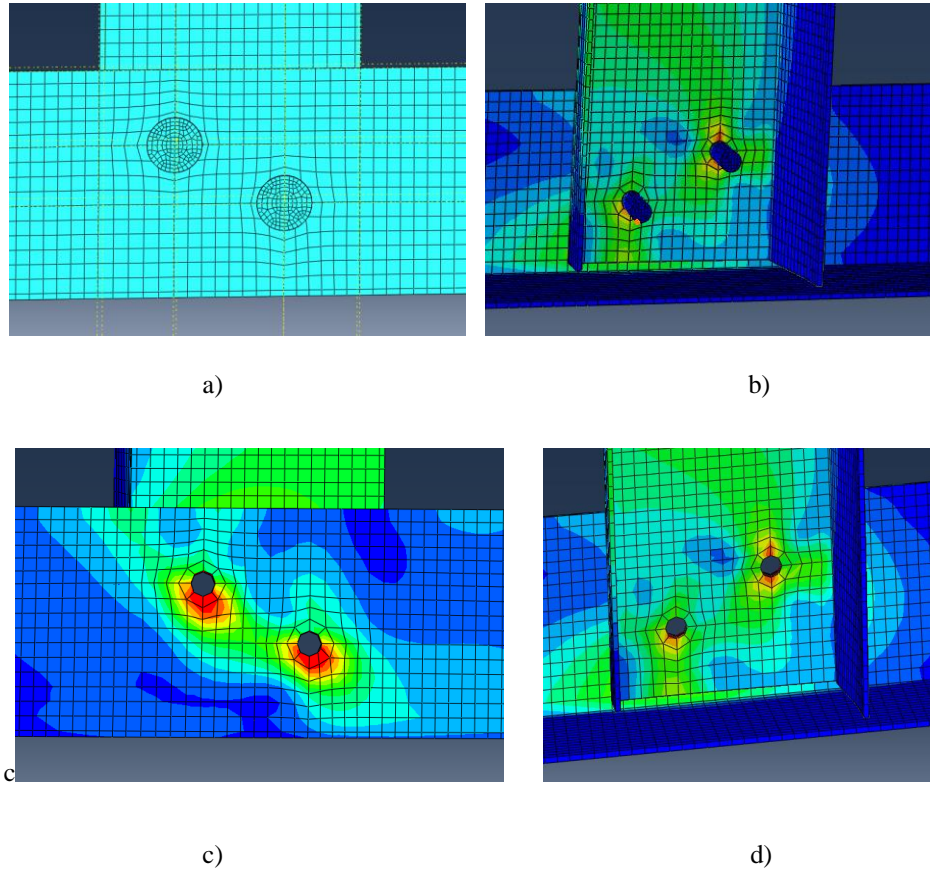
Figure 4-15 Meshed by Hex element shape (F2G1A)

Table 4-4 Comparison of numerical results

SPECIMEN	BOLT LOAD (N)	AISI specification results (AISI., 2007) (kN)	Bearing strength with gaps (kN)	Ultimate bearing capacity of initial modelling (kN)	Ultimate bearing capacity of modified modelling (kN)
F1G1A	1640	16.79[a]/21.60[b]	15.10(Yu and Panyanouvong, 2013)	47.03 (with gaps)	14.98 (with gaps)
F2G1A	N/A	25.90[c]	28.36/40.69(Kwon, 2006)	27.26 (with gaps)	11.48 (with gaps)

Note: The gap is 0.7mm. "a" means the nominal bearing strength in bearing strength between bolts and steel sheets considering the bolt hole deformation; "b" stands for the nominal bearing strength in bearing strength between bolts and steel sheets without consideration of the bolt hole deformation; "c" represents the nominal bearing strength limited by tilting. The results of screwed connection presented in this table represent the ultimate bearing capacity obtained when the gap between the connected plates is large and the gap is not considerable respectively (Kwon et al., 2008).

4.6 Parametric study

Based on the comparison, the constraint and interaction properties of the initial modelling are employed to simulate screwed connections. The simulation analysis of bolted connection adopts the modified FE method. In contrast with the bolted connections, the screwed connections provide much greater bearing capacity in the modellings (see Table 4-5 and Table 4-6).

The prediction of connections resistance provides a good agreement with the results of the semi-empirical studies (Kwon, 2006, Yu and Panyanouvong, 2013) and the prediction of current specification AISI (2007). Whereas, a deviation can be observed in the prediction of bolted connection resistance compared to the nominal bearing strength without consideration of bolt-hole deformation.

Apart from fasteners, the connection resistance is also influenced by the dimensions of the connected components, such as section depth, width and thickness. The connection featuring higher level of strength with less steel consumption presents better structural efficiency. Regarding to gaps and increasing dimensions, the relationship between the steel volume increase of the T-joints and connection resistance increase is shown in Figure 4-6.

According to numerical results of the bolted connections, the ultimate bearing capacity of the connection is improved by 14.51%, with the increasing of steel volume due to the stud thickness by 12.83%. The results of Group 2 indicate that the flange and web dimensions present insignificant effect on the load carrying capacity of the connection. As shown in group 3, when the thickness increases, the steel volume grows by 53.85% with the connection resistance improved by 136.53%. The similar trend is obtained by the screw connections.

It can be concluded that increasing stud thickness is the efficient way to enhance the bearing capacity of the stud-to-track connections. However, the influence of the thickness increasing on screwed connections with gaps is greater than that on the bolted connections with gaps in

group 1 (see Figure 4-16) which reveals that the bolted connection is more sensitive to the gap. The increasing of web depth and flange width made the ultimate resistance decreased slightly.

Table 4-5 Numerical study results of series 1

Specimen	Gap (mm)	Bolt load (N)	AISI specification results (kN)			Ultimate bearing strength of connection with gaps (Yu and Panyanouvong, 2013) (kN)	Ultimate bearing capacity obtained by FEM (kN)
			Nominal bearing strength without consideration of bolt hole deformation	Nominal bearing strength with consideration of bolt hole deformation	Ultimate shear strength/resistance of bolts		
F1G1A	0.7	0	21.60	16.79	80.38	15.10	14.16
		1640					14.98
F1G1B	0.7	0	23.40	18.38	80.38	17.52	14.86
		1640					15.38
F1G1C	0.7	0	23.40	18.38	80.38	17.52	16.40
		1640					17.15
F1G2A	0	0	36.00	30.33	80.38	32.40	36.33
		1640					37.82
F1G2B	0	0	36.00	30.33	80.38	32.40	36.82
		1640					38.15
F1G2C	1	0	36.00	30.33	80.38	32.40	33.21
		1640					34.12
F1G3A	0	0	21.60	16.79	80.38	15.10	16.83
		1640					17.03
F1G3B	0	0	36.00	30.33	80.38	32.40	36.44
		1640					38.14
F1G3C	0	0	36.00	30.33	80.38	32.40	38.06
		1640					40.29

Table 4-6 Numerical study results of series 2

| Specimen | Gap (mm) | AISI specification results (kN) | | | Ultimate bearing strength of connection with gaps (Kwon et al., 2008) (kN) | Ultimate bearing capacity obtained by FEM (kN) |
		Nominal bearing strength limited by tilting and bearing	limitations	Ultimate bearing strength/resistance of screws		
F2G1A	0.7	25.90	tilting	51.29	28.36/40.69	27.26
F2G1B	0.7	29.20	tilting	51.29	31.98/45.89	32.67
F2G1C	0.7	36.44	tilting and bearing	51.29	31.98/45.89	42.15
F2G2A	0	55.72	tilting	51.29	61.03/87.56	61.49
F2G2B	0	55.72	tilting	51.29	61.03/87.56	61.38
F2G2C	1	55.72	tilting	51.29	61.03/87.56	54.32
F2G3A	0	25.90	tilting	51.29	28.36/40.69	28.20
F2G3B	0	55.72	tilting	51.29	61.03/87.56	53.47
F2G3C	0	59.40	bearing	51.29	61.03/87.56	60.96

Note: The results of screwed connection presented in this table represent the ultimate bearing capacity obtained when the gap between the connected plates is large and the gap is not considerable respectively (Kwon et al., 2008).

a) Bolted connection

b) Screwed connection
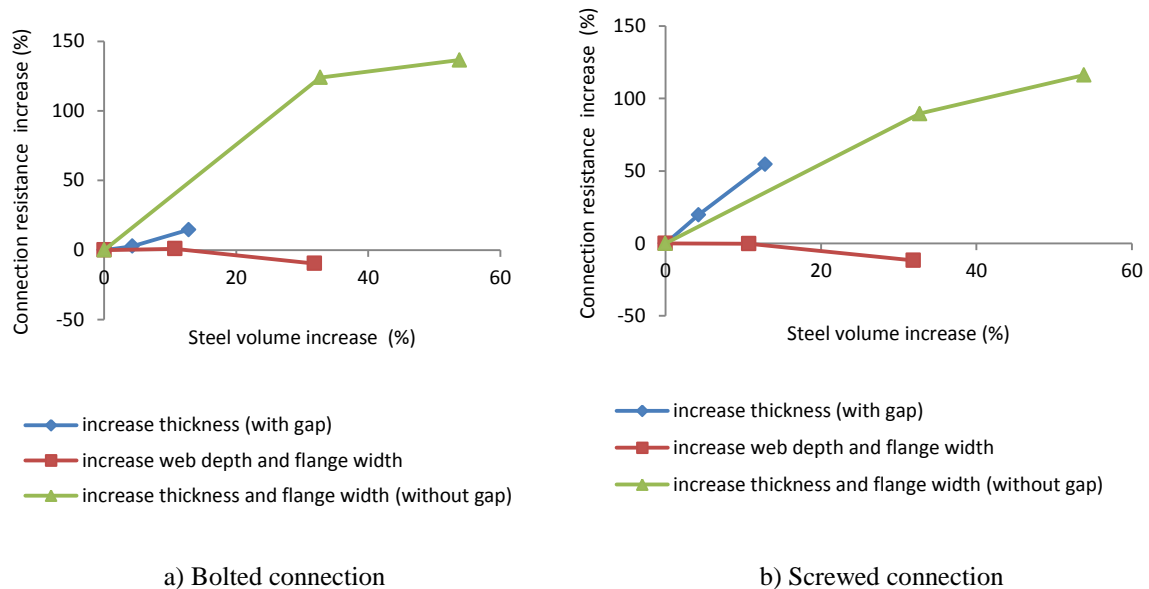
Figure 4-16 Influence of the variables

4.7 Summary

Various joining methods have been presented in this chapter. In contrast, screw and bolt with easy installation is more appropriate for CFS modular constructions. The FE models of stud-to-track connection with screw and bolt joint were discussed in this chapter. It can be found that the settings of constraint and interaction between the fasteners and the connected components significantly influence the analysis outcomes. In terms of bolted connection, the modified model with pre-tightening force and clearance between connected components presented a good agreement with the existing semi-empirical formula achieved by test results. Whereas, the initial modelling have been proved to be applicable to simulate screwed connection. The parametric study was also conducted using the dimensions of the exist products. It was concluded that increasing the component thickness is an efficient measure to improve the connection resistance. However, the gaps can significantly limit the performance improvement of the bolted connection. M8 bolt is overly strong for the thin-walled sections, whereas, double-screw joint is a relatively more effective solution in the thin-walled systems. In addition, the resistance reduction of the connection caused by the gap (1mm) was evaluated to be around 10%.

CHAPTER 5 EXPERIMENTAL STUDY OF SCREW JOINTS

5.1 Introduction

The traditional connection methods of CFS include weld, bolt and screw joints. The current codified design approaches are not adequate to consider those joints subjected to the combined loading scenario. Due to the diversely designed connections, complex loading scenarios may act on a joint. Thus, it has become significant to have a deep understanding the behaviour of a joint under combination of the different actions. In this chapter, an experimental study of screwed joints with high strength steel (S550) was conducted. The loading scenarios include the single and double shear, tension, and the combination of tension and shear. In addition, finite element models (FEMs) were developed to reproduce the physical experiments and reveal the mechanism of a joint under action. Results showed that the shearing resistance of screw joints will be decreased significantly in the presence of the combined action. In the experimental investigations reported in this chapter, the S550 steel was employed. A number of loading scenarios that can be encountered in the light steel frame or modular system were considered in the test regime. A test configuration was designed to facilitate the variation of the tension/shear ratio. The entire–process behaviours of the connections would be recorded and presented in this chapter. The first-hand test results can be used for the calibration of the parameters needed in FE modelling.

5.2 Experimental study

5.2.1 Test program

To examine the structural behaviour of S550 CFS screw and bolt joint, a series of tests were arranged using testing machine ZwickReoll-Z100. The material properties of the connection components were evaluated through the coupon tests. It was then followed by three groups of tests, i.e. (1) pure shear tests detonated as "S" for screw joints and "B" for bolt joints; (2) pure

tension test detonated as "T"; (3) combined shear and tension detonated as "TS". The group S involved three variables, i.e. the thickness of plate, the number of screws and the type of shear tests (single and double shear). The groups B and T only concerned the variable of plate thickness. The group TS included the variable of tension to shear. Each sample was tested until failure, from which the load-displacement curves and failure modes were recorded. In the test program, the 0.8mm and 1.0mm S550 steel plates were employed, which were galvanized on the surface, with the nominal yield stress 550MPa and the ultimate strength 600MPa. Thin-walled plates were connected by hexagon washer head drilling screws with tapping screw thread (see Figure 5-1). The nominal diameter (d) of the screw was 5.5mm. There was a 1mm plastic washer at the bottom of the screw head. The sketch of the hexagon head M8 bolt and nut is shown in Figure 5-2. Details of test specimens and the test instrument are illustrated in Table 5-1.
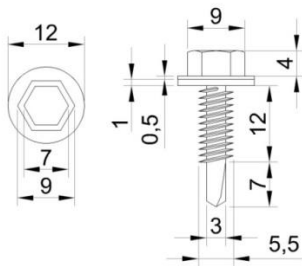
Figure 5-1 Hexagon washer head drilling screws (mm)
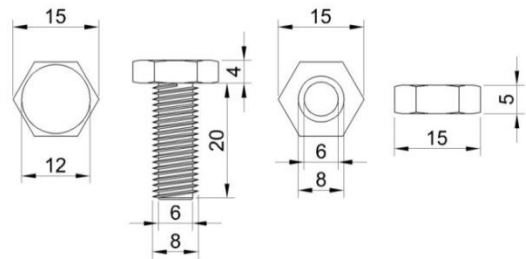
Figure 5-2 Hexagon head M8 bolt and nut (mm)

5.2.2 Test specimens and set-up

5.2.2.1 Coupon test

As shown in Figure 5-3, S550 steel strips were used to test the material properties according to ISO 6892-1:2009 B4 (ISO., 2009).
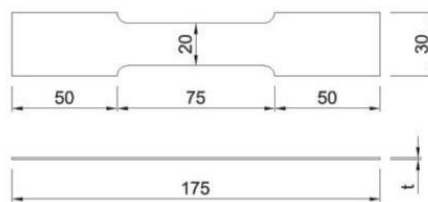
Figure 5-3 Steel strip for material property test

In this part, steel strips were clamped by the jaws of testing machine before a tensile force was applied until its rupture. The stress-strain curve was obtained by the average of three duplicate tests in each group.

5.2.2.2 Shear connection tests

The dimension of plates in shear tests was 100mm in length and 50mm in width, with 50mm overlapping length. Screws were installed by using self-tapping screw gun while pre-drilling hole was not requested for the very thin thicknesses. The distances from the centre of each screw to the edge of the plate and between the centres of screws were more than $3d$ (AISI., 2007, Eurocode, 2006b) in order to avoid screw longitudinal shearing failure and tearing failure in the net cross section respectively. Observations included failure modes and force-to-displacement curves of the joints. The thicknesses of connected plates are respectively represented by t1, t2 and t3 as indicated in Figure 5-4 to 5-7. The ID and geometric dimensions are listed in Table 5-1.
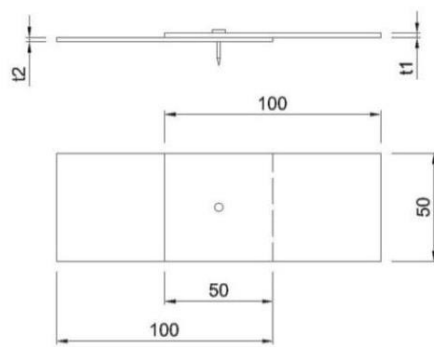
Figure 5-4 Screw shear test   Figure 5-5 Double screw shear test
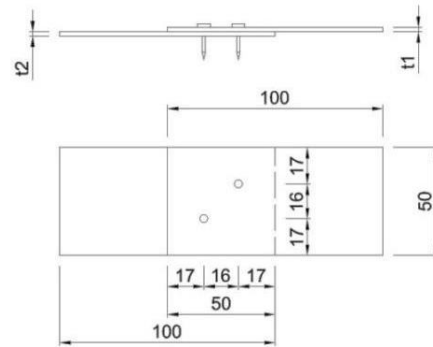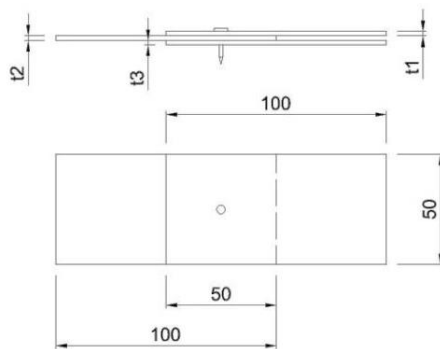
Figure 5-6 Double shear screw test   Figure 5-7 Bolt shear test
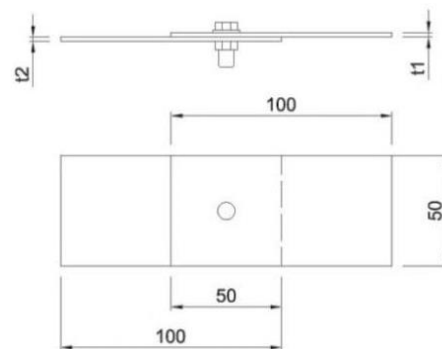
Table 5-1 Screw shear joint test samples

Specimen	Pattern	Length (mm)	Width (mm)	Over-lap (mm)	t1/t2/t3 (mm)	Duplicated
S1	single shear/one screw	100	50	50	0.8/0.8	2
S2	single shear/one screw	100	50	50	0.8/1.0	2
S3	single shear/one screw	100	50	50	1.0/0.8	2
S4	single shear/one screw	100	50	50	1.0/1.0	2
S5	single shear/two screws	100	50	50	0.8/0.8	2
S6	single shear/two screws	100	50	50	1.0/1.0	2
S7	double shear/one screw	100	50	50	All 0.8	2
S8	double shear/one screw	100	50	50	All 1.0	2
B1	single shear/one bolt	100	50	50	0.8/0.8	2
B2	single shear/one bolt	100	50	50	1.0/1.0	2

5.2.2.3 Tension connection tests

The test specimens were made by two U-sections connected back-to-back by a screw at the centre of the webs. The angle θ between web and flange of the U section is 90°. A fixture (see Figure 5-8) was designed to restrain the specimen (see Figure 5-9) to the test machine (see Figure 5-10).

The eight M8 bolts employed to connect the specimen and the fixture had adequate strength and stiffness. The fixture was clamped by jaws and can be reused. The description of samples is listed in Table 5-2.
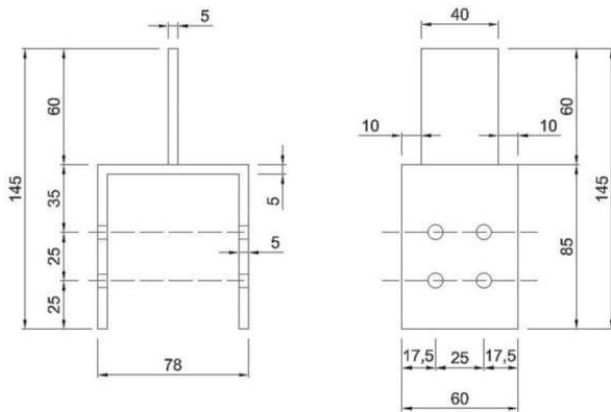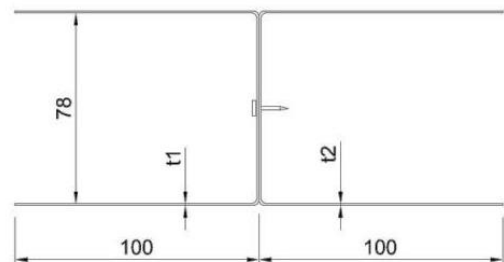
Figure 5-8 Fixture   Figure 5-9 Specimen of tension test
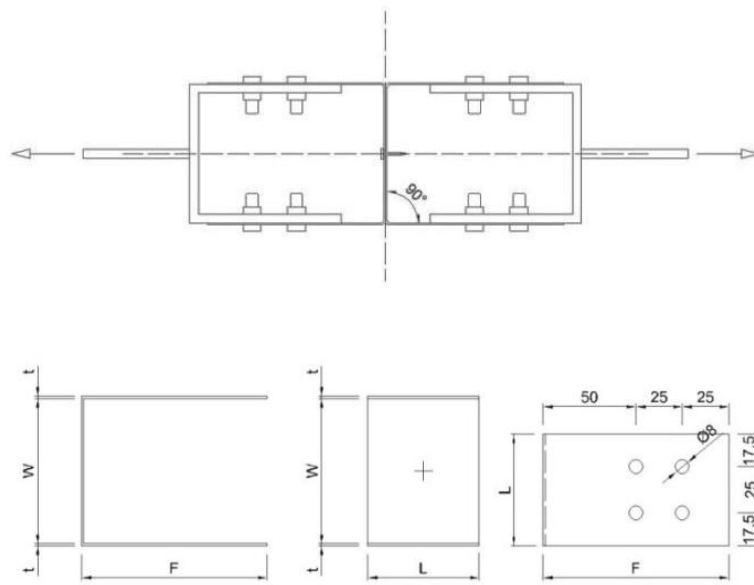
Figure 5-10 Schematic illustration of tension test

Table 5-2 Tension test samples

Specimen	Patterns	L (mm)	F (mm)	W (mm)	t1/t2 (mm)	Duplicated
T1	tension/one screw	60	100	78	0.8/0.8	2
T2	tension/one screw	60	100	78	1.0/1.0	2

5.2.2.4 Combined shear and tension tests

The combination of shear and tension was achieved by the sloped U-sections (see Figure 5-11). These components involved three different loading angles θ such as 30°, 45° and 60°, as shown in Figure 5-12.

To facilitate the application of screws by using the screw gun, two short flange lengths were designed. Two extension plates were used to connect the test samples and the fixture after the screw was applied (see Figure 5-13). The extension plates had 1.0mm thickness, 60mm width. The length was determined by the fixed length of the short flange, i.e. 110mm as indicated in Figure 5-13, and the slope angle of the web plate. The extension plates were bonded to the flanges of test samples by epoxy resin adhesive.

The strength of the adhesive joints was also verified to have shear strength 23MPa and tensile strength 35MPa, which meet the test requirements. The details of specimen dimensions are shown in Figure 5-11 and Table 5-3.

At the other ends, they were connected to fixtures by bolts. The fixtures for the combined shear and tension tests were the same as those shown in Figure 5-8 for the tension tests.
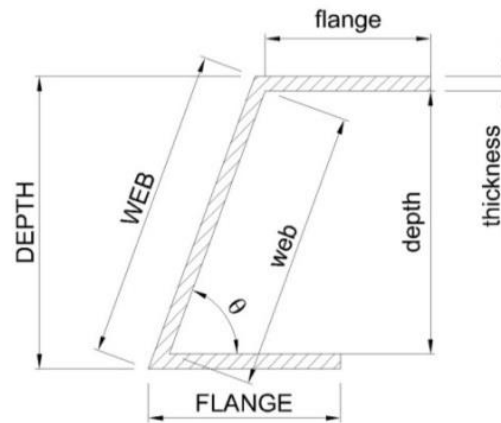
Figure 5-11 Dimensions of shear-tension test specimen

Table 5-3 Combined tension and shear test samples

Specimen	Patterns	web (mm)	Width (mm)	flange (mm)	t1/t2 (mm)	θ (°)	Duplicated
TS1	Combined load/one screw	92	60	20	1.0/1.0	60	2
TS2	Combined load/one screw	113	60	30	1.0/1.0	45	2
TS3	Combined load/one screw	160	60	40	1.0/1.0	30	2

a) Specimen TS1   b) Specimen TS2   c) Specimen TS3
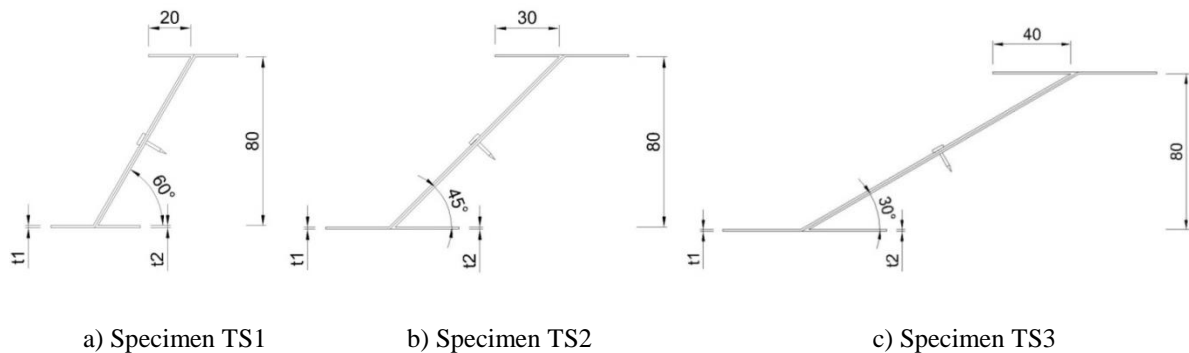
Figure 5-12 Specimens of sloped tension test

a) TS1

b) TS2

c) TS3
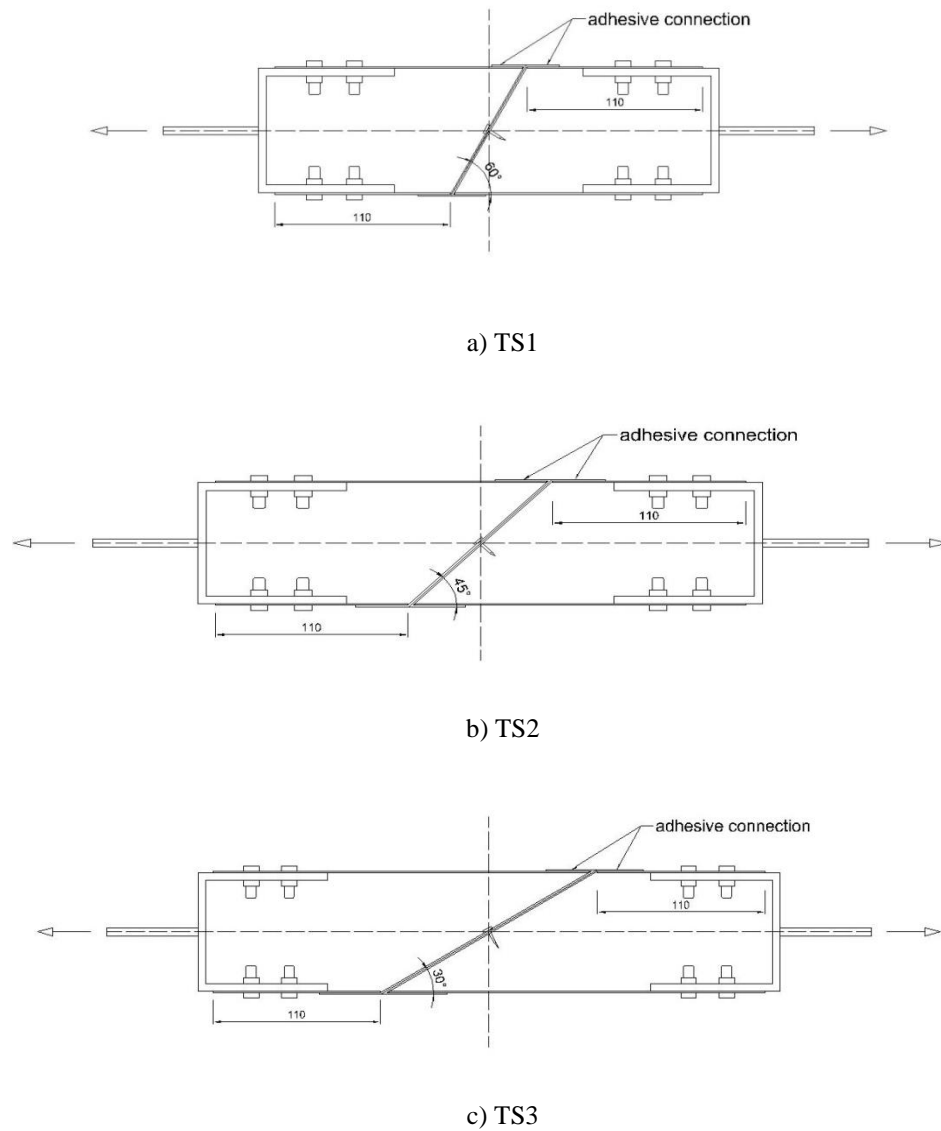
Figure 5-13 Schematic illustration of sloped tension test

5.2.3 Test procedure

The tests, including material coupon test and joint tests, were performed using the 10T ZwickRoell static material testing machine. The machine recorded the data of applied force $F_{,test}$ and cross-head displacement $D_{,test}$ every 0.1 second until the joint failed. Tests were conducted by displacement control mode at a rate of 2mm/min for screw shear test and 1mm/min for pure tension and combined shear and tension tests. When the applied load dropped more than 80% between two consecutive loading increments, the test stopped automatically. In the pure tension and combined shear and tension tests, the separations at the

web centre (D_c) and those of 30mm distance from the centre were also recorded by demec strain gauge at around 100N increments. In that case, U-section (see Figure 5-9) and sloped U-section (see Figure 5-11) components were connected by screw in the web. In fact, the cross-head displacement consists of bending in the flanges, rotation at the section corner, web deformation and the movement of the screw joint. However, the diverse dimensions of specimens brought about different deformation under loading. To make the results comparable, a 60×60 (mm) plate was taken into account.
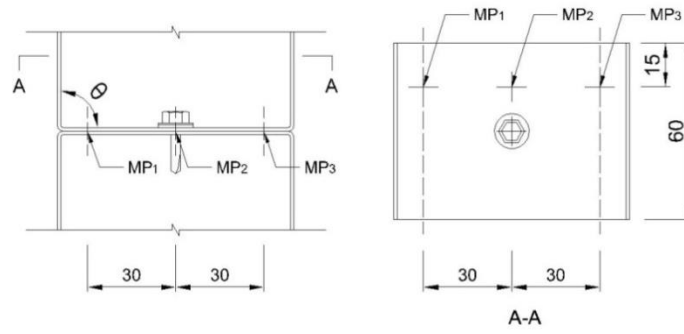
a) Locations of measuring points
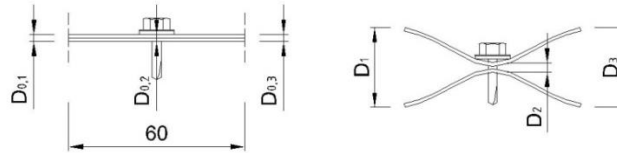
b) Initial and developed separations

Figure 5-14 Illustration of the measurement

Measure points (MPs) are shown in Figure 5-14. In details, $D_{0,1}$, $D_{0,2}$ and $D_{0,3}$ stand for the initial distance between the up and down surfaces at each MP respectively. During the test, the distance at each MP was represented by D_1, D_2 and D_3. Hence, it can be derived that the relative displacement $D_c = D_2 - D_{0,2}$. The same processing method was applied for the measurement at MP1 and MP3. Considering the symmetry of the test sample, the separation at 30mm away from the screw centre (D_{30}) was assumed to be the average of those at MP1 and MP3, i.e. $(D_1 - D_{0,1} + D_3 - D_{0,3})/2$.

5.2.4 Test results

5.2.4.1 Coupon test

Specimens were loaded until rupture (see Figure 5-15) occurred. Results are listed in Table 5-4 comprising of three duplications.

Figure 5-15 S550 steel specimens and failure mode

Table 5-4 Specimen dimensions of material property tests

Specimen	material	Thickness(mm)	b_0(mm)	E(GPa)	f_y (MPa)	f_u(MPa)
1		0.98	18.96	223	543	559.8
2	S550	1.00	21.60	257	513	514.31
3		0.99	20.82	200	483	550.46

Note: b_0 is the middle width of the specimen.

On the average, elastic module was taken as E=211.5GPa. Yield strength f_y= 513MPa was obtained when the strain reached ε_y=0.42%. The ultimate strength f_u=555MPa and the corresponding strain ε_u=4.82%. Figure 5-16 exhibits the strain-to-stress curve of the material.

In the final stage of the tests, the stress of the specimen dropped sharply. However, the fracture of the coupon occurred when the stress decreased to zero. Before the fracture, the strain still increased.
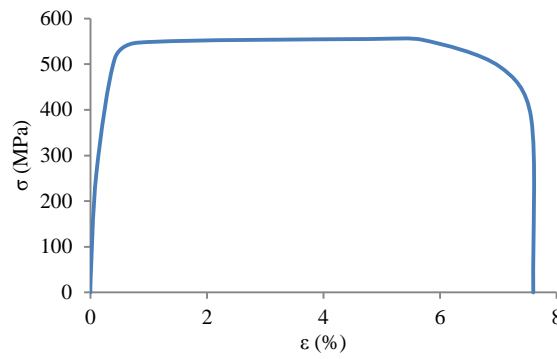
Figure 5-16 Strain-to-stress curve of S550 steel

5.2.4.2 Shear tests

5.2.4.2.1 Failure mode

Failure mode determines the response of lap shear tests (Lorenzo and Landolfo, 2004). In light-gauge steel shear joint made of mechanical fasteners, there are six main types of failure listed as follows: (1) shear failure of fastener (2) fastener fracture (3) tilting and pull-out of fastener (4) bearing failure of either both sheets or thinner sheet only (5) sheet tearing in net section and (6) longitudinal shearing of the sheet. In fact, mixed failure types often occurred in tests. During the tests, the screw appeared to be strong enough, and did not fail in the test scenarios. Due to the amply screw edge and interval distances of the specimens, (5) and (6) were also not involved in current single lap shear tests.

In this case, the combination of tilting and bearing failure of both sheets took place. Besides, in double screw single shear joint tests, screws were observed to be pulled out from the bottom sheet. As for the double shear joint, bearing failure occurred ahead of the longitudinal shearing in the middle sheet. Assuming the edge distance between screws and plate ends are sufficient, the bearing capacity of the plate, the tilting resistance and shearing strength of the screw determine the structural behaviour of the screw joint (see Figure 5-17). In the case of the single shear, tilting was supposed to be the most likely failure mode based on specifications (AISI., 2007, Eurocode, 2006b) duo to the eccentrically applied load. To minimize the tilting deformation, the double shear tests were also adopted. The latter can eliminate the effect of bending effect on the connection. Thus, the tilting effect was not

dominant. In order to find out a better connecting solution, single bolt joints were employed as a comparison of double screw joints.

a) Bearing in the sheet   b) Screw tilting   c) Shearing in the shank
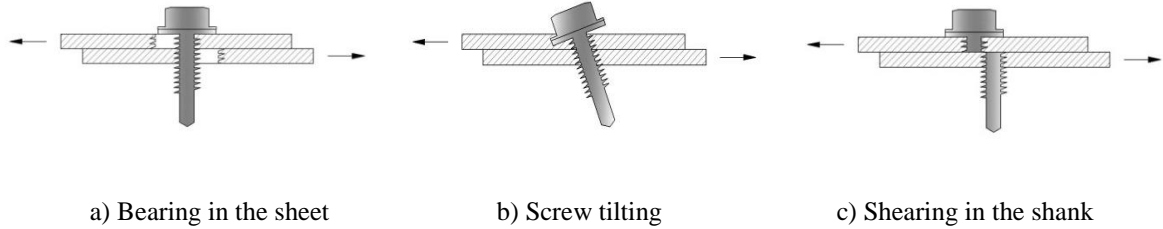
Figure 5-17 Failure modes of screw joint

In Table 5-5, specimen dimensions, failure modes (see Figure 5-18 to 5-21) and the performance of lap shear tests are reported. The comparison between single screw shear specimens (S1, S4) and double screw shear specimens (S5, S6) aims to identify the cluster effect. In terms of single screw single shear tests, it can be found that initial stiffness of the joint is quite small because of the influence of screw tilting. Taking specimen S4 for instance, as plate slip over the screw thread, the curve drops after reaching the peak point and then increases until bearing failure occurs in the sheet. The bolt joint failed with warping and bearing in the sheet (see Figure 5-21).

Table 5-5 Screw shear joint test results

Specimen	L (mm)	W (mm)	t1/t2/t3 (mm)	Failure mode in test	Fu,test (kN)	Du,test (mm)	Dm,test (mm)
S1	99.8	50.2	0.79/0.78	T+B	3.91	4.81	11.14
S2	99.7	50.0	0.80/1.01	T+B	4.18	5.76	8.16
S3	100.2	50.0	1.02/0.79	T+B	4.14	6.31	8.33
S4	99.9	49.8	1.00/1.01	T+B	4.71	4.48	8.11
S5	100.0	49.9	0.80/0.80	T+B+P	8.24	5.57	9.63
S6	99.8	50.0	0.99/1.01	T+B+P	9.66	5.10	10.97
S7	100.0	49.8	0.80/0.79/0.78/0.80	B	5.28	4.45	15.17
S8	99.8	50.2	0.99/1.01/1.00/1.01	B	8.12	7.72	15.15
B1	99.2	50.0	0.78/0.78	B+W	7.44	7.49	11.21
B2	99.1	50.1	0.99/1.01	B+W	8.90	10.88	14.01

Note: The overlapped length was 50mm. T=tilting; B=bearing in the board; P=pull out failure; W=warping in the board; Fu,test=the ultimate force; Du,test=the deformation of joint obtained by testing machine when the ultimate force was achieved; Dm,test=the deformation of joint obtained by testing machine when the joint failed.

Figure 5-18 Single screw lap joint test failure mode (S3)

Figure 5-19 Double screws lap joint test failure mode (S5)

a) Original specimen   b) Failed specimen

Figure 5-20 Screw joint double shear test failure mode (S7)
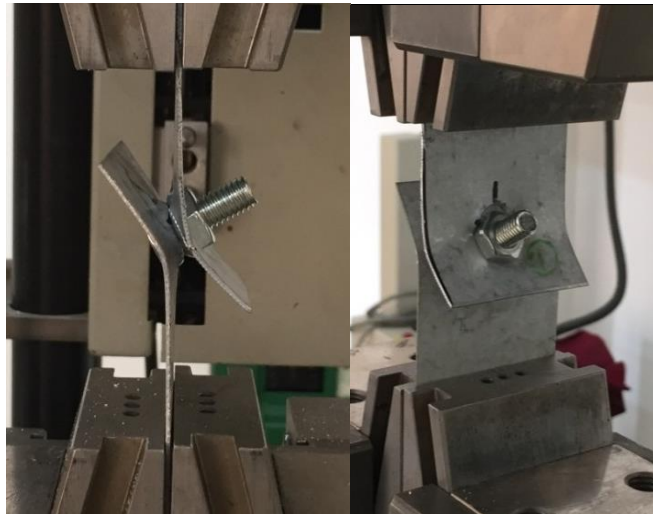
Figure 5-21 Bolt single lap-joint test failure mode (B2)

5.2.4.2.2 Bearing resistance

Force-displacement responses are presented in Figure 5-22. It is clear that double screw shear specimens achieve about twice of the carrying capacity of the single screw shear specimens with the same thick sheets (see Figure 5-22a and 5-22b), whereas a better ductility can be observed from the single bolt joint (see Figure 5-22d). As regards the design aspects, it is small enough to be neglected.

The double shear joint is also a common scenario in light steel constructions. The most striking differences between single shear joints and double shear joints were the failure mode and join motion. The bending moment was balanced by the exterior plates of the joint. These two plates effectively restrained the out of plane movement of the inner plate. Therefore, the bearing capacity of a joint depends on bearing resistance of the sheet, and fastener tilting was not occurred.

The test observation suggests the use of double shear joint when high initial stiffness or ductility-restoring connection is required (see Figure 5-22c). The analysis of the single screw test results emphasizes that the double shear joints provide greater strength and ductility accompanied by different failure modes. The wave in the cure of S7 indicates the compressive pile up of plates in front the screw.

It can be observed from Figure 5-22 that the initial force-displacement curves tend more flat before sharply increasing. This trend formed by some potential causes. Slippage existing between the clamps and specimens at the beginning of loading procedure caused extra displacement which is recorded by the test machine. Besides, the fastener is easier to tilt in the initial stages.

a) One screw single shear tests   b) Double screw shear tests

c) Screw double shear tests   d) Single bolt joint and double screw joint
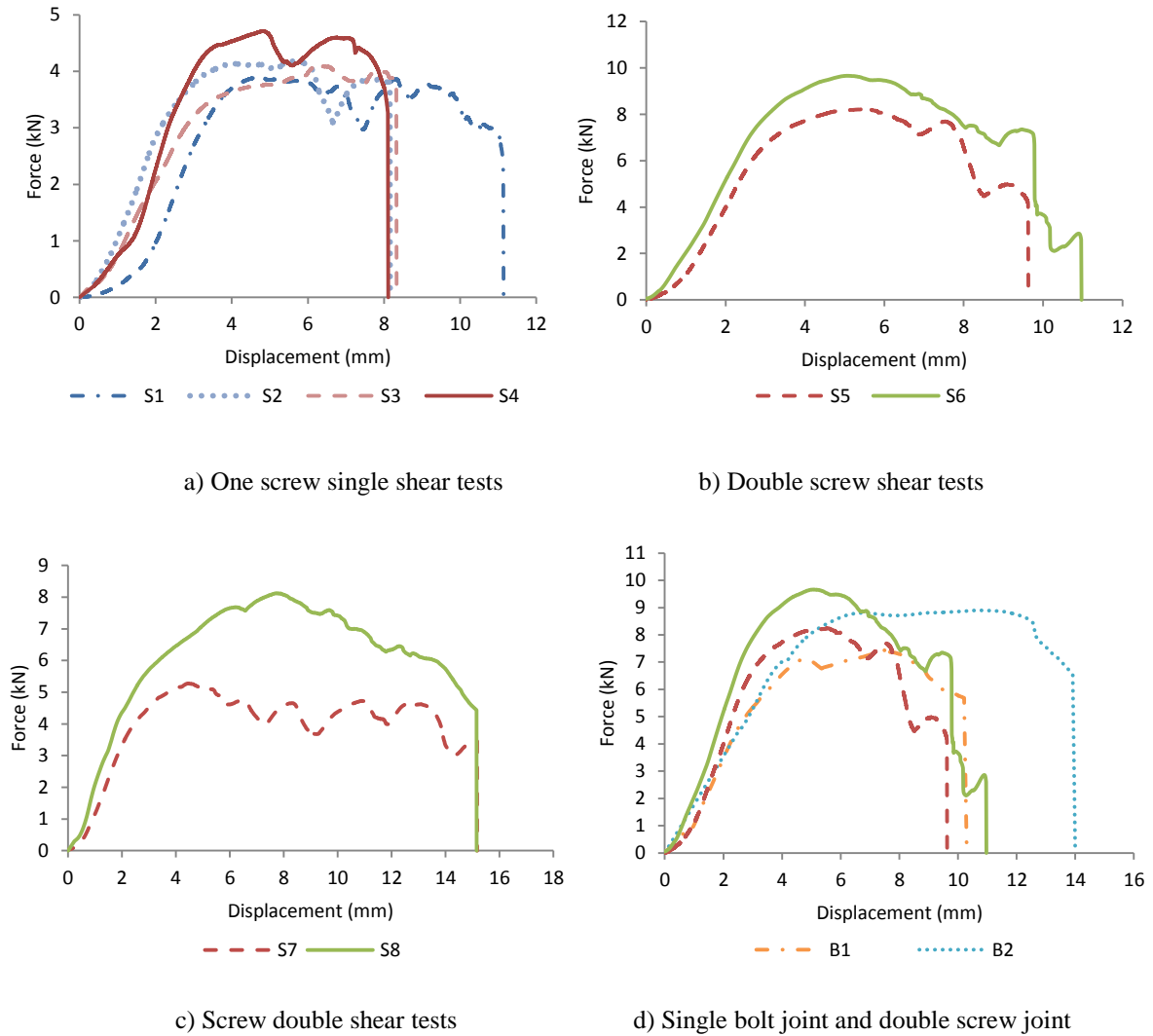
Figure 5-22 Force-to-displacement curve of screw and bolt joints

5.2.4.3 Tension test

The failure mode of tension test specimens depended on the thickness of the connected sheets. In this research t2/t1＜2.5 (AISI., 2007), the main failure mode was screw pull-out as shown in Figure 5-23. Force-displacement curves of specimens from the tension tests are shown in

Figure 5-24. An increasing of force was observed until failure occurred. Thread stripping of the bottom sheet appeared on the screw hole. There was a small linear displacement between U-sections at the connected point, while a much larger deformation of U-section components took place. As the joint was further loaded, the joint suddenly failed with screw pull-out failure. Meanwhile, a rapid resilience reduced section deflection and the plastic deformation was placed in Figure 5-23. The tensile mode exhibits much lower resistance but higher displacement relative to shear tests. There was no visible plastic deformation observed in the screw. The residue material on the screw after failure indicated that the bottom screw hole damaged due to the threads shear action. Table 5-6 lists the detailed dimensions, failure modes and responses of tension tests. It also can be found that thickness has a great influence on the peak load and corresponding deformation. As shown in the table, the ultimate force $F_{u,test}$ of specimen T2 is more than twice of that of T1 and the macroscopic displacement $D_{u,test}$ increases 48%.

Table 5-6 Tension tests

Specimen	L (mm)	F (mm)	W (mm)	t1/t2 (mm)	Fu,test (kN)	Failure mode in test	Du,test (mm)	Du,30 (mm)	Du,c (mm)
T1	60.5	101.2	78.1	0.79/0.80	1.11	P	27.08	16.20	2.13
T2	60.2	100.5	78.3	1.00/1.01	1.58	P	39.96	26.24	2.20

Note: Fu and Du represent the ultimate force and the corresponding displacement respectively. 'test' stands for the data obtained by obtained by ZwickReoll-Z100 machine.
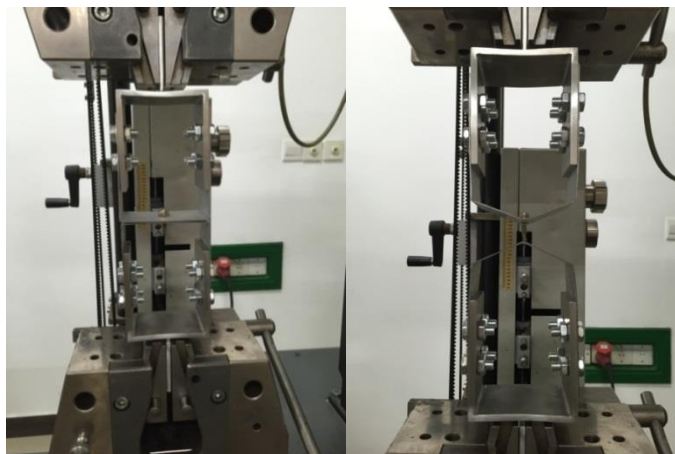
Figure 5-23 Single screw tension test failure mode
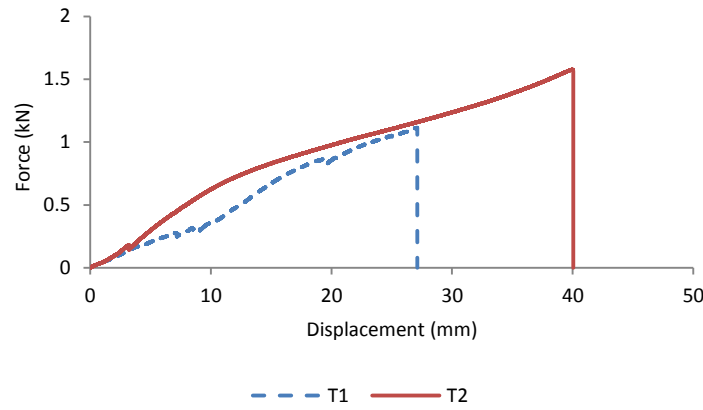
Figure 5-24 Cross-head force-displacement curves

5.2.4.4 Combined shear and tension tests

When the screw joint is subjected to tension accompanied by shear, the bearing effect on the screw and plate interface increases. Such increase may enhance the friction resistance and thus the tension resistance but may also deteriorate the bearing failure at shear. Both effects are contradictory and need to be detected in the tests. The mixed loading actions in tests TS1, TS2, TS3 have three different slope angles 30, 45 and 60 degree respectively. The experimental set-up is presented in Figure 5-25. In order to inspect the entire-process response of the specimen, the force-to-displacement curves obtained at each MP were also recorded in Figure 5-26. Figure 5-27 illustrates the screw hole deformation of the tests. Table 5-7 lists the dimensions and resistance of specimens under different loading angles.

Table 5-7 Tests under combined tension and shear force

Specimen	web (mm)	Width (mm)	flange (mm)	t1/t2 (mm)	Fu,test (kN)	Failure mode in test	Du,test (mm)	Du,30 (mm)	Du,c (mm)
TS1	92.3	60.1	21.2	1.02/1.01	1.78	P	36.48	26.10	4.40
TS2	113.2	60.5	30.3	1.01/1.00	2.16	P+B	30.52	20.94	4.34
TS3	160.8	60.2	41.1	1.01/1.0.2	2.71	B+T+S	25.30	14.41	4.30

Note: S=screw head fracture.
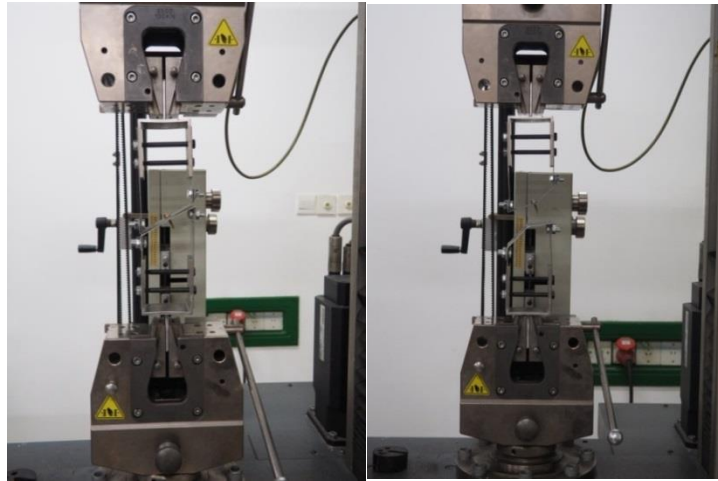
a) TS1
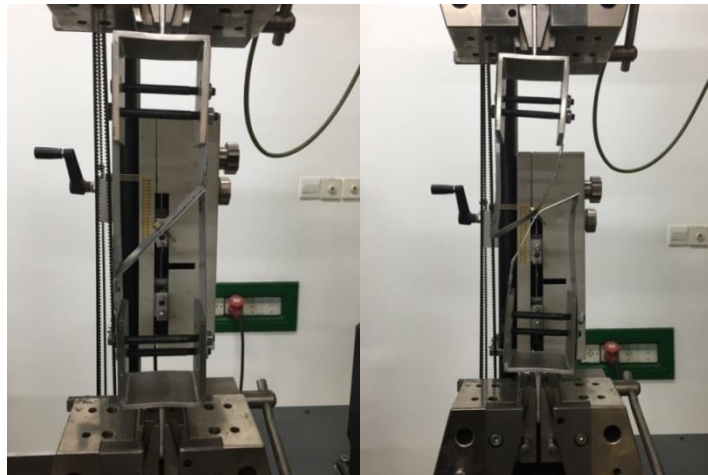
b) TS2
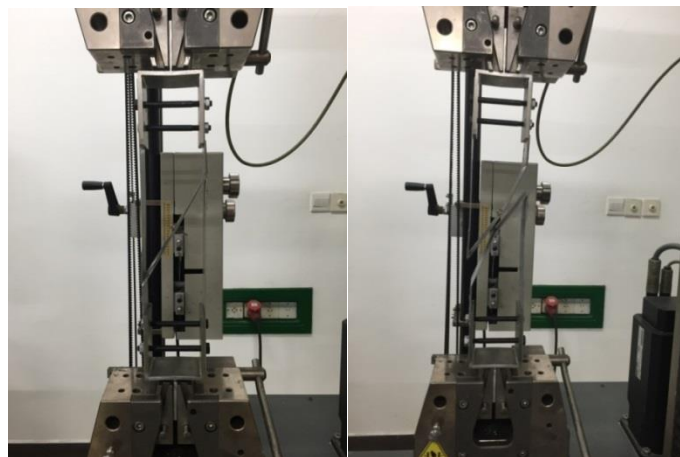
c) TS3

Figure 5-25 Failure mode of screw joint in combined shear and tension tests
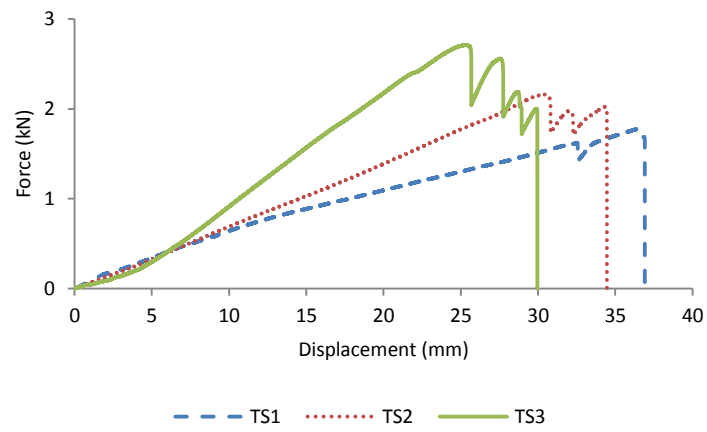
a) Measured by test machine (ZwickReoll-Z100)
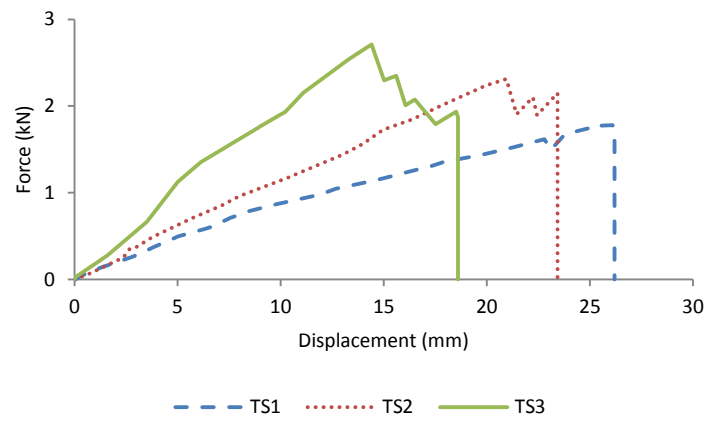
b) Measured at the 30mm point
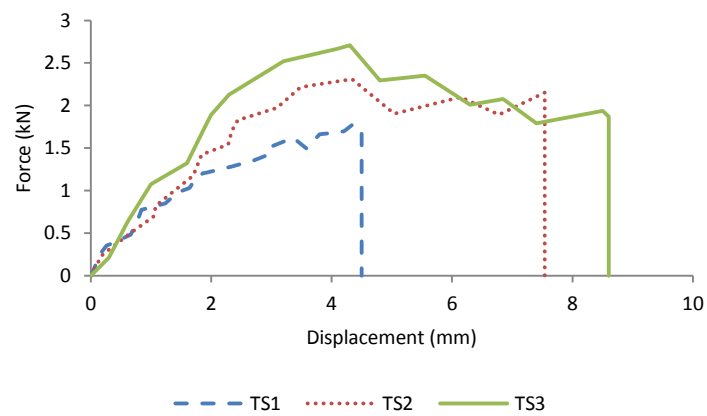
c) Measured at the centre point

Figure 5-26 Force-to-displacement curve of specimens

a) TS1   b) TS2

c) TS3

Figure 5-27 Deformation of screw hole in slop tension tests

As aforementioned, the combination of tension (Ft) and shearing (Fv) force was implemented by slope tension tests. Similar to T2, brittle failure occurred and the screw was pulled out from the bottom section in TS1 (see Figure 5-25a). With the slope angle increased in TS2 and TS3, the elongation deformation of screw hole became larger (see Figure 5-27b and 5-27c) and yielding of sheet material made joint softened after reaching the peak load until the joint failed with bearing in the sheet (see Figure 5-26). In the case of specimen TS3 screw fracture occurred without pulling out from the bottom sheet. It also can be found out that deformation of specimens decreased when the slope angle increased (see Figure 5-26a and 5-26b), whereas the screw joint showed the opposite result (see Figure 5-26c). The reason is that tension component led to screw thread slipping from the bottom sheet. Likewise, the visible waves in the curves were also caused by the threads slipping.

5.2.5 Discussion and analysis

The flexibility and bearing resistance of a joint with mechanical fasteners connecting thin-walled steel sheets have been concerned. The codes, such as Eurocode 3 (Eurocode, 2006b), AISI-S100 (AISI., 2007) and Chinese technical code (GB., 2002), specify expressions calculating joint resistance and displacement. In the specifications, tilting failure mode is occurred based on the thicknesses of the connected sheets. The range of validation in GB only refers to Q235 and Q345 steel material. Besides, based on the tests with reference to the typical case of a 16mm bolt in Z28 steel (yield stress 280N/mm^2, ultimate stress 390N/mm^2), researcher (Bryan, 1993) proposed the design expressions (see Eq. 5-1 and 5-2) for the joint flexibility C and bearing capacity Pbs of a single bolted lap joint. Although the flexibility of screw lap joint has not been developed, the comparison involved this method as a reference. Table 5-8 lists the results of predictions as a comparison.

$$C = 5n\left(\frac{10}{t_1} + \frac{10}{t_2} - 2\right) \times 10^{-3} \text{mm/kN} \qquad \text{(Eq. 5-1)}$$

$$P_{bs} = k_1 k_2 k_3 k_4 k_5 k_6 k_7 \times dt U_s \times 10^{-3} \text{kN} \qquad \text{(Eq. 5-2)}$$

where t_1、t_2 are the connected thicknesses and no more than 8mm, n is a factor which depends on the position of the shear plane and the number of utilised bolts, Us is the ultimate strength of the sheet (N/mm^2), t is the minimum thickness of the connected sheet (mm), d is the nominal bolt diameter (mm) and k_1-k_7 are influence factors, referring to bolt diameter, sheet thickness, sheet yield strength, washer diameter, number of washers end distance and shear plane respectively.

A better agreement can be found between the AISI calculations and the test results, whereas EC3 makes a conservative prediction. GB overestimates the carrying capacity of screw joint for the high strength material. According to the table, the average ratio of the predicted bearing resistance between AISI and experiment is 1.09, with a standard deviation of 0.16. The result shows that when the ultimate force is achieved, the analytical-to-test ratio is 0.80, with a standard deviation of 0.06. Eq. 5-1and 5-2 pronounce smaller flexibility than other predictions and overly large carrying capacity of the joint, which is because that bolt joint,

installed with nut, is stronger that the screw. It can be concluded that GB is not applicable to S550 material in the test scenarios. With regard to screw tension test, comparison demonstrated in Table 5-9 indicates that the joint failed before the predicted carrying force in the specifications.

Table 5-8 Resistance comparison of shear specimens

Specimen	Fu,AISI (kN)	Fu,EC3 (kN)	Fu,GB (kN)	Pbs (kN)	C (mm/kN)	Du,Bryan (mm)	Fu,AISI/ Fu,test	Fu,EC3/ Fu,test	Fu,GB/ Fu,test	Pbs/ Fu,test	Du,Bryan/ Du,test
S1	3.91	2.98	5.86	6.62	0.58	3.80	1.00	0.76	1.50	1.69	0.79
S2	5.65	3.27	6.64	6.62	0.51	3.39	1.35	0.78	1.59	1.58	0.59
S3	3.91	3.27	6.64	6.62	0.51	3.39	0.94	0.79	1.60	1.60	0.54
S4	5.47	4.17	7.33	8.43	0.45	3.79	1.16	0.89	1.56	1.79	0.78
S5	7.82	5.96	11.72	13.23	0.35	4.57	0.95	0.72	1.42	1.61	0.82
S6	10.94	8.34	14.66	16.86	0.27	4.55	1.13	0.86	1.52	1.75	0.89
S7	N/A	N/A	N/A	N/A	N/A	N/A	N/A	N/A	N/A	N/A	N/A
S8	N/A	N/A	N/A	N/A	N/A	N/A	N/A	N/A	N/A	N/A	N/A
Mean							1.09	0.80	1.53	1.67	0.74
S.D.							0.16	0.06	0.07	0.09	0.14
B1	5.95	7.6	3.55	7.98	0.58	4.59	0.80	1.02	0.48	1.07	0.61
B2	7.6	10.21	4.44	10.17	0.45	4.58	0.85	1.15	0.50	1.14	0.42

Note: AISI, EC3 and GB stand for Eurocode 3, AISI-S100 and Chinese technical code respectively. Du,Bryan is the deflection of single bolted lap joint, calculated by C times Pbs. In AISI, the failure mode of specimen S1 to S6 are tilting failure; S7 and S8 are double shear screw joints which are not involved in the above norms.

Table 5-9 Result comparison of tension specimens

Specimen	Fu,AISI (kN)	Fu,EC3 (kN)	Fu,GB (kN)	Fu,AISI/ Fu,test	Fu,EC3/ Fu,test	Fu,GB/ Fu,test
T1	2.08	1.59	1.83	1.87	1.43	1.65
T2	2.59	1.98	2.29	1.64	1.25	1.45
Mean				1.76	1.34	1.55
S.D.				0.17	0.13	0.14

The single-bolt joint is usually considered to be replaced by the double-screw joint. Based on the test results, the double-screw joint provides better resistance (S5: 8.24kN, S6: 9.66kN) than the single bolt joint (B1: 7.44kN, B2: 8.90kN) with the thicknesses of connected sheets respectively. It can be concluded that the bolt is overdesigned to the thin-walled component. However, an opposite prediction can be obtained by the norms. EC3 (Eurocode, 2005) provides the design resistance for individual fasteners subjected to shear and/or tension. Based

on the nominal shear strength P_{ns} and the nominal pull-over strength P_{nov}, screw joint failed by combined shear and pull-over action is considered in AISI-S100 (AISI., 2007). In the specification, shear force Q and tension force T should satisfy the expression Eq.5-3. However, this method shall be valid for joints that meet the following limits: The thickness should be 0.724mm≤t1≤1.130mm; the diameter of the screw head and washer should be no more than 19.1mm; F_{u1}≤483MPa; Connected sheet should meet t2/t1≥2.5. All the limitation is to ensure that the failure mode of the joint is pull-over, which does not involve pull-out failure mode.

$$\frac{Q}{P_{ns}} + 0.71\frac{T}{P_{nov}} \le 1.1\emptyset \qquad \text{(Eq. 5-3)}$$

where $\emptyset$=0.65.

Nevertheless, the gap is supplied in the Chinese technical code of cold-formed thin-walled steel structures (GB., 2002). This code provides a design method for combined tension and shear action applied between steel sheet and profiled sheet of roof, which is shown in Eq. 5-4. It is only applicable for Q235 and Q345 with nominal yield stress of 235 N/mm^2 and 345 N/mm^2 respectively, but not for high strength material S550.

$$\sqrt{\left(\frac{N_v}{N_v^f}\right)^2 + \left(\frac{N_t}{N_t^f}\right)^2} \le 1 \qquad \text{(Eq. 5-4)}$$

where N_v is the shear force, N_t is the tensile force, N_v^f is the shear bearing capacity design value, N_t^f is the tensile bearing capacity design value.

According to test and GB, the maximum allowable shear force Qm and the corresponding tensile force Tm of the joint loaded by slope angle can be obtained in Table 5-10.

Table 5-10 Ultimate force distribution in shear and tension directions

Specimen	$\theta°$	Qm,test (kN)	Tm,test (kN)	Qm,GB (kN)	Tm,GB (kN)	Qm,GB/ Qm,test	Tm,GB/ Tm,test
T2	90	0.00	1.58	0.00	2.29	N/A	1.45
TS1	60	0.89	1.54	1.30	2.55	1.46	1.66
TS2	45	1.48	1.48	2.18	2.18	1.47	1.47
TS3	30	2.35	1.36	3.49	2.02	1.49	1.49
S4	0	4.71	0.00	7.33	0.00	1.56	N/A
Mean						1.49	1.52
S.D.						0.04	0.09

The results illustrate that the average ratios of the predicted Qm and Tm between GB and the test are 1.49 and 1.52, with standard deviations of 0.04 and 0.09 respectively, implying that GB overestimated the value of the ultimate shear and tension resistances. The ultimate pure shearing and tensile resistance Qu and Tu were obtained by test S4 and T2. Thus, the nonlinear expectation function is assumed:

$$\sqrt{\left(\frac{Q_m}{Q_u}\right)^2 + \left(\frac{T_m}{T_u}\right)^2} = 1 \qquad \text{(Eq. 5-5)}$$

$$Q_m = Q_u\sqrt{1 - \left(\frac{T_m}{T_u}\right)^2} \qquad \text{(Eq. 5-6)}$$

Regression variation is

$$RSS = \sum_{i=1}^{n}(\hat{y}_i - \bar{y}_i)^2 \qquad \text{(Eq. 5-7)}$$

Residual variation is

$$ESS = \sum_{i=1}^{n}(y_i - \hat{y}_i)^2 \qquad \text{(Eq. 5-8)}$$

Total variance is

$$TSS = \sum_{i=1}^{n}(y_i - \bar{y}_i)^2 \qquad \text{(Eq. 5-9)}$$

where $\hat{y}_i = Q_m$ is the variable predicted by the regression model, $\bar{y}_i$ is the mean of the test Qm,test; RSS+ESS=TSS.

The determination coefficient

$$R^2 = RSS/TSS \qquad \text{(Eq. 5-10)}$$

is the proportion of regression variation in total variance.

Overall, the shear and tension forces should satisfy Eq. 5-11 under the mixed loading conditions.

$$\sqrt{\left(\frac{Q}{Q_u}\right)^2 + \left(\frac{T}{T_u}\right)^2} \leq 1 \qquad \text{(Eq. 5-11)}$$

where Q is the required allowable shear strength of joint, T is the allowable tension strength of joint. The tested pure shear strength and pure tension strength of the screw joint are Qu=4.71kN and Tu=1.58kN respectively.
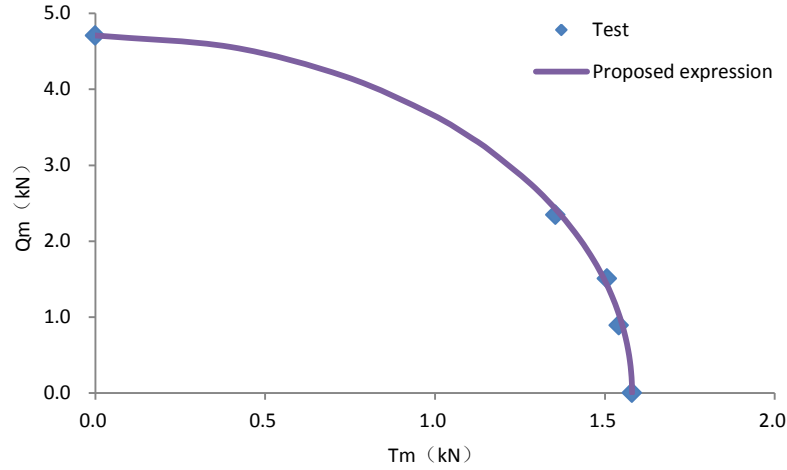
Figure 5-28 Result comparison of proposed expression and test

Regarding the test data, determination coefficient R^2=0.9954 indicates that the regression model is acceptable with a good accuracy. Thus, it is demonstrated that the combination of shear and tensile force acting on the joint, with 1mm thickness and S550 material, can be precisely predicted by the proposed expression (see Figure 5-28).

As is mentioned above, the interaction of shearing and pulling action declined the both bearing resistances in each direction. The proportional coefficient β in shear (β_v=Q_m/Q_u) and tension (β_t=T_m/T_u) directions is introduced in the analysis. Figure 5-29 presents the relationship between β and θ. It can be found that, with increasing of θ, the proportion of the maximum shear strength is declined. At the beginning, the dropping increases until the curves intersect. Then the gradient of the curve decreases. From the curve of β_t, it also can be observed that the ratio of Tm/Tu rapidly rises in the beginning. After reaching the crossover point, the value flattens out. The two curves intersect at θ=18.34°. The expressions of the proportional coefficient β_v and β_t were regressed as follows.
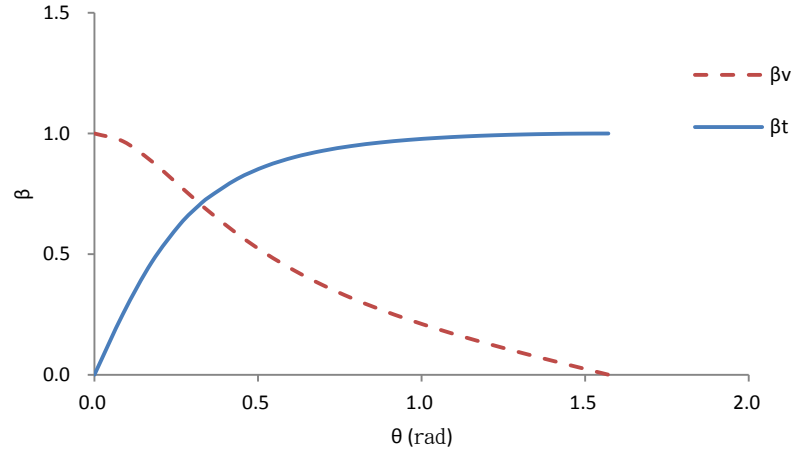
Figure 5-29 β-to-θ curve

Assume the modified ultimate strength Fu of screw joint is:

$$F_u = \sqrt{Q_m{}^2 + T_m{}^2} \qquad \text{(Eq. 5-12)}$$

$$Q_m = \beta_v Q_u \qquad \text{(Eq. 5-13)}$$

$$T_m = \beta_t T_u \qquad \text{(Eq. 5-14)}$$

$$\theta = \arctan\frac{T_m}{Q_m} \qquad \text{(Eq. 5-15)}$$

$$\beta_v = 1 - 0.35\theta - 1.73\theta^2 \quad (0 \le \theta \le 0.32\text{rad}) \qquad \text{(Eq. 5-16)}$$

with $R^2 = 0.9938$,

$$\beta_v = 0.21 - 0.45\ln\theta \quad (0.32 < \theta \le 1.57\text{rad}) \qquad \text{(Eq. 5-17)}$$

with $R^2 = 0.9998$,

$$\beta_t = 3.24\theta - 3.3\theta^2 \quad (0 \le \theta \le 0.32\text{rad}) \qquad \text{(Eq. 5-18)}$$

with $R^2 = 0.9987$,

$$\beta_t = 1.17 - 0.05\theta - \frac{0.15}{\theta} \quad (0.32 < \theta \le 1.57\text{rad}) \qquad \text{(Eq. 5-19)}$$

with $R^2 = 0.9989$.

For further details of the slope angle effect, the ultimate forces in the experiment Fu, test are listed with regard to the angle θ. Due to the softening of the joint after reaching the maximum

123

resistance, the load response of joint decreases while the deformation increases until the joint is damaged. Herein, the maximum displacements of joint at MPs are presented in Table 5-11. It shows that the Dm and the ratio between Du and Dm rises up to 1.00 with slope angle drops, implying that shear action provides better ductility of the screw joint and brittle fracture occurs with low slope angle.

Table 5-11 Displacement and force comparison

Specimen	θ (°)	Fu,test (kN)	Dm,test (mm)	Dm,30 (mm)	Dm,c (mm)	Du,test/ Dm,test	Du,30/ Dm,30	Du,c/ Dm,c
T2	90	1.58	40.05	27.00	2.20	1.00	0.97	1.00
TS1	60	1.78	36.91	26.20	4.50	0.99	1.00	0.98
TS2	45	2.61	34.46	23.44	7.54	0.89	0.89	0.58
TS3	30	2.71	29.96	18.60	8.60	0.84	0.77	0.50
S4	0	4.71	8.11	8.11	8.10	0.55	0.55	0.55

As shown in Figure 5-30, when the section acute angle θ increases, the carrying capacity decreases. On the contrary, macroscopic displacement of specimen becomes larger. Meanwhile, the change is flattening out. The same trend is observed for the displacement at 30mm measure point. However, the relative movement between the connected points present an opposite result, showing a decline with ascending of slope angle.

It is proved that shear force acting on screw joint is actually in proportion to the joint elongation. The larger macroscopic deformation of the specimen is only by the reason of the larger dimension of the sloped U-section.
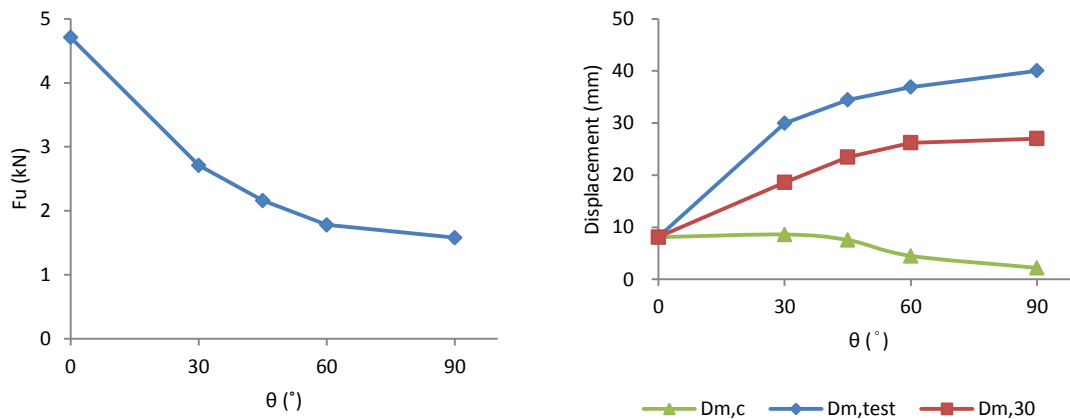
Figure 5-30 Comparison of different angles scenarios

5.3 Numerical analysis and validation

5.3.1 Modelling development

5.3.1.1 Elements

In the present study, commercial FE package ABAQUS was used to simulate the experimental results and carry out further analysis of joints implemented in modular construction. Three-dimensional SHELL element S4R (A 4-node doubly curved thin or thick shell, reduced integration, hourglass control, and finite membrane strains), SOLID element C3D8R (An 8-node linear brick, reduced integration, hourglass control) and BUSHING connector element were employed in the analysis. For 3D SOLID element, the degrees of freedom of each node include 3 translations. Shell element involves six degrees of freedom-three translations and three rotations. Bushing Connector Section (BCS) is flexible in usage without specific shape. Between the two joint points, six degrees including three translations and three rotations (see Figure 5-31) can be defined linearly or nonlinearly. The settings of damage condition of the joint were also contained in BCS. When the joint reached the defined limitation, the connector was demolished.
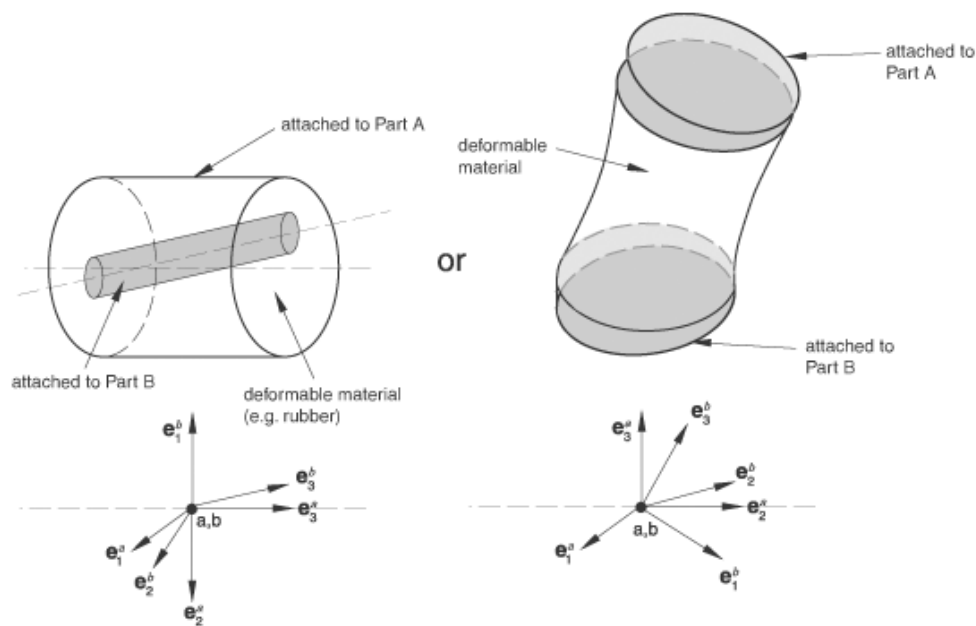
Figure 5-31 Bushing element (Abaqus-6.13, 2013)

5.3.1.2 Meshing

It was proved that Hex or Hex-dominated element shape are more regular, presenting more accurate and better convergence than other element shapes (SHI, 2006), which was employed in the meshing of solid element. The shell element shape was "Quad", with "Structured" technique. Through an extensive trial-and-error process and sensitivity analysis, the most satisfactory results were achieved when using the following discretisation pattern. The approximate global sizing of the screw was 1.6mm. In terms of CFS components, it was defined as 5mm.

5.3.1.3 Material

For the sheets, the nominal stress σ_{nom} and strain ε_{nom} were achieved by the coupon test results. In FE modelling, the stress and strain definition followed the true stress σ_t and strain ε_t

$$\varepsilon_{nom} = \frac{l - l_0}{l_0} = \frac{l}{l_0} - 1 \qquad \text{(Eq. 5-20)}$$

$$\varepsilon_t = \ln(\varepsilon_{nom} + 1) \qquad \text{(Eq. 5-21)}$$

$$\sigma_{nom} = \frac{F}{A_0} \qquad \text{(Eq. 5-22)}$$

Assuming that the plastic deformation is incompressible,

$$l_0 A_0 = lA \qquad \text{(Eq. 5-23)}$$

$$\sigma_t = \sigma_{nom}(\varepsilon_{nom} + 1) \qquad \text{(Eq. 5-24)}$$

where l is the final length of the specimen; l_0 is the original length of the specimen.

5.3.1.4 Interaction and solution

The friction coefficient of 0.3 was applied to simulate the interface between all the contact surfaces. The "hard contact" condition was applied between components. The analysis adopted the Von Mises yield criterion and a nonlinear incremental-iterative Full Newton solution technique. The displacement load was applied to the model. In the joint simulation, the setting of contact and interaction between fastener and connected sheets is the key issue. Table 5-12 illustrates six modelling methods as a comparison.

Table 5-12 Settings of joint simulation methods

Modelling	Sheet element	Fastener element	Settings
FEM1	shell	bushing	Nonlinear elasticity in shear force direction and linear elasticity in tension direction were defined based on test datum. Connector became damaged in the shear direction when the longitudinal elongation exceeded 8.10mm/15.15mm for single/double shear specimens or in the tension direction with the resistance force reached 1.58kN. The diameter of the connector was 5.5mm.
FEM2	solid	bushing	Same with FEM1
FEM3	shell	contimuum shell	All the contact surface between screw and sheets were tied together.
FEM4	solid	solid	Same with FEM3
FEM5	solid	solid	A quarter of the screw head interface was tied to the sheet as emphasized in Figure 5-31. Besides, the interaction of the shank surface and the edges of the holes was defined by finite-sliding.
FEM6	solid	solid	This method considered friction to simulate the interaction between thread and contacted plates. The friction coefficient was assumed to be 5.0. The interaction between the contact surfaces was set to finite-sliding.
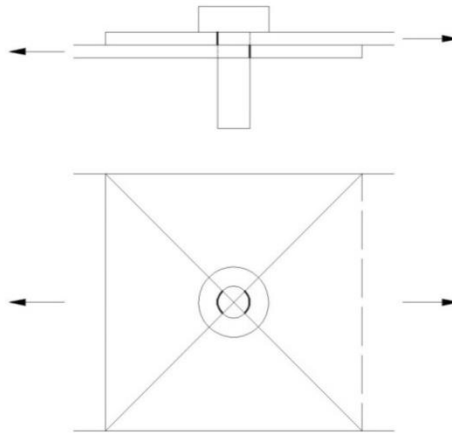
Figure 5-32 Sketch diagram of "tie" contact in FEM5

5.3.1.5 Fastener modelling

As for the pure shear test, the macroscopic displacement of the joint along the load direction includes material elongation, warping in the plate and joint motion. In fact, the motion of screw joint under different loading scenarios consists of several factors, involving screw rotation, screw-hole deformation, tension in the sheets, screw sliding from the connected sheets and screw deflection. Based on the test results, the failure conditions and all stages of joint nonlinear responses were defined in the connector settings, representing screw joint

motion. Regarding to material elongation, the response of bushing connector was achieved based on the following expressions. Account to the post-failure reaction, the maximum sliding distance determines the damage point of bushing connector under shear force.

$$F_{bushing} = F_{test} \tag{Eq. 5-25}$$

$$U_{bushing} = U_{test} - U_{material} \tag{Eq. 5-26}$$

where $F_{bushing}$ and $U_{bushing}$ stand for the force and displacement bushing connector, F_{test} and U_{test} are the force and displacement of the test, $U_{material}$ is the material elongation.

According to the specimens T1 and T2, brittle fracture was observed when the joint reach the bearing capacity. Thus, the critical condition in tension direction was the maximum load obtained by the pure tension test. The linear stiffness of screw joint was assumed based on the test results. For the screw modeled solid elements. The material property of the shaped screw was given by a bilinear stress-strain curve with nominal yield strengths of 415MPa, ultimate strengths of 540MPa respectively. The simplified screw included screw head and flat shank with the diameter of 5.5mm.

5.3.2 Numerical results

5.3.2.1 Coupon analysis

The experimental and numerical results of coupon test are shown in Figure 5-33. The comparison demonstrates a good agreement, implying the material setting is valid.
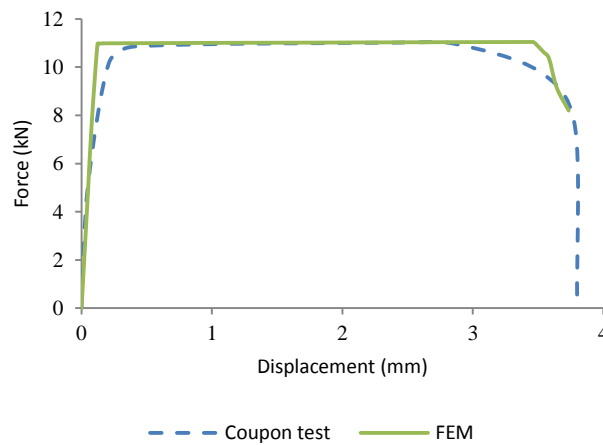
Figure 5-33 Force-to-displacement curves of coupon test and FEM simulation

5.3.2.2 Shear joint

Each modelling of joint has certain superiority and certain limitation. In order to obtain the fit FEM, taking 1mm sheets for instance, numerical investigation on the different elements and modelling settings were carried out. Figure 5-34 presents the Von Mises stress distribution when the specimen S4 achieved the ultimate resistance force. The comparison of force-to-displacement curves obtained by each FEM1 and FEM2 are also shown in Figure 5-34.

According to Table 5-13, FEM1 and FEM2 show good precision in joint behaviour prediction. On the other hand, the numerical calculation of bushing connector has less time consumption. When the joint reach the critical limitation, the connector was demolished in the modelling. To some extent, it is considered as the best choice to simulation fasteners of the connection in full-scaled construction simulation. However, this method is not applicable in parametric study. Table 5-13 indicates that ultimate force of single lap joint was overrated by FEM3 and FEM4, with figure of 14.15kN and 9.47kN. On the contrary, the corresponding displacements are only 12% and 25% out of the test results. That means the fully tie contact overly enhanced the joint in the modelling. It also can be observed from Table 5-13 that shell sheet presented better ductility after yielding. Better predictions in carrying capacity of screw joint were made by FEM5 and FEM6, with simulation-to-test ratios are 1.12 and 0.81 respectively. Nevertheless, the displacements obtained by these methods still cannot meet the requirement.

Table 5-13 Comparison of test and FEM with macroscopic results

Modelling	Specimen	$F_{u,test}$ (kN)	$D_{u,test}$ (mm)	$F_{u,FEM}$ (kN)	$D_{u,FEM}$ (mm)	$F_{u,FEM}/F_{u,test}$	$D_{u,FEM}/D_{u,test}$
FEM1				4.71	4.95	1.00	1.02
FEM2				4.71	4.98	1.00	1.03
FEM3	S4	4.71	4.84	14.15	0.58	3.00	0.12
FEM4				9.47	1.23	2.01	0.25
FEM5				5.28	0.62	1.12	0.13
FEM6				3.82	1.26	0.81	0.33

Table 5-14 Comparison of test and FEM with macroscopic results

Specimen	$F_{u,test}$ (kN)	$D_{u,test}$ (mm)	$F_{u,FEM}$ (kN)	$D_{u,FEM}$ (mm)	$F_{u,FEM}/F_{u,test}$	$D_{u,FEM}/D_{u,test}$
S8	8.12	7.72	7.75	9.03	0.95	1.17
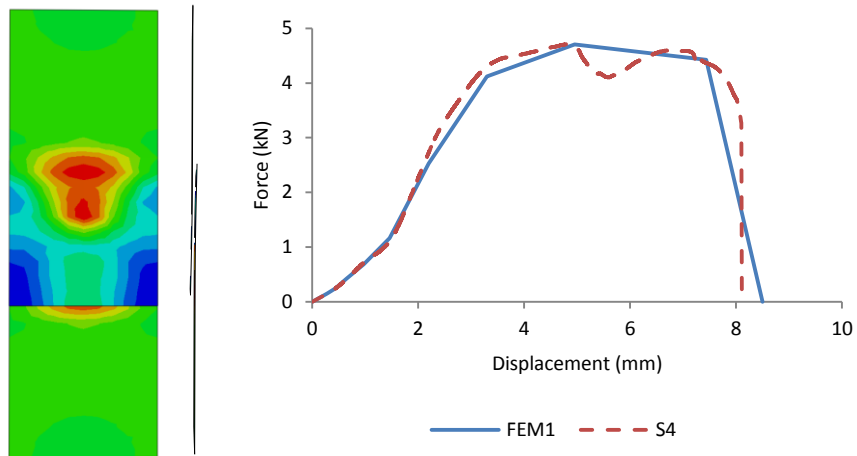
a) FEM1
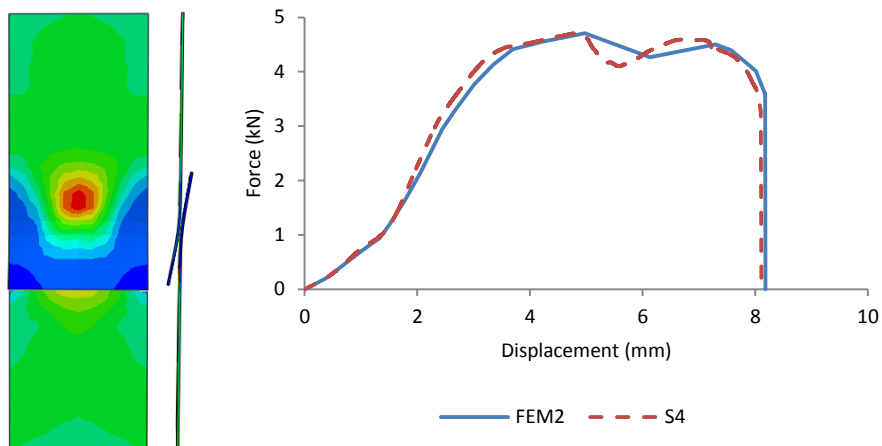
b) FEM2

Figure 5-34 Von Mises stress diagram and force-to-displacement curve of S4
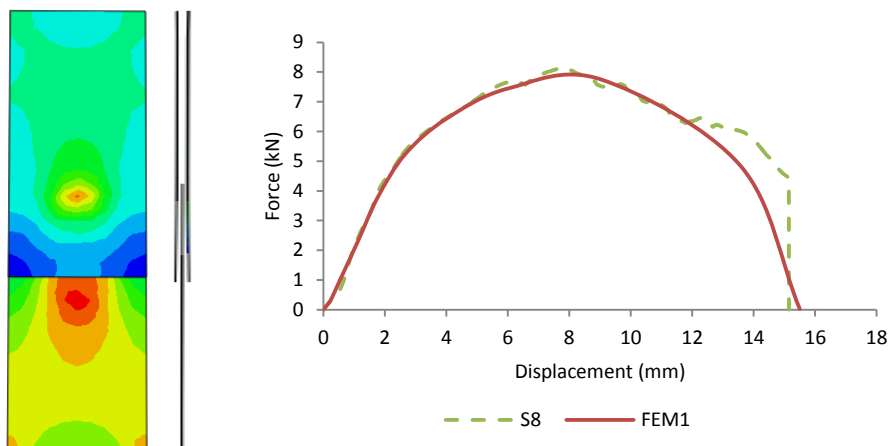
Figure 5-35 Von Mises stress diagram and force-to-displacement curve of S8

In terms of double shear scenario S8, the results in Figure 5-35 and Table 5-14 are achieved by using FEM1. It demonstrates that the bushing connector is applicable in predicting structural behaviour of double shear screw joint.

5.3.2.3 Single tension joint

Based on the same settings of bushing connector in FEM1 and material property, specimen T2 was simulated under tension. The following figures and table presents ultimate force, displacement (see Figure 5-36) and the loading process (see Figure 5-37) from the simulation.

As shown in Figure 5-36, bushing connector accurately predicted the behaviour of the joint. However, the deformation of connected sections shows discrepancy in FEM2. Obviously, a better agreement was obtained by FEM1, implying that shell element is more compatible with the CFS component simulation than solid element and the numerical model is valid. As a result, Table 5-15 shows that the ratio of the predicted ultimate resistance between numerical model and the test is 1.00. As for the displacement, the ratio is obtained with the figure of 1.02.

The stress of the specimen varies as the displacement increases. Deformation of the section can be observed in the central web and the corner of each C-section. The stress increases significantly in these areas (see Figure 5-37a). The steel material at the corner of the section firstly reaches the plastic phase with the load increasing (see Figure 5-37b). When the tension load exceeds the load carrying capacity of the fastener, the bushing connector is disabled leading to the stress relieved instantly (see Figure 5-37c).

Table 5-15 Comparison of test and FEM with macroscopic results

Modelling	Specimen	$F_{u,test}$ (kN)	$D_{u,test}$ (mm)	$F_{u,FEM}$ (kN)	$D_{u,FEM}$ (mm)	$F_{u,FEM}$/ $F_{u,test}$	$D_{u,FEM}$/ $D_{u,test}$
FEM1	T2	1.58	39.96	1.58	40.91	1.00	1.02
FEM2				1.56	41.92	0.99	1.04
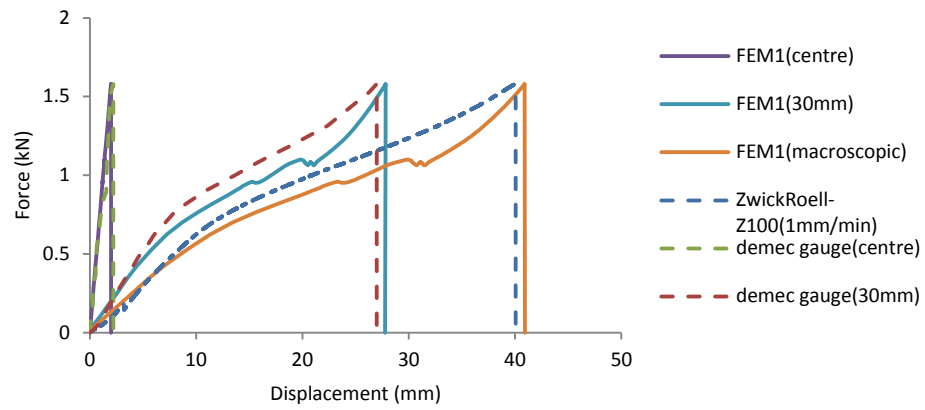
a) FEM1
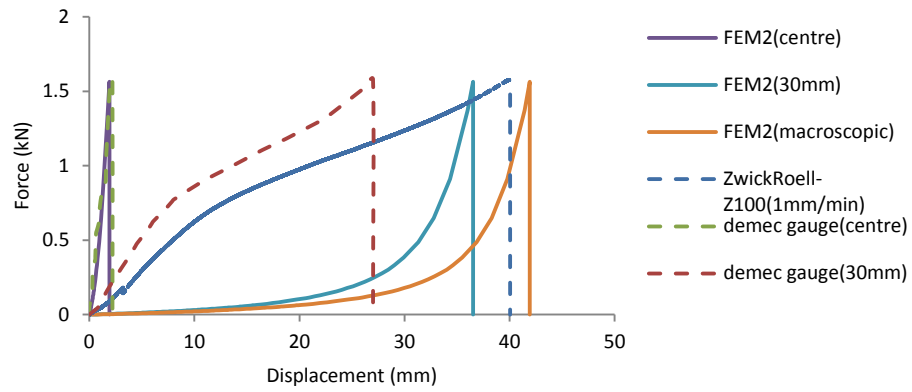
b) FEM2

Figure 5-36 Force-to-displacement curve of T2
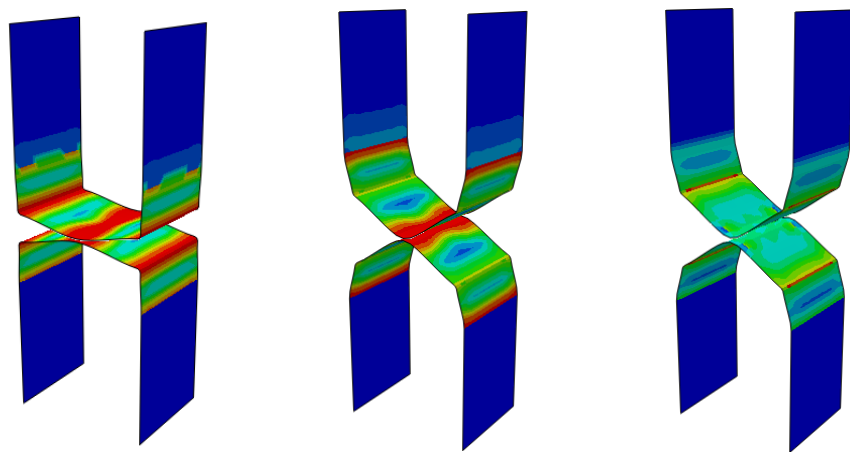
a) Stage I initial loading   b) Stage II maximum loading   c) Stage III pull-out failure

Figure 5-37 Von Mises stress distribution diagram of FEM1

5.3.2.4 *Combined shear and tension joint*

The slope tension imposed mixed shear and tension forces on the screw joint. The bushing elements provide a connection between two nodes that allows independent behaviour. It was assumed that the shear and tension response of the joint were independent in model A. The pure shear and tension resistance of the screw joint in the tests were employed in the modelling. Thus, based on the verified models, the features of joint in shear and tension directions followed FEM1 in the mixed loading scenarios. However, with regard to interaction between mixed actions, proportional coefficients β_v and β_t were also employed in the bushing connector settings of model B. The comparison of the force-to-displacement curves are shown in Figure 5-38 to 5-40. The detailed results are presented in Table 5-16.

The failure of joint did not occur in TS1 model as shown in Figure 5-38a. The reason for the divergence is the failure in the sloped U section at the connected point. For TS2 and TS3, the ductility of the test joint is larger than the prediction (see Figure 5-39a and 5-40a). However, the initial stiffness of the joints acted in accordance with the test. When the proportional efficient β was introduced in modelling, a better agreement can be observed in Figure 5-38b, 5-39b and 5-40b. The ductility of screw joint was predicted but slightly overestimated in TS1, which was undervalued in TS2 and TS3. During the tests, tension action accelerated the failure in shear direction leading to the failure occurred earlier than the prediction in model A. On the other hand, screw sliding was larger than that in the pure tension test, which is not involved in the modelling. Thus, there is a gap can be observed in the ductility between models and tests (see Figure 5-39b and 5-40b).

Table 5-16 shows that the model overestimated the carrying capacity of the joint under combined actions by 1.85 times in average. However, the ultimate force was obtained at the similar displacement with the experiment outcome. It indicates that combined shear and tension significantly declined the screw joint resistance. The average values of $F_{u,b}/F_{u,test}$ and $D_{u,b}/D_{u,c}$ are 0.95 and 1.00, with the standard deviations being 0.05 and 0.04, respectively.

Table 5-16 Comparison of test and FEM1 with macroscopic results

Specimen	Fu,a (kN)	Du,a (mm)	Dm,a (mm)	Fu,b (kN)	Du,b (mm)	Dm,b (mm)	Fu,a/ Fu,test	Du,a/ Du,c	Dm,a/ Dm,c	Fu,b/ Fu,test	Du,b/ Du,c	Dm,b/ Dm,c
TS1	3.31	3.53	5.36	1.60	4.37	4.85	1.86	0.80	1.19	0.90	0.99	1.08
TS2	4.42	4.59	6.85	2.03	4.20	6.75	2.05	1.06	0.91	0.94	0.97	0.90
TS3	4.47	4.35	7.39	2.70	4.48	7.90	1.65	1.01	0.86	1.00	1.04	0.92
Mean							1.85	0.96	0.99	0.95	1.00	0.96
S.D.							0.20	0.14	0.18	0.05	0.04	0.10

Note: "a" stands for independent resistance in each direction (model A), "b" represents that the interaction of shear and tension responds (model B) was taken into account.
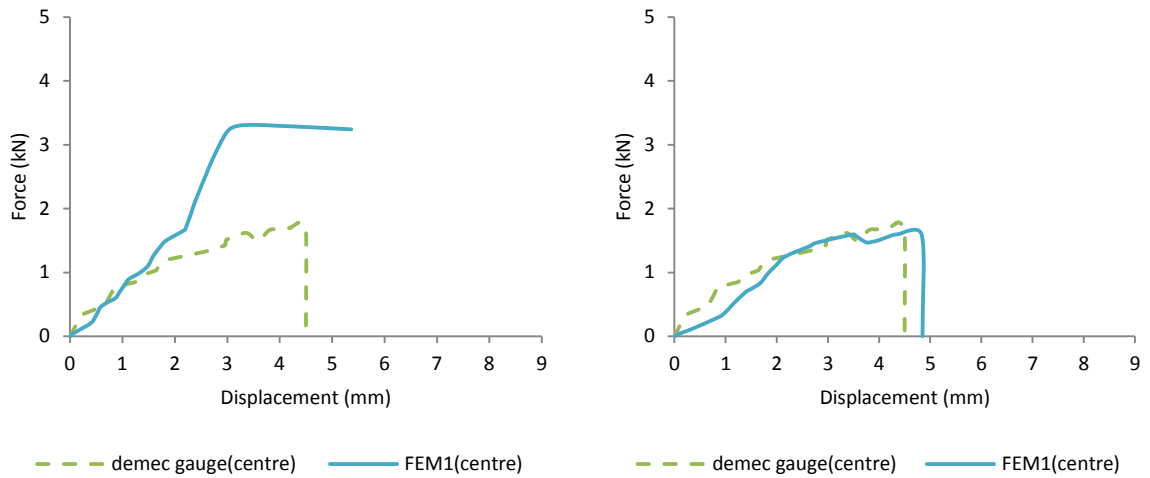
a) Model A independent action   b) Model B interaction action

Figure 5-38 Force-to-displacement curve of the joint in TS1
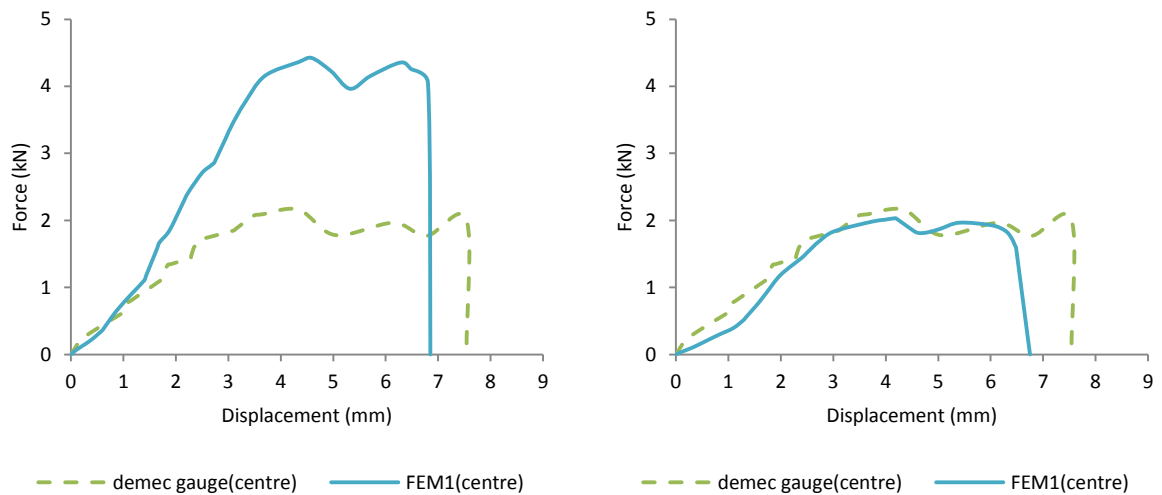
a) Model A independent action   b) Model B interaction action

Figure 5-39 Force-to-displacement curve of the joint in TS2

a) Model A independent action   b) Model B interaction action
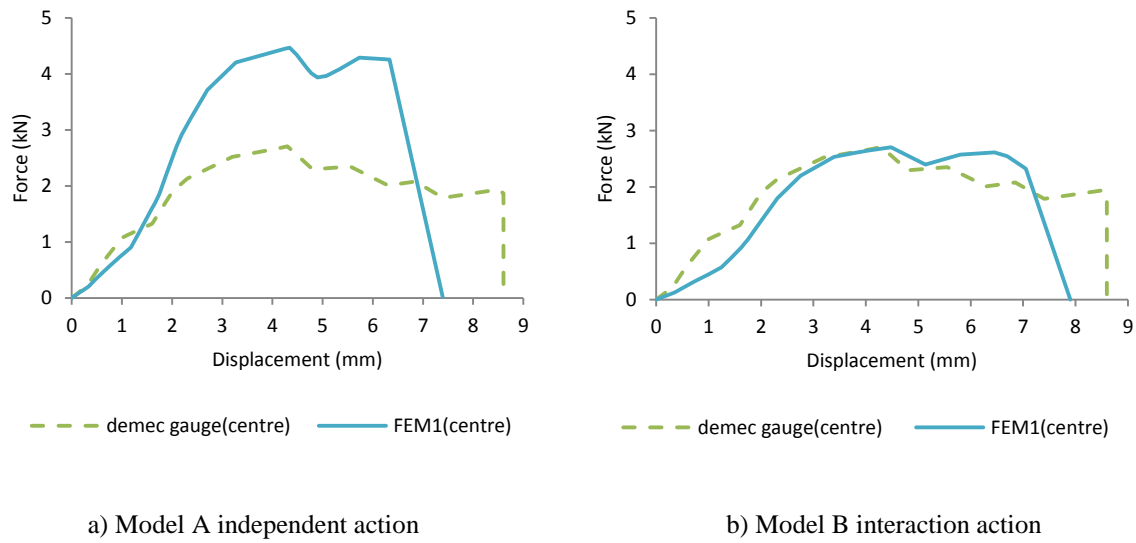
Figure 5-40 Force-to-displacement curve of the joint in TS3

5.4 Summary

Experimental and numerical investigation on screw joint with thin thickness high strength material S550 has been presented. The test included three typical loading scenarios including shear, tension and mixed actions. The slope U section was proposed to implement the combination of shear and tension force in the tests. The bearing capacity, flexibility, and failure modes were identified in the test. A comparative study between the test results and the analytical values predicted by specifications was presented. Based on the current code and test results, this chapter developed expressions to prediction the ultimate resistance of screw joint suffering combined shear and tension action, and the proportional coefficient β was also proposed. In the numerical study, bushing connector shows good agreement with experimental and analytical studies. The coefficient β introduced to the modelling further proved the numerical validation. It was revealed that combined shear and tensile force can significant reduce the resistance in the shear direction further accelerate the failure process of the joint but enlarge the ductility. Furthermore, the interaction of the bearing capacity of screw joint under mix loadings was detected in the paper. The developed simulation method in this chapter can be applied in design process of screwed connections.

CHAPTER 6   CONNECTION BETWEEN MODULAR PANELS

6.1 Introduction

In recent years, high strength CFS sections have begun to be commonly used as load-bearing members in constructions especially in the low-rise dwellings. Designing an efficient connecting method for such structures is imperative as it is a vital factor affecting the cost and the safety controls in the CFS modular structures. This chapter presents a study of several connection configurations. For improving the structural properties of the typical connecting method, three connection configurations were proposed in this research. In order to reveal the entire process response of the different connections, the numerical study was conducted by using finite element software ABAQUS. The structural properties of each screw joint were tested in the Chapter 5 and introduced in the connection simulation. As a result, the force-to-displacement relationships were achieved to illustrate the resistance of the connection in shear, tension and rotation directions. With regards to the connection structural properties, the robustness of the CFS modular panel structure was estimated through the full-scaled 3D modelling and 2D frame modelling. The cases involved the removal of the external and internal wall panels, respectively.

6.1 Connection investigation

6.1.1 Connection configurations

The CFS modular panel system is composed of stud, track, pipes, thermal and acoustic insulation, as well as internal and external decorations. The galvanized cold-formed structural elements in the modular panels usually adopt C-section and U-section (see Figure 6-1a and 6-1b). As is shown in Figure 6-1c, section 1 is the joist in the floor; section 2 is the floor track; section 3 is the wall track and section 4 is the post of the load bearing wall panel.
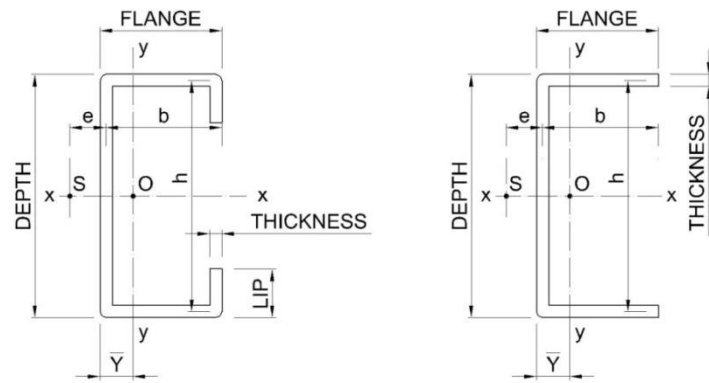
| a) C-section | b) U-section |
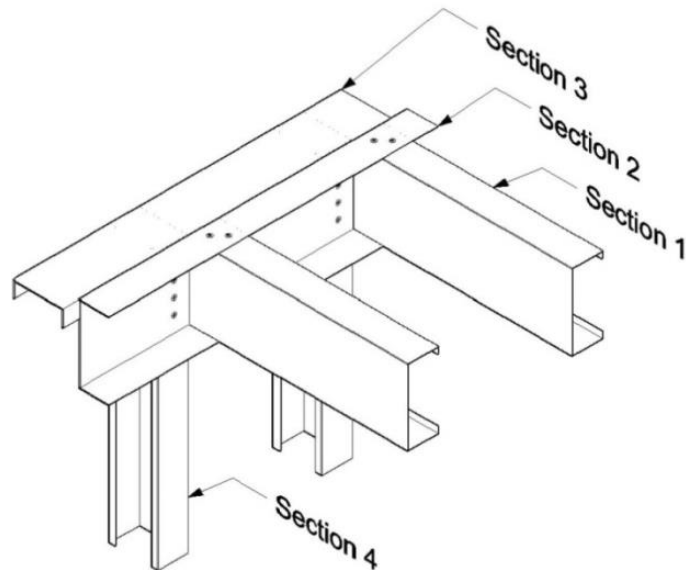
c) Section assembly

Figure 6-1 Sections in CFS modular panel system

In this research, screws (see Figure 5-1) were employed assembling the connections between the wall panel and the floor panel. Although the floor panel can be either assembled on the side of wall panel or placed on the top of wall, in a high-rise building, the vertical forces is suggested to be transferred directly go through the wall panels in the wall bearing modular system. Therefore, connection between floor and wall panels dominantly carries a shear force under normal loading condition.

When the abrupt removal of the ineffective component occurs, the force transferring path may be changed. Assuming the ductility and strength meet the requirement of catenary action, the load acting on the connection consists of shear and moment. Specific to the screw joint between jointed panels, each screw may be subject to combined shear and tension in the typical connection method. Intermediate stiffer is supposed to improve the tension and moment resistance, which is employed in the connection innovation. The details of the connection configurations are described as follows.

The typical connection method introduced in this thesis is presented as connection type A (see Figure 6-2). Load acting on the joists is transferred to the floor panel track through screw joints on the flange. The track is restrained to the post flange with four screw joints.
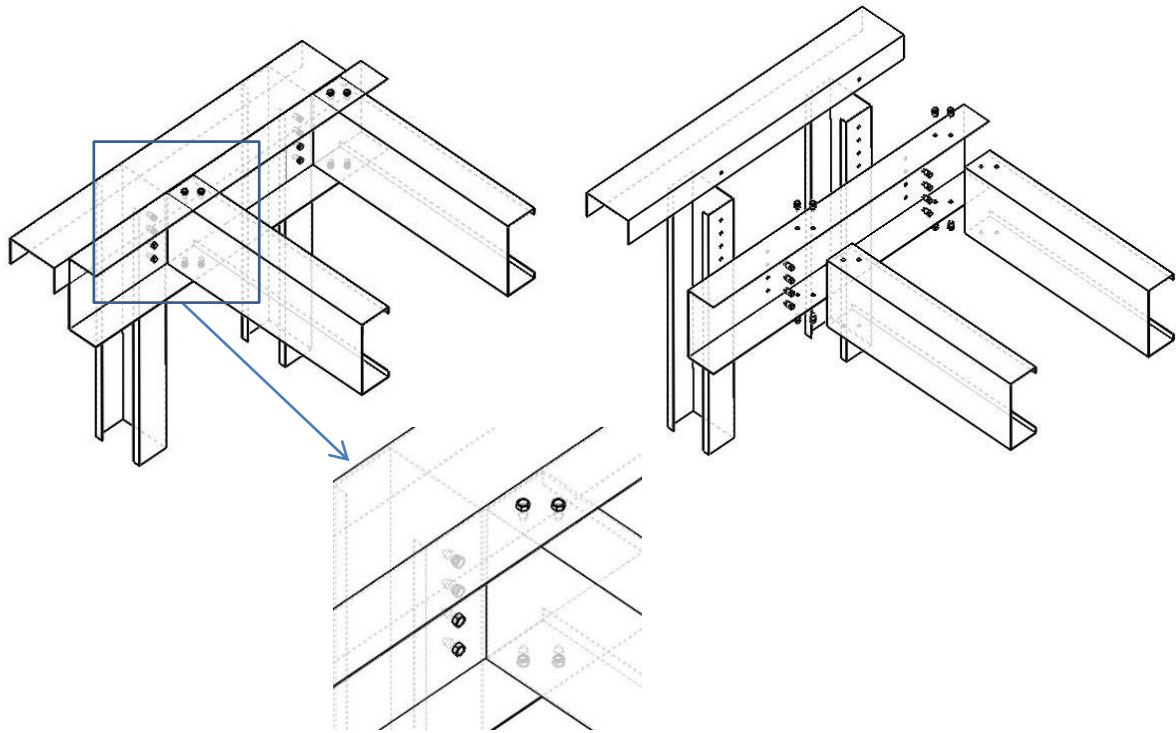
Figure 6-2 Perspective and explosion diagram of connection type A

To enhance the flange and web of joist, a modified bracket was suggested as connection type B (see Figure 6-3). The bracket connects to the webs of wall track and post by screw joints. There is a rectangular pre-opening in the web of floor track to ensure that the bracket can pass through and connect to the floor panel. In that case, the transverse load transfers to post through the bracket instead of the floor panel track.

Bracket
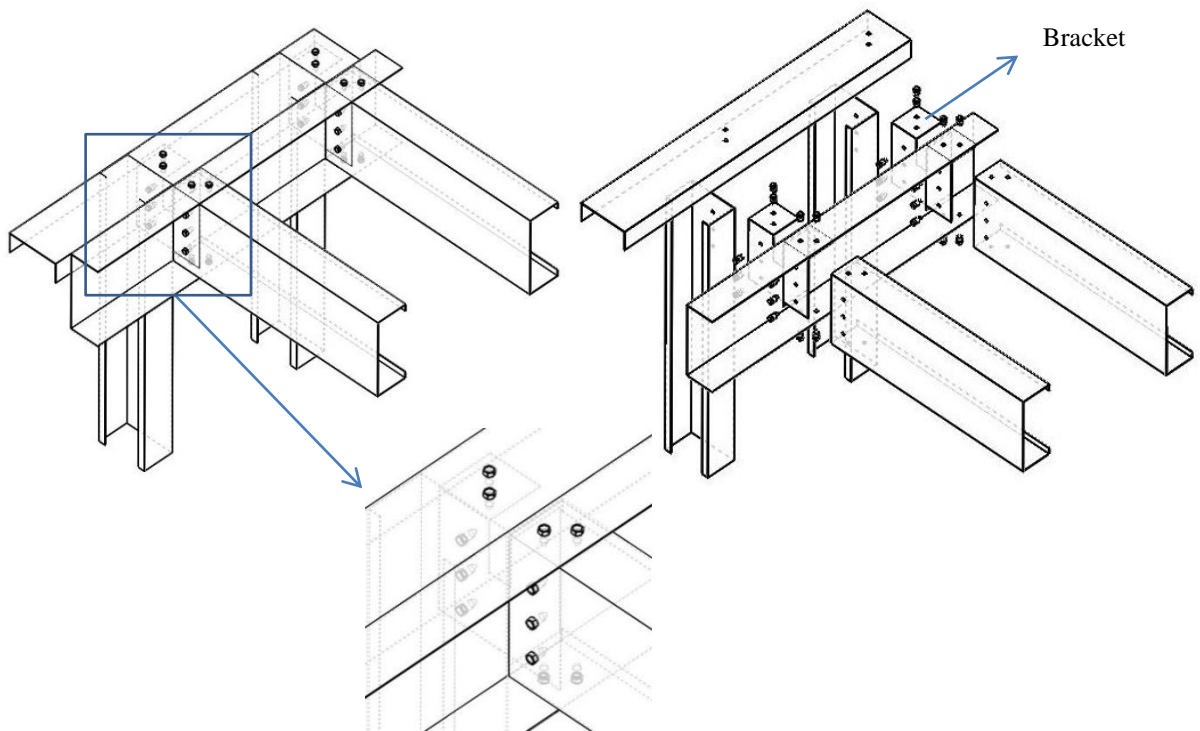
Figure 6-3 Perspective and explosion diagram of connection type B

Double cleats
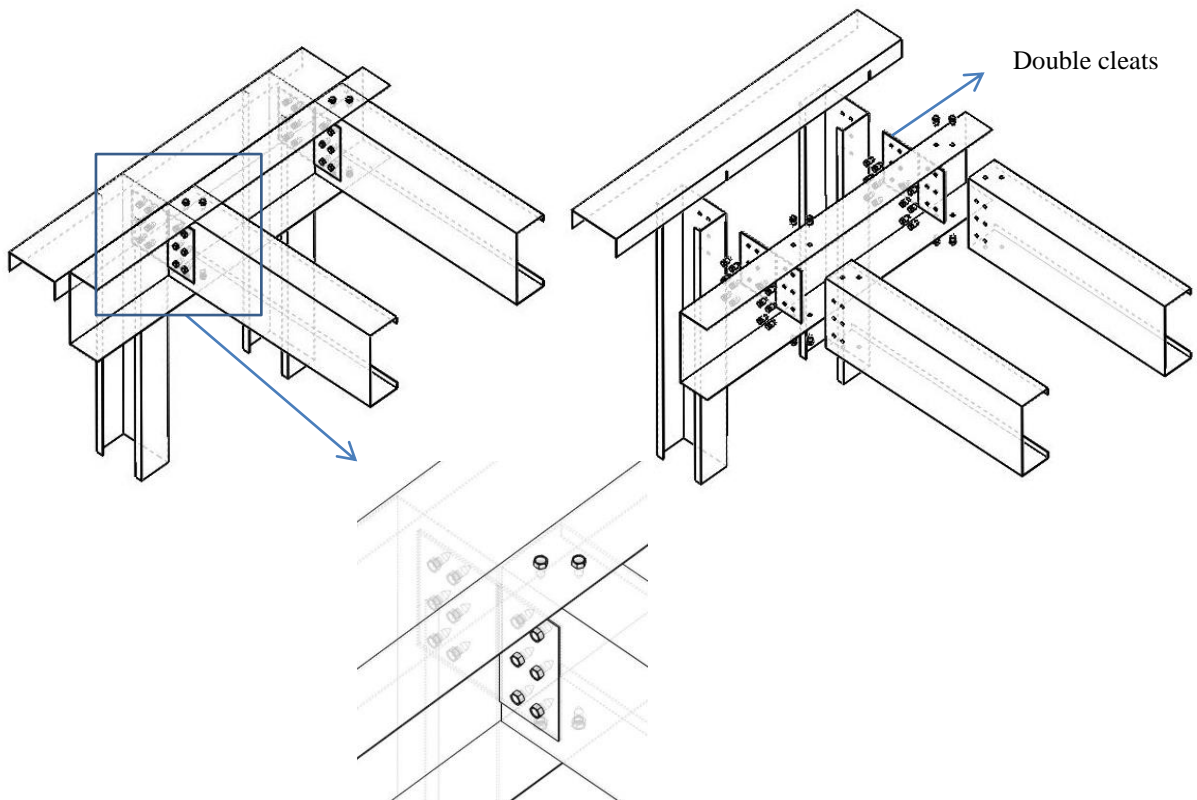
Figure 6-4 Perspective and explosion diagram of connection type C

The connection type C consists of two rectangular cleats assembled through the pre-opening in tracks and post (see Figure 6-4). The cleats are put both sides of the connected webs. As shown in Figure 6-5, only one rectangular cleat is employed in connection type D to connect the back-to-back compound sections. The screw joints in connection C and D are performed as double shear joint.
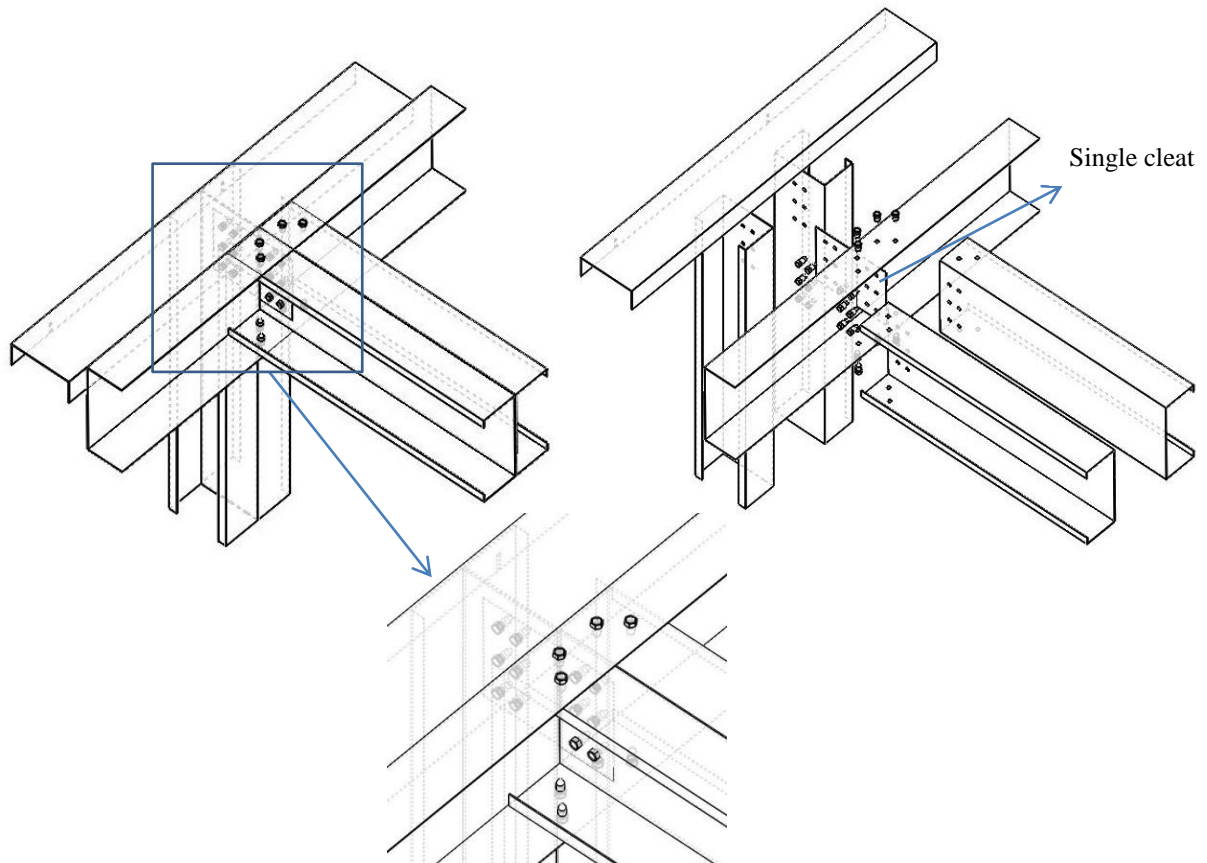
Figure 6-5 Perspective and explosion diagram of connection type D

6.1.2 Theoretical analysis

6.1.2.1 Assumptions

The structural behaviour of the screw joint follows the experimental results obtained in Chapter 5. It should be noted that, the floor slab, brick wall, oriented strand board (OSB) or cement particle board (CPB) are general attached in the construction system (Lawson et al., 2012) and the lateral torsional distortion caused by the eccentricity of the open section can be

restrained (Lawson and Ogden, 2008). Compared with the ductility of the each connection, the elongation of the joist section is small enough to be ignored.

The in-plane strength (U) and stiffness (K) of the connection between two modular panels consist of (1) joist section in-plane deformation (U_j, K_j), (2) deformation of joint between joist and track (U_{jt}, K_{jt}), (3) floor track deformation (U_t, K_t), (4) the deformation of connector between the floor panel and wall panel (U_c, K_c), including joint, cleat or bracket, and (5) deformation of the post section (U_p, K_p). T_u is the tension resistance of the screw joint; Q_u is the ultimate resistance of single shear screw joint; the $Q_u{}'$ is the ultimate resistance of the double shear joint; k_1 is the stiffness of the screw single shear joint; k_2 is the stiffness of the double shear joint; k_3 is the stiffness of the single tension joint.

$$\frac{1}{K} = \frac{1}{K_j} + \frac{1}{K_{jt}} + \frac{1}{K_t} + \frac{1}{K_c} + \frac{1}{K_p} \tag{Eq. 6-1}$$

$$U = \min(U_j, U_{jt}, U_t, U_c, U_p) \tag{Eq. 6-2}$$

6.1.2.2 Longitudinal tension resistance

The longitudinal stiffness K_l and strength U_l of the connection are:

$$\frac{1}{K_l} = \frac{1}{K_{jt,l}} + \frac{1}{K_{t,l}} + \frac{1}{K_{c,l}} + \frac{1}{K_{p,l}} \tag{Eq. 6-3}$$

$$U_l = \min(U_{jt,l}, U_{t,l}, U_{c,l}, U_{p,l}) \tag{Eq. 6-4}$$

For connection type A, joist and track are connected by four screws subjected to single shear force pattern, therefore,

$$\frac{1}{K_{jt,l}} = \frac{1}{4k_1} \tag{Eq. 6-5}$$

$$U_{jt,l} = 4Q_u \tag{Eq. 6-6}$$

The track and post are connected by four screw single tension joints, the connection properties can be expressed by,

$$\frac{1}{K_{c,l}} = \frac{1}{4k_3} \tag{Eq. 6-7}$$

$$U_{c,l} = 4T_u \tag{Eq. 6-8}$$

The stiffness and strength of the floor track ($K_{t,l}$, $U_{t,l}$) and post ($K_{p,l}$, $U_{p,l}$) depend on the section material and dimensions.

For connection type B, the wall panel and floor panel are only connected through bracket. The five joints connecting bracket and joist are subjected to shear force. The longitudinal stiffness K_l and strength U_l of the connection are only related to $K_{c,l}$ and $U_{c,l}$.

$$\frac{1}{K_l} = \frac{1}{K_{c,l}} = \frac{1}{5k_1} \qquad \text{(Eq. 6-9)}$$

$$U_l = U_{c,l} = 5Q_u \qquad \text{(Eq. 6-10)}$$

For connection type C, floor panel and wall panel are assembled by double cleats with six double shear screw joints.

$$\frac{1}{K_l} = \frac{1}{K_{c,l}} = \frac{1}{6k_2} \qquad \text{(Eq. 6-11)}$$

$$U_l = U_{c,l} = 6Q_u' \qquad \text{(Eq. 6-12)}$$

Connection D is the same with connection C.

6.1.2.3 Vertical shear resistance

The vertical stiffness K_v and strength U_v are:

$$\frac{1}{K_v} = \frac{1}{K_{t,v}} + \frac{1}{K_{c,v}} \qquad \text{(Eq. 6-13)}$$

$$U_v = \min(U_{t,v}, U_{c,v}) \qquad \text{(Eq. 6-14)}$$

For connection type A, the vertical load is carried by the four fasteners linking floor panel and wall panel. The stiffness and strength of the connector can be calculated by:

$$\frac{1}{K_{c,v}} = \frac{1}{4k_1} \qquad \text{(Eq. 6-15)}$$

$$U_{c,v} = 4Q_u \qquad \text{(Eq. 6-16)}$$

For connection type B, each module is connected to the bracket with five fasteners, including two screws on the top and three screws in the middle. The calculations can be obtained:

$$\frac{1}{K_v} = \frac{1}{K_{c,v}} = \frac{1}{3k_1} + \frac{1}{2k_3} \qquad \text{(Eq. 6-17)}$$

$$U_v = U_{c,v} = 3Q_u + 2T_u \qquad \text{(Eq. 6-18)}$$

The stiffness and strength of the floor track ($K_{t,v}$, $U_{t,v}$) depend on the section material and dimensions.

For connection type C, floor panel and wall panel are assembled by double cleats with six double shear screw joints.

$$\frac{1}{K_v} = \frac{1}{K_{c,v}} = \frac{1}{6k_2} \qquad \text{(Eq. 6-19)}$$

$$U_v = U_{c,v} = 6Q_u{}' \qquad \text{(Eq. 6-20)}$$

Connection D is the same with connection C.

6.1.2.4 Rotation resistance

Assuming the rotation centre is at the bottom corner of the floor panel track, the rotation stiffness K_r and moment carrying capacity U_r can be figured out. As for connection type A, rotation stiffness K_r is contributed by screw joints between joist and track $K_{jt,r}$, track $K_{t,r}$, screw tension joints between track and post $K_{c,r}$, and the rotation stiffness of post flange $K_{p,r}$.

$$\frac{1}{K_r} = \frac{1}{K_{jt,r}} + \frac{1}{K_{t,r}} + \frac{1}{K_{c,r}} + \frac{1}{K_{p,r}} \qquad \text{(Eq. 6-21)}$$

$$U_r = \min(U_{jt,r}, U_{t,r}, U_{c,r}, U_{p,r}) \qquad \text{(Eq. 6-22)}$$

$$K_{jt,r} = \frac{M}{\theta} = \frac{2\Delta k_1 h}{\theta} \qquad \text{(Eq. 6-23)}$$

Assuming that θ is small enough, $\sin\theta = \Delta/h \approx \theta$, then

$$K_{jt,r} = 2k_1 h^2 \qquad \text{(Eq. 6-24)}$$

$$U_{jt,r} = 2D_{u1}k_1 h \qquad \text{(Eq. 6-25)}$$

D_{u1} is the deformation when the screw joint reach the maximum shear resistance.

For the screw tension connection between wall panel and floor panel,

$$K_{c,r} = \frac{M}{\theta} = \frac{\sum \Delta_i k_3 d_i}{\theta} \text{ (i = 1,2,3,4)} \qquad \text{(Eq. 6-26)}$$

$$U_{c,r} = \sum \Delta_i k_3 d_i \text{ (i = 1,2,3,4)} \qquad \text{(Eq. 6-27)}$$

where θ is the rotation angle, h the height of the joist, Δ_i is the deflection of each screw, d_i is the distance of screw to the inflection point, $\Delta_{max} = D_{u3}$ which is the screw joint deformation when the maximum tension force is achieved; $K_{t,r}$, $K_{p,r}$ and $U_{t,r}$ can be examined by FEM.

For connection type B, the five single shear screw joints resist transverse bending:

$$\frac{1}{K_r} = \frac{1}{K_{c,r}} + \frac{\sum \Delta_i k_1 d_i}{\theta} \text{ (i = 1,2,3,4,5)} \qquad \text{(Eq. 6-28)}$$

$$U_r = U_{c,r} + \sum \Delta_i k_1 d_i \text{ (i = 1,2,3,4,5)} \qquad \text{(Eq. 6-29)}$$

$K_{c,r}$ and $U_{c,r}$ are the stiffness and strength of the bracket that can be examined by FEM.

For connection type C, there are six double shear screw joints resisting the moment:

$$\frac{1}{K_r} = \frac{1}{K_{c,r}} + \frac{\sum \Delta_i k_2 d_i}{\theta} \ (i = 1,2,3,4,5,6) \tag{Eq. 6-30}$$

$$U_r = U_{c,r} + \sum \Delta_i k_2 d_i \ (i = 1,2,3,4,5,6) \tag{Eq. 6-31}$$

$K_{c,r}$ and $U_{c,r}$ are the stiffness and strength of the cleat that depend on the section material and dimensions. Connection D is the same with connection C.

6.1.3 Numerical analysis

6.1.3.1 Normal loading conditions

6.1.3.1.1 Modelling process

In the models, the internal space between joists or posts was 300mm. The floor panel was 3 metres in width and 6 metres long. The wall panel was 3m high and 6m in length. The stud and track sections were selected based on the current productions from the Albion Sections Ltd. Table 6-1 presents the dimension properties of the sections.

Table 6-1 Dimensions and properties of the connected sections

SECTION	DEPTH mm	FLANGE mm	LIPS mm	THICKNESS mm	I_{xx} cm^4	Z_{xx} cm^3	R_{xx} cm	b/h mm
Section 1 AS1506115	150	61	15	1.5	158.68	21.16	5.98	60.25/148.50
	154	57	0	1.5	142.45	18.50	5.99	56.25/152.50
	154	57	0	1.5	142.45	18.50	5.99	56.25/152.50
Section 2 AT1545715	150	61	15	1.5	158.68	21.16	5.98	60.25/148.50
	I_{yy} cm^4	Z_{xxc} cm^3	Z_{yy} cm^3	R_{yy} cm	$\overline{Y}$ cm	AREA cm^2	WEIGHT Kg/m	e mm
Section 3 AT1545715	22.31	19.39	5.24	2.24	1.84	4.44	3.41	14.24
	12.14	13.08	2.74	1.75	1.27	3.97	3.09	12.91
Section 4 AS1506115	12.14	13.08	2.74	1.75	1.27	3.97	3.09	12.91
	22.31	19.39	5.24	2.24	1.84	4.44	3.41	14.24

The screw joints and material were established based on the modified modelling process mentioned in Section 4.3. The screw shank was constrained with the edge of the hole by "tie".

In terms of the boundary conditions, the bottom of the post was fixed. To simplify the calculations, symmetrical modelling was employed. At the end of the joist and tracks, symmetry constraints (ZSYMM, XSYMM) were utilised respectively.

The uniform distributed load was directly applied at the flange of the joist. Riks solution was adopted in the nonlinear analysis to find out the critical bearing capacity of the systems.

6.1.3.1.2 Results

The lateral torsion caused by the eccentricity to the shear centre was observed under normal loading conditions (see Figure 6-6 and 6-7). According to the numerical analysis, the ultimate resistance of connection type A is 4.87kN. The maximum stress occurred in the screw joint of the bottom flange. As shown in Figure 6-6, the bearing capacity of the joist-to-post connection is limited by the local failure.
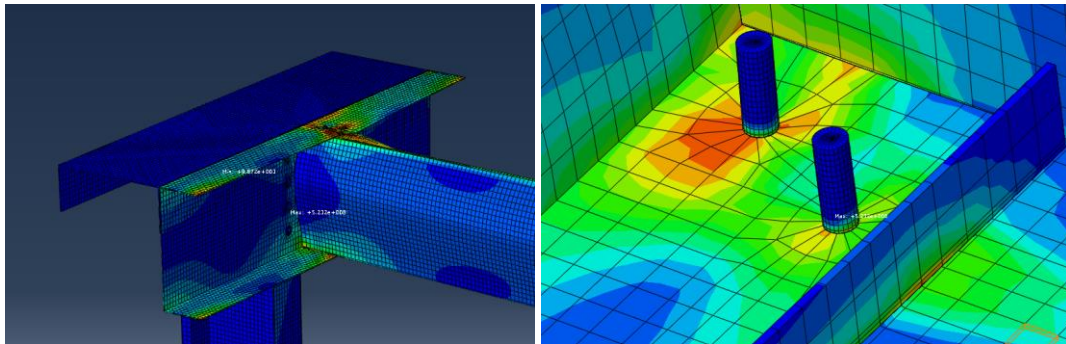
Figure 6-6 Meshing and stress contour of the connection type A

As is mentioned above, the typical joist-post connection in modular structure presents ineffective force transferring path. According to the results, the floor panel track carried most of the allowable load. In order to take full advantage of each member and improve the resistance of the connection, a bracket was proposed as shown in connection type B (see Figure 6-7). The thickness of the bracket is 3mm. The material of the bracket is the same with the sections. The floor panel track is no longer to be considered as the load carrying member, which is removed from the modelling. Based on the analysis, it can be observed that the failure occurs in the proposed bracket.
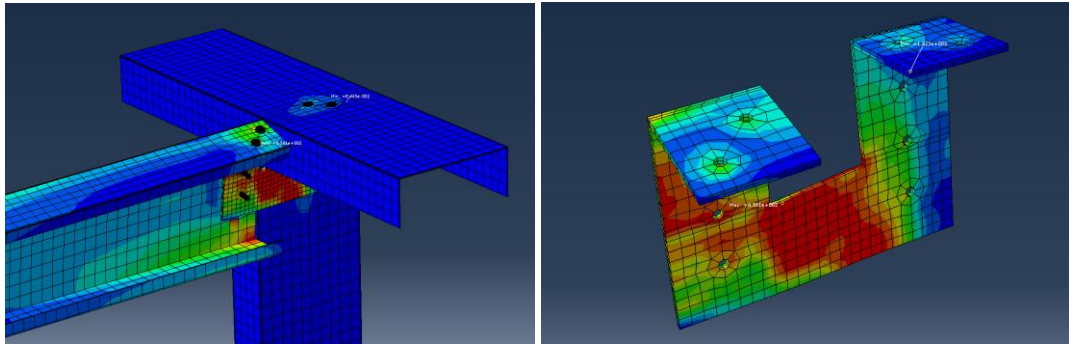
Figure 6-7 Meshing and stress contour of the connection type B

The resistance of the system with connection B is significantly improved with the carrying capacity of the connection being 7.60kN, which is 56% higher than the system assembled by the typical connecting method. The deformation and Von Mises stress distribution of the bracket are shown in Figure 6-7.

6.1.3.2 Abnormal loading conditions

The numerical analysis of connection performance involves the potential loading scenarios of shear, tension and rotation. The structural properties of each screw joint are assumed to follow the numerical analysis in Section 5.3. When the connection is subjected to pure bending action, it is assumed that the connection characterises sufficient rotation capacity. In the post-failure stage, plastic hinge can be formed when the connection loses the moment resistance.

6.1.3.2.1 Modelling process

6.1.3.2.1.1 Material and dimension

The connection impacting zoon in the analysis is assumed to be limited in 200mm of the post and 100mm of joist, which is based on the potential deformation of the joint and connected members. In order to identify the connection response, 200mm post and 100mm joist related to the connection were established in the FE modelling. The tracks were 300mm long. The section selection was based on SSMA ICBO ER-4943P.

This system consists of the CFS components using S550 steel plate. The material property was based on Section 5.2.4.1 and 5.3.1.3. Table 6-2 shows the dimension properties of the stud and track sections.

Table 6-2 Dimensions and properties of the connected sections

SECTION	DEPTH mm	FLANGE mm	LIPS mm	THICKNESS mm	Ixx cm^4	Zxx cm^3	Rxx cm	Mmax kN·m
Section 1 600S200-43	152	51	16	1	99.99	13.15	5.95	6.75
	154	51	0	1	87.78	11.4	5.9	5.85
Section 2 600T200-43	91	41	0	1	22.07	4.85	3.61	2.49
	89	41	13	1	24.76	5.56	3.58	2.85
	Iyy cm^4	Zxxc cm^3	Zyy cm^3	Ryy cm	$\overline{Y}$ cm	AREA cm^2	WEIGHT Kg/m	e mm
Section 3 350T162-43	10.27	6.91	2.84	1.9	1.48	2.82	2.21	16.85
	5.7	5.58	1.39	1.5	1.02	2.52	1.97	16.78
Section 4 350S162-43	2.66	2.74	0.85	1.25	0.97	1.69	1.32	14.78
	4.76	3.41	1.76	1.57	1.39	1.93	1.51	14.87

6.1.3.2.1.2 Element and meshing

In the study, the commercial FE package ABAQUS was used to carry out further analysis of joints implemented in modular construction. Three-dimensional SHELL element S4R (A 4-node doubly curved thin or thick shell, reduced integration, hourglass control, and finite membrane strains) was employed to predict the behaviour of the thin-walled components.

This element involves six degrees of freedom-three translations and three rotations. The screw joint in the connection was simulated by Bushing Connector Section (BCS) which is flexible in usage without specific shape and provides a bushing-like connection between two nodes. Between the nodes, six degrees including three translations and three rotations of bushing element (see Figure 5-30) can be defined linearly or nonlinearly with the damage criteria. BCS does not constrain any components of relative motion and uses local orientation definitions, which is equivalent to combining connection types Projection Cartesian and Projection Flexion-torsion. The responses of the connection in three local directions are specified by the Projection Cartesian connection. This connection applies orthonormal system that follows the systems at both nodes *a* and *b* (see Figure 6-8). Thus, the change in position of node *b* relative to node *a* along the (projection) coordinate directions (e_1, e_2, e_3) are

measured. Connection type Projection Flexion-torsion provides rotational properties between two nodes, accounting two component flexion angles as shown in Figure 6-8.
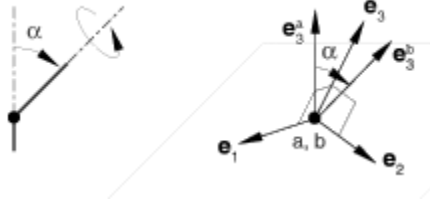
Figure 6-8 Illustration of connection translation and rotation (Abaqus-6.13, 2013)

In the modeling, nonlinear elasticity in shear and tension direction were defined based on test data in Section 5.2.4. As a result, the connectors became damaged when the longitudinal elongation exceeded 8.10mm/15.15mm for single/double shear specimens in the shear direction. The maximum tension resistance of BCS was limited by 1.58kN. The diameter of the connector was 5.5mm. Meshing is closely related to the convergence and precision of FEM modelling. The shell element shape was "Quad" with "Structured" technique. Through an extensive trial-and-error process and sensibility analysis, the most satisfactory results were achieved while using the following discretisation pattern: the approximate global sizing of the screw was 1.6mm; in terms of CFS components, that value was defined as 5mm.

6.1.3.2.1.3 Boundary condition and loadings

The end of the post was fixed. At the end of the track, a symmetry constraint (ZSYMM) was applied. Displacement load was applied in the simulation in each scenario. The lateral movement of the joist was restrained.

6.1.3.2.1.4 Interaction and solution

The friction coefficient of 0.3 was applied to the interfaces. The "hard contact" condition was defined between components. The Von Mises yield criterion was adopted for the analysis along with nonlinear incremental-iterative Full Newton solution technique. Material and geometric nonlinearity were taken into account. The investigation did not involve the buckling analysis of the joists. Therefore, the initial imperfection was not introduced in the simulation.

6.1.3.2.2 Results

As shown in Figure 6-9, when the connection type A under a tension force, the tension force rises linearly with an increase of the displacement. When the displacement reaches 8.36mm, the side screw joints are supposed to be pulled out firstly, with ultimate loading force 3.73kN. Hence, the tension force drops down. After that the middle screw begins to carry the load until the failure occurred. The maximum horizontal movement of connection A is 13mm. Figure 6-10 shows that when the connection is subjected to pure shear force, the screw joints provide amply resistance. However, when the displacement reaches 4mm, the local buckling in the web of the joist is observed, leading to the vertical stiffness of the connection reduced sharply. When the deflection of the joist reaches 20mm, the shear resistance of connection A is 5.51kN. The rotation response of connection type A is mainly determined by the screw pull-out resistance. There are four steps during the simulation (see Figure 6-11). As shown in Figure 6-12, the screw joints connecting the floor and wall panels fail orderly from top to bottom. The ultimate moment of 0.22kN·m is obtained when the rotation angle is 0.06rad.

Figure 6-9 Connection type A subjected to pure tension
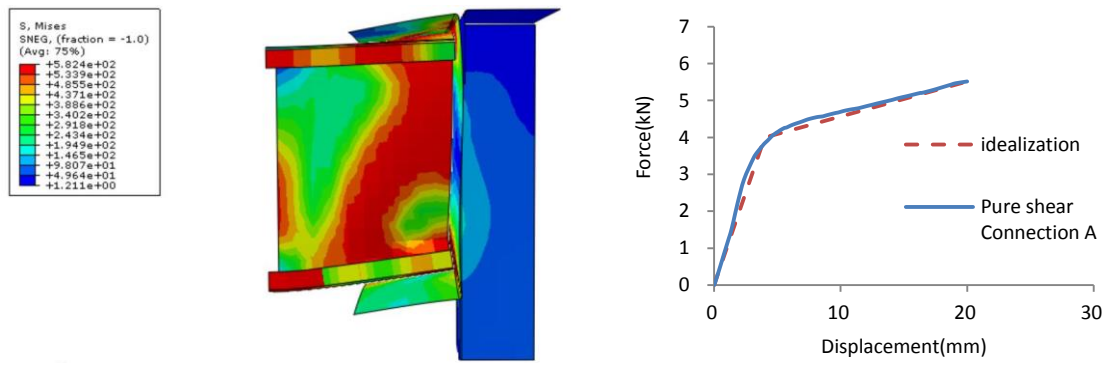
Figure 6-10 Connection type A subjected to pure shear

Figure 6-11 Moment-rotation curve of connection A subjected to bending
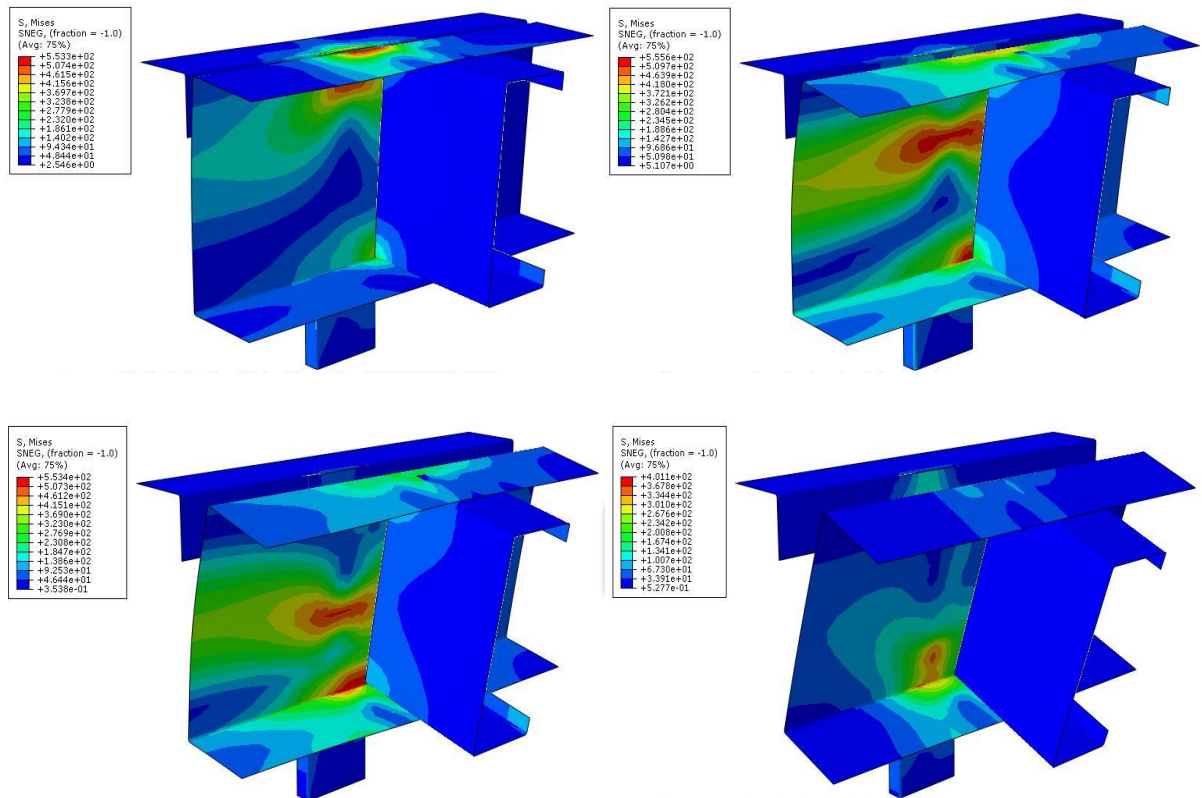
Figure 6-12 Connection type A subjected to bending

150
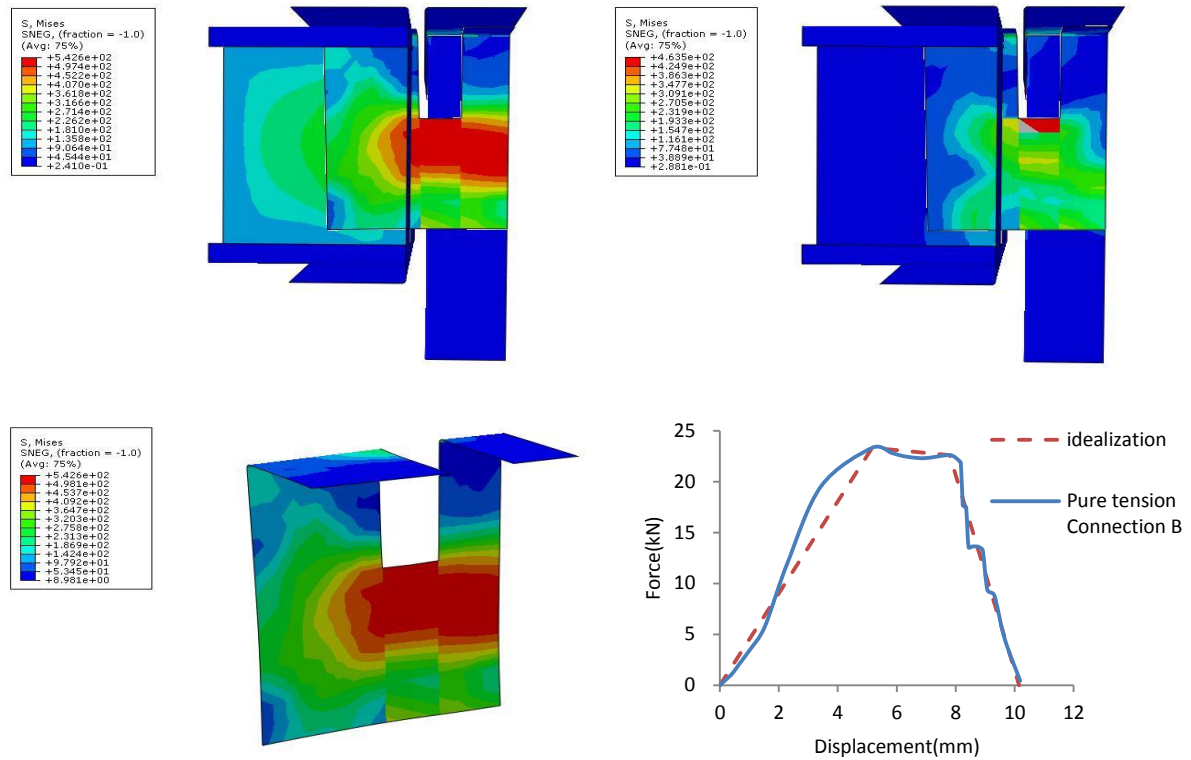
Figure 6-13 Connection type B subjected to pure tension

The ultimate tension resistance of connection type B is 23.32kN, with the displacement of 5.17mm (see Figure 6-13), indicating that the enhancement of the introduced bracket is sound. The tension resistance of connection B is around six times of that of connection A, whereas the horizontally allowable movement (10.15mm) is smaller than connection type A.

It can be found that the fastener was supposed to be wrecked before the failure occurred in the connected component. In the pure shearing scenario (see Figure 6-14), due to the deformation of the bracket, the initial stiffness of connection type B is only 910kN/m, and the stiffness is further reduced after the shear force reaching 6.98kN. Herein, a notable local buckling occurs in the bracket. The ultimate shear force is 8.47kN, which is improved 54% of the resistance of connection type A.
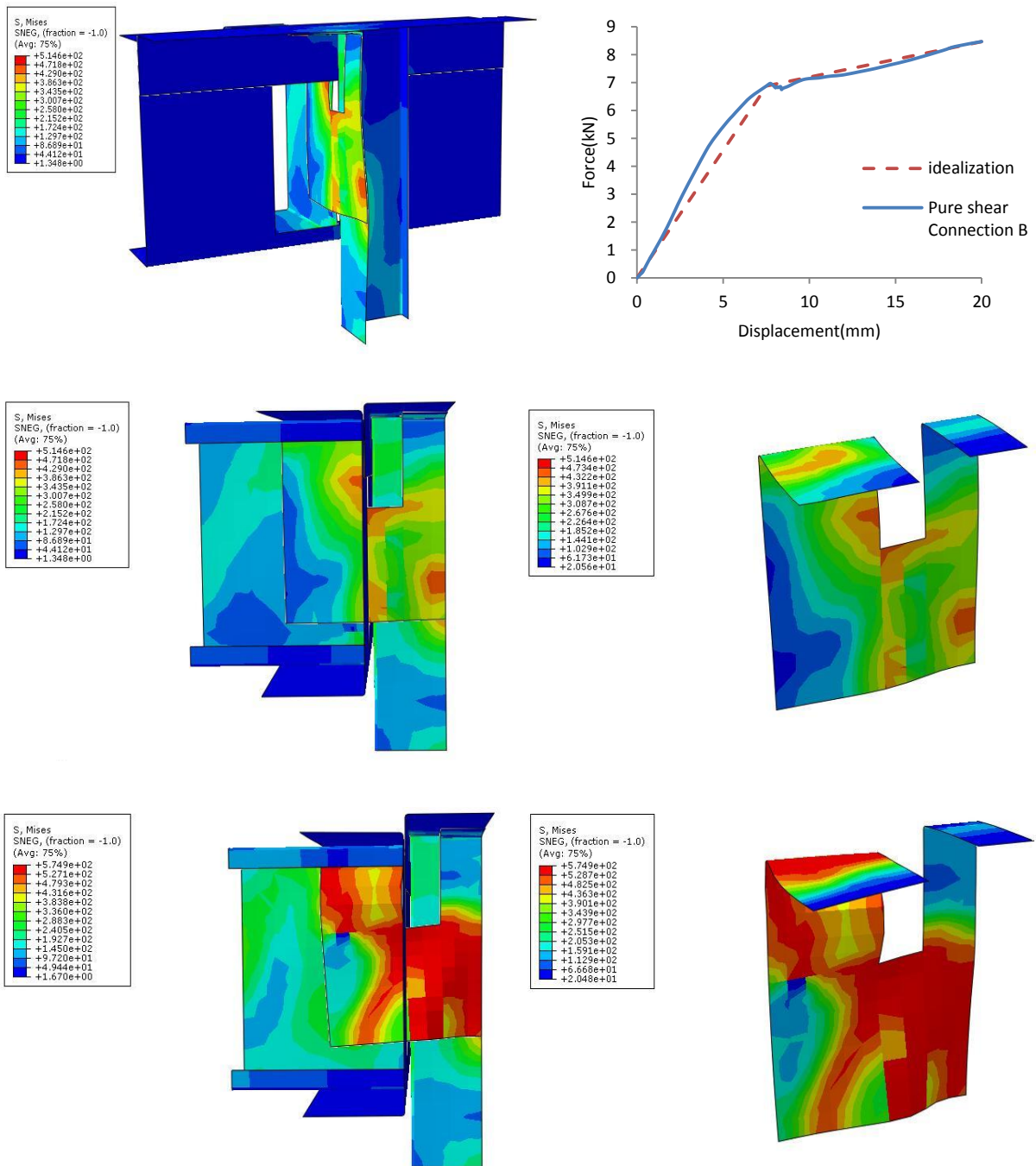
Figure 6-14 Connection type B subjected to pure shear
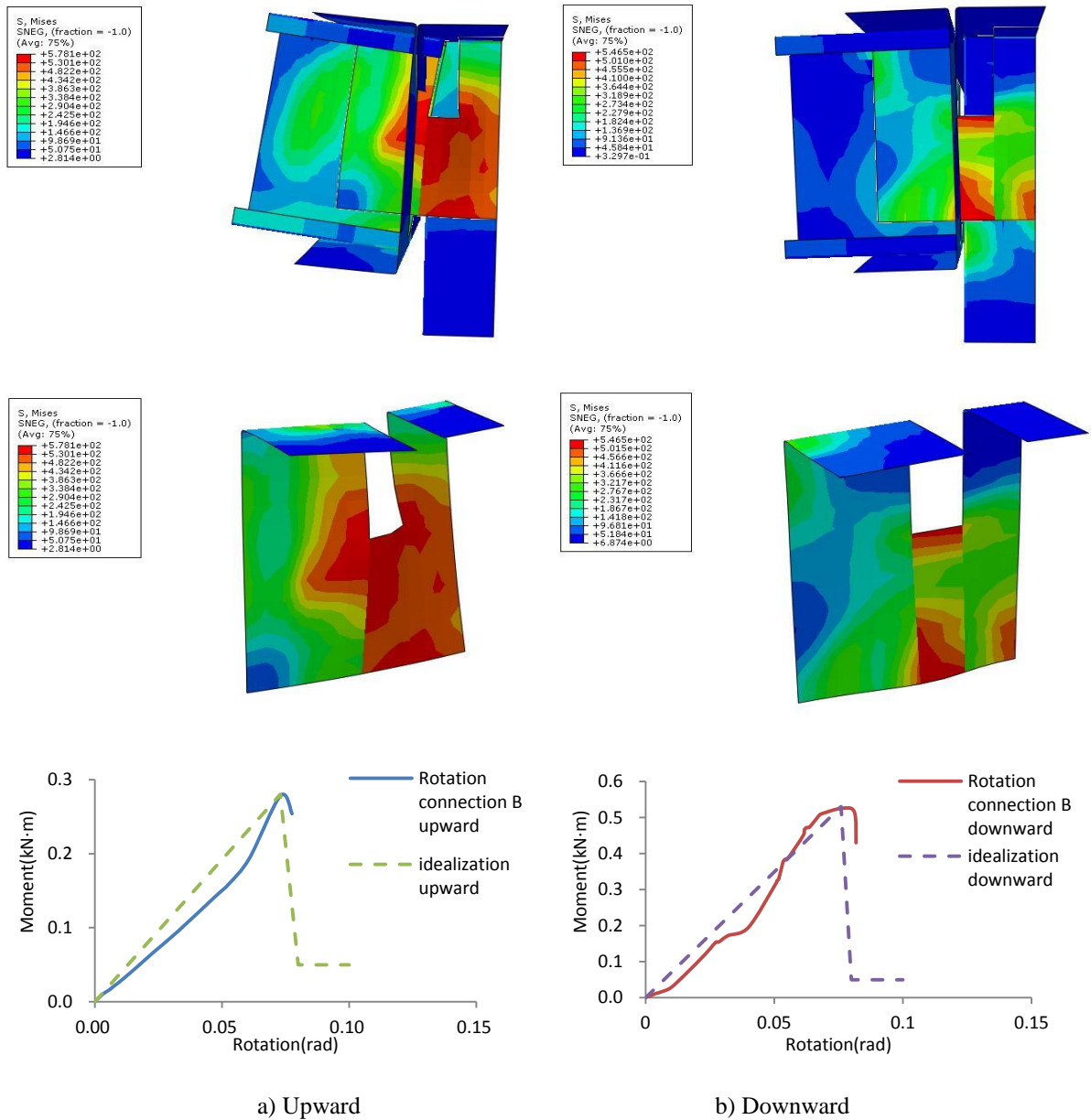
a) Upward   b) Downward

Figure 6-15 Connection type B subjected to bending

As shown in Figure 6-15, the upward and the downward rotation resistance are 0.28kN·m and 0.53kN·m respectively. The connection compromises after the rotation angle exceeding 0.073rad and 0.076rad. The allowable rotation angle is larger than that of connection type A in either upward or downward direction.
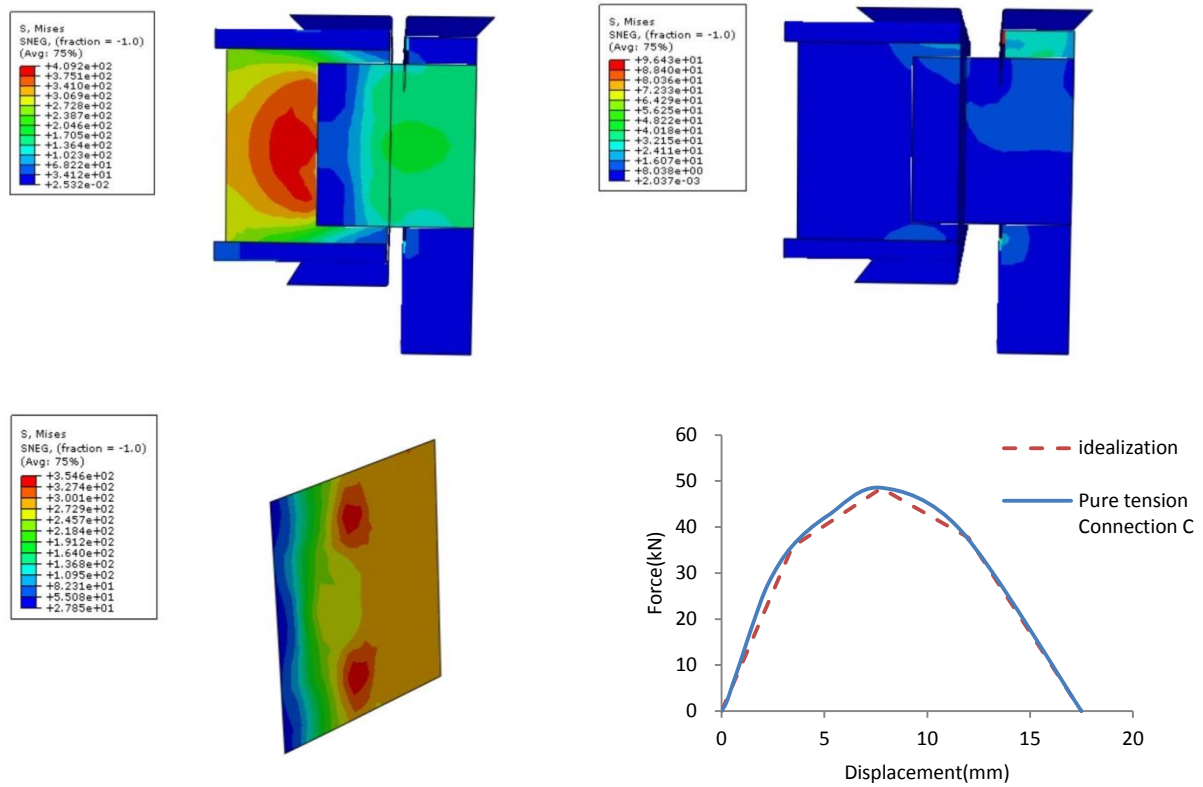
Figure 6-16 Connection type C subjected to pure tension

Figure 6-16 shows that the tension resistance (48.54kN) can be achieved with the horizontal movement being 7.76mm. It is found that the double cleat connection configuration significant increase the tension resistance of the joist-to-post connection. The maximum displacement is 17.5mm which is also greater than others. However, when the connection is subjected to pure shear load, the resistance of the connection is limited by the local bucking occurred around the opening in the web (see Figure 6-17). The displacement-to-force curve shows moderate trend after reaching the peak load 11.20kN. Figure 6-18 illustrates that the ultimate bending moment (1.05kN·m) can be obtained when the rotation angle is 0.17rad. The stress concentration appears in the post leading to the softening after reaching the peak load.
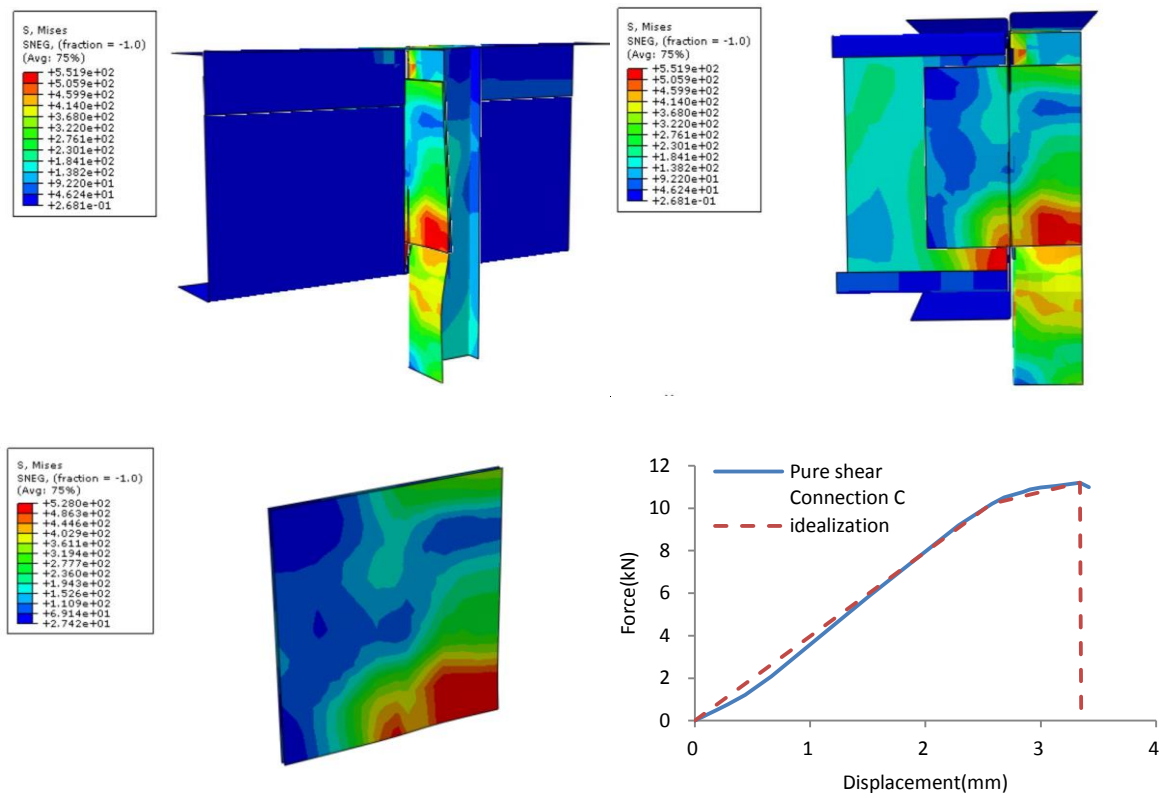
Figure 6-17 Connection type C subjected to pure shear
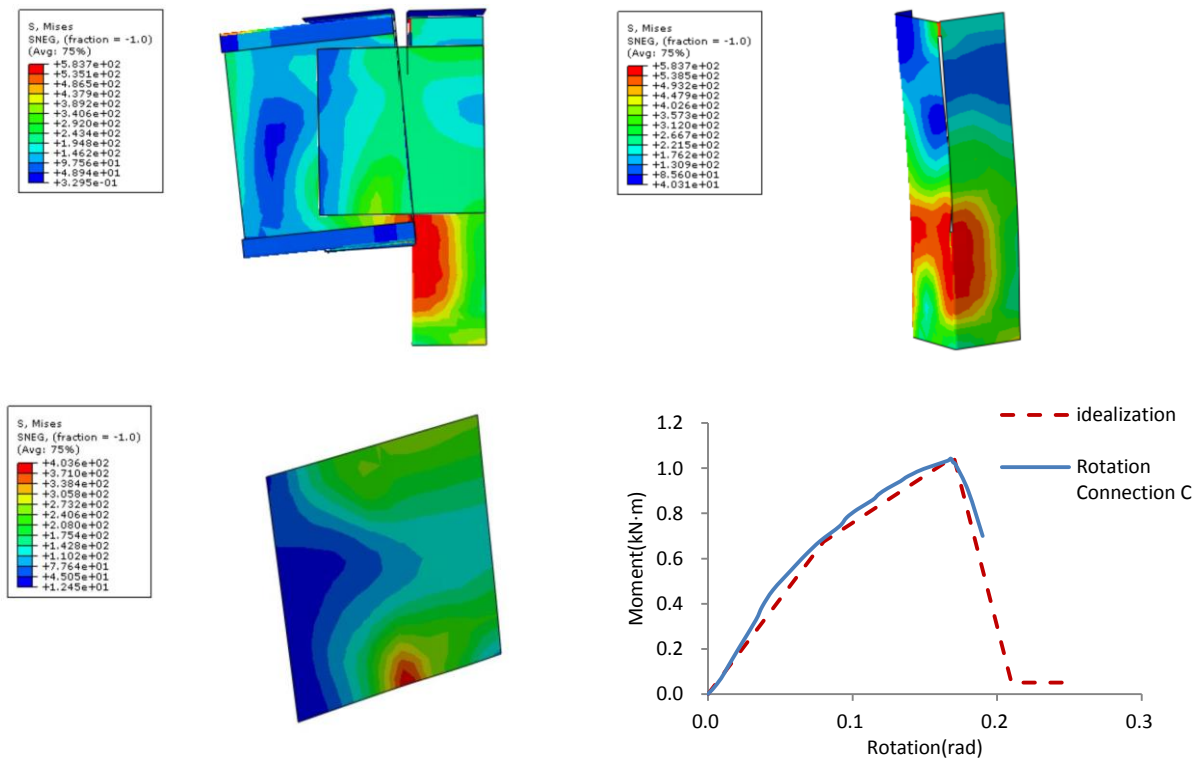
Figure 6-18 Connection type C subjected to bending

As shown in Figure 6-19, the number of the fasteners in connection D is the same with connection type C. As a result, the tension resistances of connection C (48.50kN) and connection D (48.41kN) are almost the same. However, the connection D provides better shearing resistance than connection C when the vertical displacement reaches 5.26mm, with the ultimate force of 32kN (see Figure 6-20). This type of connection also provides the greatest ultimate bending moment and initial rotation stiffness (see Figure 6-21). The peak moment can be obtained when the rotation angle of the connection is 0.08rad. The structural behaviour of each connection configuration and the corresponding idealized curves are listed in Table 6-3.
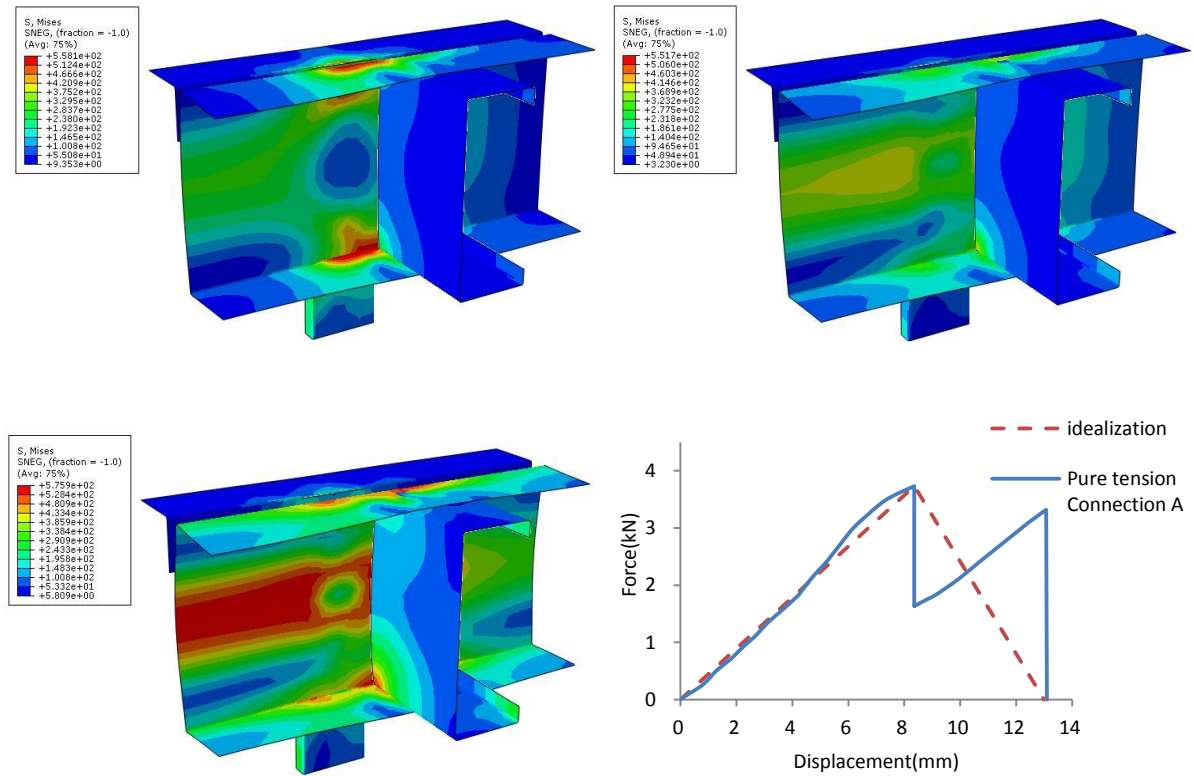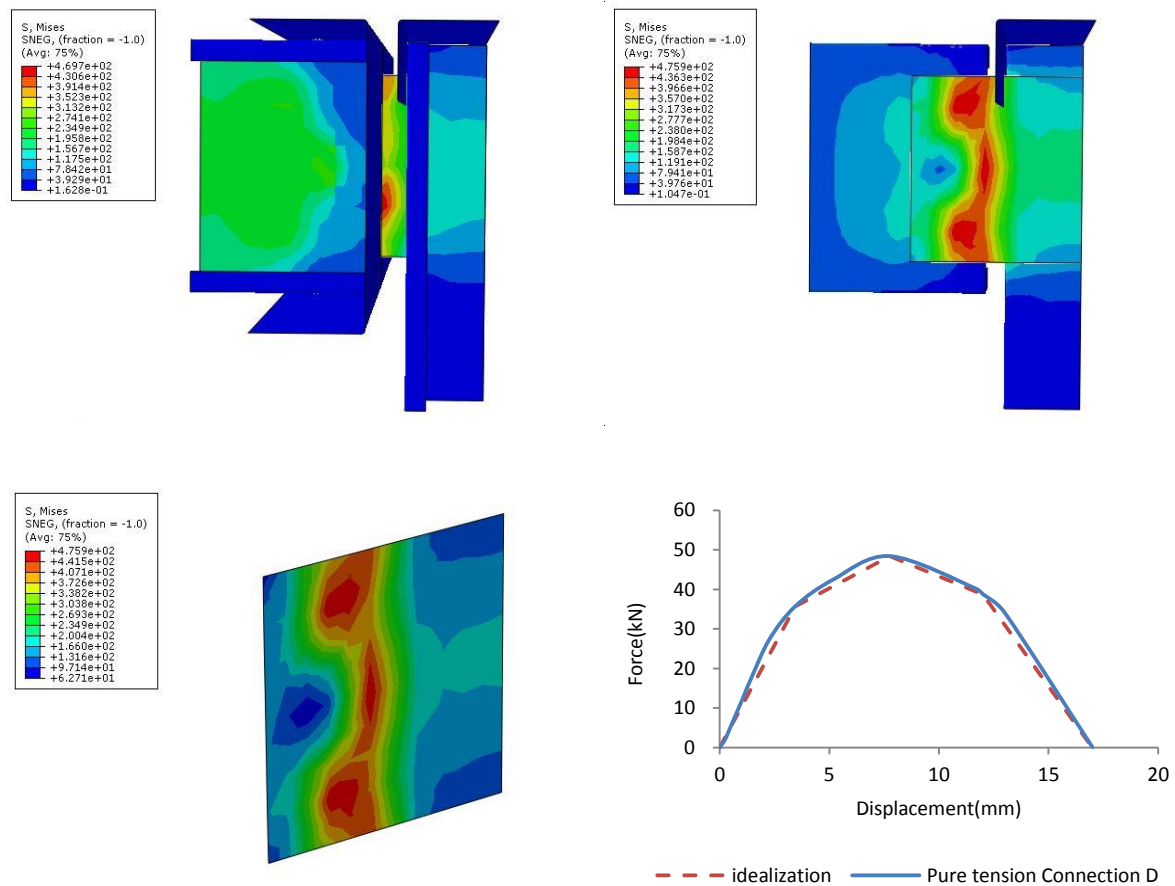

Figure 6-19 Connection type D subjected to pure tension
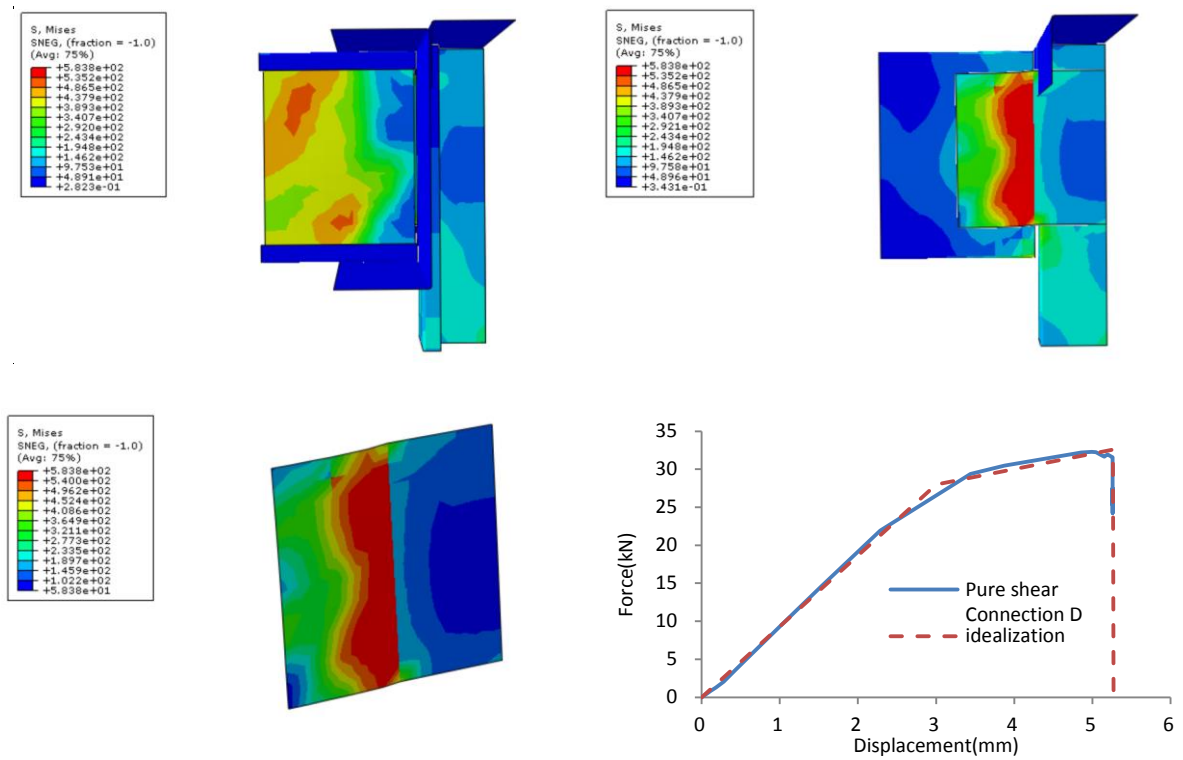
Figure 6-20 Connection type D subjected to pure shear
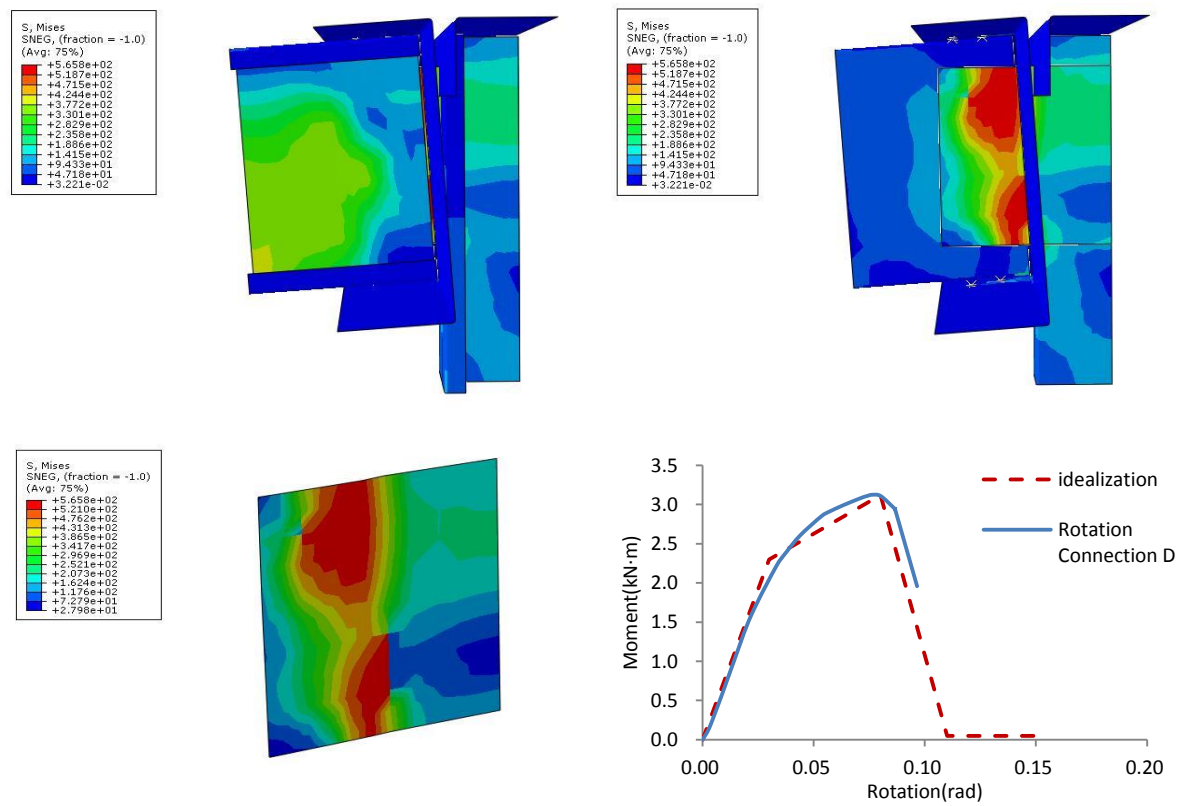
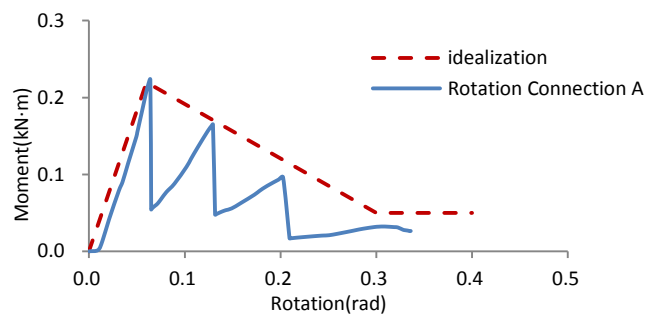Figure 6-21 Connection type D subjected to bending

Table 6-3 Connection simulation results

Connection type	Load pattern	Ultimate force (moment) Umax kN (kN·m)	Displacement (Rotation) δ mm (rad)	Failure mode	Initial stiffness k0 kN/mm (kN·m/rad)	Idealized lines	
A	Tension	3.73	8.36	Screw pull-out	0.45	y=0.45x y=-0.80x+10.45	0≤x≤8.36 8.36＜x≤13
	Shear	5.51	20.00	Buckling in the joist and floor track sections	1.00	y=x y=0.09x+3.62	0≤x≤4 4＜x≤20
	Bending	(0.22)	(0.06)	Screw pull-out	(3.67)	y=3.67x y=-0.71x+0.26 y=0.05	0≤x≤0.06 0.06＜x≤0.30 x＞0.3
B	Tension	23.32	5.17	Screw joint shear failure	4.51	y=2.26x y=-0.14x+12.37 y=-4.62x+47.31	0≤x≤5.17 5.17＜x≤7.8 7.80＜x≤10.15
	shear	8.47	20.00	Buckling in the bracket	0.91	y=0.91x y=-0.13x+8.77	0≤x≤7.54 7.54＜x≤8.77
	Bending	Upward (0.28) Downward (0.53)	Upward (0.073) Downward (0.076)	Buckling in the bracket	Upward (3.84) Downward (6.97)	Upward: y=3.84x y=-32.86x+2.68 y=0.05 Downward: y=6.97x y=-120x+9.65 y=0.05	0≤x≤0.073 0＜x≤0.08 x＞0.08 0≤x≤0.076 0＜x≤0.08 x＞0.08
C	Tension	48.54	7.76	Screw joint shear failure	10.43	y=10.43x y=2.93x+25.82 y=-2.41x+67.22 y=-6.70x+117.32	0≤x≤3.44 3.44＜x≤7.76 7.76＜x≤12 12＜x≤17.5
	Shear	11.20	3.34	Buckling in the post web	3.97	y=3.97x y=1.29x+6.91 y=-70x+245	0≤x≤2.57 2.57＜x≤3.34 3.34＜x≤3.5
	Bending	(1.05)	(0.17)	Buckling in the post	(8.44)	y=8.44x y=4.17x+0.34 y=-25x+5.30 y=0.05	0≤x≤0.08 0.08＜x≤0.17 0.17＜x≤0.21 x＞0.21
D	Tension	48.41	7.76	Screw joint shear failure	10.37	y=10.37x y=2.95x+25.53 y=-2.28x+66.10 y=-7.77x+132.11	0≤x≤3.44 3.44＜x≤7.76 7.76＜x≤12.81 12.81＜x≤17
	Shear	32.58	5.26	Failure in the cleat	9.33	y=9.33x y=2.03x+21.92 y=0	0≤x≤3 3＜x≤5.26 x＞5.26
	Bending	(3.12)	(0.08)	Screw joint shear failure	(76.67)	y=76.67x y=16.40x+1.81 y=-102.33x+11.31 y=0.05	0≤x≤0.03 0.03＜x≤0.08 0.08＜x≤0.11 x＞0.11

6.2 Robustness investigation

Constructions undergo disproportional/progressive collapse when the primary elements fail. Investigations have been conducted to prevent disproportional/progressive collapse and have been reflected in design codes, specifications and guidelines, including the British Standard

(BS., 1997, BS., 1996) and Regulation (ODPM., 2004), Eurocode (Eurocode, 2004, Eurocode, 2006a), NBCC (2005), ASCE7-05 (2005), ACI318 (2011), GSA guidelines (GSA., 2000, GSA., 2003) and DoD guidelines (DoD., 2005, DoD., 2013). However, none of them has taken into account of CFS structure that has different connection configurations and has been commonly used as load-carrying members in constructions.

6.2.1   Cantilever and beam action of floor panels

This investigation aims to figure out the influence of the connection resistance on the robustness of the CFS modular panel system. With the removal of an external panel, the failure area of the construction and the collapse components are considered as the evaluation criterion. In order to prevent the progressive collapse, DoD guidelines requires the collapse area of the floor directly above the comprised member should be less than the minimum value of $70m^2$ and 15% of the total area of the floor.

6.2.1.1 Modelling process

The software package SAP2000v14.1 was employed in the 3D structural analysis. The modular construction was assembled with floor panels, wall panels and the equivalent connections (see Figure 6-22 and 6-23). As shown in Figure 6-22, the wall panel was composed of stud, track and lateral bracing. The floor panel consists of stud and track sections. The construction was a three-floor four-bay residence hall. The post spacing around the window satisfies the requirement of Metsec SFS Installation Manual. The structural stud and track sections (see Table 6-4) were selected according to the Steel Stud Manufacturers Association (ICBO ER-4943O). Each modular panel was composed with stud and track sections. The section selection was based on SSMA ICBO ER-4943P. The section material was considered as S550 CFS with the material property according to curves captured from coupon tests. The equivalent connection is illustrated in Figure 6-23. The short beams installed in the modelling between the floor track and wall track was used to replace the structural properties of the connection. According to the connection properties, the tension, shear and rotation stiffness of the connections were assigned in the joint between the short

beam and the wall panel post. The equivalent section was applied to the short beam describing the carrying capacity of the connection. The length of the short beam was 50mm.

In addition, 50mm thick concrete slab was laid on the floor panel, with a reinforcement ratio of 0.15%. The structure was not designed by progressive collapse process. Thus, it is necessary to be checked in the following cases and find out the component which should be re-designed or enhanced.

The loading condition was assumed as shown in Table 6-5. The load combination was based on the DoD guidelines during the numerical analysis. With regard to the dynamic influence (Ruth et al., 2015), the amplified factor 2 was applied as the provision in DoD guidelines on the components above the ineffective panel. The carrying capacity of each cold-formed section was checked by using specifications in AISI-LRFD 96.

Table 6-4 Section properties

Storey	Wall panel stud	Wall panel track	Brace	Floor panel stud	Floor panel track
3rd	350S162-43	350T162-43	075U50-54	600S200-43	600T200-43
2nd	600S200-43	600T200-43	075U50-54	600S200-43	600T200-43
1st	800S250-43	800T250-43	075U50-54	600S200-43	600T200-43

Table 6-5 Construction loading condition

Load pattern	Live load	Dead load
Roof	1.0 kN/m2 (kPa)	0.9 kPa
Floor	2.0 kPa	50 mm in lightweight concrete including metal deck 0.9 kPa Cold forming framing panel depends on the designed sections 10 mm Gypsum/wood board 0.15 kPa 150 mm Mineral wool 0.03 kPa Total 1.16 kPa
Wall	N/A	Cold forming framing panel depends on the designed sections 10 mm Gypsum/wood board 0.15 kPa 90 mm Mineral wool 0.02 kPa Total 0.235 kPa Window glass and mullion system 0.5 kPa Interior 0.5 kPa
Snow	1.44 kPa	N/A

a) Wall panels

b) Floor panels

Figure 6-22 Modular construction configurations

Blue line – post section
Purple line – wall track section
Green line – joist section
Yellow line – floor track section
Red line – equivalent short beam

Figure 6-23 Equivalent connection

GSA guidelines have also provided a determination of demand-capacity ratio DCR=Q_{UD}/Q_{CE}, in which Q_{UD} represents the acting force and Q_{CE} stands for the resistance of the component.

It was suggested to find out the distribution and magnitude of potential inelastic demands of the structure in linear elastic analysis. In the redundancy analysis process, the member has the DCR value larger than 2.0 was considered to be severely damaged. The connection was supposed to be damaged with the DCR of 1.0. The damaged components were removed in the further analysis process. It should be noted that when the connection was damaged, the related component was supposed to be ineffective as well. Figure 6-24 illustrates the procedure of the 3D progressive collapse analysis.

STEP 1
Remove the assumed ineffective wall panel as shown in Case 1 and 2

STEP 2
Perform linear analysis according to DoD guidelines

STEP 3
Check the cold-formed members by using AISI-LRFD 96 and the equivalent connections by using AISI-LRFD 99.
If DCR value of the members and connections less than 2.0 and 1.0 respectively, go to STEP 5; otherwise, go to STEP 4

STEP 4
Remove the members featuring DCR values more than or equal to 2.0; remove the connection and connected joist featuring DCR values more than or equal to 1.0 from the modelling and go to STEP 2

STEP 5
According to DoD guidelines, check the damage member and the collapse area

Figure 6-24 Analytical process of progressive collapse resistance

6.2.1.2 Results

The investigation involved cases as shown in Figure 6-25. In Case 1, the construction was not collapse with each connection type as shown in Figure 6-26. After removing the damaged members, all elements and connections have the stress ratio less than 0.7. The progressive collapse did not occur.

As shown in the pictures (see Figure 6-27) for Case 2, the compound sections between the modular panels resist the exerted loads in the initial modellings. The compound sections act as a frame in the structure. When collapsed elements are removed in the modelling, the

structure reacts with cantilever action mechanism. In contrast, connection type C is stiffer than other connection types, leading to the large magnitude of the negative moment in the cross sections of the joists. The reason is supposed to be that the connection stiffness determined the tension, shear and moment distribution. When the rotational stiffness increased, the bending moment raised at the end section of the joist, which caused the joist failure. Thus, the construction assembled by connection C presents more serious collapse. The diagram of acting force-to-carrying capacity ratio is presented in Figure 6-27. It can be found that none of the connection failed in the analysis, and the collapse area was only counted by the failed joists and posts.

a) Case 1   b) Case 2
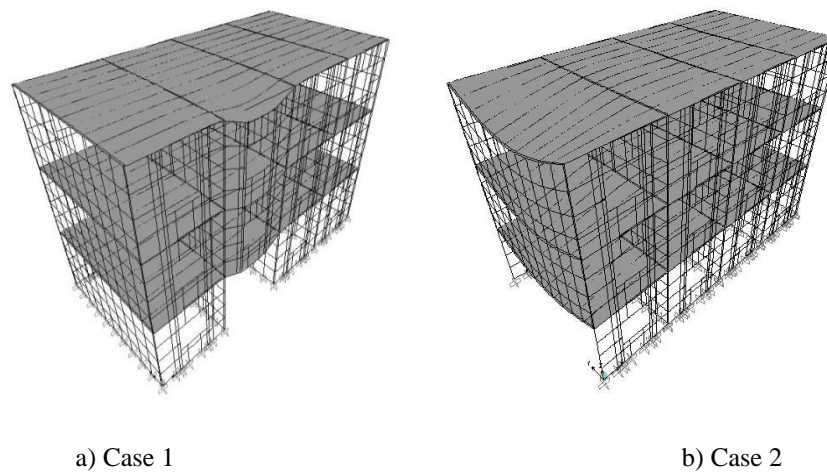
Figure 6-25 Analysed cases of progressive collapse resistance

a) Initial result   b) Final result
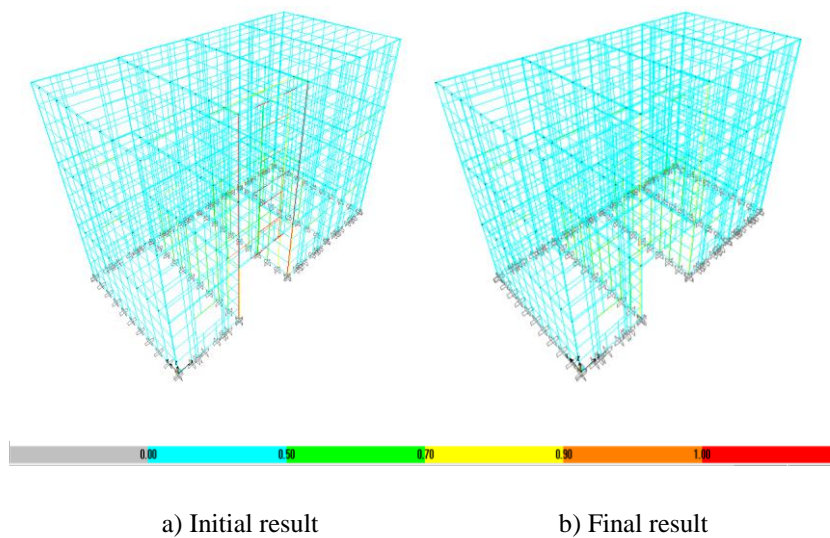
Figure 6-26 DCR result of construction collapse in Case 1
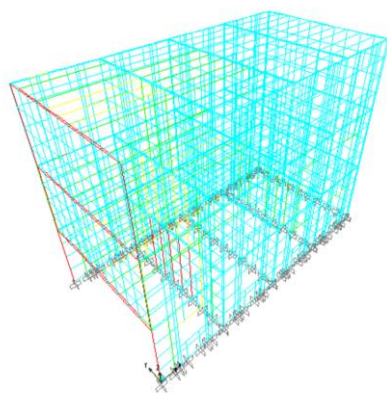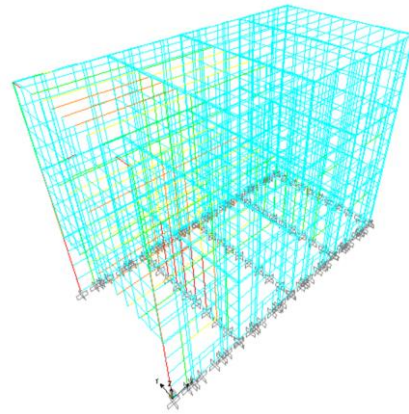
a) Initial result with connection A   b) Final result with connection A
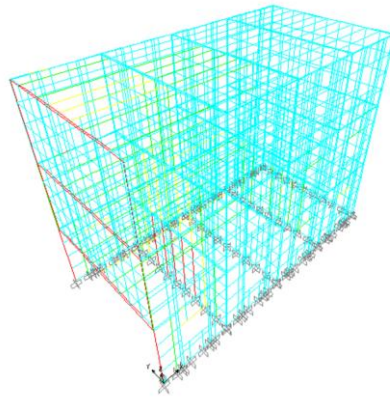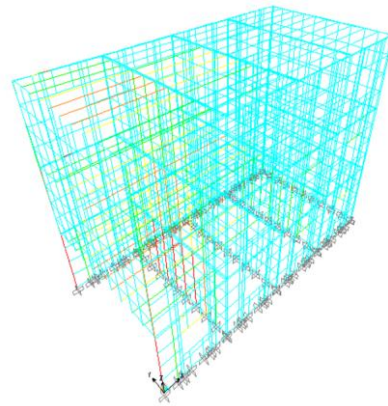
c) Initial result with connection B   d) Final result with connection B
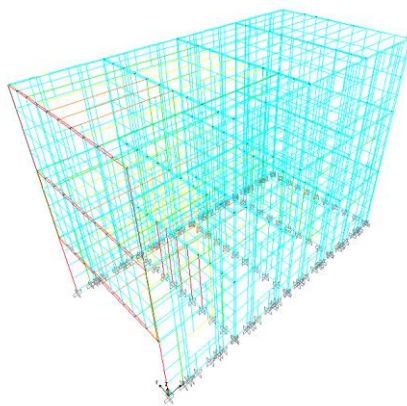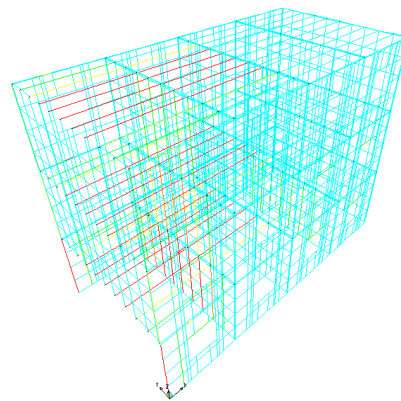
e) Initial result with connection C   f) Final result with connection C
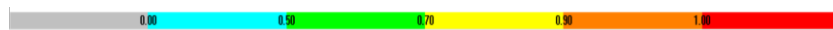
Figure 6-27 DCR result of construction collapse in Case 2

Table 6-6 Analysis results of cases

Connection method	Case	Storey	Number of removed damage members DCR≥2	Number of damage connection DCR≥1	Number of failure members 1.5≤DCR≤2	Number of failure members 1≤DCR≤1.5	Collapse area of the floor m²	Collapse area/total floor area %
Connection A	1	3rd	4	0	0	0	0	0
		2nd	6	0	0	0	0	0
		1st	2	0	0	0	0	0
	2	3rd	14	0	2	0	0	0
		2nd	16	0	0	0	0	0
		1st	16	0	0	7	10.8	15
Connection B	1	3rd	4	0	0	0	0	0
		2nd	6	0	0	0	0	0
		1st	2	0	0	0	0	0
	2	3rd	16	0	0	0	0	0
		2nd	16	0	0	0	0	0
		1st	16	0	0	7	10.8	15
Connection C	1	3rd	4	0	0	0	0	0
		2nd	6	0	0	0	0	0
		1st	2	0	0	0	0	0
	2	3rd	16	0	2	8	18	25
		2nd	16	0	4	6	18	25
		1st	16	0	4	13	19.8	27.5

Table 6-6 shows the analysis results. It demonstrates that, the number of the damage members is proportional to the rotation stiffness of the connection. The ratio of the collapsed area to the total area of the floor (27.5% for the first floor, 25% for the second and third floor respectively) in the construction assembled by connection type C exceeded the criteria of DoD guidelines. Therefore, it can be concluded that the structure with stiffer connection is more susceptible to progressive collapse regarding the removal of the external wall panel.

6.2.2 Nonlinear catenary action analysis

The progressive collapse of a structure depends on its redundancy and may involve three steps. When the middle column is removed, the upper loading is firstly carried by the moment resistance of the structure. The plastic hinge may form and develop in its beams. If the horizontal tie force can satisfy the required tie force and deformation, the catenary action will be initiated. The joists will be subjected to longitudinal tension as well as the connections. The successive removal of the cross wall panel P3 may leads to the load transfer path change. The structure directly above the removed element is potentially subjected to beam action or catenary action which is determined by the stiffness and strength of the connections.

The tension resistance of the connection is supposed to be the critical factor when the catenary action is performed. In fact, the combined action including tension, shear and rotation acts in the connections simultaneously. The interaction of tension, shear and rotation actions may reduce the resistance of the connection. However, in order to simplify the analysis process, it assumed to be neglected in this investigation. The load bearing capacity of a structure in progressive collapse process is limited by the properties of members as well as the connections.

P-post; J-joist; C-connection
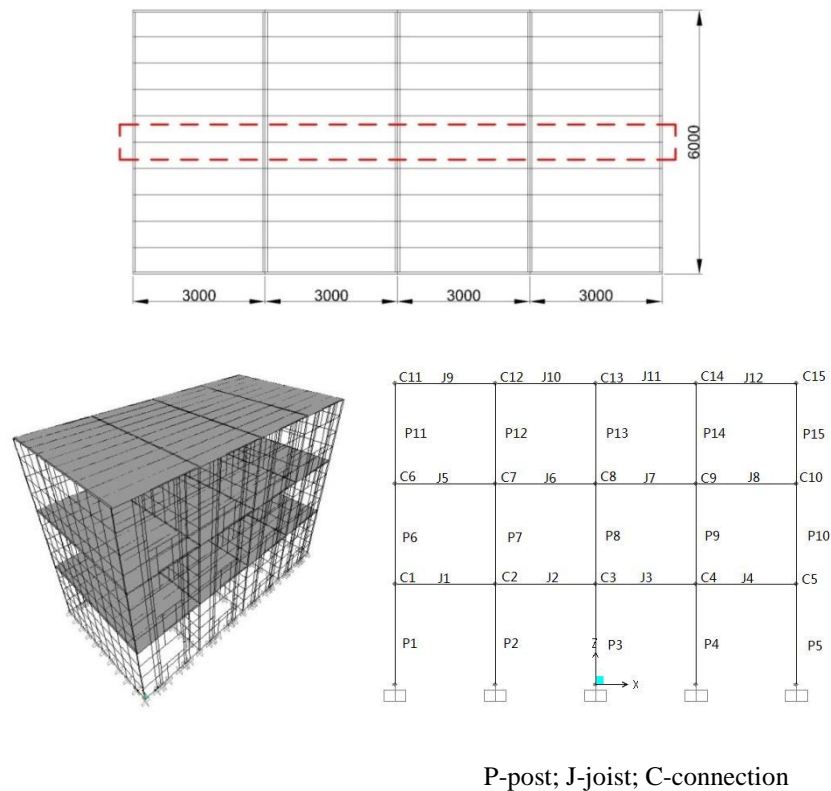
Figure 6-28 Components in the modelling

In order to study the influence of the connection resistance on the structural robustness and understand the entire process response of the connection to progressive collapse scenario, the analysis of a nonlinear 2D frame selected in the modular panel system (see Figure 6-28) was conducted. Herein, the influence of the concrete floor is neglected. It was assumed that the lateral bracing of the structure is sufficient so that the horizontal movement of the posts were restrained in the modelling. The uniformly distributed load (UDL) was added on each floor.

As mentioned above, the amplified factor 2 was applied on the floors directly above the removed member.

6.2.2.1 Modelling process

The commercial finite element package ABAUQ 6.13 was employed for developing the numerical model. The posts and joists were modelled by the 2-node beam element B21. The material was S550 CFS. The material property was obtained by the curves captured from coupon tests in Chapter 5.
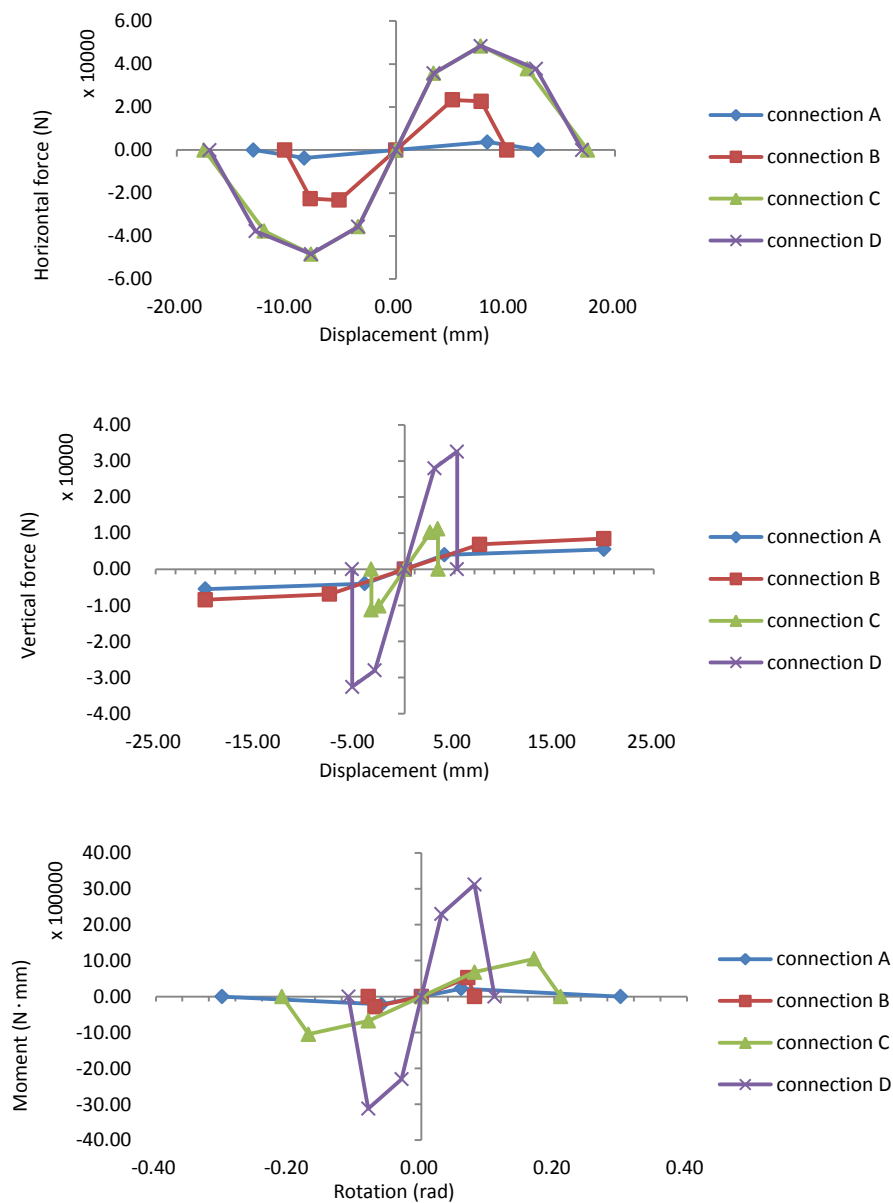
Figure 6-29 Connection idealized properties

The dimension property of each member was assigned according to Table 6-4. The posts and joists were assembled by nonlinear spring connections. The shear, tension and rotation properties of each connection solution were based on the corresponding idealized multi-linear results (see Figure 6-29). The bottom of the ground floor posts was fixed. The horizontal movement of the posts were restrained. Based on the balance of precision and computing time, the most satisfactory results were achieved when mesh size was 50mm. The solution of the analysis adopted a nonlinear incremental-iterative Full Newton solution technique.

6.2.2.2 Results and discussion

Ultimate line load: 22.92N/mm   Ultimate line load: 9.71N/mm

a) Pinned connection

Ultimate line load: 3.66N/mm   Ultimate line load: 0.32N/mm

b) Connection type A
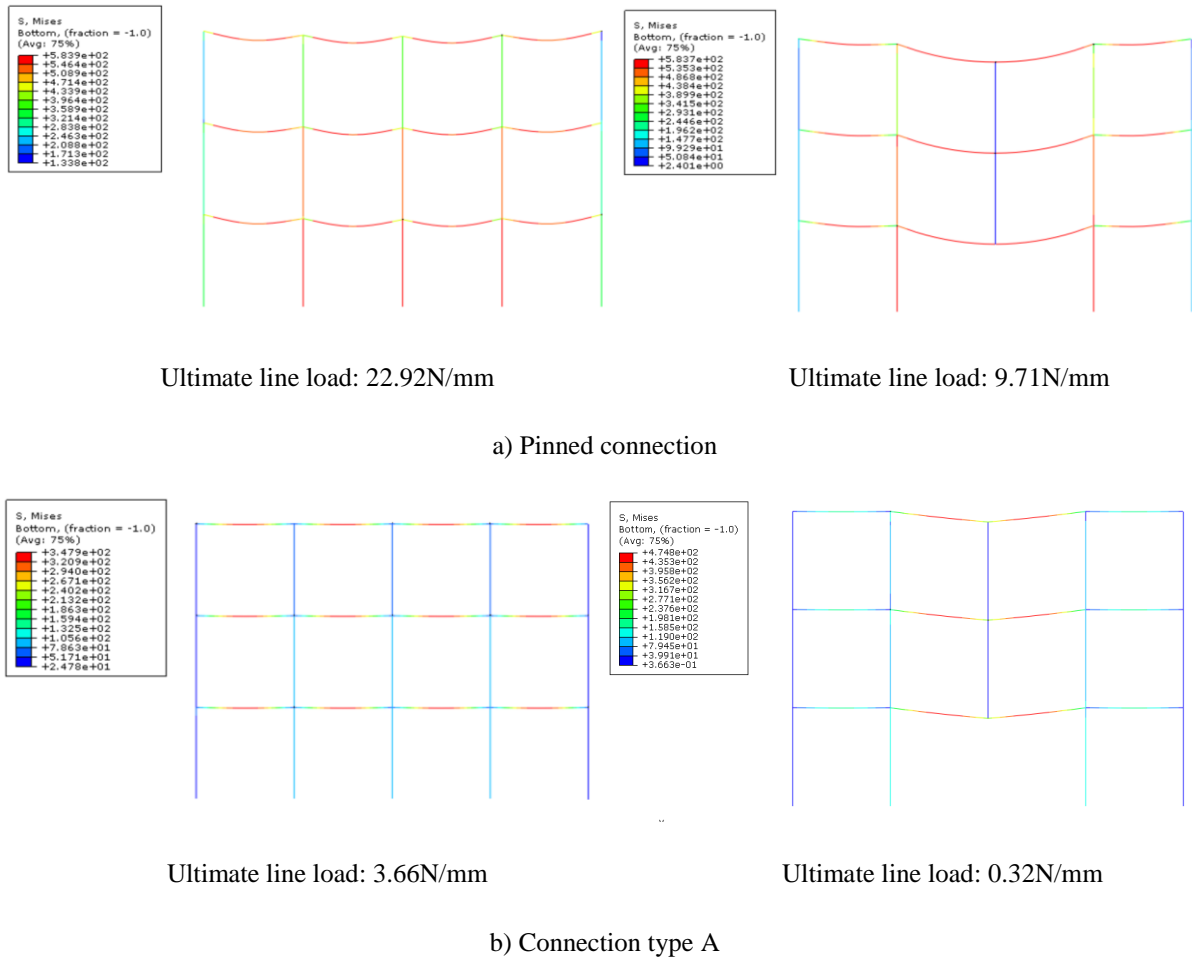
Figure 6-30 Stress envelope of modular structure

Figure 6-30 shows that if a single internal wall panel is lost, the connection C3 would undergo a downward displacement. With floor load increase, the resistance of the structure increases until the connections compromise. The change of the force transfer path caused by the

removal of the primary element is revealed by the stress patterns of the modelling. In the initial modelling, the ultimate load of the structure was controlled by the joist bending resistance. The middle post carried more load than others. Due to the removal of the structural element, the load added on the post directly above the removed element was reduced and the adjacent joists were subjected to combined bending and tension leading to the stresses of the joists increased. It indicates that the connection resistance governs the ultimate load of the structure. The responses of each connection solution are illustrated in Figure 6-31 to 6-34.
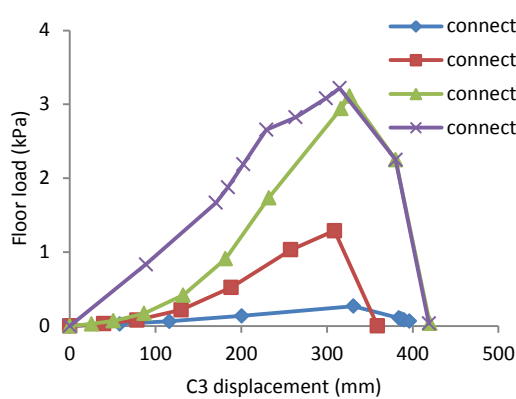
Figure 6-31 UDL to displacement curve
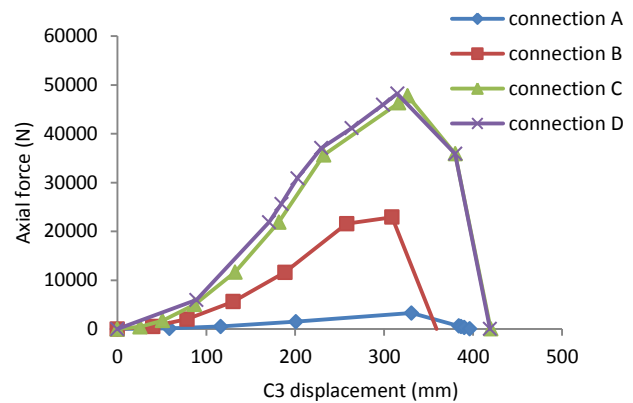
Figure 6-32 Axial tensile force in J2
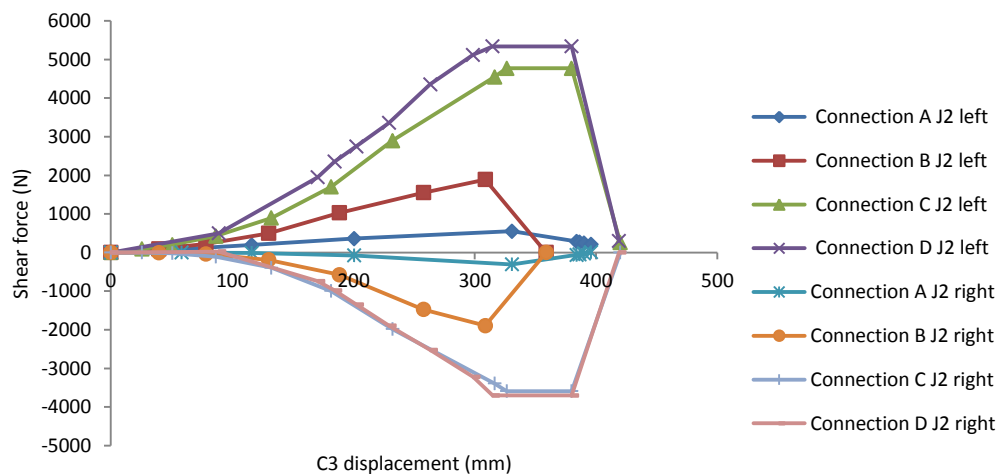
Figure 6-33 Shear force in J2
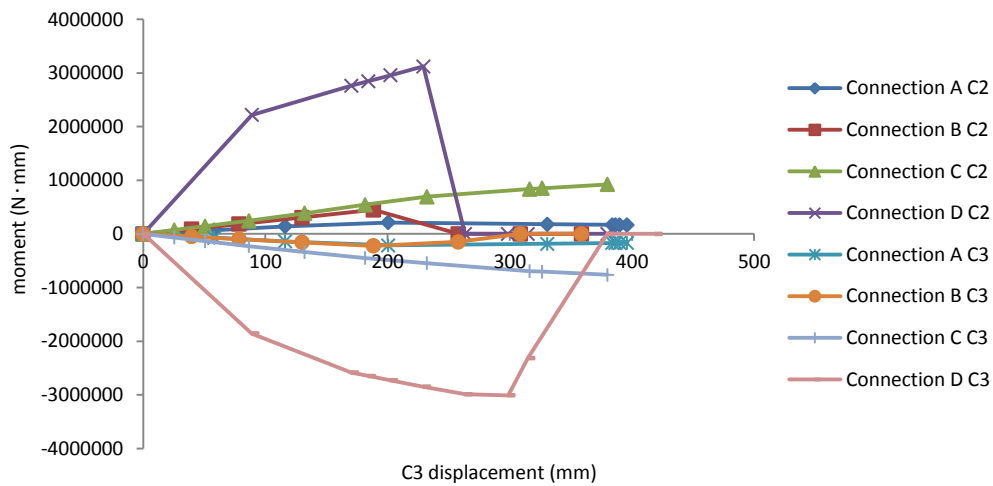
Figure 6-34 Bending moment in C2 and C3

Connection type A: The force acting on the connection A increases until the ultimate load (0.54kPa) of the structure was achieved. In the meantime, the tension resistance was obtained with the value of 3.26kN, whereas the shear forces acting on the connection C2 and C3 are only 70% and 40% of the carrying capacity (0.74kN). Correspondingly, the rotation angle of connection C2 and C3 are 0.11rad and 0.107rad respectively. It can be concluded that, the resistance of connection type A is limited by the tension resistance in this scenario. The failure of the connection occurred, when the displacement of C3 is 396mm.

Connection type B: Connection type B provides greater ultimate strength but less allowable deformation than connection A. The connection lost the bending moment resistance when the axial tension force of J2 reached 11.6kN, which is only 49.8% of the carrying capacity. Therefore, a plastic hinge is supposed to be formed in the connection. The ultimate load (2.58kPa) can be obtained when the displacement of C3 is 309mm. The connection failed at the displacement of C3 being 359mm.

Connection type C: The axial force carrying capacity of connection type C also determined the resistance of the structure. The axial tension force of J2 rises to 47.78kN with increasing displacement of C3 from zero to 237mm. Then, the load drops until the connection fails, with vertical displacement of C3 being 420mm. When the ultimate floor load (6.23kPa) is achieved, the shear forces acting on J2 left and right are 4.78kN and -4.78kN respectively, and the

rotation angles of C2 and C3 are 0.12rad and 0.09rad, which is below the ultimate limit of connection type C.

Connection type D: Base on the connection investigation results, connection type D shows the greatest strength and stiffness compared with other connecting methods. The bending moment resistance of connection D begins to drop sharply after the displacement of C3 being 263mm (see Figure 6-34). The failure mode of screw double shear tests indicates that the deformation of the screw-hole circumference and the wrinkling in front of the screw by tension leads to the screw joint softening, which is the reason of the decreasing of bending resistance in connection D. In the end, it is supposed that the plastic hinge is formed in the connection before the ultimate tension force (48.41kN) achieved. The ultimate floor load of the structure (6.44kPa) can be obtained when the vertical displacement of C3 reaches 315mm.

Figure 6-33 shows the shear force at the ends of the joist, which indicates that the connections can provide sufficient shearing strength (see Figure 6-29) during the change of force transfer path in the CFS structure. The failure of the connection is controlled by the tensile resistance.

In traditional concrete frame structures, the load redistribution mechanism of progressive collapse includes three stages: beam action, compressive arching action and catenary action. After the removal of load carrying element, the connection provides moment resistance. The plastic hinge is firstly formed in the middle connection and then spread to the end supports. The load acting on the connection transfers from bending to tension. Thereafter, the resistance of the structure will increase until the connection fails by tension. In terms of the traditional hot-rolled steel section frame structures which usually adopt semi-rigid or rigid connections, the beam action and catenary action can also be observed in progressive collapse process.

However, the sections and connections in the CFS structure systems have thinner thickness and higher flexibility. Due to the smaller initial stiffness than the traditional frame structures, the tension resistance of the connection increases from the beginning (see Figure 6-32). According to the classification in EC3 (Eurocode, 2005), the initially rotational stiffness of connection type A, B and C are less than 0.5EI/L which are pinned connection.

In contrast, the connection D is classified to be semi-rigid connection. As shown in Figure 6-35, the declining rate of the surface load is presented when the plastic hinge is firstly formed at the ends of the joists. After forming the plastic hinge, the surface load rapidly increases and the catenary action develops in the bottom beams directly above the removed element. In the last stage, the structure compromises by the tensile failure of the connections.
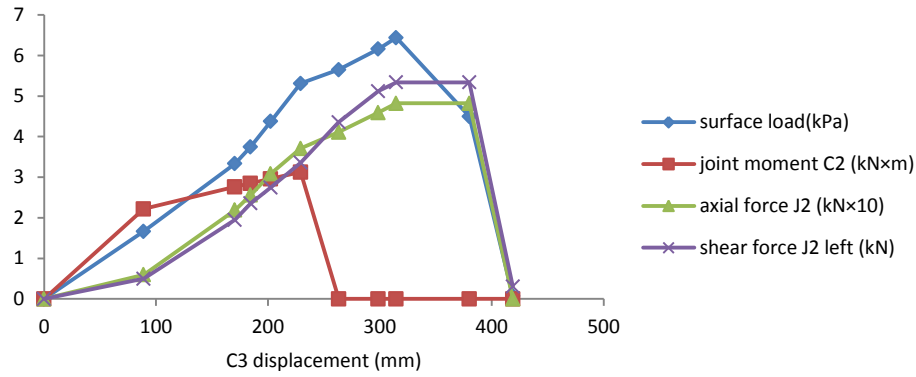
Figure 6-35 Reactions of C2 with connection D

As for connection B, plastic mechanism is also completely formed at the side supports during the analysis. In other cases (connection A and C), the plastic hinge has not been formed when the tensile failure occurs (see Figure 6-34). The distinction of beam and catenary stages is not notable in the CFS structure. In the comparison of connection C and D, the similar axial force and shear force are presented in Figure 6-32 and 6-33. In contrast, the connection D shows better load carrying capacity in the early stage (see Figure 6-31) because of the greater rotational stiffness. It indicates that the upper loading is carried by connection moment, tension and shear simultaneously (see Figure 6-36).
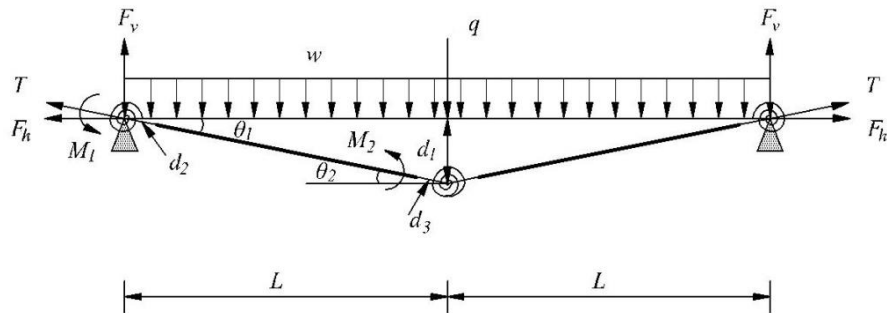
Figure 6-36 Resistance mechanism of the CFS panel system

172

The maximum floor load is determined by the connection elongation (d_2 and d_3), connection horizontal resistance (F_h), connection moment resistance (M_1 and M_2) and connection vertical resistance (F_v). Thus, the total load can be divided into two parts:

Load carried by connection tension resistance w_1 and q_1:

$$F_h = \frac{(2w_1 L + q_1)bL}{2d_1}$$
(Eq. 6-32)

Load carried by connection moment resistance w_2 and q_2:

$$M_1 + M_2 = \frac{w_2 bL^2 + q_2 bL}{2}$$
(Eq. 6-33)

Load carried by connection shear resistance w_2 and q_3:

$$F_v = \frac{2w_3 bL + q_3 b}{2}$$
(Eq. 6-34)

The total load carrying capacity of the structure:

$$w = w_1 + w_2 + w_3$$
(Eq. 6-35)
$$q = q_1 + q_2 + q_3$$
(Eq. 6-36)

It can be observed in the modelling, q is very small. If ignore the influence of q,

$$w_1 = \frac{d_1 F_h}{bL^2}$$
(Eq. 6-37)

$$w_2 = \frac{2(M_1 + M_2)}{bL^2}$$
(Eq. 6-38)

$$w_3 = \frac{F_v}{bL}$$
(Eq. 6-39)

If

$$d_1 = \sqrt{(d_2 + d_3 + L)^2 - L^2}$$
(Eq. 6-40)

then

$$w = \frac{\sqrt{(d_2 + d_3 + L)^2 - L^2}\, F_h + 2(M_1 + M_2)}{bL^2} + \frac{F_v}{bL}$$
(Eq. 6-41)
$$F_h = K_h \cdot d_2 \cos\theta_1$$
(Eq. 6-42)
$$F_v = K_v \cdot d_2 \sin\theta_1$$
(Eq. 6-43)
$$M_1 = K_{r1} \cdot \theta_1$$
(Eq. 6-44)
$$M_2 = K_{r2} \cdot \theta_2$$
(Eq. 6-45)

where μ is the proportion of the load carried by connection moment resistance; w is the uniformly distributed floor load; b is the internal spacing of joists; L is the floor span length; d_1 is the vertical displacement at the middle wall support; d_2 and d_3 represent the extension experienced at the side and middle supports respectively; θ_1 and θ_2 stand for the rotation experienced at the side and middle supports respectively; K_{r1} and K_{r2} represent the rotational stiffness of the connection at the side and middle respectively; K_h and K_v stand for the horizontal and vertical stiffness of the connection respectively; q is the line load imposed by the upper wall panel; F_v is the vertical resisting force at the connection; T is the axial tension force of the joist and F_h is the horizontal resisting force at the connection. The predictions of the surface load carrying capacity achieved by the proposed expression present a good agreement with the simulation outcomes (see Figure 6-37).
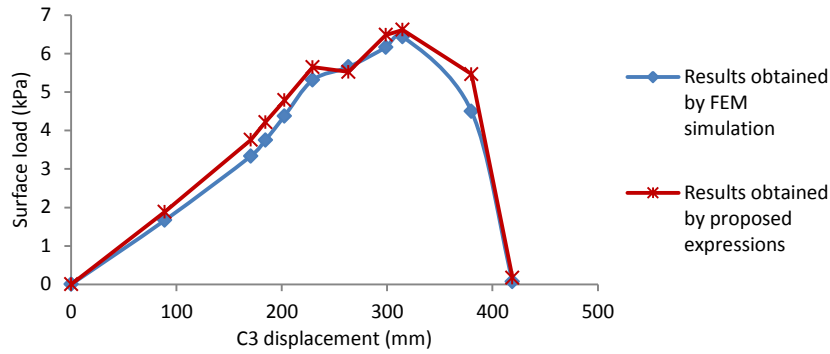
Figure 6-37 Surface load of the structure with connection D

The deviation is supposed to be cause by ignoring the load imposed by the upper element. If $\mu w = w_2, \mu q = q_2$, then

$$M_1 + M_2 = \frac{\mu wbL^2}{2} \tag{Eq. 6-46}$$

$$F_h = \frac{(1-\mu)wbL^2}{d_1} \tag{Eq. 6-47}$$

Assuming that $\theta_1 = \theta_2, M_1 = M_2$, then

$$M_1 = \frac{\mu wbL^2}{4} = K_{r1} \cdot \theta_1 \tag{Eq. 6-48}$$

Because of $\theta_1 \ll 1, \tan\theta_1 \approx \theta_1 \cdot \text{rad}^{-1}$.

$$d_1 = L \cdot \tan\theta_1 = \frac{\mu w b L^3}{4K_{r1}} \cdot \text{rad}^{-1} \qquad \text{(Eq. 6-49)}$$

The proportion of the load carried by connection moment resistance is

$$\mu = \frac{4K_{r1}d_1}{wbL^3} \cdot \text{rad} \qquad \text{(Eq. 6-50)}$$

The percentage of the load carried by connection moment resistance is directly proportional to the rotational stiffness of the connection.

6.3 Summary

This chapter presents the investigation on connection between CFS modular panels. The comparative study between the current and the proposed connection configurations was conducted by numerical analysis. The structural properties of screw joints obtained by the experimental study were introduced in the modelling. According to the numerical study, the proposed connecting method for floor and wall panels achieved greater structural performance in shear, tension and rotation resistance.

Through 3D modelling pilot study, this thesis studied the robustness of the three-floor four-bay CFS modular panel structure. Based on GSA guidelines and DoD guidelines, the evaluation was performed. It was found that a removal of the external wall in Case 1 did not lead to progressive collapse. Since the modular floor panel is one-way board, the removed wall panel is not primary load carrying element. But the failure of members occurred in the panels of the second and third floor which is directly above the removed element. In Case 2, the connected tracks formed a compound section to transfer the load. However, the track sections were damaged, leading to further damage in the floor panel. It can be concluded that the enhancement of track sections is supposed to be a potential measure to improve the structural performance in progressive collapse. The equivalent connection was applied in the modelling. As a result, the construction with stiffer connection was more susceptible to progressive collapse. When the external wall was removed, the greater rotation stiffness gave rise to the moment distributed on the joist in Case 2.

The removal of internal wall panel was also considered in this chapter. In general, the construction failure is on account of the resistance of structural members and the connections. The 2D frame nonlinear analysis was carried out to evaluate the robustness of the structure with different connection configurations. Based on the analysis, the axial tension force of the joist increased due to the alternative load transfer path appeared in the structure. In contrast, connection type D is stronger and stiffer other proposed connections. The structure with connection type D provided the greatest load carrying capacity. However, this connection consumes much more steel and leads to an inconspicuous improvement to connection type C. The results demonstrated that connection C is the most efficient connection solution for the joist-to-post connection. The plastic hinge was formed in connection B and connection D before the ultimate force achieved, leading to catenary action occurred in the structure. It was proved that the tension resistance and deformation capacity of the connection determined the load carrying capacity under abnormal loading conditions, and the connections most likely fail with the tension failure. When the internal wall panel is ineffective, the floor load of the CFS structure is carried by connection moment resistance and tension resistance of the upper elements. The expressions for calculating the maximum floor load w and the proportion μ of the load carried by connection moment resistance were proposed.

CHAPTER 7   CONCLUSIONS AND FUTURE WORKS

7.1   Introduction

The aforementioned aim and objectives of the research have been achieved through the experimental, numerical and analytical analysis. According to the results obtained from this investigation, the main contributions and conclusions could be drawn as follows.

7.2   Contributions and conclusions

7.2.1   Benefits and challenges of CFS modular building constructions

This thesis has summarized the benefits and challenges of CFS modular building constructions through extensive literature review and case studies. In practice, reduced construction time on site, economic benefits, energy saving, low waste, health and safety in production, environmental protection, good thermal and acoustic insulation, and high automation and productivity have been achieved by adopting off-site CFS modular building structures. The potential merits of material properties and recyclability should also be considered in the decision making process. The key barriers to the implementation of off-site construction are focused upon the lack of norms and standards, and conventional social concepts. In additional to these obstacles, high initial cost, low level supply chain, the lack of a developed legal system and government incentives, poor productivity, low skilled labour and product quality problems also impact the construction industrialisation in developing countries.

7.2.2   Investigation on purlin-to-sheeting connections

This thesis has developed a FE model to simulate the purlin-sheeting system and predict rotational stiffness of the purlin-sheeting connection. The rigid plate has been introduced in the simulation to simulate screw joint. The results of the FE model are in great accordance with the experiment results.

Based on the numerical analysis, this thesis quantified the factors that influence on the purlin rotation stiffness and proposed the accurately predicting solution. It was shown that the rotational stiffness increases remarkably with increasing section thickness for both downward and uplift load scenarios. There is a deviation between the analytical results obtained by design approach in EC3 and the test outcomes, because the effects of purlin thickness and the flange width are underestimated in EC3. Based on the numerical analysis, the compensation coefficient that relate to shell thickness (β_t) and flange width (β_F) was proposed, leading to a better agreement with the test results for Σ purlins. This approach is approved to be applicable on Z and C purlins.

A series of parametric studies have been conducted to investigate the influence of the fastener spacing, sheeting thickness and the depth of the purlin on the rotational stiffness. The results have demonstrated that the rotational stiffness decreases with increasing of fastener spacing, which can be predicted by EC3. The sheet thickness has a significant effect on the rotational stiffness. In contrast, the effect of the depth of the purlin can be neglected.

7.2.3 Investigation on screwed and bolted connections

The FE models of stud-to-track connection with screw and bolt joint have been discussed in this thesis. It was found that the settings of constraints and interactions between the fasteners and the connected components significantly influence structural performance of the connections.

Validated by existing test results, the finite element models were proposed to predict the ultimate resistance of screwed and bolted connections. Additionally, it was found that the pre-tightening force can improve the performance of the bolted connections but in a limited range.

It was proved that the gap between connected components led to warping in the early stages, which reduced the carrying capacity of the bolted and screwed connections. With the stud thickness increasing, the overall resistance of the bolted connections without the gap improved tremendously, and was much greater when compared to the connections with a gap.

However, this trend was not embodied in screwed connections, as the bolted connection is more sensitive to the clearance.

The parametric study was also conducted in the analysis. It was found that increasing the component thickness is an efficient measure to improve the resistance of the stud-to-track connections.

A series of screw and bolt joint tests have been carried out to reveal the entire response of the joint applied in the high strength material (S550) plates. A new test facility has been developed to investigate the screw joint subjected to pure and mix loads. The test results and observations have revealed the structural properties and identified the failure modes of the joints. A comparative study has been conducted with the current codes and analytical method. It was found that AISI can provide more accuracy than other related norms and specifications in predicting the ultimate resistance.

The expressions were proposed to describe the interaction between the tensile and shear actions, which can be used to predict the tensile or shear resistance of the screw joint. In addition, the study proposed the proportional coefficients to adjust the calculations of screw joint resistance under combined shear and tension loading conditions.

A FE model with bushing elements has been proposed to reproduce the test results, which presented good accuracy.

7.2.4 Investigation on the connection behaviour between modular panels

The study developed three connection configurations attaching reinforcing pieces for CFS modular panel system. The amount of increasing in weight of steel brought by the reinforcing pieces is small. These configurations can provide great improvement of the resistance and stiffness to the current typical connecting method when the connection was subjected to shear, tension or rotation action. The proposed connection assembled by double shear joints provides greater structural performance and efficiency compared with single shear joints.

The sudden failure and ineffectiveness of the structural element may lead to progressive collapse. The progressive collapse resistance depends on the type selection, arrangement and details of structure. The alternative load path method is widely employed to examine the structural progressive collapse in engineering practice. It has been found that the structural behaviour of the connection between primary load carrying elements highly collaborates with the robustness and load redistribution mechanism due to the removal of load carrying element.

The numerical analysis has been conducted to evaluate the robustness of the modular construction with the removal of either internal or external wall panels by using commercial software package ABAQUSv6.13 and SAP2000v14.1. Based on the joint test results, the obtained entire connection performance including stiffness and strength under normal and abnormal loading conditions was embedded in the developed FE models through equivalent connecting method for the investigation of modular panel system. Quantitative objectives for the influence of connection configuration on the structural robustness have been established by using collapse area of the floor and ultimate floor load of the structure as criteria in analysis processes.

From the numerical analysis, it was found that when the external wall panel was removed from the structure, cantilevered beam action occurred. The analysed connections can provide ample strength. The moment redistribution of the floor panel above the removed element depends on the rotational stiffness of the connection between floor panel and wall panel. The connection with higher rotational stiffness is more likely to cause the metal component failure, leading to larger collapse area in the floor.

On the contrary, when the internal wall panel was removed, beam action and catenary action may be successively observed in the analysis accompanied by alternative force transfer path. The numerical results indicated that the tension resistance and the rotation capacity of the connections are the principal factors determining the structural behaviour of the CFS panel system under abnormal loading conditions.

During the numerical analysis, it was observed that the upper loading is carried by connection shear, tension and moment simultaneously. When the plastic hinge formed at the end connections and then transferred to the middle connections, the catenary action occurred.

In the catenary action, the load carrying capacity of the modular panel structure is controlled by the tension resistance of the connections. Compared with the traditional connection solution, the proposed connection configurations with the enhanced connecting methods presented a great improvement, especially for connection type C and D.

From the progressive collapse analysis of CFS modular panel structure, the resistance mechanism of the CFS systems is identified to be different from the traditional frame structures. The expressions for calculating the ultimate floor load w and the proportion μ of the load carried by connection moment resistance were proposed. The prediction of the expressions is in good accordance with the numerical result.

7.3 Limitations and future works

This thesis has provided some solutions to address the current problems in CFS modular panel constructions. Nevertheless, the connection types studied so far are only appropriate for limited applications. There are still many challenges in connections of CFS modular building structures. To achieve further contributions in this field, this section lists the potential works which need to be conducted in the future:

- To conduct an experiment study for the stud-to-track connections. The simulation method should be further validated by the test outcomes. The influence of variables, such as component material, fastener alignment, needs to be discussed.
- To carry out the experiment study for each proposed connection solution. The validation of the numerical analysis only refers to the screw joints. Based on the assumptions in the analysis, the interaction between the structural properties of the connection in shear, tension and rotation directions was neglected. The resistance of the connection may be overrated by the modelling. The numerical prediction of each connection solution needs

to be further examined by the full-scaled tests.

- To evaluate the influence of the accessories, such as the in-filled materials, on the structural robustness. The structure accessories can potentially improve the stability and resistance of the main structure. The stiffness and strength enhanced by the accessories should be identified in the future.

- To develop an effective and efficient connection solution for steel frame modular cassette system. The connection investigated in the thesis is only related to CFS modular panel systems. However, the connection between frame modular cassettes is also a challenge in steel modular construction.

7.4 Summary

The mean findings have been briefly stated in this chapter in aspects of features of modular constructions, rotational stiffness of the purlin-to-sheeting system, joints and connections between modular panels. These findings regarding connections employed in modular systems provide instructions in construction design. However, there are still limitations and knowledge gaps in this field, which also have been listed in this chapter.

Appendix I

Semi-empirical design rules for bolt joint of steels with variable ductility and strength by Chung and Ip (2001)

For design rules comparison, the bearing resistance $\emptyset P_n$, $\emptyset V_b$, P_{bs}, B_r and $F_{b,Rd}$, respectively in AISI, AS/NZ4600, BS5950 Part 5, CSA:S136 and Eurocode 3 Part 1.3 were presented in the paper.

- AISI:1996 Clause E3.3 and Table E3.3-1

$$\emptyset P_n$$

where $P_n = 3.00dtf_u$, $\emptyset = 0.6$ for LRED; d is the bolt diameter; t is the thickness of the steel; f_u is the tensile strength of steel strips.

- AS/NZ 4600:1996 Clause 5.3.4 and Table 5.3.4.1

$$\emptyset V_b$$

where $V_b = 3.00d_f tf_u$; $\emptyset = 0.6$ for LRED; d_f is the bolt diameter; t is the thickness of the steel; f_u is the tensile strength of steel strips. This is the same as design rules given by AISI.

- BS5950 Part 5:1998 Clause 8.2.5.2

$$P_{bs} = (1.65 + 0.45t) \, dtp_y$$

where d is the bolt diameter; t is the thickness of the steel; p_y is the yield strength of steel strips.

- CSA:S136:1994

$$B_r = \emptyset_u Cdtf_u$$

where $\emptyset_u = 0.67$; when $d/t < 10 \ C \quad 3$; when $10 < d/t < 15 \ C \quad 30t/d$; when $d/t > 15 \ C \quad 2$; d is the bolt diameter; t is the thickness of the steel; f_u is the tensile strength of steel strips.

- Eurocode 3 Part 1.3 Clause 8.4 and Table 8.4

$$F_{Rd} = \frac{2.5 d t f_u}{\gamma_{M2}}$$

where $\gamma_{M2}=1.25$; d is the bolt diameter; t is the thickness of the steel; f_u is the tensile strength of steel strips.

- New design rule in the paper

$$F_{b,Rd} = F_{bf,Rd} + F_{ff,Rd}$$

$$F_{b,Rd} = \frac{\alpha d t f_u}{\gamma_M}$$

$$\alpha = \frac{1}{\beta}\frac{f_u}{d}$$

$$\beta = 15 + 35\gamma$$

$$\gamma = \frac{f_y - 280}{1000}$$

$$F_{ff,Rd} = \frac{n \mu t F_{BT,Rd}}{\gamma_M}$$

where $F_{bf,Rd}$ is the resistance contribution due to bearing action (kN); α is the strength coefficient for bolt joints; d is the bolt diameter (mm) and t is the thickness of the steel (mm); γ_M is the partial safety factor for joints at 1.25; f_u is the design tensile strength of steel strips and f_y is the yield strength (N/mm^2); $F_{ff,Rd}$ is the resistance contribution due to frictional action (kN); μ is the coefficient of friction assigned to be 0.2 for galvanized cold-formed steel strips; n is the number of contact surfaces with a value of 2 for typical joints; $F_{BT,Rd}$ is the clamping force developed at bolt shank assigned to be 12.0 kN for typical joints.

Appendix II

Strength function for circular press-joints (Di Lorenzo and Landolfo, 2004)

The design resistance is shown as follow,

$$F_{\mathrm{Rd}} = \alpha_{\mathrm{c}} \cdot f_{\mathrm{u}} \cdot d_{\mathrm{p}} \cdot t_{\mathrm{p}} / \gamma_{\mathrm{M2}}$$

where α_{c} is the clinching bearing coefficient (see Table II-1); d_{p} is the internal diameter measured on punch side; t_{p} is the sheet thickness of punch side; γ_{M2} is the partial factor for calculating the design resistance of mechanical fasteners.

Table II-1 Assessment of the bearing coefficient α for circular press-joints

General information		Bearing coefficient α_{c}
Type of specimen	Specimen notation	$F_{\mathrm{u,e,i}}/(F_{\mathrm{u,i}} d_{\mathrm{p}} t_{\mathrm{ep,i}})$
Asymmetrical C'_{ci} (specimens with two sheets and two clinches manufactured by Avdel Textron) d_{p}=5.0mm, d_{d}=6.5mm	Tests carried out in Ben Vautier laboratory (Italy) C'_{c1}	0.86
	C'_{c2}	0.90
	C'_{c3}	0.91
	C'_{c4}	0.86
	C'_{c5}	0.95
	Tests carried out in Avdel-Textron laboratory (Germany) C'_{c6}	0.89
	C'_{c7}	0.89
	C'_{c8}	0.87
	C'_{c9}	0.89
	C'_{c10}	0.93
	C'_{c11}	0.87
	C'_{c12}	0.85
	Statistical evaluation Mean	0.89
	Standard deviation	0.02
	Characteristic value	0.84

Appendix III

Prediction of the stiffness of bolted moment connections between cold-formed steel components of portal frames by Lim and Nethercot (2004)

For the rotational stiffness of bolt group, the resistance F_i of each bolt-hole is positive proportional to its distance d_i from the rotation centre (see Figure III-1).

$$F_i = cd_i; \quad \sum_{i-1}^{n} F_i d_i = M; \quad c = \frac{M}{\Sigma_{i-1}^{n} d_i}$$

where c is a constant; n is the number of the bolts in the group.

a)   b)
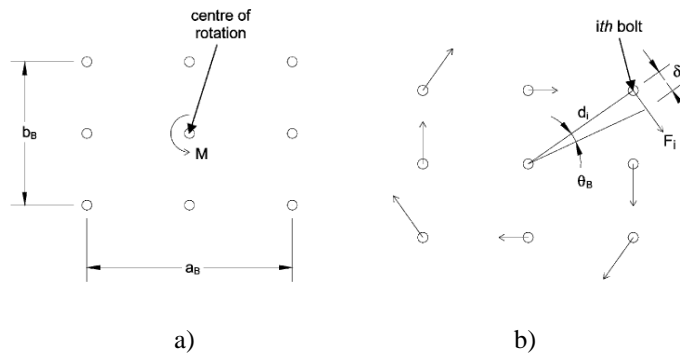
Figure III-1 Bolt group details

The elongation stiffness of the bolt-hole is k_b.

$$\delta_i = \frac{F_i}{k_b} = \frac{cd_i}{k_b}$$

The rotation can be calculated from

$$\theta_B = \frac{\delta_i}{d_b} = \frac{c}{k_b}$$

The rotational stiffness of the bolt-group is

$$k_B = \frac{M}{\theta_B} = \frac{Mk_b}{c} = k_b \sum_{i-1}^{n} d_i^2$$

The calculation of rotational stiffness k_B of bolt-group for different arrays of bolts is shown in Table III-1.

Table III-1 Rotational stiffness of bolt-group for different arrays of bolts

Arrays of bolts	k_B
2×2	$(a_B^2 + b_B^2)k_b$
3×3	$\dfrac{3}{2}(a_B^2 + b_B^2)k_b$
4×4	$\dfrac{20}{9}(a_B^2 + b_B^2)k_b$
5×5	$\dfrac{25}{8}(a_B^2 + b_B^2)k_b$

Appendix IV

Flexibility prediction for bolted moment connections (Yu et al., 2005)

The rotational stiffness of bolted moment connections is mainly influenced by such as the connection configurations, load paths, friction in interfaces between washers and steel sections, clamping forces developed in bolt shanks, etc. In terms of the bolted moment connections in the paper, the effect elements for flexibility of the bolted moment connections contain the bearing deformation around bolt holes edges; the clearance in bolt holes; flexural and shear deformations; slippage against friction between the washers and the connected components. A semi-empirical design rule for the flexibility prediction was proposed as follows:

$$\frac{1}{K_{con}} = \frac{1}{K_{cfs}} + \frac{1}{K_b} + \frac{1}{K_{gp}}$$

where $\frac{1}{K_{con}}$ is the overall flexibility of the connection; $\frac{1}{K_{cfs}}$ is the flexibility due to bending deformation of the cold-formed steel section within the connection; $\frac{1}{K_b}$ is the flexibility due to bearing deformation of the connected section web of the cold-formed steel section around the bolt hole; $\frac{1}{K_{gp}}$ is the flexibility due to bending deformation of the hot-rolled steel gusset plate within the connection;

$$K_{cfs} = \frac{3(EI)_{cfs}}{l_{con}}$$

$$K_b = \frac{M}{\theta_b}; \theta_b = \frac{\Delta_b}{r}$$

$$K_{gp} = \frac{3(EI)_{gp}}{l_{con}}$$

where $(EI)_{cfs}$ is the flexural rigidity of the cold-formed steel section; $(EI)_{gp}$ is the flexural rigidity of the gusset plate; l_{con} is the length of the connection; r is the distance from the bolt

group centre to the outermost bolt; Δ_b is the bearing deformation of the section web around bolt hole to be specified.

Appendix V

Calculations of buckling length of truss web members, rotational stiffness and axial stiffness of the bolted connections (Zaharia and Dubina, 2000, Zaharia and Dubina, 2006)

With the same partial safety factor γ_R=1.25 in Eurocode 3, the stiffness of a single lap bolt joint can be predicted

$$K = 6.8 \frac{\sqrt{D}}{(\frac{5}{t_1} + \frac{5}{t_2} - 1)} \quad \text{(kN/mm)}$$

where D is the nominal diameter of the bolt; t_1, t_2 are the thicknesses of the connected sheets.

For computation of rotational stiffness of truss connections, as the model is shown in Figure V-1.
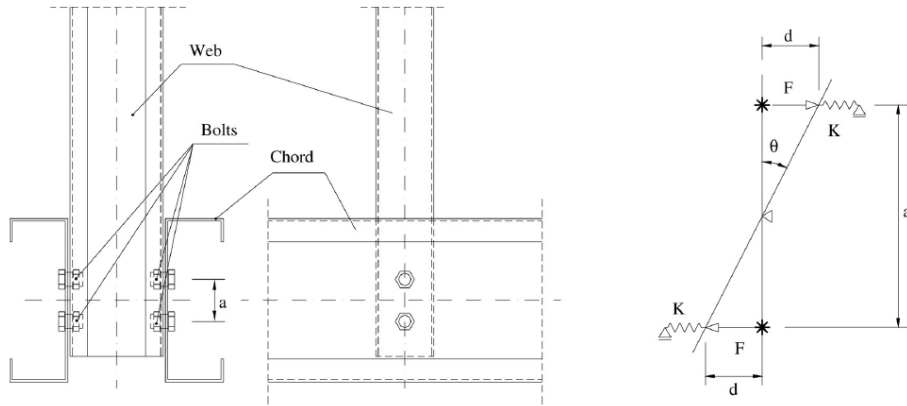
Figure V-1 Four bolt connection computation model

The expression with γ_R=1.25 is shown as follows:

$$K_{\text{node,t}} = \frac{M_{\text{tot}}}{\theta} = \frac{2(Fa)}{\tan\theta} = \frac{2Kda}{\left(\frac{d}{0.5a}\right)} = Ka^2$$

$$= \frac{6.8a^2\sqrt{D}}{(\frac{5}{t_1} + \frac{5}{t_2} - 1)} \quad (\text{kN} \cdot \text{mm/rad})$$

where M_{tot} is the total bending moment; θ is the corresponding rotation; a is the distance between bolts; D is the nominal diameter of the bolt; t_1, t_2 are the thicknesses of the connected sheets.

Considering the rotational centre is in the axis of the middle bolt (see Figure V-2), the rotational stiffness for a similar truss connection model with six bolts can be calculated by the following equation,

$$K_{\text{node,t}} = \frac{M_{\text{tot}}}{\theta} = \frac{2(F \times 2a)}{\tan\theta} = \frac{4Kda}{\left(\frac{d}{a}\right)} = 4Ka^2 = \frac{27.2a^2\sqrt{D}}{(\frac{5}{t_1} + \frac{5}{t_2} - 1)} \quad (\text{kN} \cdot \text{mm/rad})$$
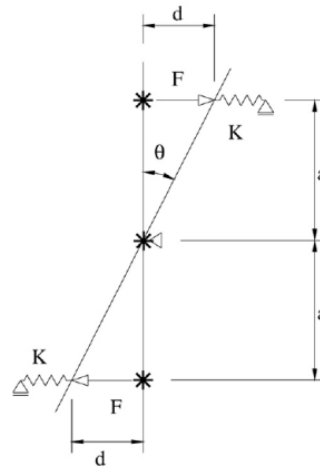
Figure V-2 Six bolt connection computation model

The rotational stiffness can be used to determine the buckling lengths of the web members.

$$L_{\text{b,web}} = \mu L_{\text{web}}$$

$$\mu = 0.5 + 0.14(\eta_1 + \eta_2) + 0.055(\eta_1 + \eta_2)^2$$

$$\eta_1 = \frac{K_{\text{web}}}{K_{\text{web}} + K_{\text{node,1}}}; \eta_2 = \frac{K_{\text{web}}}{K_{\text{web}} + K_{\text{node,2}}}$$

$$K_{\text{web}} = \frac{EI_{\text{web}}}{L_{\text{web}}}$$

where L_{web} is the length of the web member measured between centre lines of connections; I_{web} is the second moment of area of the web member; $K_{node,i}$ presents the rotational stiffness of the connection connecting the web member on the chord.

Because of the connection eccentricities (see Figure V-3), for the six bolt connection, expression of axial stiffness of the connection is as follow:

$$K_{axial} = 6 \times 6.8 \frac{\sqrt{D}}{(\frac{10}{t} - 1)} = \frac{EA_{ech}}{L_{ech}} \quad (kN/mm)$$
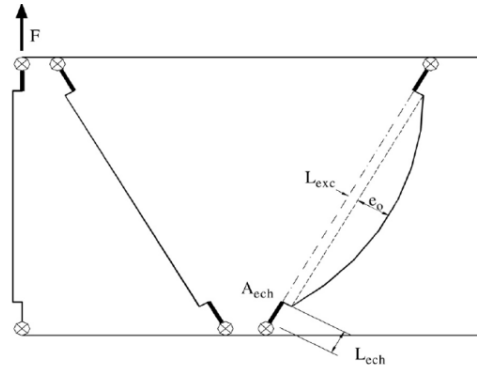
Figure V-3 Experimental model of truss

Appendix VI

Formulas for connection stiffness and moment resistance presented by Dubina (2008)

As is shown in Figure VI-1, the elements impacting the stiffness of the connection include bolts in shear ($k_{v,f}$ for flange bolts; $k_{v,w}$ for web bolts), bolts in bearing on cold-formed member ($k_{b,cff}$ for flange bolts; $k_{b,cfw}$ for the web bolts) and bolts in bearing on the bracket ($k_{b,bf}$ for flange bolts; $k_{b,bw}$ for web bolts) (see Figure VI-2).
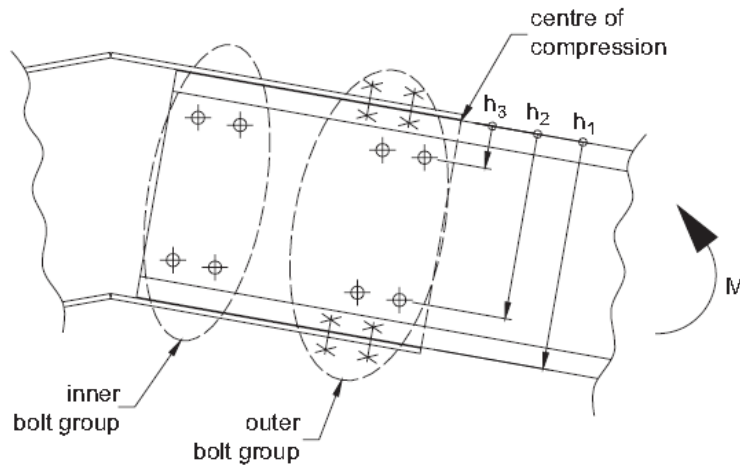
Figure VI-1 Bolt groups in the analysis

According to Eurocode 3 (Eurocode, 2005), for each of the bolt rows r, an effective stiffness coefficient $k_{eff,r}$ can be determined by individual stiffness coefficients:

$$k_{eff,r} = \frac{1}{\sum_i (1/k_{i,r})}$$

The effective stiffness coefficients of the bolt rows in 'tension' zone are instead of an equivalent spring with the stiffness k_{eq}:

$$k_{eq} = \frac{\sum_r k_{eff,r} h_r}{z_{eq}}$$

where h_r is the distance between bolt row r and the centre of compression.

$$Z_{eq} = \frac{\sum_r k_{eff,r} h_r^2}{\sum_r k_{eff,r} h_r}$$

The initial connection stiffness is:

$$S_{j,ini} = \frac{E z_{eq}^2}{\sum_i (1/k_i)}$$
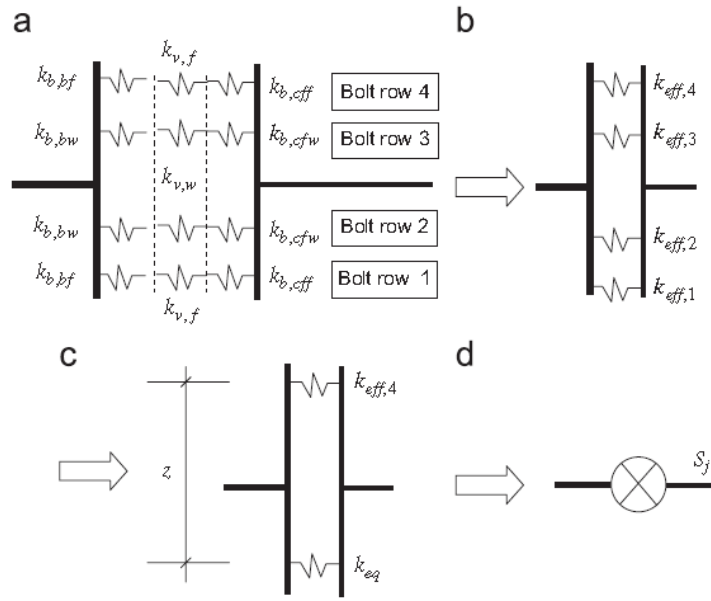
Figure VI-2 Main steps of the connection stiffness determination

The moment resistance of the bolt connection was divided into two steps. In the first step, only members related to bolt resistance were considered. The moment resistance of the bolted connection is $M_{C,Rd}^b$. In the second step, the moment resistance is the minimum of moment resistance of the bolted connection $M_{C,Rd}^b$ and one of the connected cold-formed steel members $M_{beam,Rd}$:

$$M_{C,Rd} = \min(M_{C,Rd}^b, M_{beam,Rd})$$

$$M_{C,Rd}^b = \sum_r F_{tr,Rd} h_r$$

$$F_{tr,Rd} \leq F_{t1,Rd} \frac{h_r}{h_1}$$

where $F_{tr,Rd}$ presents the effective tension resistance of the bolt row r.

Appendix VII

The shear resistances of the screwed connections (Kwon et al., 2008)

The width of the gap between the connected plates impacts the deformation mode and the shear resistances. Considering the gap and different thicknesses of connected plates, calculations for the shear resistances of the screwed connections was proposed.

When the gap between the connected plates is large:

$$P_{max} = 4.6(t_2^3 d)^{1/2} F_{u2}$$

When the gap is not considerable:

$$P_{max} = 6.6(t_2^3 d)^{1/2} F_{u2}$$

where t_2 is the thinner thickness of the connected plate; d is the diameter of the screw; F_{u2} is the ultimate tensile strength of the thinner plate. It should to be noted that the results of the expressions are correspondingly larger than the value from AISI by 10% and 57%.
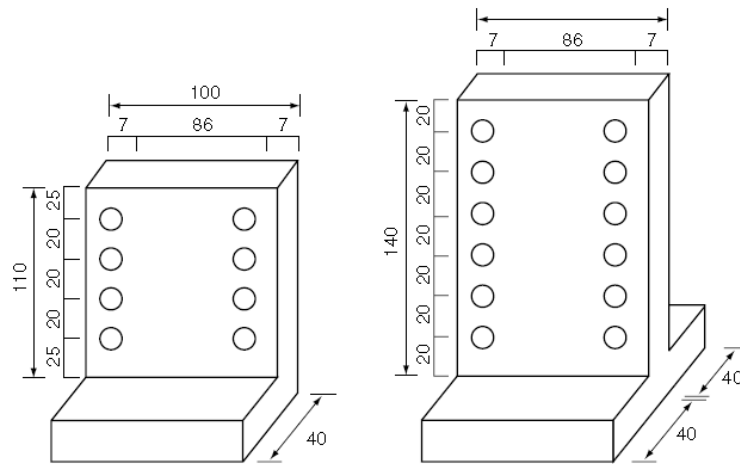
Figure VII-1 Shapes of connectors

Appendix VIII

Calibration factors for the truss connections with gaps (Yu and Panyanouvong, 2013)

The bearing strength of the connection depends on the strength of the connected plates, the fasteners, the sheet thickness, the type of connection, etc.

In AISI S100 (2007), without considerations of the holes deformation, the bearing strength of the connection can be calculated by the following expression.

$$P_\mathrm{n} = m_\mathrm{f} C d t F_\mathrm{u}$$

where m_f is the modification factor (see Table VIII-1); C is the bearing factor for bolted connections (see Table VIII-2); d is the bolt diameter; t is the thickness of the thinnest sheet; F_u presents the tensile strength of the sheets. According the comparison with test, the results of AISI S100 (2007) is unconventional. The author presented new modification factor m_f (see Table VIII-3) and bearing factor C (see Table VIII-4) in the paper (Yu and Panyanouvong, 2013).

Table VIII-1 Modification factor m_f for bolted connections (AISI S100 (2007))

Type of bearing connection	m_f
Single shear and outside sheets of double shear connection with washers under both bolt head and nut	1.0
Single shear and outside sheets of double shear connections without washers under both bolt head and nut, or with only one washer	0.75
Inside sheet of double shear connection with or without washers	1.33

Table VIII-2 Bearing factor C for bolted connections (AISI S100 (2007))

Ratio of fastener diameter to member thickness, d/t	C
d/t < 10	3
10 ≤ d/t ≤ 22	4-0.1(d/t)
d/t > 22	1.8

Table VIII-3 New modification factor m_f for bolted connections

Type of bearing connection	m_f
Single shear connection without restraints on both sides	0.675

Table VIII-4 New bearing factor C for bolted connections

Ratio of fastener diameter to member thickness, d/t	C
d/t < 5	3
5 ≤ d/t ≤ 28	0.33+13.33/(d/t)
d/t > 28	0.81

Appendix IX

Nonlinear flexural stiffness of the sleeved MZ connections (Ye et al., 2013)

Rotational behaviour model and the stiffness calculations was proposed by Bryan (1993). However, this linear model is inapplicable for the nonlinear feature of the sleeved connections.
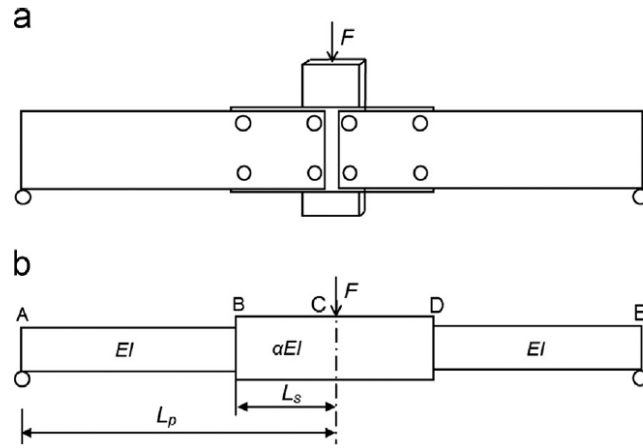
Figure IX-1 a) Experimental model and b) Analytical model

The effective flexural stiffness ratio α is defined as follow

$$\alpha = \frac{EI_s}{EI}$$

where I_s is the second moment of area of the sleeved connection and I is the second moment of the purlin section.

According to Figure IX-1, the deflection at point C is

$$\delta_C = -\frac{F}{4\alpha EI}\left[-\frac{2L_p^3}{3} + \frac{(2-2\alpha)(L_p-L_s)^3}{3}\right]$$

Because two beams are tested together, the load applied is *P=2F*.

$$\delta_C = -\frac{P}{12\alpha EI}\left[(1-\alpha)(L_p-L_s)^3 - L_p^3\right]$$

The rotation angle of the beam is

$$\theta = \frac{\delta}{L_p}$$

So that,

$$\alpha = \frac{P[L_p^3-(L_p - L_s)^3]}{12EI\delta-P(L_p - L_s)^3}$$

The mid-span moment (kN · m) on one beam is

$$M = \frac{1}{1000} \cdot \frac{P}{2} \cdot \frac{2L_p}{4} = \frac{PL_p}{4000}$$

The moment resistance ratio is as follow

$$\gamma = \frac{M_{\max}}{M_{\mathrm{con}}}$$

where $M_{\max}$ is the moment resistance of the MZ connection; M_{con} is the moment resistance of the continuous purlin section.

According to the numerical study,

$$\gamma = \begin{cases} \dfrac{0.2L_s}{D} + 0.05 & L_s/D \leq 4.0 \\ 0.85 & L_s/D > 4.0 \end{cases}$$

$$P_{\max} = \begin{cases} 4000(\dfrac{0.2L_s}{D} + 0.05)M_{\mathrm{con}}/L_p & L_s/D \leq 4.0 \\ 3400M_{\mathrm{con}}/L_p & L_s/D > 4.0 \end{cases}$$

Based on the test results and parametric study, the effective flexural stiffness ratio is

$$\alpha = (0.0012L_s - 0.20)M^{(0.0009L_s-0.67)}$$

where L_s is the length of the sleeve; M is the mid-span moment. The sleeve length to span ratio in the test is ranging from 18% to 39%. The expression may also applicable in a larger scope.

REFERENCES

ABAQUS-6.13 2013. *Analysis User's Manual*, SIMULIA.

ABRUZZO, J., MATTA, A. & PANARIELLO, G. 2006. Study of Mitigation Strategies for Progressive Collapse of a Reinforced Concrete Commercial Building. *Journal of Performance of Constructed Facilities,* 20**,** 384-390.

ACI. 2011. Building code requirements for structural concrete (ACI 318-11).

AISI. 2007. North American Specification for the Design of Cold-Formed Steel Structural Members, 2007 Edition. (AISI-S100). Washington, DC: American Iron and Steel Institute.

ASCE. 2005. American Society of Civil Engineers (ASCE). Minimum design loads for buildings and other structures. (ASCE7-05). Reston, VA.

ASME, M. 2003. Ultimate strength and failure mechanism of resistance spot weld subjected to tensile, shear, or combined tensile/shear loads. *Journal of Engineering Materials & Technology,* 125**,** 125-132.

BAE, S. W., LABOUBE, R. A., BELARBI, A. & AYOUB, A. 2008. Progressive collapse of cold-formed steel framed structures. *Thin-Walled Structures,* 46**,** 706-719.

BAMBACH, M. R., RASMUSSEN, K. J. R. 2007. Behavior of Self-Drilling Screws in Light-Gauge Steel Construction. *journal of Structural Enginnering.*

BARKER, K. 2003. Review of Housing Supply: Securing our Future Housing Needs. *Interim Report: Analysis, HMSO.* London.

BARKEY, M. E. & KANG, H. 2010. Tesing of spot welded coupons in combined tension and shear. *Experimental Techniques,* 23**,** 20-22.

BEWICK, B. & WILLIAMSON, E. 2014. Computational Modeling of Steel Stud Wall Systems for Applications to Blast-Resistant Design. *Journal of Structural Engineering,* 140**,** A4014007.

BEWICK, B. T., O'LAUGHLIN, C. G. & WILLIAMSON, E. B. 2013. Evaluation of Conventional Construction Techniques for Enhancing the Blast Resistance of Steel Stud Walls. *Journal of Structural Engineering Asce,* 139**,** 1992-2002.

BLISMAS, N. & WAKEFIELD, R. 2009. Drivers, constraints and the future of offsite manufacture in Australia. *Construction Innovation: Information, Process, Management,* 9**,** 72-83.

BONDOK, D., SALIM, H., SAUCIER, A. & DINAN, R. 2015. Static resistance function of cold-formed steel stud walls. *Thin-Walled Structures,* 94**,** 177-187.

BRYAN, E. R. 1993. The design of bolted joints in cold-formed steel sections. *Thin-Walled Structures,* 16**,** 239-262.

BS. 1996. British Standard (BS). Loading for buildings, Part 1: Code of practice for dead and imposed loads. (BS6399). London, United Kingdom.

BS. 1997. British Standard (BS). "The Structural use of concrete in building (BS8110-1:1997)". Part1: Code of practice for design and construction.

BSI. 2009. BS EN ISO 6892-1. Metallic materials. Tensile testing: Method of test at ambient temperature.

BURSI, O. S. & JASPART, J. P. 1997. Benchmarks for finite element modelling of bolted steel connections. *Journal of Constructional Steel Research,* 43**,** 17-42.

CHEN, C. H., ZHU, Y. F., YAO, Y., HUANG, Y. & LONG, X. 2016. An evaluation method to predict progressive collapse resistance of steel frame structures. *Journal of Constructional Steel Research,* 122**,** 238-250.

CHU, X.-T., RICKARD, J. & LI, L.-Y. 2005. Influence of lateral restraint on lateral-torsional buckling of cold-formed steel purlins. *Thin-Walled Structures,* 43**,** 800-810.

CHUNG, K. F. & IP, K. H. 2000. Finite element modelling of bolted connections between cold-formed steel strip and hot rolled steel plates under static shear loading. *Engineering Structures,* 22**,** 1271-1284.

CHUNG, K. F. & IP, K. H. 2001. Finite element investigation on the structural behaviour of cold-formed steel bolted connections. *Engineering Structures,* 23**,** 1115-1125.

CHUNG, K. F. & LAU, L. 1999. Experimental investigation on bolted moment connections among cold-formed steel members. *Engineering Structures,* 21**,** 898-911.

CHUNG, K. F. & LAWSON, R. M. 2000. Structural performance of shear resisting connections between cold-formed steel sections using web cleats of cold-formed steel strip. *Engineering Structures,* 22**,** 1350-1366.

COIMBRA, J. & ALMEIDA, M. 2013. Challenges and benefits of building sustainable cooperative housing. *Building and Environment,* 62**,** 9-17.

DAVIES, R., PEDRESCHI, R. & SINHA, B. P. 1997. Moment-rotation behaviour of groups of press-joins in cold-formed steel structures. *Thin-Walled Structures,* 27**,** 203-222.

DI LORENZO, G. & LANDOLFO, R. 2004. Shear experimental response of new connecting systems for cold-formed structures. *Journal of Constructional Steel Research,* 60**,** 561-579.

DOD. 2005. DoD. Design building to resist progressive collapse. Unified Facilities Criteria (UFC-04-023-03). USA: Department of Defence.

DOD. 2009. Unified facilities criteria: design of buildings to resist progressive collapse. UFC 4-023-03. United States Department of Defense.

DOD. 2013. DoD. Design building to resist progressive collapse. Unified Facilities Criteria (UFC-04-023-03). USA: Department of Defence.

DOD. 2016. DoD. Design building to resist progressive collapse. Unified Facilities Criteria (UFC-04-023-03). USA: Department of Defence.

DORAN, D. & GIANNAKIS, M. 2011. An examination of a modular supply chain: a construction sector perspective. *Supply Chain Management: An International Journal,* 16**,** 260-270.

DRAGANIĆ, H., DOKŠANOVIĆ, T. & MARKULAK, D. 2014. Investigation of bearing failure in steel single bolt lap connections. *Journal of Constructional Steel Research,* 98**,** 59-72.

DUBINA, D. 2008. Structural analysis and design assisted by testing of cold-formed steel structures. *Thin-Walled Structures,* 46**,** 741-764.

DUNDU, M. & KEMP, A. R. 2006. Plastic and Lateral-Torsional Buckling Behavior of Single Cold-Formed Channels Connected Back-to-Back. *Journal of Structural Engineering,* 132**,** 1223-1233.

EGAN, J. 1998. Rethinking Construction. London: Construction task force.

EUROCODE 2004. European Committee for Standardization. Eurocode 2: Design of concrete structures. Part 1: General rules and rules for buildings (EN 1992-1-1). Brussels, Belgium.

EUROCODE 2005. European Committee for Standardization. Eurocode 3: design of steel structures-cold formed structures. (EN 1993-1-8). *part 1-8: Design of joints.* British Standards Institution.

EUROCODE 2006a. European Committee for Standardization. Eurocode 1: Actions on structures. Part 1-7: General Actions - Accidental actions. (EN 1991-1-7). Brussels, Belgium.

EUROCODE 2006b. European Committee for Standardization. Eurocode 3: Design of Steel Structures: Part-1-3 General rules- Supplementary rules for cold-formed members and sheeting. (EN 1993-1-3).

FAN, L., RONDAL, J. & CESCOTTO, S. 1997a. Finite element modelling of single lap screw connections in steel sheeting under static shear. *Thin-Walled Structures,* 27**,** 165-185.

FAN, L. X., RONDAL, J. & CESCOTTO, S. 1997b. Numerical simulation of lap screw connections. Thin-walled structure. *Thin-Walled Structures,* 29**,** 235-241.

FIORINO, L., DELLA CORTE, G. & LANDOLFO, R. 2007. Experimental tests on typical screw connections for cold-formed steel housing. *Engineering Structures,* 29**,** 1761-1773.

FOLEY, C. M., MARTIN, K. & SCHNEEMAN, C. 2007. Robustness in structural steel framing systems. *Milwaukee, WI: Marquette University.*

GAO, T. & MOEN, C. D. 2012. Predicting rotational restraint provided to wall girts and roof purlins by through-fastened metal panels. *Thin-Walled Structures,* 61**,** 145-153.

GB. 2002. Technical code of cold-formed thin-wall steel structures. (GB50018-2002). Beijing: China Planning Press.

GERASIMIDIS, S. & BANIOTOPOULOS, C. 2015. Progressive collapse mitigation of 2D steel moment frames. *Stahlbau,* 84**,** 324-331.

GERASIMIDIS, S., BISBOS, C. D. & BANIOTOPOULOS, C. C. 2014. A computational model for full or partial damage of single or multiple adjacent columns in disproportionate collapse analysis via linear programming. *Structure and Infrastructure Engineering,* 10, 670-683.

GIBB, A. G. F. & ISACK, F. 2003. Re-engineering through pre-assembly: client expectations and drivers. *Building reseach & information,* 31**,** 146-160.

GOODIER, C. & GIBB, A. 2005. The value of the UK market for offsite. *Buildoffsite: promoting construction offsite.* Buildoffsite: promoting construction offsite.

GORGOLEWSKI, M., GRUBB, P. & LAWSON, R. 2001a. Building design using cold formed steel sections: light steel framing in residential buildings. *The Steel Construction Institute P,* 301.

GORGOLEWSKI, M. T., GRUBB, P. & LAWSON, R. M. 2001b. *Modular Construction Using Light Steel Framing: Desing of Residential Buildings*, Steel Construction Institute.

GSA. 2000. United States General Services Administration (GSA). Progressive collapse analysis and design guidelines for new federal office buildings and major modernization projects. Washington, DC: General Services Administration.

GSA. 2003. United States General Services Administration (GSA). Progressive collapse analysis and design guidelines for new federal office buildings and major modernization projects. Washington D.C.

GSA. 2016. United States General Services Administration (GSA). Alternate path analysis & Design guidelines for progressive collapse resistance. Washington D.C.

GUTIERREZ, R., LOUREIRO, A., LOPEZ, M. & MORENO, A. 2011. Analysis of cold-formed purlins with slotted sleeve connections. *Thin-Walled Structures,* 49**,** 833-841.

HAMPSON, K. & BRANDON, P. 2004. *Construction 2020: A vision for Australia's property and construction industry.*, Cooperative research centre for construction innovation.

HE, Y. C. & WANG, Y. C. 2011. Load–deflection behaviour of thin-walled plates with a single bolt in shearing. *Thin-Walled Structures,* 49**,** 1261-1276.

HO, H. C. & CHUNG, K. F. 2006. Structural behavior of lapped cold-formed steel Z sections with generic bolted configurations. *Thin-Walled Structures,* 44**,** 466-480.

ISO. 2009. International Organization for Standardization (ISO 6892-1), metallic materials –tensile testing – part 1: method of test at room temperature. Geneva, Switzerland: ISO.

JU, S. H., FAN, C. Y. & WU, G. H. 2004. Three-dimensional finite elements of steel bolted connections. *Engineering Structures,* 26**,** 403-413.

KIM, J., YOON, J.-C. & KANG, B.-S. 2007. Finite element analysis and modeling of structure with bolted joints. *Applied Mathematical Modelling,* 31**,** 895-911.

KIRK, P. 1986. Design of a cold formed section portal frame building system. *Eighth International Specialty Conference on Cold-Formed Steel Structures.* St. Louis, Missouri, U.S.A.

KRAUS, C. A. 1997. *Floor vibration design criterion for cold-formed C-Shaped supported residential floor systems.* Virginia Polytechnic Institute and State University.

KWON, Y. B., CHUNG, H. S. & KIM, G. D. 2008. Development of cold-formed steel portal frames with PRY sections. *Advances in Structural Engineering,* 11**,** 633-649.

KWON, Y. B., CHUNG, H. S., KIM, G. D. 2006. Experiments of cold formed steel connections and portal frames. *Journal of Structural Engineering*.

LANDOLFO, R., FIORINO, L. & IUORIO, O. 2010. A specific procedure for seismic design of cold-formed steel housing. *Advance Steel Construction,* 6**,** 603-618.

LANDOLFO, R., MAMMANA, O., PORTIOLI, F., DI LORENZO, G. & GUERRIERI, M. R. 2009. Experimental investigation on laser welded connections for built-up cold-formed steel beams. *Journal of Constructional Steel Research,* 65**,** 196-208.

LARSSON, J., ERIKSSON, P. E., OLOFSSON, T. & SIMONSSON, P. 2014. Industrialized construction in the Swedish infrastructure sector: core elements and barriers. *Construction Management and Economics,* 32**,** 83-96.

LAWSON, R. M. & OGDEN, R. G. 2008. 'Hybrid' light steel panel and modular systems. *Thin-Walled Structures,* 46**,** 720-730.

LAWSON, R. M., OGDEN, R. G. & BERGIN, R. 2012. Application of Modular Construction in High-Rise Buildings. *Journal of Architectural Engineering,* 18**,** 148-154.

LAWSON, R. M., OGDEN, R. G., PEDRESCHI, R. & POPO-OLA, S. O. 2008. Developments of Cold-Formed Steel Sections in Composite Applications for Residential Buildings. *Advances in Structural Engineering,* 11**,** 651-660.

LAWSON, R. M. & RICHARDS, J. 2010. Modular design for high-rise buildings. *Proceedings of the Institution of Civil Engineers-Structures and Buildings,* 163**,** 151-164.

LEE, Y. L., WEHNER, T. J., LU, M. W., MORRISSETT, T. W. & PAKALNINS, E. 1998. Ultimate Strength of Resistance Spot Welds Subjected to Combined Tension and Shear. *Journal of Testing & Evaluation,* 26**,** 213-219.

LI, L.-Y. 2004. Lateral–torsional buckling of cold-formed zed-purlins partial-laterally restrained by metal sheeting. *Thin-Walled Structures,* 42**,** 995-1011.

LI, L.-Y., REN, C. & YANG, J. 2012. Theoretical analysis of partially restrained zed-purlin beams subjected to up-lift loads. *Journal of Constructional Steel Research,* 70**,** 273-279.

LI, Y., LU, X., GUAN, H. & YE, L. 2011. An improved tie force method for progressive collapse resistance design of reinforced concrete frame structures. *Engineering Structures,* 33**,** 2931-2942.

LIM, J. & KRAUTHAMMER, T. 2006. Progressive collapse analyses of 2D steel-framed structures with different connection models. 43**,** 201-215.

LIM, J. B. P. & NETHERCOT, D. A. 2004. Stiffness prediction for bolted moment-connections between cold-formed steel members. *Journal of Constructional Steel Research,* 60**,** 85-107.

LIN, S. H., PAN, J., WU, S. R., TYAN, T. & WUNG, P. 2002. Failure loads of spot welds under combined opening and shear static loading conditions. *International Journal of Solids & Structures,* 39**,** 19-39.

LIU, J. L. 2010. Preventing progressive collapse through strengthening beam-to-column connection, Part 1: Theoretical analysis. *Steel Construction,* 66**,** 229-237.

LIU, Q., YANG, J., CHAN, A. H. C. & LI, L. Y. 2011. Pseudo-plastic moment resistance of continuous beams with cold-formed sigma sections at internal supports: A numerical study. *Thin-Walled Structures,* 49**,** 1592-1604.

LORENZO, G. D. & LANDOLFO, R. 2004. Shear experimental response of new connecting systems for cold-formed structures. *Journal of Constructional Steel Research,* 60**,** 561-579.

LU, X., LI, Y. & YE, W. 2011. *Theory and design method for progressive collapse provision of concrete structures,* Beijing, China Building Industry Press.

MILES, J. & WHITEHOUSE, N. 2013. Offsite housing review. London: Construction industry council.

MILLS, J. E., LABOUBE, R. 2004. Self-Drilling Screw Joints for Cold-Formed Channel Portal Frames. *Journal of Structural Enginnering,* 130**,** 8.

MOHAMED, I., RAHMAN, N. A. & SERACINO, R. Investigation of Cold-Formed Steel Wall Reinforcement Systems to Resist Progressive Collapse. Structures Congress, 2013. 960-969.

MUCHA, J. & WITKOWSKI, W. 2013. The experimental analysis of the double joint type change effect on the joint destruction process in uniaxial shearing test. *Thin-Walled Structures,* 66**,** 39-49.

MÄKELÄINEN, P. & KESTI, J. 1999. Advanced method for lightweight steel joining. *Journal of Constructional Steel Research,* 49**,** 107-116.

NAIR, R. S. 2004. Progressive collapse basics. *Modern Steel Construction*.

NBCC. 2005. Canadian Commission on Building and fire Codes, National Research Council of Canada. National Building Code of Canada. Ottawa, Canada.

NETHERCOT, D. A., LI, T. Q. & AHMED, B. 1998. Unified classification system for beam-to-column connections. *Journal of Constructional Steel Research,* 45**,** 39–65.

ODPM. 2004. Office of the Deputy Prime Minister. Office of the Deputy Prime Minister. The building regulations 2000, Part A, Schedule 1: A3, Disproportionate collapse. London, United Kingdom.

OUTINEN, J., PERTTOLA, H., HARA, R., KUPARI, K. & KAITILA, O. 2000. Seminar on steel structures: Design of cold-formed steel structures. Helsinki University of Technology Laboratory of Steel Structures Publications 15.

PAN, W., GIBB, A. & DAINTY, A. 2005. Offsite modern methods of construction in housebuilding: Perspectives and practices of leading UK housebuilders. Leicestershire: Loughborough University.

PAN, W., GIBB, A. G. F. & DAINTY, A. R. J. 2007. Perspectives of UK housebuilders on the use of offsite modern methods of construction. *Construction Management and Economics,* 25**,** 183-194.

PCA. 1979. Portland Cement Association (PCA). Design Methodology. Design and Construction of Large-Panel Concrete Structures, report 1- 6 and supplementary A, B, C.

PEDRESCHI, R. F., SINHA, B. P. & DAVIES, R. 1997. Advanced connection techniques for cold-formed steel structure. *Journal of Structural Engineering,* 123**,** 138-144.

REN, C., LI, L.-Y. & YANG, J. 2012. Bending analysis of partially restrained channel-section purlins subjected to up-lift loadings. *Journal of Constructional Steel Research,* 72**,** 254-260.

RUTH, P., MARCHAND, K. A. & WILLIAMSON, E. B. 2015. Static Equivalency in Progressive Collapse Alternate Path Analysis: Reducing Conservatism while Retaining Structural Integrity. *Journal of Performance of Constructed Facilities,* 20**,** 349-364.

S NSTAB , J. K., HOLMSTR M, P. H., MORIN, D. & LANGSETH, M. 2015. Macroscopic strength and failure properties of flow-drill screw connections. *Journal of Materials Processing Technology,* 222**,** 1-12.

SCI. 2006. Sustainability of steel in housing and residential buildings. The steel construction institute.

SCI. 2007. Market study of modular construction in Europe and design of residential building using modular construction. The steel construction institute.

SCI. 2015. Modular construction using light steel framing-design of residential buildings. The steel construction institute.

SHI, Y. P. & ZHOU, Y. R. 2006. The finite element analysis example explanation. 45-51.

SHI, Y. P. Z., Y. R. 2006. *The finite element analysis example explanation*.

STODDART & E., P. 2012. *Development of component-based connection modelling for steel framed structures subjected to blast or progressive collapse.* University of Southampton.

STYLIANIDIS, P. M. & NETHERCOT, D. A. 2015. Modelling of connection behaviour for progressive collapse analysis. *Journal of Constructional Steel Research,* 113**,** 169-184.

TAN, K. H., SEAH L. K., FOK, S. C. 1996. Connections in cold-formed thin-walled structures. *Computers and Structures,* 60**,** 4.

TOHIDI, M., YANG, J. & BANIOTOPOULOS, C. 2014a. An Improved Tie Force Method for Progressive Collapse Resistance of Precast Concrete Cross Wall Structures. *International Journal of Civil, Structural, Construction and Architectural Engineering,* 8**,** 1-9.

TOHIDI, M., YANG, J. & BANIOTOPOULOS, C. 2014b. Numerical evaluations of codified design methods for progressive collapse resistance of precast concrete cross wall structures. *Engineering Structures,* 76**,** 177-186.

TOM , A., SEDLACEK, G. & WEYNAND, K. 1993. Connections in cold-formed steel. *Thin-Walled Structures,* 16**,** 219-237.

TRAHAIR, N. S., BRADFORD, M. A., NETHERCOT, D. & GARDNER, L. 2007. *The behaviour and design of steel structures to EC3*, CRC Press.

VLASSIS, A. G., IZZUDDIN, B. A., ELGHAZOULI, A. Y. & NETHERCOT, D. A. 2009. Progressive collapse of multi-storey buildings due to failed floor impact. *Engineering Structures,* 31**,** 1522-1534.

VRAN , T. 2002. Torsional restraint of cold-formed beams provided by corrugated sheeting for arbitrary input variables. *Eurosteel the 3rd European conference on steel structures.* Coimbra, Portugal.

VRAN , T. 2006. Effect of loading on the rotational restraint of cold-formed purlins. *Thin-Walled Structures,* 44**,** 1287-1292.

WAHYUNI, E. 2015. Axial and Flexural Performance of Adhesive Connection on Cold-Formed Steel Structures. *International Journal of Technology,* 6**,** 699-708.

WINTER, G. 1956. Tests on bolted connections in light gage steel. *Journal of the Structural Division, Proc. ASCE,* 82, No. ST2.

WONG, M. F. & CHUNG, K. F. 2002. Structural behaviour of bolted moment connections in cold-formed steel beam-column sub-frames. *Journal of Constructional Steel Research,* 58**,** 253-274.

YANG, J. & LIU, Q. 2012. Sleeve connections of cold-formed steel sigma purlins. *Engineering Structures,* 43**,** 245-258.

YE, W., WANG, C. J., MYNORS, D. J., KIBBLE, K. A., MORGAN, T. & CARTWRIGHT, B. 2013. Load–deflection behaviour of sleeved joints in modified Z purlin system. *Thin-Walled Structures,* 73**,** 318-328.

YE, Z.-M., KETTLE, R. & LI, L.-Y. 2004. Analysis of cold-formed zed-purlins partially restrained by steel sheeting. *Computers & Structures,* 82**,** 731-739.

YE ZM, K. R., LI LY, SCHAFER BW 2002. Buckling behavior of cold-formed zed-purlins partially restrained by sheeting. *Thin-Walled Structures,* 40**,** 853-864.

YU, C. & PANYANOUVONG, M. X. 2013. Bearing strength of cold-formed steel bolted connections with a gap. *Thin-Walled Structures,* 67**,** 110-115.

YU, W. K., CHUNG, K. F. & WONG, M. F. 2005. Analysis of bolted moment connections in cold-formed steel beam–column sub-frames. *Journal of Constructional Steel Research,* 61**,** 1332-1352.

YUAN, W.-B., CHENG, S., LI, L.-Y. & KIM, B. 2014. Web-flange distortional buckling of partially restrained cold-formed steel purlins under uplift loading. *International Journal of Mechanical Sciences,* 89**,** 476-481.

ZABIHI, H., HABIB, F. & MIRSAEEDIE, L. 2013. Definitions, concepts and new directions in Industrialized Building Systems (IBS). *KSCE Journal of Civil Engineering,* 17**,** 1199-1205.

ZADANFARROKH, B. F. & BRYAN, E. R. 1992. Testing and design of bolted connections in cold formed steel sections. *Eleventh International Specialty Conference on Cold-Formed Steel Structures.* St. Louis, Missouri, U.S.A.

ZAHARIA, R. & DUBINA, D. 2000. Behaviour of cold-formed steel truss bolted joints. *In: The IV'th international workshop on connections in steel structures*.

ZAHARIA, R. & DUBINA, D. 2006. Stiffness of joints in bolted connected cold-formed steel trusses. *Journal of Constructional Steel Research,* 62**,** 240-249.

ZHAI, X., REED, R. & MILLS, A. 2014. Factors impeding the offsite production of housing construction in China: an investigation of current practice. *Construction Management and Economics,* 32**,** 40-52.

ZHANG, X., SKITMORE, M. & PENG, Y. 2014. Exploring the challenges to industrialized residential building in China. *Habitat International,* 41**,** 176-184.

ZHAO, C., YANG, J., WANG, F. & CHAN, A. H. C. 2014. Rotational stiffness of cold-formed steel roof purlin–sheeting connections. *Engineering Structures,* 59**,** 284-297.

ZHU, J., CHEN, J. & REN, C. 2013. Numerical study on the moment capacity of zed-section purlins under uplift loading. *The 2013 World Congress on Advances in Structural Engineering Mechanics (ASEM 13).* Jeju, Korea.